



Vinícius Gabriel Segala Simionatto

The Use of Centrifugal Pendulums for Torsional Vibration Control in Automotive Powertrains

*O Uso de Pêndulos Centrífugos para
Controle de Vibrações Torcionais em
Trens de Potência Automotivos*

43/2015

CAMPINAS
2015



UNIVERSIDADE ESTADUAL DE CAMPINAS
FACULDADE DE ENGENHARIA MECÂNICA

Vinícius Gabriel Segala Simionatto

**The Use of Centrifugal Pendulums for Torsional Vibration
Control in Automotive Powertrains**

*O Uso de Pêndulos Centrífugos para Controle de Vibrações
Torcionais em Trens de Potência Automotivos*

Doctoral Thesis presented to the School of Mechanical Engineering of the University of Campinas in partial fulfillment of the requirements for the degree of Doctorate in Mechanical Engineering, in the Area of Solid Mechanics and Mechanical Design.

Tese de Doutorado apresentada à Faculdade de Engenharia Mecânica da Universidade Estadual de Campinas como parte dos requisitos exigidos para obtenção do título de Doutor em Engenharia Mecânica, na Área de Mecânica dos Sólidos e Projeto Mecânico.

Orientador: Prof. Dr. Milton Dias Junior

ESTE EXEMPLAR CORRESPONDE À VERSÃO
FINAL DA TESE DEFENDIDA PELO ALUNO
Vinícius Gabriel Segala Simionatto E ORIENTADA
PELO Prof. Dr. Milton Dias Junior.



Prof. Dr. Milton Dias Junior

CAMPINAS
2015

Ficha catalográfica
Universidade Estadual de Campinas
Biblioteca da Área de Engenharia e Arquitetura
Elizangela Aparecida dos Santos Souza - CRB 8/8098

Si45u Simionatto, Vinícius Gabriel Segala, 1986-
The use of centrifugal pendulums for torsional vibration control in automotive powertrains / Vinícius Gabriel Segala Simionatto. – Campinas, SP : [s.n.], 2015.

Orientador: Milton Dias Junior.
Tese (doutorado) – Universidade Estadual de Campinas, Faculdade de Engenharia Mecânica.

1. Automóveis - Vibração. 2. Movimento pendular. 3. Automóveis - Dinâmica. 4. Veículos - Controle de ruído. I. Dias Junior, Milton, 1961-. II. Universidade Estadual de Campinas. Faculdade de Engenharia Mecânica. III. Título.

Informações para Biblioteca Digital

Título em outro idioma: O uso de pêndulos centrífugos para controle de vibrações torcionais em trens de potência automotivos

Palavras-chave em inglês:

Automobiles - Vibration

Pendular motion

Automobiles - Dynamics

Vehicles - Noise control

Área de concentração: Mecânica dos Sólidos e Projeto Mecânico

Titulação: Doutor em Engenharia Mecânica

Banca examinadora:

Milton Dias Junior [Orientador]

Robson Pederiva

Pablo Siqueira Meirelles

Sérgio Junichi Idehara

Marcelo Becker

Data de defesa: 26-02-2015

Programa de Pós-Graduação: Engenharia Mecânica

UNIVERSIDADE ESTADUAL DE CAMPINAS
FACULDADE DE ENGENHARIA MECÂNICA
COMISSÃO DE PÓS-GRADUAÇÃO EM ENGENHARIA MECÂNICA
DEPARTAMENTO DE SISTEMAS INTEGRADOS

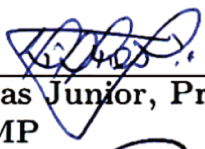
TESE DE DOUTORADO

**The Use of Centrifugal Pendulums for Torsional
Vibration Control in Automotive Powertrains**
*O Uso de Pêndulos Centrífugos para Controle de
Vibrações Torcionais em Trens de Potência
Automotivos*

Autor: Vinícius Gabriel Segala Simionatto

Orientador: Prof. Dr. Milton Dias Junior

A Banca Examinadora composta pelos membros abaixo aprovou esta Tese:



Prof. Dr. Milton Dias Junior, Presidente
DSI/FEM/UNICAMP



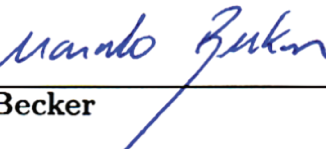
Prof. Dr. Robson Pederiva
DSI/FEM/UNICAMP



Prof. Dr. Pablo Siqueira Meirelles
DMC/FEM/UNICAMP



Prof. Dr. Sérgio Junichi Idehara
UFSC/Joinville



Prof. Dr. Marcelo Becker
SEM/EESC/USP

Campinas, 26 de fevereiro de 2015.

Dedico este trabalho à minha amada esposa e eterna companheira Vanessa.

I dedicate this work to my beloved wife and eternal companion Vanessa.

Agradecimentos

Em Português

A execução deste trabalho e o meu desenvolvimento como profissional e como pessoa jamais seriam possíveis sem a valiosa ajuda e o valioso suporte que recebi destas pessoas tão especiais a quem desejo expressar minha gratidão neste momento.

À família,

Primeiramente, gostaria de agradecer imensamente à minha esposa, amiga, namorada, fiel e eterna companheira Vanessa, que esteve ao meu lado durante todos os momentos me dando muito amor, carinho, compreensão, motivação e inspiração para que eu pudesse sempre dar o meu melhor e ultrapassar todas as dificuldades que encontrei neste período.

Gostaria de agradecer também aos meus pais, sogro e sogra, irmão e cunhadas, por todo o carinho, apoio e torcida que recebo de vocês.

Aos amigos,

Nesta parte dos agradecimentos, gostaria de agradecer a todos aqueles que estiveram do meu lado na execução deste trabalho, e que contribuíram valiosamente na troca de experiências tanto profissionais quanto pessoais.

Aos amigos da UNICAMP, meu agradecimento especial aos companheiros de longa data Fábio Menegatti de Melo e Hugo Heidy Miyasato, com quem tanto convivi e aprendi nos últimos anos. Devo agradecimentos especiais ao colega Alberto Oliveira Jr., pela amizade e pela valiosa ajuda concedida em sua passagem por Londres.

Aos amigos da ZF do Brasil, gostaria de agradecer especialmente a Hélio Shiguenori Sacagami, Ricardo Itoo, Eduardo da Silva, Wilson Rodrigo de Sousa, Luiz Alberto Caires Lima, Edmar Chaves Ferreira e Humberto Jorge Miranos de Golvea, pela amizade e pela rica troca de experiências e conhecimento que tanto contribuíram em minha formação.

Também devo agradecimentos a Douglas Vinícius Lemes, Leandro Tadeu Roldão Perestrelo, Lucas Santana Aurélio, Giezel Dias da Trindade e Giezel Dias da Trindade Junior, que contribuíram imensamente não só na realização deste trabalho, mas também em minha formação como profissional e ser humano.

Finalmente, gostaria de agradecer a Klaus Steinel por toda a atenção dada a nossos trabalhos e pelos valiosos conselhos ao longo desta jornada.

Aos professores,

Gostaria de agradecer primeiramente ao meu orientador, mentor, amigo e parceiro de longa data Milton Dias Jr. Seus ensinamentos e suporte transcendem em muito a realização deste trabalho e surtem efeitos que levarei comigo para toda a vida.

Agradeço imensamente à professora Kátia L. C. Dedini, que além de uma excelente professora, também é um excelente ser humano. Como para muitos alunos da Faculdade de Engenharia Mecânica, a senhora para mim é um grande exemplo e uma grande fonte de inspiração.

À ZF do Brasil,

Gostaria de agradecer imensamente à ZF do Brasil, não só por todo o suporte fornecido, mas também por todas as oportunidades de aprendizado e desenvolvimento que tivemos neste período. Assim como a empresa, eu tive ganhos de conhecimento que seriam inatingíveis sem a existência da parceria. Espero que este relacionamento possa se sustentar por muitos e muitos anos.

A Deus,

Gostaria de agradecer a Deus por me iluminar nos momentos em que me encontrei na escuridão, por me dar forças nos momentos em que eu acreditava que não poderia mais seguir em frente, por me dar clareza de pensamento nos momentos de confusão, inspiração nos momentos de dificuldade, e por me dar esta incrível vontade de seguir meus objetivos e alcançar meu propósito, mesmo eu não sendo capaz de entender por completo a minha missão.

In English

The execution of this work and my personal and professional development would never have been possible without the valuable help and support from all the special people, to whom I wish to express my thankfulness in this moment.

To my Family,

Firstly I would like to deeply thank my wife, friend, girlfriend, loyal and eternal companion Vanessa, who has been there for me through all the moments, giving me lots of love, affection, comprehension, motivation and inspiration, so that I could always give my best and overcome all the difficulties experienced in this period.

I would also like to thank my parents, brother and in-laws, for all the affection and support devoted to me.

To my friends,

In this part of my acknowledgments, I would like to thank all those who have been beside me during the execution of this work, and who have given valuable contributions on the exchange of personal and professional experience.

To my friends from UNICAMP, my special thanks to the longtime friends and companions Fábio Menegatti de Melo and Hugo Heidy Miyasato, with whom I lived and learnt a lot in the past years. I also owe special thanks to my friend Alberto Oliveira Jr. for the friendship and for the valuable help provided during his stay in London.

To my friends from ZF do Brasil, I would like to thank specially Hélio Shiguenori Sacagami, Ricardo Itoo, Eduardo da Silva, Wilson Rodrigo de Sousa, Luiz Alberto Caires Lima, Edmar Chaves Ferreira and Humberto Jorge Miranos de Golvea, for the friendship and rich exchange of experience and knowledge, which have contributed very much in my development.

I also have to thank Douglas Vinícius Lemes, Leandro Tadeu Roldão Perestrelo, Lucas Santana Aurélio, Giezel Dias da Trindade and Giezel Dias da Trindade Junior, who have contributed immensely not only for the execution of this work, but also in my development as a professional and human being.

I would finally like to thank Klaus Steinel for all the attention given to our work and for the valuable advice given throughout this journey.

To the professors,

I would firstly like to thank my advisor, mentor and longtime companion and friend Milton Dias Jr. His teachings and support transcend by far the execution of this work, and produce effects that I will carry with me throughout all my life.

I would also like to immensely thank professor Kátia L. C. Dedini, who is, besides an excellent professor, an excellent human being. As for many students of the Faculty of Mechanical Engineering, you are to me a great example and source of inspiration.

To ZF do Brasil,

I would like to thank very much ZF do Brasil, not only for all the support provided, but also for all the learning and development opportunities we had in this period. As the company, I had valuable knowledge gains that would have been unachievable without the existence of the

partnership. I sincerely hope that this relationship lasts for many years.

To God,

I would like to thank God for giving me illumination in the moments when I found myself in the darkness. For giving me strength in the moments when I believed I could not go any further and for giving me clearness of thought in the moments of confusion. For giving me inspiration in the moments of difficulties, and for giving me this amazing will of achieving my objectives and reach my purpose, even though I am not capable of fully understanding my mission.

“... tive uma vida muito boa. Mas tudo isso que eu consegui foi através de dedicação, perseverança, e muito desejo de atingir os meus objetivos, muito desejo de vitória. Vitória na vida, não vitória como piloto. E a vocês todos que assistirem e estão assistindo agora, eu digo que, seja quem você for, seja qualquer posição que você tenha na vida, um nível altíssimo ou o mais baixo, social, tenha sempre como meta muita força, muita determinação, e sempre faça tudo com muito amor, e com muita fé em Deus, que um dia você chega lá. De alguma maneira você chega lá.”

Ayrton Senna da Silva

Resumo

Absorvedores de Vibração Pendulares Centrífugos (ou CPVAs) são uma tecnologia criada em 1911, que trouxe excelentes resultados na redução de vibração torcional de muitos sistemas. Porém, sua aplicação em trens de potência automotivos para redução de vibração no virabrequim tornou-se inviável ao final da década de 1940 pela existência de *dampers* viscosos à base de silicone, uma solução mais barata e com desempenho similar em certas aplicações. Contudo, a vibração torcional transmitida a transmissões manuais ou automatizadas, em certas velocidades críticas, pode gerar ruído em níveis inaceitáveis, e as soluções atuais para a atenuação deste tipo de vibração, em algumas aplicações, são ou pouco efetivas, como o atrito em discos de embreagem, ou muito custosas, como volantes de dupla massa. Por isso, neste trabalho busca-se a aplicação de absorvedores de vibração pendulares em um disco de embreagem de um trem de potência automotivo equipado com uma transmissão automatizada para a redução de vibração torcional na transmissão, reduzindo possivelmente o ruído de *rattle*. Para este fim, primeiramente são realizados testes no veículo em estudo para o levantamento de dados torcionais do trem de potência, e em seguida, um modelo linear torcional é proposto, para que a dinâmica torcional do trem de potência seja representada. Em seguida, uma análise extensiva dos principais tipos de CPVA é realizada. São realizadas análises lineares e não lineares em modelos com parâmetros adimensionais de um e dois rotores com pêndulos centrífugos, e nas análises não lineares, o Método de Múltiplas Escalas é utilizado; um método mais robusto e preciso do que o método que vem sendo utilizado nos principais trabalhos nesta área. Além disso, as análises são feitas considerando-se que os pêndulos possuem trajetória genérica, e ênfase é dada às trajetórias clássicas: circular, cicloide e epicycloide. Com base nestas análises, duas metodologias de projeto de pêndulos centrífugos são propostas. Além disso, um protótipo de disco de embreagem com pêndulo é proposto. Então, baseando-se nas limitações do projeto, simulações são feitas utilizando o modelo proposto para o trem de potência e o modelo não linear do pêndulo. As primeiras simulações são feitas obedecendo as limitações do projeto, que propiciam um pequeno raio de instalação do pêndulo e permitem que ele possua massa muito menor do que o valor ideal. Estas simulações mostram que, neste caso o pêndulo se torna instável e ineficaz. Nas simulações seguintes, as limitações de projeto são desprezadas e ambos os projetos de pêndulo são testados. Com maior inércia, o absorvedor pendular é capaz de reduzir substancialmente a vibração torcional na transmissão sem que seja necessário introduzir atrito no disco de embreagem. Contudo, pêndulos com maior inércia podem comprometer a vida útil dos sincronizadores da transmissão, e por isso estudos devem ser realizados para verificar este efeito colateral.

Palavras Chave: Absorvedor de vibração; Pêndulo centrífugo; Vibração torcional; Trens de potência automotivos.

Abstract

Centrifugal Pendulum Vibration Absorbers (or CPVAs) are a technology which dates back to 1911, and which has brought excellent results on the reduction of torsional vibrations in many systems. Its application in automotive powertrains for the reduction of vibration on the crankshaft became impracticable by the second half of the 1940s due to the existence of silicone based viscous dampers, a cheaper solution that had similar performance in many applications. However, torsional vibration transmitted to manual or semi-automatic gearboxes may cause unacceptable noise in some critical speeds, and the current solutions for the mitigation of this kind of vibration are, in some cases, either not effective, as torsional friction in clutch disks, or too expensive, as dual mass flywheels. For this reason, in this work, the use of centrifugal pendulum vibration absorbers on a clutch disk of a vehicle powertrain equipped with a semi-automatic gearbox is studied, aiming at reducing torsional vibration at the gearbox, leading to possible reduction of *rattle* noise. For this means, firstly tests are performed on the vehicle under investigation in order to obtain torsional data from its powertrain, and a linear torsional model of it is proposed next, so that the torsional dynamics of the powertrain can be represented. Then, an extensive analysis of the main types of CPVA are performed. Linear and nonlinear analyses are made in models with dimensionless parameters composed by one of two rotors and centrifugal pendulums. For the nonlinear analyses, the Method of Multiple Scales is used; a more robust and precise method than the one which has been used on the main literature in this area. Besides, the analyses are performed considering general-path pendulums and emphasis is given to the classical paths: circular, cycloid and epicycloid. Based on these analyses, two design techniques for CPVAs are proposed. Furthermore, a prototype of a clutch disk with pendulum absorbers is proposed. Then, based on project limitations, simulations are performed using the powertrain model and the nonlinear model of the CPVA. The first simulations are performed taking into consideration the project limitations, which allow a small radius for pinning the pendulum and also for a small mass of the pendulum bob, much lower than the ideal value. These simulations show that, in this case, the pendulum becomes unstable and ineffective. On the forthcoming simulations, project limitations are neglected and both pendulum design techniques are tested. With higher inertia, the pendulum absorbers are capable of providing a substantial reduction on the amplitude of vibration of the gearbox without the need for adding torsional friction to the clutch disk. However, pendulum bobs with high inertia may harm the service life of the gearbox's synchronizers, and further studies must be performed to evaluate this side effect.

Keywords: Vibration absorber; Centrifugal pendulum; Torsional vibration; Automotive powertrains.

List of Figures

1.1	A clutch disk.	6
1.2	Torsional characteristics of a clutch disk.	7
1.3	Several designs of CPVAs. Reproduced from Wilson (1969)	13
1.4	Bifilar absorbers attached to Lynx type helicopter rotor head. Reproduced from the work of Bramwell <i>et al.</i> (2001)	16
2.1	Vehicle under investigation.	22
2.2	Scheme of the powertrain of the vehicle under investigation.	23
2.3	Tandem axle configuration.	24
2.4	<i>Left:</i> One end of the longest propeller shaft with auxiliary lever. <i>Right:</i> Displacement sensor touching auxiliary lever.	26
2.5	<i>Left:</i> Band used to pull vehicle. <i>Right:</i> Experiment setup.	27
2.6	Data fit to calculate the stiffness of the long propeller shaft.	27
2.7	Data fit to calculate the stiffness of the short propeller shaft.	28
2.8	Data fit to calculate the stiffness of the front right side shaft.	28
2.9	Data fit to calculate the stiffness of the front left side shaft.	29
2.10	Data fit to calculate the stiffness of the rear left side shaft.	29
2.11	Data fit to calculate the stiffness of the rear right side shaft.	30
2.12	Layout of the ZF 16AS 2631 TO gearbox.	33
2.13	Results of the 3 rd order obtained in Run 1 at 7 th gear.	34
2.14	Results of the 3 rd order obtained in Run 2 at 7 th gear.	35
2.15	Results of the 6 th order obtained in Run 1 at 7 th gear.	36
2.16	Results of the 6 th order obtained in Run 2 at 7 th gear.	37
2.17	Results of the 3 rd order obtained in Run 3 at 7 th gear.	37
2.18	Results of the 3 rd order obtained in Run 4 at 7 th gear.	38
2.19	Results of the 6 th order obtained in Run 3 at 7 th gear.	39
2.20	Results of the 6 th order obtained in Run 4 at 7 th gear.	39
2.21	Results of the 3 rd order obtained in Run 1 at 8 th gear.	40
2.22	Results of the 3 rd order obtained in Run 2 at 8 th gear.	41
2.23	Results of the 3 rd order obtained in Run 3 at 8 th gear.	42
2.24	Results of the 3 rd order obtained in Run 4 at 8 th gear.	42
2.25	Results of the 6 th order obtained in Run 4 at 8 th gear.	44

2.26	Results of the 3 rd order obtained in Run 1 at 9 th gear.	44
2.27	Results of the 3 rd order obtained in Run 2 at 9 th gear.	45
2.28	Results of the 3 rd order obtained in Run 3 at 9 th gear.	46
2.29	Results of the 3 rd order obtained in Run 4 at 9 th gear.	46
2.30	Results of the 3 rd order obtained in Run 1 at 10 th gear.	48
2.31	Results of the 3 rd order obtained in Run 1 at 11 th gear.	48
2.32	Results of the 3 rd order obtained in Run 1 at 12 th gear.	49
2.33	Results of the 3 rd order obtained in Run 1 at 13 th gear.	49
2.34	Results of the 3 rd order obtained in Run 1 at 14 th gear.	50
2.35	Angular acceleration of the flywheel at third order for different gears.	51
2.36	Angular acceleration of the flywheel at sixth order for different gears.	52
2.37	Time response of the measurement points immediately before and after the first amplification (Run 1 - 8 th gear).	57
2.38	Idealization of the powertrain.	58
2.39	Measured and simulated amplitude responses for 8 th gear - Run 1.	62
2.40	Physical mode and mode without gearings for gear rattle at 8 th gear.	63
2.41	Physical mode and mode without gearings for second amplification at 8 th gear.	64
2.42	Measured and simulated amplitude responses for 9 th gear - Run 1.	65
2.43	Physical mode and mode without gearings for gear rattle at 9 th gear.	66
2.44	Physical mode and mode without gearings for second amplification at 9 th gear.	67
3.1	A one degree of freedom carrier structure with a TMD.	70
3.2	Dimensionless frequency gap as a function of β	72
3.3	Dimensionless frequency gap as a function of μ	73
3.4	One degree of freedom structure with n tuned mass dampers.	75
3.5	Scheme of a single torsional disk with a CPVA attached to it.	77
3.6	Stability diagram for homogeneous Mathieu equation.	83
3.7	Two elastically coupled disks, one of them with a CPVA.	86
3.8	Eigen-orders of a two disk system with a CPVA.	89
3.9	Eigenfrequencies of a two disk system with a CPVA.	90
3.10	Modal ratios of a two disk system with a CPVA.	92
3.11	Order Response Function of carrier disk.	94
3.12	Maximum absolute value of the eigenvalues of the system for several (Ω, v) points.	96
3.13	Geometry for the generation of the cycloidal path.	103
3.14	Graphical representation of the implicit relationship $\theta_r(\theta_a)$ for the cycloidal path.	104

3.15	Second, 4 th , 6 th and 8 th order approximations for the cycloidal path.	106
3.16	Percent estimation error for the 2 nd , 4 th , 6 th and 8 th order approximations for the cycloidal path.	106
3.17	Geometry for the generation of the epicycloidal path.	108
3.18	Graphical representation of the implicit relationship $\theta_r(\theta_a)$ for the epicycloidal path.	109
3.19	Second, 4 th , 6 th and 8 th order approximations for the epicycloidal path.	110
3.20	Percent estimation error for the 2 nd , 4 th , 6 th and 8 th order approximations for the epicycloidal path.	111
3.21	Roots of the numerator of v_c	121
3.22	Normalized variation of A_1 from Eq. (3.156) along β with $q = 0.003125$	136
3.23	Normalized variation of A_1 from Eq. (3.157) along β with $q = 0.003125$	136
3.24	Normalized variation of A_1 from Eq. (3.156) along β with $q = 0.32031$	137
3.25	Normalized variation of A_1 from Eq. (3.157) along β with $q = 0.32031$	138
3.26	Normalized variation of A_1 from Eq. (3.156) along β with $q = 0.95469$	138
3.27	Normalized variation of A_1 from Eq. (3.157) along β with $q = 0.95469$	139
3.28	Normalized variation of A_2 from Eq. (3.158) along β with $q = 0.003125$	141
3.29	Normalized variation of A_2 from Eq. (3.159) along β with $q = 0.003125$	141
3.30	Normalized variation of A_2 from Eq. (3.158) along β with $q = 0.32031$	142
3.31	Normalized variation of A_2 from Eq. (3.159) along β with $q = 0.32031$	142
3.32	Normalized variation of A_2 from Eq. (3.158) along β with $q = 0.95469$	143
3.33	Normalized variation of A_2 from Eq. (3.159) along β with $q = 0.95469$	143
3.34	Normalized variation of the ratio A_2/A_1 from Eq. (3.160) along β with $q =$ 0.54688	145
3.35	Normalized variation of the ratio A_2/A_1 from Eq. (3.161) along β with $q =$ 0.54688	145
3.36	Normalized variation of the ratio A_1/A_2 from Eq. (3.162) along β with $q =$ 0.003125	147
3.37	Normalized variation of the ratio A_1/A_2 from Eq. (3.163) along β with $q =$ 0.003125	147
3.38	Normalized variation of the ratio A_1/A_2 from Eq. (3.162) along β with $q =$ 0.95469	148
3.39	Normalized variation of the ratio A_1/A_2 from Eq. (3.163) along β with $q =$ 0.95469	148
4.1	Parameters for tuning of CPVAs considering the No-Resonance Zone.	154
4.2	ZF prototype layout of clutch disk with bifilar CPVAs.	162

4.3	Contour levels of the surface of swing angles through (B_w, δ) for 8 th gear. . .	164
4.4	Contour levels of the surface of mass of bifilar pendulum bob through (B_w, δ) for 8 th gear.	164
4.5	Contour levels of the surface of swing angles through (B_w, δ) for 9 th gear. . .	165
4.6	Contour levels of the surface of mass of bifilar pendulum bob through (B_w, δ) for 9 th gear.	166
4.7	Angular acceleration from Simulation 1 from Set 2.	169
4.8	Swing angle of the pendulum bob from Simulation 1 from Set 2.	169
4.9	Angular acceleration from Simulation 2 from Set 2.	170
4.10	Swing angle of the pendulum bob from Simulation 2 from Set 2.	171
4.11	Angular acceleration from Simulations 1 to 3 from Set 3.	172
4.12	3 rd order swing angle response of the pendulums from Simulations 1 to 3 from Set 3.	173
4.13	6 th order swing angle response of the pendulums from Simulations 1 to 3 from Set 3.	174
4.14	Angular acceleration from Simulations 4 to 6 from Set 3.	174
4.15	3 rd order swing angle response of the pendulums from Simulations 4 to 6 from Set 3.	175
4.16	6 th order swing angle response of the pendulums from Simulations 4 to 6 from Set 3.	175
A.1	Powerflow diagram of ZF 16AS 2631 TO Gearbox	192
A.2	Example of system to be simplified (System A).	193
A.3	Simplification of torsional system (System B).	193
B.1	Free body diagrams for disk and pendulum.	207
B.2	Representation of a general path pendulum.	222
B.3	Free body diagrams for disk with general path CPVA.	224

List of Tables

1.1	Firing frequency according to number of cylinders of a four stroke engine. . .	3
2.1	Estimated stiffness and correlation coefficient for each shaft.	30
2.2	Torsional characteristics of clutch disks used on recognition measurements. .	32
3.1	Stability results from general and extended Floquet theory for homogeneous and inhomogeneous systems.	85
3.2	First coefficients of $f_a(\theta_a)$	105
4.1	Values of $\min(\mu_{\max})$ for usual values of n_t	157
4.2	Summarized information about the simulations.	168
4.3	Design and physical parameters for simulations 1 to 3 from Set 3.	176
4.4	Design and physical parameters for simulations 4 to 6 from Set 3.	176
4.5	Recalculated design and physical parameters for simulations 1 to 3 from Set 3.	178
4.6	Recalculated design and physical parameters for simulations 4 to 6 from Set 3.	178
B.1	Some values of $p_1(v)$	227

List of Abbreviations and Acronyms

The items in this list are sorted in order of appearance. If a symbol is not mentioned on the section referring to a given chapter, it means that the previous definition of such symbol is still valid.

Chapter 1

Ω - Engine speed

Chapter 2

\mathbf{M} - A given mass matrix

\mathbf{K} - A given stiffness matrix

\mathbf{x} - Vector of physical coordinates

$\mathbf{f}(t)$ - Vector of efforts or physical excitation

Φ - Modal matrix

ω_i - Diagonal matrix containing the eigenfrequencies of the system

\mathbf{q} - Vector of generalized coordinates

ζ_i - Diagonal matrix containing modal damping ratios.

\mathbf{C} - A given damping matrix

Chapter 3

Section 3.1

m_a - Mass of the absorber

k_a - Stiffness of the absorber

m_t - Mass of the main structure

k_t - Stiffness of the main structure

$F(\omega, t)$ - Excitation

t - Time

ω - Frequency of excitation

x_a - Absolute displacement of the absorber mass

x_t - Absolute displacement of the mass of the main structure
 ω_a - Eigenfrequency of the absorber when isolated from the main structure
 ω_t - Eigenfrequency of the main structure when isolated from the absorber
 μ - Mass ratio
 β - Eigenfrequency ratio
 τ - Dimensionless time
 r - Normalized frequency of excitation or frequency ratio
 $s_{1,2}$ - Eigenvalues of the system
 $r_{1,2}$ - Eigenfrequencies of the system

Section 3.2

$m_a^{(p)}$ - Mass of the p -th absorber
 $k_a^{(p)}$ - Stiffness of the p -th absorber
 $x_a^{(p)}$ - Absolute displacement of the p -th absorber
 n - Number of absorbers

Section 3.3

θ_t - Absolute angular displacement of the disk
 θ_a - Swing angle of the pendulum, relative to the disk
 ϵ_a - Distance between the center of mass of the pendulum and its pinning point
 R_p - Distance between the geometrical center of the disk and the pinning point of the pendulum
 I_t - Polar moment of inertia of the disk
 I_a - Polar moment of inertia of the pendulum bob
 m_a - Mass of the pendulum bob
 g - Acceleration of gravity
 Ω - Rotating speed of the carrier disk
 δ - Reference angle
 ω_a - Eigenfrequency of the pendulum when the disk spins at constant angular speed
 v - Eigen-order of the pendulum when the disk spins at constant speed
 r_{ga} - Radius of gyration of the pendulum bob
 τ - Dimensionless time
 κ - Stiffness coefficient of Mathieu equation
 η - Coefficient of the time varying part of Mathieu equation
 $y(\tau)$ - Unknown variable from Hill's equation

- $f(\tau)$ - Time varying coefficient of Hill's equation
- $\varphi(t)$ - Periodic part of the solution from Floquet theory
 - α - Floquet exponent
 - a_i - Coefficients of the Fourier series
 - b_i - Coefficients of the Fourier series
 - σ_i - i -th Floquet multiplier
- K_t - Torsional stiffness of the two-degrees-of-freedom system
- $\tilde{\theta}_t$ - Oscillation of the disk around $\Omega t + \delta$
 - a - Dimensionless increase on the inertia of the disk due to the presence of the pendulum
 - b - Dimensionless increase on the inertia of the pendulum due to its pinning
 - μ - Ratio between the final inertia of the pendulum and the final inertia of the disk
 - p - Ratio between ϵ_a and R_p
- ω_t - Eigenfrequency of the system without pendulums
 - β - Ratio between the eigenfrequency of the pendulum when the disk spins at constant angular speed and the eigenfrequency of the system without pendulums.
- $f(\tau)$ - A given function
 - $s_{1,2}$ - Eigenvalues of the two-degrees-of-freedom system in dimensionless time
 - q - Stability coefficient of the system
 - $\chi_{1,2}$ - Eigen-orders of the 2DOF system
 - $\omega_{1,2}$ - Eigenfrequencies of the 2DOF system
 - $\tilde{\Theta}_t$ - Modal amplitude of oscillation of the disk
 - Θ_a - Modal amplitude of the pendulum bob
 - $\Gamma_{1,2}$ - Modal ratios of the 2DOF system
- $T(n\Omega, t)$ - Excitation torque in physical time domain
- $T(n, \tau)$ - Excitation torque in dimensionless time domain
 - n - Order of excitation
 - g_ϵ - Dimensionless gravity
- $r_a(\theta_a)$ - Radius of the path performed by the center of mass of the pendulum bob
 - $\bar{\alpha}_i$ - Coefficients of $r_a(\theta_a)$
 - ρ_i - Radius of curvature of the path in the work of Denman (1992)
 - ρ_{i0} - Radius of curvature at the vertex of the path in the work of Denman (1992)
 - S_i - Arc-length performed by the center of mass of the pendulum bob in the work of Denman (1992)
 - λ - Path parameter in the work of Denman (1992)
 - \tilde{n}_i - Order of the epicycloidal path in the work of Denman (1992)
- $f_a(\theta_a)$ - Shape function of the pendulum path

- α_k - Coefficients of $f_a(\theta_a)$
- $\tilde{\theta}_a$ - Oscillation of θ_a about ι
- ι - Equilibrium position of the pendulum bob when the disk accelerates
- θ_r - Rolling angle used on the description of the cycloid and epicycloid curves
- $(x_p(\theta_r), y_p(\theta_r))$ - A point on a cycloid or an epicycloid
- $g(\theta_r(\theta_a))$ - Function which eases the differentiation process
- $f_a^{(i)}(\theta_a)$ - Function $f_a(\theta_a)$ truncated at the i -th term
- $E_{2k}(p)$ - Polynomials on p for the calculation of the shape function of the epicycloid
- z_i - Unknown variables for the application of the method KB-Averaging
- $a(\tau)$ - Slowly varying function of τ
- $\beta(\tau)$ - Slowly varying function of τ
- u - Variable in Duffing's equation
- ϵ - A small parameter
- $u_i(t)$ - Expansion terms of u
- T_i - i -th time scale ($e^i t$)
- $\varphi(t)$ - Phase of the solution
- v_c - Detuning term due to the shape of the path
- θ_{ai} - i -th term of the expansion of θ_a
- $\tilde{\theta}_{ti}$ - i -th term of the expansion of θ_t
- $\Theta_{arg}^{(s)}$ - Amplitude of the term $\sin(arg)$
- $\Theta_{arg}^{(c)}$ - Amplitude of the term $\cos(arg)$
- g_c - Detuning term due to the presence of gravity
- G - Normalized amplitude of the oscillating torque
- G_0 - Dimensionless version of G
- θ_i - array of variables
- \mathbf{M}_ϕ - Dimensionless mass matrix of 2DOF system
- \mathbf{K}_ϕ - Dimensionless stiffness matrix of 2DOF system
- ∂_i^n - n -th derivative with respect to the time scale T_i
- ψ_i - i -th eigenvector
- Δ - Characteristic polynomial of the dimensionless 2DOF system
- Λ - Receptance matrix of the dimensionless 2DOF system
- A_i - Amplitude calculated from initial conditions
- β_i - Phase calculated from initial conditions
- ω - Order that is close to an eigen-order
- σ - Proximity of ω to an eigen-order
- $\theta_{sec}^{(i)}$ - Terms that would generate secular terms on the solution of the i -th equation

γ_1 - Auxiliary variable

Chapter 4

n_t - Target order

B_w - Order bandwidth of the pendulum

δ - Order placement parameter

q_{\max} - Maximum allowable value for q

μ_{\max} - Maximum allowable value for μ

ϱ - Manufacturing error

ϱ_{\max} - Maximum allowable manufacturing error

$|\theta_a|_{\text{lin}}$ - Linear estimation of the maximum amplitude of θ_a

CONTENTS

1	INTRODUCTION	1
1.1	Vehicle Powertrains and NVH	2
1.2	An introduction to Centrifugal Pendulum Vibration Absorbers	12
1.3	Motivations	18
1.4	Objectives	18
1.5	Outline of the Work	19
2	The Powertrain: Recognition and Modeling	21
2.1	Part I: Vehicle Data and Technical Specifications	22
2.2	Part II: Experimental Estimation of Torsional Stiffness of Axles	24
2.3	Part III: Drive Rattle Measurements	31
2.3.1	Analysis of the Torsional Behavior at 7 th Gear	34
2.3.2	Analysis of the Torsional Behavior at 8 th Gear	40
2.3.3	Analysis of the Torsional Behavior at 9 th Gear	43
2.3.4	Analysis of the Torsional Behavior at 10 th to 14 th Gears	47
2.4	Part IV: Mathematical Modeling and Model Validation	50
2.4.1	Development of Linear Conservative Model of the Powertrain	58
2.4.2	Calculation of Equivalent Damping for the Linear Model of the Powertrain	60
3	Theoretical Aspects of Passive Vibration Absorbers	69
3.1	Review on Tuned Mass Dampers	69
3.2	Dynamics of a system with multiple tuned mass dampers	74
3.3	Centrifugal Pendulum Vibration Absorber: a thorough analysis	76
3.3.1	Single torsional disk with a Circular Path CPVA	77
3.3.1.1	Linear analysis at constant angular speed and zero gravity	78
3.3.1.2	Linear analysis at constant angular speed considering gravitational terms	79
3.3.2	Elastic two-disk system with a Circular Path CPVA	86
3.3.2.1	Linear analysis with zero gravity and small oscillations on the carrier disk's angular speed	87

3.3.2.2	Linear analysis considering gravity and small oscillations on the carrier disk's angular speed	93
3.3.3	Systems with General Path CPVA	96
3.3.3.1	Shape function for the cycloidal path	102
3.3.3.2	Shape function for the epicycloidal path	107
3.3.3.3	Multiple Scales Method	110
3.3.3.4	Nonlinear analysis at constant angular speed and zero gravity	117
3.3.3.5	Nonlinear analysis at constant angular speed considering gravitational terms	121
3.3.3.6	Nonlinear analysis with zero gravity and small oscillations on the carrier disk's angular speed	127
4	Application of the CPVA on the Clutch Disk of the Powertrain	151
4.1	Design Techniques for CPVAs	151
4.1.1	Resonance Tuning vs. Inertia Tuning	152
4.1.2	Design Technique 1: Design for Tuning	159
4.1.3	Design Technique 2: Design for Geometry	160
4.2	Simulations	161
4.2.1	Layout of The Clutch Disk with a CPVA and Project Limitations . .	162
4.2.2	Simulation Planning	167
4.2.3	Simulation Results	168
5	Conclusion	179
5.1	Discussion and Conclusions	179
5.2	Contributions	182
5.3	Future Research	185
	References	187
	Appendix A Auxiliary information from the powertrain	191
A.1	Powerflow Diagram of the ZF 16AS 2631 TO Gearbox	191
A.2	Energy Equivalence Approach for powertrain modeling	191
A.3	Generalized method to impose motion of known degrees of freedom on linear time invariant systems	197
	Appendix B Auxiliary results for the Review on Tuned Mass Dampers	199
B.1	Proof: Radicand real and nonnegative	199
B.2	Proof: Square of dimensionless eigenfrequency is always real and positive . .	200

B.3	Proof: Smallest dimensionless eigenfrequency is less than or equal to β . . .	200
B.4	Proof: Greatest dimensionless eigenfrequency is greater than or equal to β . .	201
B.5	Proof: Asymptotic behavior of gap between dimensionless eigenfrequencies as a function of β	202
B.6	Proof: Asymptotic behavior of gap between dimensionless eigenfrequencies as a function of μ	204
B.7	Proof: Normalized FRF for a 1-DOF system with multiple similar TMDs . .	205
B.8	Derivation: Equations of motion for a single torsional disk with a CPVA . .	207
B.9	A brief introduction to the Floquet theory applied to one-degree-of-freedom systems	209
B.10	Introduction to the general Floquet theory	211
B.11	Introduction to the extended Floquet theory	213
B.12	Proof: s_i^2 from Eq. (3.33) is negative	216
B.13	Proof: Asymptotic behavior of eigen-order χ_1	217
B.14	Proof: Asymptotic behavior of eigen-order χ_2	219
B.15	Proof: Maximum value of eigen-order χ_1	220
B.16	Proof: Minimum value of eigen-order χ_2	221
B.17	Derivation: Equations of motion for a single torsional disk with a General Path CPVA	222
B.18	List of derivatives of the radius of the general path in terms of the function $g(\theta_r)$	225
B.19	List of functions from $E_0(p)$ to $E_8(p)$ for the epicycloid	226
B.20	Table of values of $p_1(v)$ for given values of v	226

1 INTRODUCTION

The development of a vehicle powertrain is a multidisciplinary task, and has to take into consideration some key (and not independent) requirements, such as performance, efficiency, durability, comfort, cost, safety and laws. The current trend on the development of new vehicles is, besides reducing costs, to find innovative solutions to obey the ever tightening emission laws, which define global standards.

In Brazil the laws demand the production of trucks and buses, which are diesel fueled, to follow the *European Emission Standards* (EURO V up to 2015 and probably EURO VI from 2016 on). Additionally, there is the governmental program *Inovar Auto*, which grants up to 30% of deduction on the national tax on manufactured products (IPI) for vehicle manufacturers that join the program. Those who have joined the program but were not able to achieve the program's milestones are subjected to severe financial penalties.

In order to meet these requirements, the solution found by manufacturers is to reduce vehicle weight as much as possible, and to produce smaller but more powerful and efficient engines. This trend is often referred to as *downsizing*, and has led to several consequences on the design of the powertrain.

One of the main consequences in which this work is focused on, is comfort. Lighter and more powerful engines tend to be important sources of torsional and translational vibration. Also, lighter structures are more prone to vibrate and less favorable to sound insulation. These factors worsen the physical and acoustic comfort which are decisive on the consumer's choice.

In order to present the motivations and objectives of this work in a clear and understandable way, it is necessary to present some technical aspects on powertrains and on Centrifugal Pendulum Vibration Absorbers (CPVAs), which are done in the next two sections. After that, the motivations, objectives and the outline of the work are presented.

1.1 Vehicle Powertrains and NVH

The acronym NVH on the title of this section stands for *Noise, Vibration and Harshness*, and refers to the research area which studies noise and vibration mitigation on ground vehicles, more often cars, trucks and buses. There are many NVH phenomena to be studied, which regard many types of noise, from squeaking between polymeric parts of the vehicle interior up to noise and vibration caused by engine, gearbox, joints, friction induced instabilities and even more complex subjects.

In the scope of this work, among all the NVH phenomena, the phenomenon of interest is a powertrain generated noise, resulting from the interaction of the powertrain itself and the torsional vibration provided by the vehicle. The powertrain parts and the NVH phenomena generated by their interaction are presented below, with sufficient details for this work. However, further reading is suggested for the readers who seek for deep understanding of these phenomena.

Among all the types of engines, the by far most usual type in Brazilian market are the *internal combustion* (IC) engines. There are many types of IC engines, but the one being studied in this work is the *four stroke* engine, which also represents the greatest majority of the national fleet.

The term “four stroke” stands for the working principle of each cylinder, which is divided in four stages: intake, compression, combustion and exhaust. On a gasoline fueled engine, the intake stage is defined by the opening of the intake valves and the descent of the piston allowing the air-fuel mixture in. On the second stage, this mixture is compressed by the rise of the piston. After that, when the piston begins its second descent, the engine plugs produce an electric spark that gives start to the combustion, raising the pressure in the combustion chamber and pushing the piston all the way down. Finally, on the exhaust stage, the exhaust valves are opened and the piston rises once more, pushing the burnt mass out.

Diesel fueled engines are also four stroke engines. The difference between them and gasoline fueled engines is that on the first two stages, only air is injected on the combustion chamber and compressed. Also, the compression rate is usually much higher than on gasoline engines. The combustion stage is started by the spraying of diesel directly on the combustion

chamber at high pressure, with no need of sparks (and hence plugs). The combustion starts through the contact between diesel and high pressure atmospheric air. The exhaust stage is similar to the gasoline engine case.

Because of this working principle, on engines with an even number of cylinders the pistons work in pairs, so that when one of them is on the intake stage, the other is on the combustion stage, i.e. each pair of cylinders produce one combustion per revolution of the engine. Three cylinder engines work with different phases between the cylinders, producing three combustion every two revolutions.

Once the combustion stage is the one that propels the piston, and therefore the crankshaft, the torque produced by the engine is composed basically by a number of pulses per revolution that is related to the number of cylinders of the engine, which originates the concept of *firing frequency*. The firing frequency of an engine is the number of pulses of torque the engine produces per revolution multiplied by the rotating speed of the crankshaft. Considering that the rotating speed of the engine is Ω , the most usual values of firing frequencies related to the number of cylinders of a four stroke engine is shown in Table 1.1.

Table 1.1: Firing frequency according to number of cylinders of a four stroke engine.

Number of Cylinders	1	2	3	4	5	6	8
Firing Frequency ($\times\Omega$)	0,5	1	1,5	2	2,5	3	4

The torque pulses produced by the engine are sharp and their sharpness has increased in order to increase efficiency and improve combustion. Therefore, torque produced by an engine with a given firing frequency, or firing orders (in the angle domain), has a spectrum that contains not only the fundamental frequency, but also its multiples. Increased sharpness of the pulses increases the amplitude of the multiples of the firing frequency, and modern engines may present fundamental and second harmonic components of the engine torque with equivalent amplitudes.

Therefore, it is known that the torque produced by the engine is oscillatory and the main components on the spectrum of this torque are the ones at the first and second harmonics of the firing frequency. This torque has to be distributed to the other parts of the powertrain up to the wheels, allowing the vehicle to move. Although there are many layouts of vehicle powertrains, some parts are common to almost all of them and are mentioned briefly.

Linked to the flywheel of the engine there is usually a part that allows the powertrain to be connected to or disconnected from the engine, which can be a clutch set or a torque converter. This part usually transmits torque to a transmission that provides different gear ratios suitable for different operating regimes. Transmissions are discussed in detail further on the text. Depending on the layout of the powertrain, a differential gear can be directly connected to the output of the transmission or through a propeller shaft. There may also be more than one differential gear. This part allows the transmission of torque for multiple driving wheels allowing their rotating speeds to be different, and hence enabling the vehicle to perform turning maneuvers.

The transmission or gearbox is an important part of the powertrain, for providing different gear ratios. It allows the driver to choose between high torque and low speeds or lower torque and higher speeds, whichever suits best the driving conditions. The five most common types of transmission are the manual, the automatic, the semi-automatic, the CVT (continuously variable transmission) and the DCT (dual clutch transmission). Each one of them have advantages and drawbacks to be discussed.

The most usual transmissions on North-American passenger cars are the automatic and the CVT. The market share of vehicles with this type of transmission is rapidly increasing among the luxurious vehicles in Brazil. These transmissions provide the driver with a very good driving experience, once they are not required to actuate clutch pedals or shift gears, and do not need to be concerned about engine stall. However, these gearboxes have a limited torque capability, making them unsuitable for heavy duty applications or above.

Manual, semi automatic and dual clutch transmissions have unlimited torque capacity and increased efficiency¹. The advantage of the latter two types over the manual transmission is that the user is not required to actuate the clutch pedal. Additionally, the semi automatic transmission is a manual transmission with a mechatronic unit that controls two hydraulic or pneumatic actuators, one for the clutch and the other for the selector forks.

These transmissions are composed by many gear pairs that are constantly meshed, but one of the gears is not necessarily connected to its shaft, i.e. it may be free to spin. When both gears of the gear pair are connected to their respective shafts, this gear is transmitting torque, and hence it is called *loaded gear pair*. If one of the gears is not connected to its

¹Fuel consumption is usually lower on vehicles with CVTs because these transmissions allow the engine to operate on its most efficient range. However, in terms of energy dissipation, CVTs are less efficient than manual, semi automatic or dual clutch transmissions.

shaft, then this gear pair does not transmit torque and is called *unloaded gear pair*.

All the gear meshes in the transmission have clearances that allow the gear teeth to perfectly mesh. This is not a problem for the loaded gear pairs, because even in the presence of vibration, the gear teeth remain in contact in most operating regimes. However, once the inertia of the unloaded gear pairs is low, if the shafts of the gearbox start to vibrate torsionally with relevant intensity, then it may cause the teeth of the unloaded gear pairs to collide against each other producing an undesirable noise, called *gear rattle*, to be discussed in detail further in this text.

From this point on, once the vehicle under investigation in this work is equipped with a semi automatic gearbox, the scope of the discussion is limited to applications of this type. On vehicles with semi automatic or manual gearbox, the transmission of torque from the engine to the gearbox is done through a clutch set, which is composed of a clutch cover and a clutch disk.

The clutch cover is composed by a housing of metal that supports a Belleville spring and a pressure plate. The Belleville spring presses the pressure plate against the friction facings of the clutch disk, which is in contact with the flywheel. The friction between these parts allow the transmission of torque. The clutch cover must be modeled in detail if coupling phenomena are to be studied. On the operating regime studied in this work, however, the clutch set must be fully coupled, and hence this part must not be detailed.

The clutch disk is a more complex part, which plays an important role on the dynamics of the powertrain, and hence it must be explained in detail. An example of a clutch disk is shown in Fig. 1.1.

The dark gray part on the outer portion of the disk is called friction facing. This facing is made of a composite material and is applied on both sides of the disk. It touches the pressure plate, on the transmission side and the flywheel on the flywheel side. The light gray portion in the middle of the disk is called torsional damping pack². It has an inner flange that is connected to the friction facings and is free to move inside the pack. The springs, visible in Fig. 1.1 are fitted into windows that exist on the flange and also on the outer metal plate, so that when the friction facing moves in any direction, the springs are compressed and

²The terms *damping* and *damper*, on the names of the clutch disk parts are due to manufacturer's choice. These parts help to attenuate some vibration problems, but are composed by stiffness and a small amount of friction. There is no actual damper in a clutch disk.



Figure 1.1: A clutch disk.

push the outer plate on the same direction. This outer plate is connected to the clutch hub through another part called “pre-damper”, which works only for small amplitudes of torque.

The first important aspect of the clutch disk is that it allows a relative angular motion between the friction facing and the clutch hub, and provides controllable torsional stiffness. Once relative motion is possible between the two ends of the clutch disk, in addition to the stiffness, the clutch disk also has a controllable amount of inner friction, which allows it to dissipate energy. Therefore, the clutch disk has two friction mechanisms, being one of them on the outer portion to provide transmission of torque, and another one inside the torsional damping pack, which allows the disk to dissipate energy.

Technically, considering that the clutch set is fully coupled, the clutch disk provides torsional stiffness and damping between the engine flywheel and the input shaft of the gearbox. The torsional damping pack is usually divided in two parts, namely the “main damper” and the “pre-damper”. These parts provide different stages of friction and stiffness according to the relative angular displacement between the flywheel and the gearbox input shaft, as shown in Fig. 1.2.

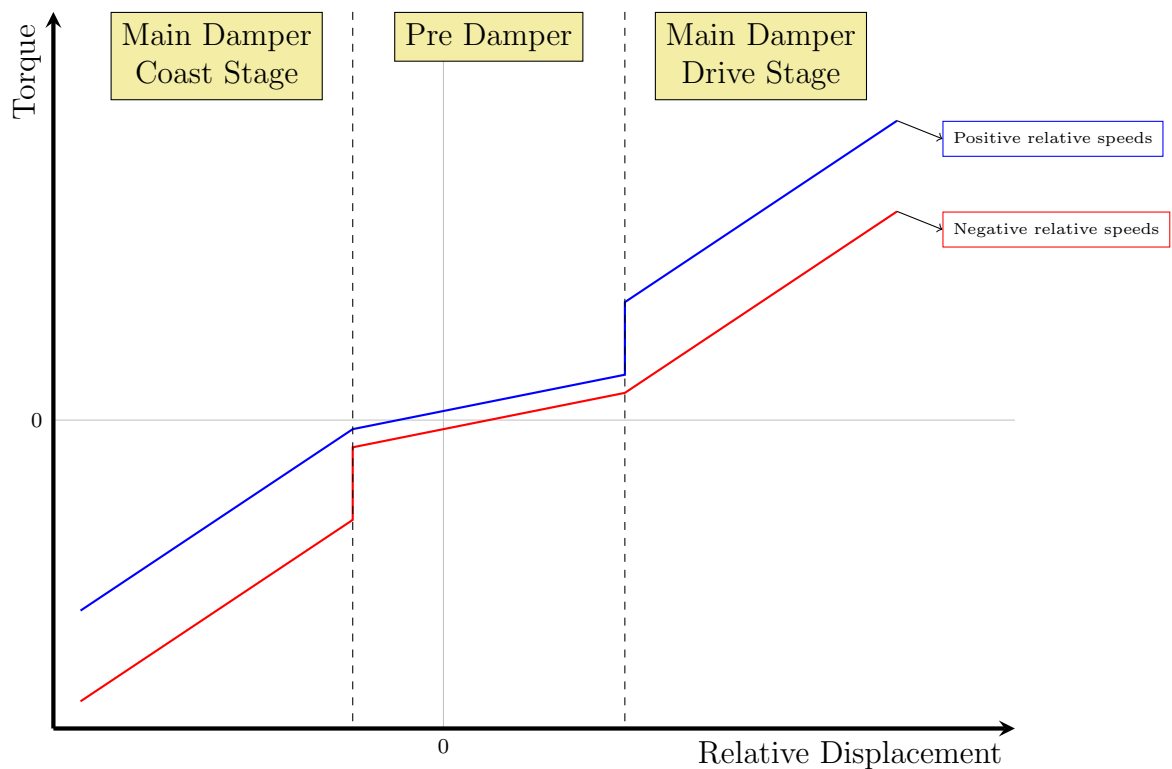


Figure 1.2: Torsional characteristics of a clutch disk.

The torque provided by the engine can be thought of as the sum of a very slow varying part, known as the mean torque, and a fast varying part, called torque fluctuation. High levels of the mean torque occur when the driver presses the throttle pedal requiring the vehicle to accelerate. This creates a considerable positive relative displacement on the clutch disk, so that it operates only at the Drive stage of the main damper, the right-hand part of the graphic shown in Fig. 1.2. The torque oscillation makes the point of operation to oscillate about a given position on this stage.

Negative relative displacements occur on engine braking maneuvers. In this case the engine decelerates the vehicle, and hence the disk operates on the Coast stage of the main damper, the left-hand part of the graphic in Fig. 1.2.

The pre-damper, the center part of Fig. 1.2 operates when the mean torque of the engine is so low that it is not capable of causing the disk to operate at drive condition. If the clutch is engaged and the neutral gear is selected, then the vehicle is at idle condition, and the low stiffness of the pre-damper reduces the transmission of torque fluctuation to the gearbox, avoiding gear rattle. If a low gear is selected, then the vehicle moves very slowly,

and the pre-damper has to be designed so that in this condition the rolling resistance of the vehicle does not induce the disk to operate on the Drive stage of the main damper, avoiding gear rattle.

Therefore, on vehicles equipped with dry clutches, the torsional characteristics of the clutch disk play a very important role on the mitigation of vibration and noise originated at the powertrain. For this reason, a brief description of the most important NVH phenomena related to this type of powertrain is presented. It is important to notice that, sometimes the NVH phenomenon and the condition at which it occurs are confusing. Hence, only the NVH phenomena are presented first, and the operating regimes are presented next.

The NVH phenomena related to vehicles with dry clutches can be classified into three categories: phenomena that occur before coupling, during coupling and after coupling. The ones that occur before coupling are the *roar noise* and *unwanted torque transmission*.

The roar noise is caused by vibration of the pressure plate at high engine speeds when the clutch is decoupled. This condition is certainly not a usual operating condition, but this problem can be solved by the installation of soft springs to control the motion of the pressure plate. The unwanted torque transmission occurs when the flywheel vibrates with large amplitudes and touches the friction facing of the clutch disk, even when the clutch set is fully decoupled. This torque transmission makes synchronizers ineffective, and worsens shiftability of some gears. In order to minimize this problem, modifications must be performed on the crankshaft.

During coupling, there are two important and very interesting phenomena to be mentioned: *judder* and *clutch squeal*.

The judder occurs at drive-off conditions, and is mainly caused by irregularities on the contact surface between the clutch disk and the flywheel, and also by friction induced instability caused by the negative slope of the curve of the coefficient of friction along the relative speed between the contact surfaces. It is characterized by low to mid frequency longitudinal vibrations of the vehicle during the coupling of the clutch set, and it is purely torsional. A very detailed study and description of this problem is found on the work of Perestrelo (2013).

The clutch squeal is characterized by a high frequency noise that occurs during coupling.

It is generated because of other type of friction induced instability, the *sprag-slip*, therefore not purely torsional, and is usually very difficult to attenuate. A deep and very complete work on this problem was done by Miyasato (2015).

The NVH phenomena that occur after coupling are the ones which can be affected by the torsional characteristics of the clutch disk. They are the *gear rattle*, the *shuffle* and the *clunk*.

Shuffle and clunk are two different phenomena which occur at the same driving conditions and can be explained together. Shuffle is characterized by low frequency longitudinal oscillations of the vehicle, typically between 2 and 8 Hz, and is caused by sudden load reversals on the vehicle, i.e. conditions at which the driver requires maximum torque of the engine through pressing the throttle pedal up to its limit, or conditions at which the driver releases the throttle pedal quickly and the mean torque generated by the engine substantially drops.

If the shuffle oscillations are too severe, the loaded gear pairs may lose contact and strongly collide against each other, causing an undesirable clunking noise, which is the clunk phenomenon. Both of these phenomena can be attenuated through engine calibration, and a detailed investigation on these phenomena made by the author of this work is found on Simionatto (2011).

The last phenomenon to be mentioned that occurs with the clutch set fully coupled is the gear rattle. It is generated by excessive torsional vibration in the gearbox, causing the teeth on the unloaded gear pairs to collide against each other, producing noise. The high amplitude vibration in the gearbox is typically caused by system amplification. In other words, the oscillating torque of the engine excites some critical frequencies at which the amplitude of vibration, mainly on the gearbox, is amplified. Linear models represent it as an eigenfrequency.

A detailed study on how to model the nonlinear part of the system is found in the work of Miyasato (2011), and a complete analysis on the ways to attenuate this amplification through the inner friction of the clutch disk is found on the work of Lemes (2015 *planned*).

There are several operating conditions to be tested regarding the performance of the torsional characteristics of the clutch disk on attenuating gear rattle, shuffle and clunk. These conditions are sought to simulate the possible use scenarios of the vehicle. The most relevant

conditions are listed below:

- **Idle:** This condition requires the vehicle to be stopped, the engine to be running at idle speed, the neutral gear to be selected and the clutch set to be engaged. The purpose of this test is to evaluate the performance of the pre-damper and to evaluate possible gear rattle noise generated at idle condition, usually referred to as *idle rattle*.
- **Start/Stop:** This condition requires the vehicle to be stopped, the clutch set to be fully engaged and the neutral gear to be selected. The engine is turned on and off repeatedly, in order to evaluate the performance of the pre-damper at attenuating possible gear rattle for engine speeds below the idle speed.
- **Clap:** This condition requires the vehicle to be stopped, the engine to be running at idle speed and the neutral gear to be selected. The clutch set is engaged and disengaged rapidly in order to verify if the pre-damper parameters are able to avoid the clutch disk to reach the main damper. In case it occurs, loud gear rattle is expected.
- **Creeping:** In this condition the engine must be running at idle speed, the clutch set must be fully engaged and a low gear must be selected. The purpose of this test is to verify if in this condition the rolling resistance of the vehicle is able to force the clutch disk to reach the Drive stage. In case it occurs, intermittent rattling noise is expected.
- **Drive:** This test is usually performed at all gears, except for the first ones. The vehicle must be fully loaded and is driven at wide open throttle condition. Engine speed is varied from idle speed to the maximum engine speed, and the performance of the drive stage of the main damper at attenuating gear rattle at all rotating speeds is evaluated. This is usually referred to as *drive rattle*.
- **Coast:** The conditions are exactly the same for the Drive test, but in this case the engine speed starts at the maximum value and an engine braking maneuver is performed.
- **Tip-in/Tip-out:** This condition requires the clutch set to be engaged and a low gear to be selected. The driver is required to press the throttle pedal for one or two seconds and then to release it rapidly. They must do it repeatedly until the maximum speed of the engine is reached. The purpose of this test is to evaluate possible shuffle and clunk, but gear rattle is also found in this procedure.

One must notice that the gear rattle shows up in all the tests performed with the clutch set fully coupled, and hence the attenuation of this phenomenon is of utmost importance for vehicle manufacturers, especially for companies that produce clutch disks.

One of the most usual ways to attenuate gear rattle is to add torsional friction to the clutch disk. It is usually possible to set two levels of friction, one for the pre-damper and other for the main damper. Once rattle is caused by a system amplification, an increase of torsional friction makes the system dissipate energy when vibrating, which helps to control the amplitude of the main amplification and hence the gear rattle noise. This works well for the drive condition, but for the coast condition, usually less friction lead to less rattle noise.

Regarding the pre-damper, low amount of friction helps to reduce rattle at idle condition, because in this case the transmissibility of displacement must be minimal, and the main resonance is below the idle speed. This resonance may be excited when turning the engine on or off, and if no friction is present, high amplitudes may occur, leading to loud rattle noise when turning the vehicle on or off.

Another drawback of this solution is that it is effective for limited amplitudes and frequencies. The damping effect caused by friction may degenerate for higher amplitudes and higher frequencies, leading to still undesirable rattle noise.

In cases at which friction is not capable of controlling rattle, a dual mass flywheel can be used. It is basically composed of two large inertias linked through a usually soft and long travel spring. This device shifts the eigenfrequencies of the system so that the frequency related to the amplification that originally caused gear rattle becomes out of the operating range of speeds. In some cases, eigenfrequencies that were originally unreachable may lie on the operating range, and these cases must be carefully treated. However, the main drawback of this solution is that it is extremely expensive in comparison to the usual single mass flywheel, and hence it is typically avoided by manufacturers.

A third way which is still not usual to deal with gear rattle is the use of centrifugal pendulums vibrations absorbers. These absorbers are analogous to the well known tuned mass dampers, with the difference that their tuning frequency is proportional to the rotating speed of the system, i.e. it is possible to tune it to absorb a given order of vibration. This feature makes it especially suitable for vehicle applications, because the torsional vibrations are caused by orders of vibration generated at the engine.

In some applications, these absorbers, also referred to as CPVAs, are applied to the dual mass flywheel. On more recent applications, like on the patent by Rusch *et al.* (2014), it has been applied to clutch disks, but this usage is still rare. However, if the parameters of such pendulum are set correctly, gear rattle must vanish for all driving conditions, what makes of this pendulum a promising solution, and therefore the object of study of this work.

For this reason the next section is devoted to the presentation of the basic working principle of the CPVA, some historical features and the most usual layouts for its application.

1.2 An introduction to Centrifugal Pendulum Vibration Absorbers

Although CPVAs are currently the object of many researches, too few of its history is documented and available. All the historic facts presented in this section are found in the laborious and complete work of Wilson (1969).

The history of centrifugal pendulum vibration absorbers dates back to 1911, when Kutzbach proposed a damper which was a carrier disk with fluid in U-shaped channels. This design can be found in the sketch A of Fig. 1.3. Eighteen years later, Duesenberg proposed a system composed of metal capsules partly filled with heavy fluid attached to a rotating body. These designs have not attracted much contemporary interest because the dynamics of such systems had not been investigated and there was no urgent need for these devices at that time.

In 1930, Meissner published the first complete discussion on such devices. His findings had been obtained through experiments with water columns in U-tubes. His results were able to show the effectiveness of this solution and started a trend to find practical forms of CPVAs, which lasted between 1930 and 1940. This trend led to the designs B to F, found in Fig. 1.3.

The simplest form of implementing a CPVA is the roll-form, found on sketch B of Fig. 1.3. The great obstacle for its implementation is to predict whether the roll slides or rolls on the contact surface, which may generate considerable amount of detuning. Experience with this device has shown that if swing angles are kept lower than $\pm 15^\circ$, then the roll only rolls on the contact surface. In 1938 Carter proposed a roll-form CPVA with gear teeth,

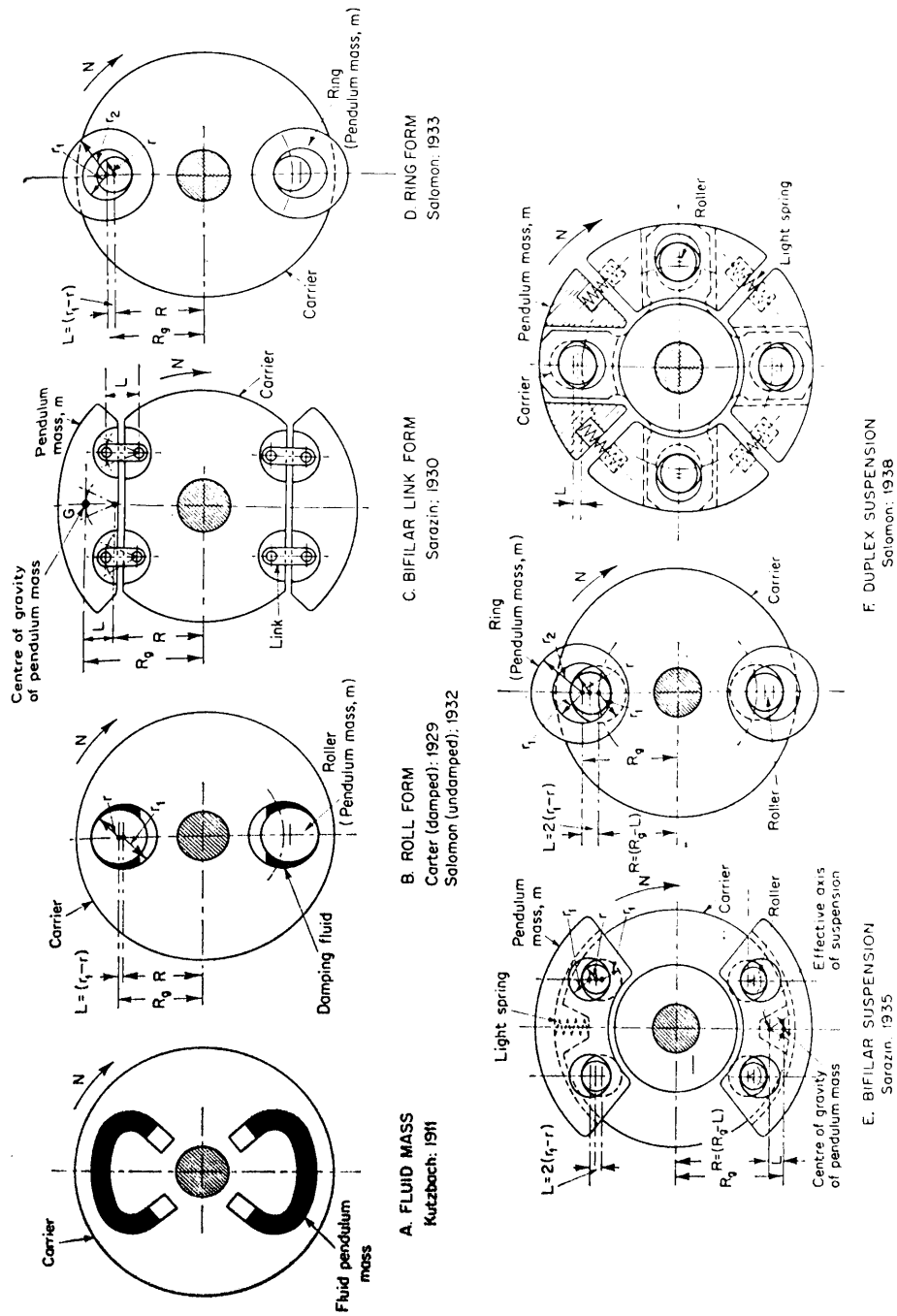


Figure 1.3: Several designs of CPVAs. Reproduced from Wilson (1969)

to avoid slipping. However, gear teeth only added mechanical complication to the project and increased the amount of damping on the pendulum, which worsens its performance substantially.

Regarding damping reduction, in 1932 F. M. M. B. Salomon proposed several designs in order to try to obtain less damping on the pendulum. He tried simple and composite assemblies, solid and hollow cylinders, metal spheres and fluids as pendulum masses and used epicycloidal paths to improve the stability on conditions where pendulum amplitudes became larger.

The design found on the sketch C of Fig. 1.3 is the bifilar link form, or parallel link form. This design was proposed by R. R. R. Sarazin in 1930, and its great advantage over the roll form is that the mass of the pendulum bob is not required to roll. Therefore, the rotational inertia of the pendulum mass does not affect its tuning. Also, it is usually possible to add more mass on this design than on roll forms. It also behaves better than the roll form for not being required to roll or slide, and hence the maximum permissible amplitudes are up to $\pm 25^\circ$.

The disadvantages of this specific layout are that for orders above the 2nd, the links may have to be so short that they become difficult to manufacture. Furthermore, the links have shown to present high amount of friction at high rotating speeds, worsening the performance of the pendulum.

On sketch D of Fig. 1.3, a ring form type of CPVA is represented. The disadvantages of this type of pendulum are exactly the same of the roll form type, with the drawback that the transition from rolling to slipping may cause even greater detuning. It has been proposed by Salomon in 1933.

The bifilar suspension type is found on sketch E of Fig. 1.3, and has several advantages compared to the previous designs. The surfaces of the tracks and the pin are hardened, what significantly reduces damping and wear. Also, the effective length of the pendulum bob is given by the difference between the radii of the bore and the pin, making it easy to provide much smaller effective lengths than using the bifilar link type. This allowed for the tuning of the pendulum for much higher orders.

The path of the pendulum bob for large amplitudes is not circular, and grants better

stability for large motions. Also, the light springs on the design are meant to hold the pendulum in position for low to stationary speeds and to prevent knocking at start/stop, but do not influence the behavior of the pendulum on its operating range. The patent on this design has been placed by Sarazin in 1935.

Finally, on sketch F the duplex suspension type is shown. The main difference from this design to the previous ones is that it has two degrees of freedom. However, only one of its vibration modes can be used, because the second one is related to high amplitudes, what is undesirable. This design has been applied successfully in some applications, though.

An important comment that must be made on the pendulum designs is that none of them comprises a simple usual pendulum. This is due to the fact that the length of the pendulum bob would often be too short to manufacture, and the pin which would hold the bob attached to the carrier disk would have to resist to extreme shear stress. However, it is very usual that problems on this area are formulated considering a simple pendulum attached to a rotating disk. The parameters of this pendulum can be translated into the parameters of any of the pendulums from the aforementioned layouts, and this eliminates the need for a specific modeling for each type of CPVA.

Apart from the technical details of each design, there are also interesting facts on the general history of centrifugal pendulums. One of the facts that motivated its usage was that, in 1936, in a meeting on the Institute of Aeronautical Sciences, a leading American aeronautical engineer expressed his opinion that, undoubtedly, the development of rotating pendulums was one of the most valuable contributions to aircraft engine design in years.

Because of this fact, the first large scale applications of CPVAs were to radial aero-engines. One of the first engines to be equipped with this technology was the Series G Wright Cyclone, a 9 cylinder four stroke engine rated with 1,000 bhp ³ at 2,200 rpm.

A pendulum tuned to the 4.5th order was used and the benefits were huge. It was possible to find reduction on vibratory stresses in the airscrew blades, and also on the occurrence of wear and tear of the power plant and of attached variable-pitch metal-bladed airscrew assembly. On later version of this engine, the Series G-100, rotating pendulums were installed at the front and rear crankwebs, allowing the engine rating to be increased to 1,200 bhp at

³The unity bhp refers to *brake horsepower*. It is the power of the engine itself regardless of the losses caused by gearboxes and other parts of the powertrain. The DIN standard and the SAE standard set rules for the measurement of bhp.

2,400 rpm with actual decrease on airscrew stress.

This stress is usually due to mixed torsional-bending modes, at which torsional vibration from the engine may induce the airscrew blades to flap. This is usually the case on helicopters, where centrifugal pendulums are used on modern applications, as shown in Fig. 1.4.

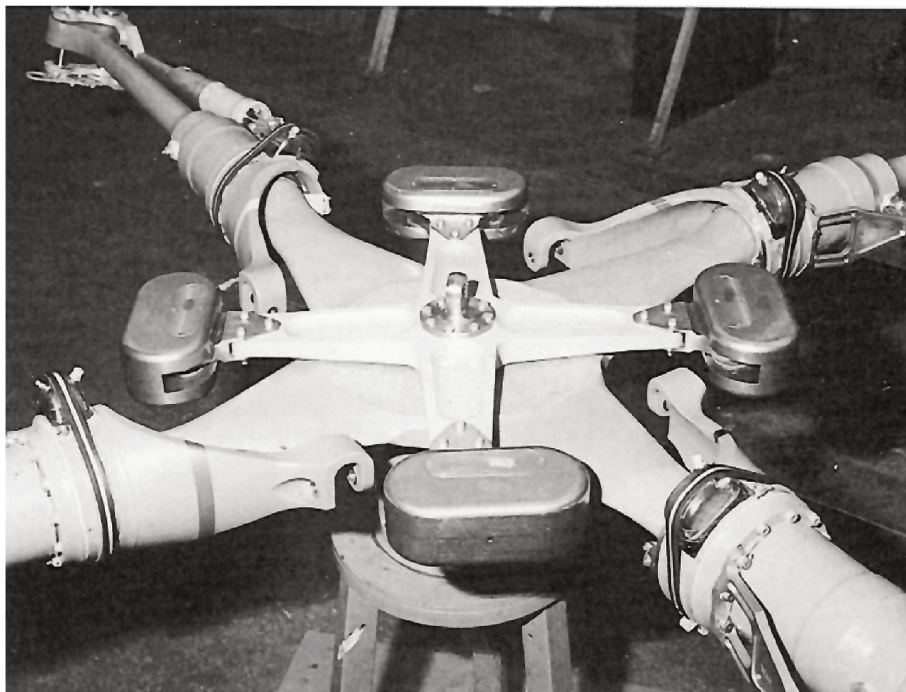


Figure 1.4: Bifilar absorbers attached to Lynx type helicopter rotor head. Reproduced from the work of Bramwell *et al.* (2001)

Great development work actually took place from 2 to 3 years before the 1939-1945 war (WWII). The applications were so successful that the crankweb counterweights of large quantities of British and American wartime radial aero-engines were designed to work as CPVAs. They were usually of bifilar or roll form.

Rotating pendulums have also been applied successfully on in-line engines, either replacing the crankweb counterweights or on a common carrier at a free end of a crankshaft. The first alternative has the advantage of adding little to no extra weight to the original engine, while the latter one leads to a more accessible device and it is easier to manufacture.

One of the first in-line engine manufacturers to develop CPVAs for high and medium compression engines was Sulzer Brothers. They were usually bifilar pendulums attached to a common carrier. One of their first engines to be equipped with this technology was a 6

cylinder four stroke in-line engine rated at 300 bhp. It presented peak amplitudes of $\pm 1.1^\circ$ at 630 rpm, excited by the 6th order, and $\pm 0.5^\circ$ at 420 rpm, excited by the 9th order. With the application of the CPVA, no resonances were found and the maximum amplitude of vibration was of $\pm 0.3^\circ$ for the entire range.

During the following 20 years, Sulzer used CPVAs on its engines, especially on railroad locomotives running at speeds up to 1,000 rpm. The smallest damper produced by this company had an external diameter of $17in$ ($0.4318m$) and total weight of $55lb$ ($24.978kg$). It had two bifilar pendulums and was installed on a free end of a crankshaft on a 6 cylinder four stroke in-line engine rated with 300 bhp at 1,200 rpm.

The largest one they produced had an external diameter of $39.5in$ ($1.0m$) and weighed $1950lb$ ($884.505kg$), representing 1% of the total mass of the engine. It was composed of four bifilar pendulums and was installed between the main crankshaft of a 7 cylinder two stroke in-line engine, rated with 2,500 bhp at 250 rpm, and the crankshaft of a reciprocating scavenge pump. This damper was able to eliminate a strong 7th order resonance.

None of the absorbers produced by Sulzer suffered any noticeable wear or needed replacement after tens of thousands of hours in service. Similar excellent results were obtained by other engine manufacturers, enforcing the belief that if the parameters of the pendulum were correctly set, the performance of this device was superior to that of contemporary devices for torsional vibration control.

The popularity of the CPVA began to decline during the latter part of the 1950s. It occurred due to the successful development of a viscous damper from 1946 on, using silicone fluid for energy dissipation, which was suitable for all engine sizes. This device was usually larger and heavier than a pendulum damper, but it was sealed and required low to zero attention during service life. One must notice that, at that time, there were much less concerns with fuel consumption, emissions and efficiency than there is today.

A similar situation was faced in 1940, when CPVAs were tried experimentally in research laboratories on automobile industry. The results shew that it was the most efficient of all devices tested, but it was not chosen to be used because cheaper rubber-in-shear absorbers were available. These were replaced after some years by the silicone dampers, because vehicle manufacturers were seeking for standardization for mass production.

This has been the status quo of the automotive industry regarding torsional dampers up to current days. However, it may possibly be changed due to the laws and constraints mentioned on the beginning of this chapter, which motivates the study of these vibration absorption devices.

At this point, all the technical features about powertrains, NVH and CPVAs, necessary for a clear understanding of the motivations and objectives of this work have been presented. On the next sections, motivations, objectives and an outline of this work are presented.

1.3 Motivations

As it has been mentioned on previous sections of this work, in some cases the amount of torsional friction provided by the clutch disk is not capable of attenuating some amplification conditions, leading to still undesirable rattle noise. It usually happens on trucks and buses. The standard solution for these cases is to use a dual mass flywheel, which has elevated cost.

A still unusual alternative solution to this problem is the use of CPVAs on the clutch disk. Its effectiveness has not been tested yet, but this solution is potentially less expensive than a dual mass flywheel and has shown to be effective on a large number of cases.

Additionally, it is known that European and South-American consumers of truck and buses are not as demanding in terms of sound comfort as the consumers of passenger vehicles. Hence, even if the use of CPVAs show to be less effective than the use of dual mass flywheels, but more effective than torsional friction, this solution would still be considered acceptable.

Therefore the motivation of this work is to verify if the use of CPVAs on a clutch disk is a suitable solution for the drive rattle problem on heavy commercial vehicles, and if so, to build a prototype for field tests and further investigations.

1.4 Objectives

This work has five main objectives, which are listed below:

- 1) Build a simple and representative torsional model of the powertrain of the vehicle under investigation.
- 2) Make a complete analysis on the linear and nonlinear dynamics of general path CPVAs. This analysis must comprise:
 - a) The derivation of a nonlinear model in terms of the swing angle of the pendulum, which is unavailable on the literature.
 - b) The analysis of the influence of gravity on tuning and stability.
 - c) The representation of paths as polynomial functions in terms of the swing angle of the pendulum bob.
 - d) The derivation of shape functions for the most usual pendulum paths.
 - e) The application of the Multiple Scales Method, instead of the limited Krylov-Bogoliubov Method of Averaging, the most used method on the literature on this subject.
- 3) Derive two different design techniques for CPVAs based on the existence of the No-Resonance Zone, still unavailable on the literature.
- 4) Design pendulums to be installed on the clutch disk of the vehicle under investigation based on project limitations.
- 5) Perform simulations and assess the suitability of such solution.

1.5 Outline of the Work

This work is composed of five chapters as described in the following.

The first chapter of this work is an introductory chapter, and presents basic features about vehicle powertrains, NVH and CPVAs, and also the objectives, motivations and outline of this work.

The second chapter is devoted to the presentation of the powertrain and some tests performed on it in order to obtain necessary data to build a mathematical model. The mathematical model that represents the dynamics of the powertrain is also built on this chapter.

On the third chapter, all the technical aspects on the dynamics of general path centrifugal pendulum vibration absorbers are presented. It was chosen not to devote a chapter to the bibliography review on this work, but to present it continuously as the theoretical features are explored. This is done extensively in this chapter.

Chapter four is devoted to the application of the CPVA on the powertrain. Hence, the design techniques and project limitations are shown in this chapter. Simulations using the previously built model of the powertrain and the recently designed CPVA are performed and results are commented and explored.

The last chapter is devoted to the conclusions of this work, the consolidation of the contributions and the perspectives for future research.

2 The Powertrain: Recognition and Modeling

The goal of this chapter is to introduce all the relevant technical features of the powertrain under investigation and to generate a reliable mathematical model of its torsional dynamics. This model is necessary for the design and simulation of the pendulums that are going to be placed on its clutch disk. For this reason, it is composed of four parts described below:

- **Part I: Vehicle Data and Technical Specifications.** On this part, the vehicle is introduced and its the technical features are described in detail.
- **Part II: Experimental Estimation of Torsional Stiffness of Axles.** On the second part, results from an experiment involving two vehicles are presented. The goal of this experiment was to estimate the torsional stiffness of the axle shafts, Cardan joints and propeller shafts.
- **Part III: Drive Rattle Measurements.** The powertrain has been subjected to tests that capture the worst case scenarios for the generation of rattle noise. These tests were performed with four different clutch disks and the results are presented in the third part of this chapter.
- **Part IV: Mathematical Modeling and Model Validation.** Using data provided by the vehicle manufacturers and results from the previous parts of this chapter, a torsional model of the powertrain is presented and validated for further use.

It is really important to emphasize that all the data presented in this chapter were obtained from a prototype vehicle designed to accentuate key undesired behaviors of the powertrain, such as generation of rattle noise, for better investigation. *End user vehicles of the same brand and model do not exhibit the same behavior.*

2.1 Part I: Vehicle Data and Technical Specifications

The vehicle under investigation is a ultra heavy duty truck, shown in Fig. 2.1. It has a 12.88 liters, four stroke 6 cylinder Diesel engine, capable of delivering 412kW^1 of maximum power at 1,900 rpm and 2,500 Nm of maximum torque between 1,000 and 1,550 rpm. The maximum engine speed recommended by the manufacturer is of 2,400 rpm and the emissions law considered for its design is Euro V.



Figure 2.1: Vehicle under investigation.

These are valuable information. For being a four stroke 6 cylinder engine, it is known that the firing frequency is three times the rotating speed of the engine, i.e. it is at the third order. Hence, the main order of excitation must be the third. For being an engine designed according to Euro V law of emissions, it is also known that the second harmonic of the firing frequency may also be critical. This is due to the fact that these engines are designed so that the efficiency of the combustion is increased, and this induces the torque pulses generated by the engine to be sharper, increasing the importance of the higher harmonics. Therefore, the sixth order must also be taken into account.

The torque transmission between the engine and the gearbox is done through a single clutch disk which has an external diameter of 430 mm. The increased diameter of the disk

¹Equivalent to 560cv or 553hp

allows for the reduction of thermal load during the coupling of the clutch, and hence improves the service life of the clutch facings.

The gearbox is a 16 speed automated manual transmission from ZF called ZF 16AS 2631 TO with Intarder². It actually has 16 speeds towards plus two reverses. The highest gear ratio provided by this gearbox is of 0.83 : 1, at the 16th speed.

One propeller shaft is connected to the end of the gearbox and it transmits torque to a set of two differential gears. Hence, the truck is a 6x4 with rear traction. The first differential gear, also referred to as front differential gear, distributes the torque between the first two side shafts and the second propeller shaft, which is shorter and is connected to the second differential gear. The latter one, sometimes referred to as rear differential gear, distributes the torque to the remaining side shafts. This configuration is also known as tandem axle. The pair of differentials is manufactured by Meritor, and is referred to as MT-50-168³. A scheme of the powertrain of the vehicle under investigation is shown in Fig. 2.2.

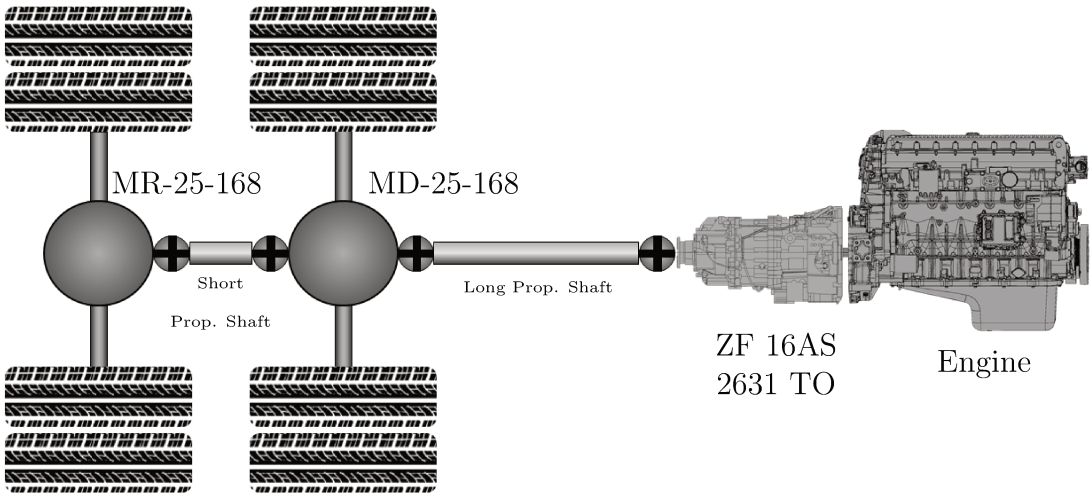


Figure 2.2: Scheme of the powertrain of the vehicle under investigation.

In order to obtain a representative model of the powertrain, it is necessary to obtain the torsional stiffness of some elements such as the side shafts, propeller shafts, cardan joints. However, once the stiffness is not a direct design parameter of any of these parts, the manufacturers don't usually have it available. Also, the side shafts are assembled with the differential gears inside a case, as shown in Fig. 2.3, which reduces the observability of such system.

²Intarder is a device that works as a hydraulic braking system. It was disabled during the tests.

³The front one is called MD-25-168 and the rear one MR-25-168. Their final ratio is of 3.42 : 1.

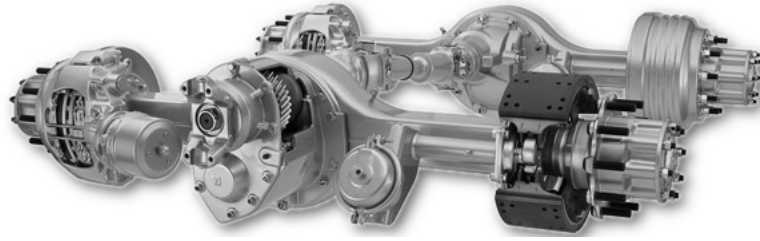


Figure 2.3: Tandem axle configuration.

For this reason, an experimental procedure was adopted in order to estimate the stiffness of each of these axles. This procedure is explained in the following section.

2.2 Part II: Experimental Estimation of Torsional Stiffness of Axles

The experiment to be explained in this section has already been performed in previous cases at ZF, and good results have been obtained.

The objective of this experiment was to estimate the torsional stiffness of the side shafts, propeller shafts and cardan joints aiming to build a representative mathematical model of the torsional dynamics of the vehicle. Hence, it consisted in basically applying torque and measuring deflections of each element. What turned it into a complex task was that the vehicle could not be disassembled, some parts were not accessible, the amount of torque needed to induce relevant deflection on the system was considerable and the clutch and the gearbox were not controllable when the engine was off, because they were all automated. Each of these issues have been circumvented as explained below.

As the vehicle could not be disassembled and torque had to be applied on the system, the only alternative left was to apply torque on its wheels. Needless to say that applying torque directly to the wheels would not be feasible, because the amount of torque had to be high and it would have to be applied equally and simultaneously on the four driving wheels. Instead, it was chosen to use another truck of the same capacity to pull the one being studied backwards. It was then able to offer the necessary amount of torque to deflect all the parts and it would also apply torque on the wheels equally, as desired.

The vehicle being studied had to be off during the test. After all, its brakes could not

actuate on the system, because they would balance the torque on the wheels and hence there would be no torque acting on the powertrain, resulting in no measurable deflection. On the other hand, as the vehicle would be pulled, if there was no reaction on the powertrain it would move and the inner parts would not be deflected, which were both undesirable. Hence, it was necessary to lock the flywheel and keep the clutch and also one of the speeds engaged. The lower the speed left engaged, the lower the reaction on the flywheel would be, which was favorable to its structural integrity.

In order to lock the flywheel, an existing window on the bell housing was used. It allowed access to some of the teeth of the flywheel, which are usually connected to the engine starter. A metal part that fits this window and locks the flywheel teeth has been manufactured and was able to lock it successfully. However, keeping the clutch and one of the gears engaged required a more sophisticated solution.

As the vehicle has an automated manual transmission, when the engine is turned off, the neutral gear is automatically selected. When the engine is on and some gear is selected, the clutch is kept disengaged until the driver releases the brake pedal and presses the throttle pedal. The objective was then to force the gearbox to do what it is programmed not to do: keep a gear engaged while turning the engine off and then engage the clutch.

The actuation on the gearbox, differentials and brakes is all pneumatic, and hence, simply disconnecting a hose could cause the whole system to lose pressure and if it happened the brakes could lock the wheels, which was undesired. The solution was to install a valve on the pneumatic intake of the gearbox and clutch actuators. With the engine on, a low gear was selected and then this valve was shut. After that, the hose on the gearbox actuator intake was disengaged, disabling this actuator. The pressure on the clutch actuator was kept and it would be disengaged until the engine was off. When the driver turned the engine off, the pressure on the clutch actuator decreased because the compressor was turned off, and the clutch automatically engaged back. The pressure on the brake system was kept, and hence the brakes remained open during the tests.

The last issue to be dealt with was the observability of the side shafts. In the case of the propeller shafts, it was possible to install levers on its ends. These levers would actuate displacement sensors that were placed on the chassis of the vehicle. Once the displacements on this test were small, this system was able to measure the angular deflection of these axles. One of the levers and one of the displacement sensors are shown in Fig. 2.4

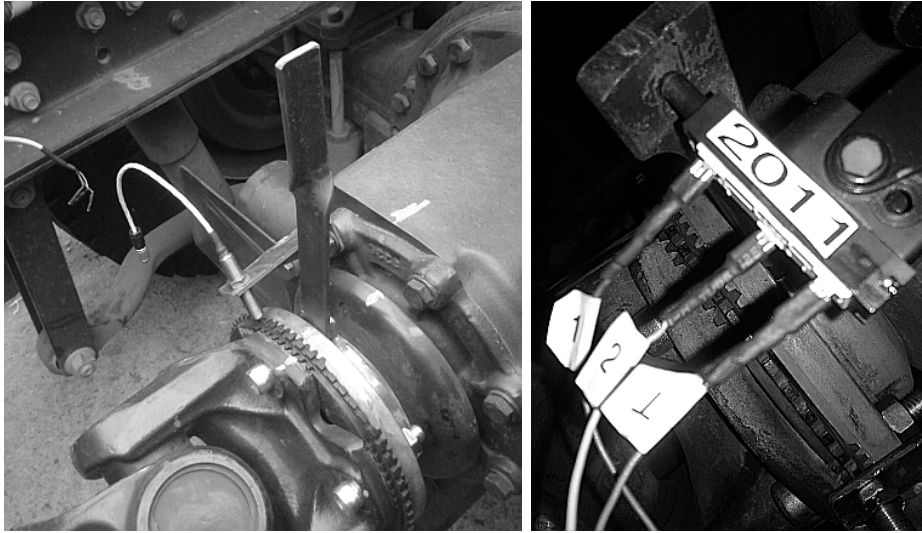


Figure 2.4: *Left:* One end of the longest propeller shaft with auxiliary lever.
Right: Displacement sensor touching auxiliary lever.

The ends of the side shafts, however, are not observable for being placed inside a case, as in Fig. 2.3. For this reason, on both rear axles the procedure was to measure the angle at the differential gear input, which will always be one end of a propeller shaft, and the angle at the wheel. Using the gear ratio of the differential gear it is possible to estimate the angular position of its crown, which is at the end of both side shafts. Using the angle at the wheel, it is then possible to estimate the deflection of each side shaft.

With all these considerations, nine sensors were necessary to carry this experiment. Eight displacement sensors have been used, one at each driving wheel and one at each end of the two propeller shafts. The ninth sensor is a load cell that was installed on the band that was used to pull the vehicle, so that the tractive force could be measured and the torque at each wheel could be estimated. Figure 2.5 shows the experiment. The truck at the back is the one being investigated while the one closer to the camera was used to pull it.

Once the data was collected, the angles at each sensor were calculated, and so was the torque acting on each shaft. The resulting samples were plotted on a torque versus deformation diagram, and, as expected, they correlated well with an affine function. The slope of such function was calculated using least squares approximation, and it represents the stiffness of each shaft. The results are shown in Figs. from 2.6 to 2.11.

The results from the data fitting are presented on Table 2.1. On this table the first



Figure 2.5: *Left*: Band used to pull vehicle.
Right: Experiment setup.

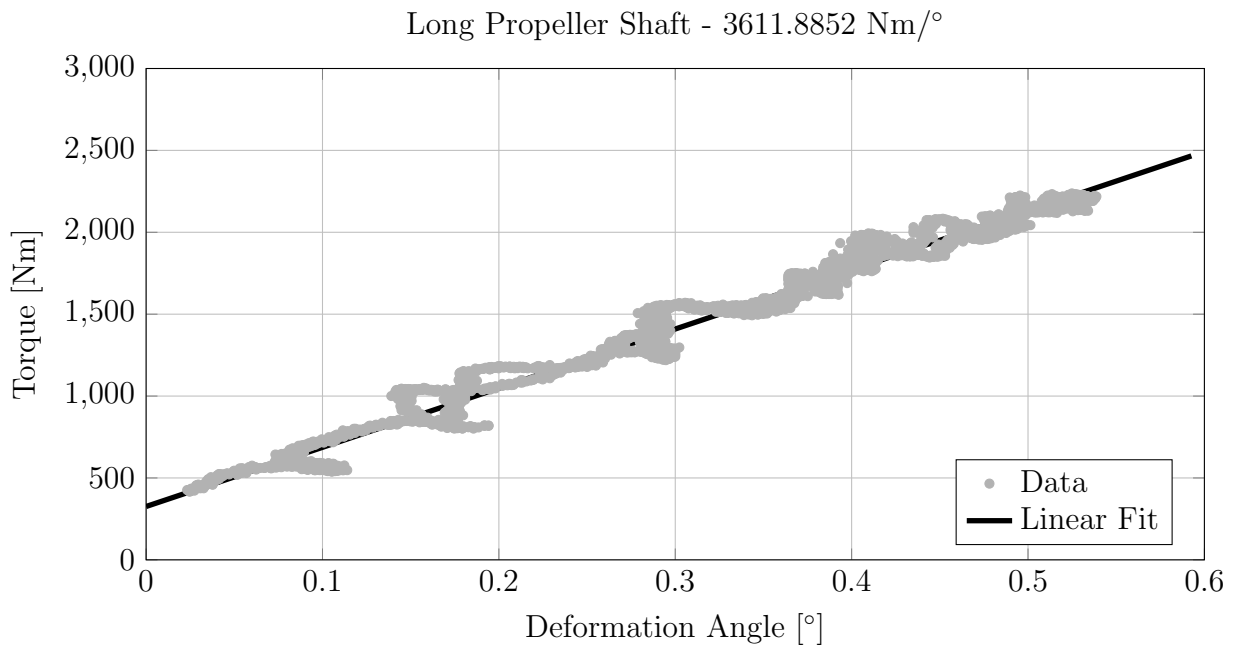


Figure 2.6: Data fit to calculate the stiffness of the long propeller shaft.

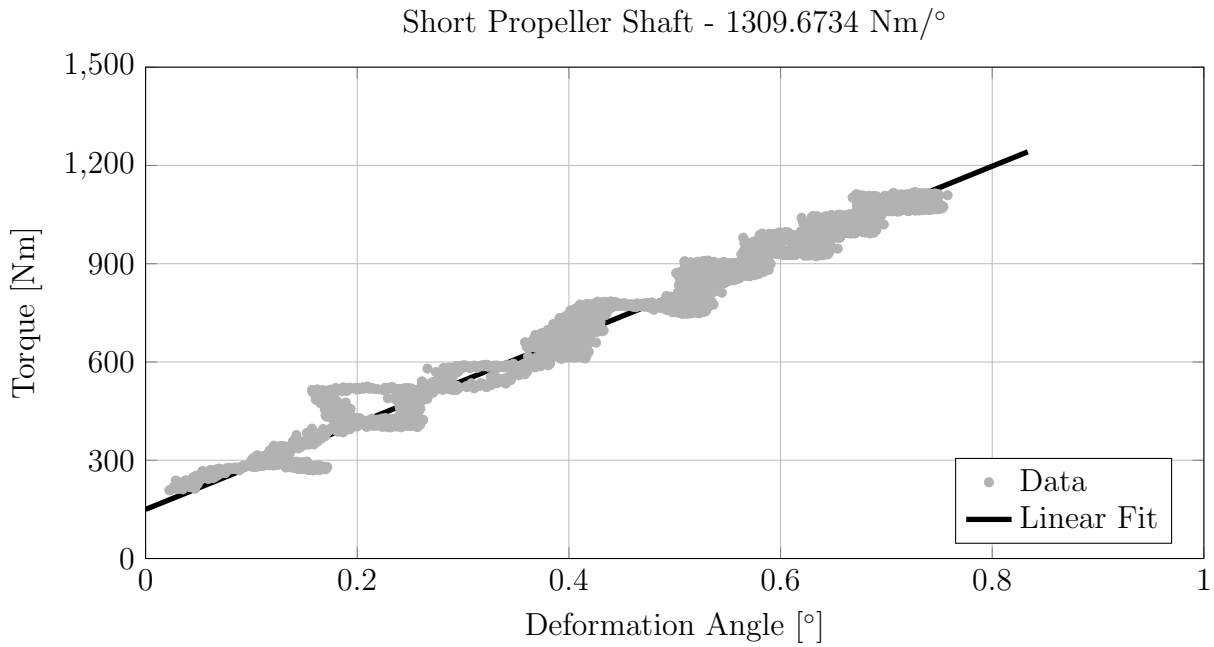


Figure 2.7: Data fit to calculate the stiffness of the short propeller shaft.

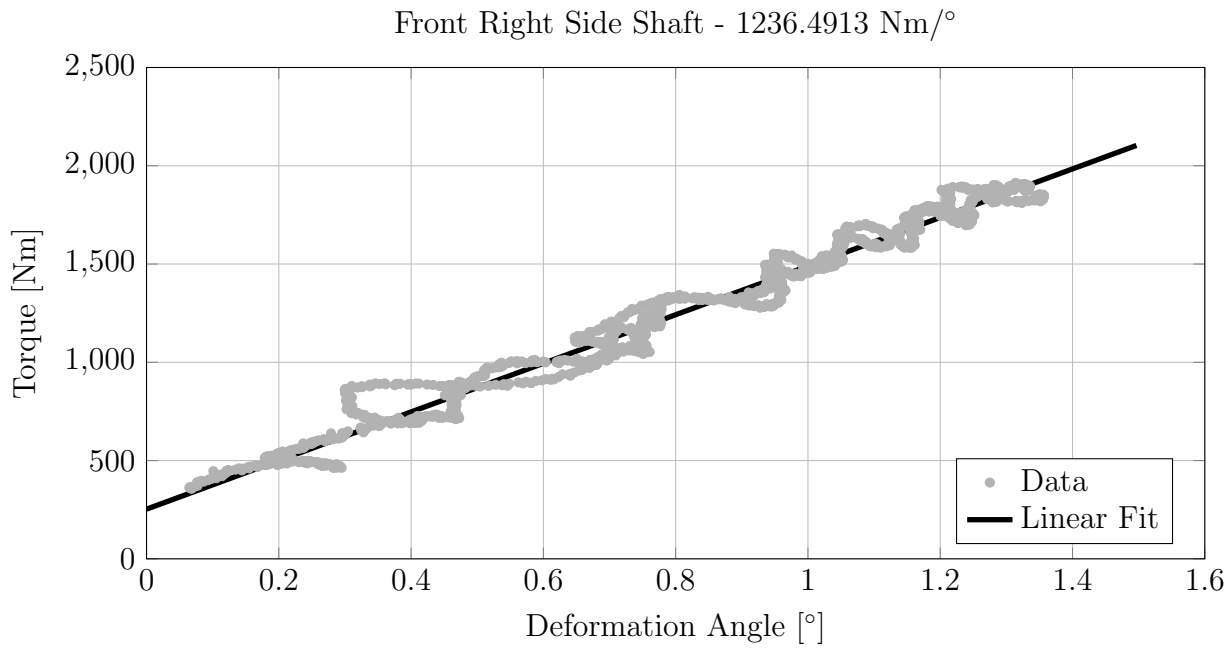


Figure 2.8: Data fit to calculate the stiffness of the front right side shaft.

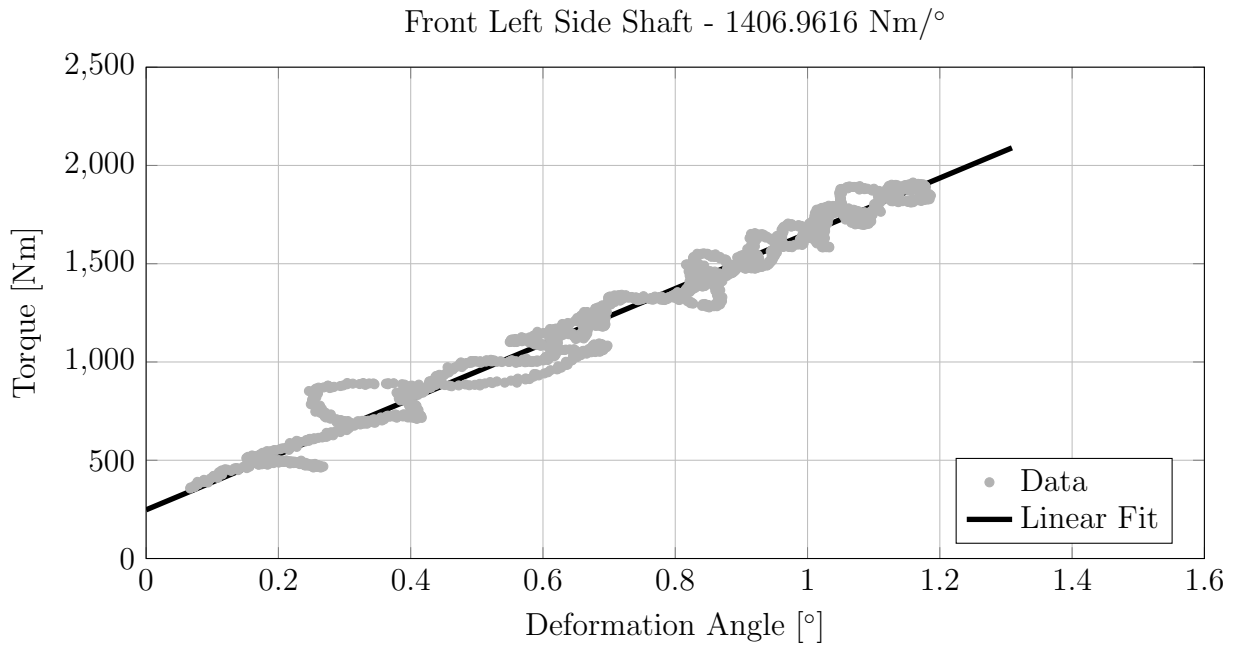


Figure 2.9: Data fit to calculate the stiffness of the front left side shaft.

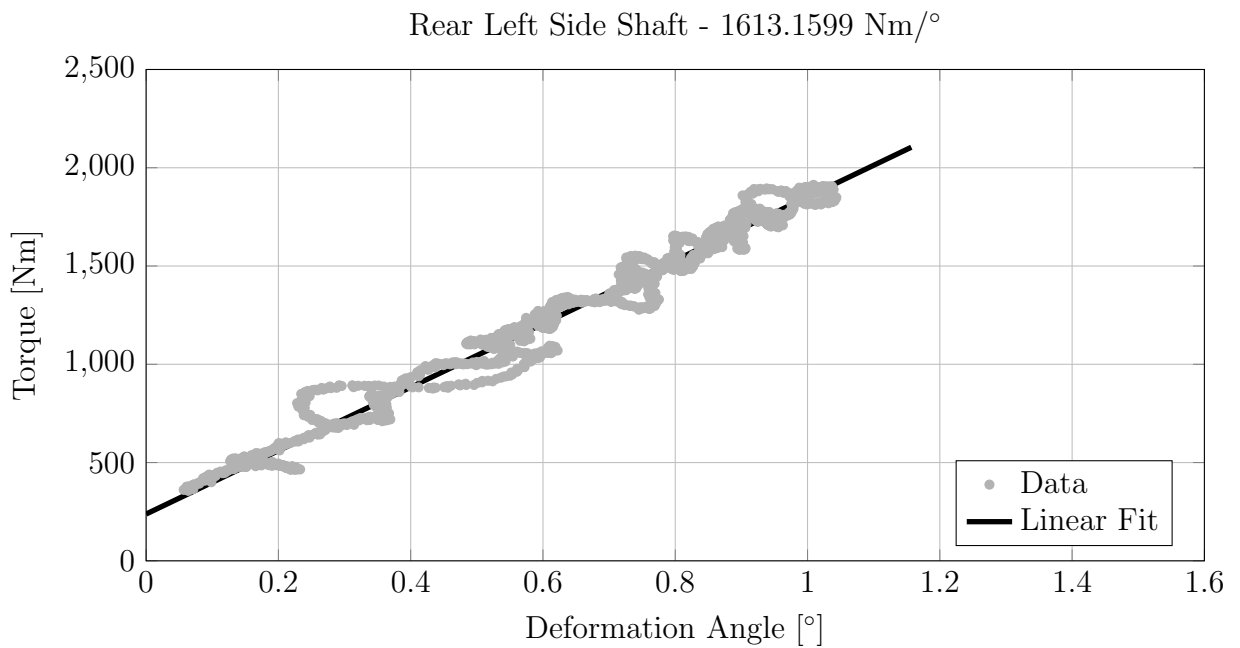


Figure 2.10: Data fit to calculate the stiffness of the rear left side shaft.

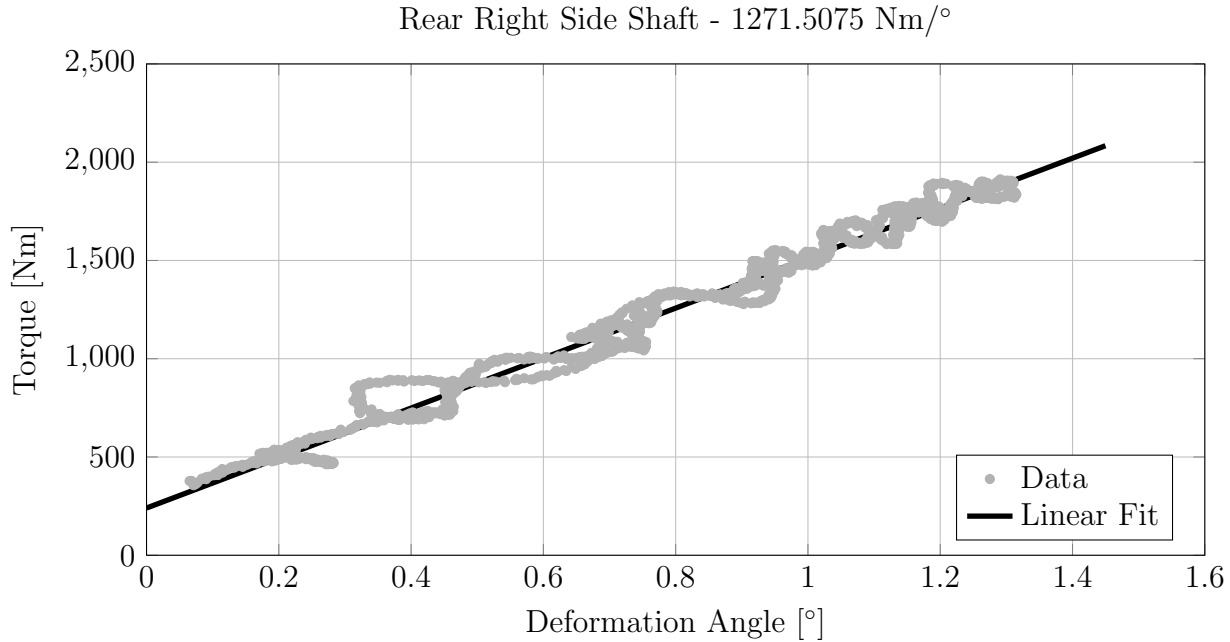


Figure 2.11: Data fit to calculate the stiffness of the rear right side shaft.

data column has the value obtained for the stiffness of each shaft while the second one is the correlation coefficient of each set.

Table 2.1: Estimated stiffness and correlation coefficient for each shaft.

Shaft	Stiffness [Nm/°]	$r_{x,y}$ [%]
Long Prop. Shaft	3611.89	99.0557
Short Prop. Shaft	1309.67	99.0268
Front Right Side Shaft	1236.49	99.0055
Front Left Side Shaft	1406.96	98.8416
Rear Left Side Shaft	1613.16	98.8494
Rear Right Side Shaft	1271.51	99.1163

The correlation coefficients obtained shows that the six sets of samples can be well represented by an affine function, once the lowest one is of 98.8416%. Consequently, the values obtained for the stiffness of each shaft are considered to have low error. It is also possible to depict different values for the stiffness of each side shaft. Although the powertrain is symmetric, for constructive reasons the side shafts may have different stiffnesses. In this case, the right ones are more compliant than the left ones. This difference tends to be much higher in lightweight vehicles. However, it does not bring unexpected vibrational behavior

to the powertrain.

2.3 Part III: Drive Rattle Measurements

The rattle noise is an NVH phenomenon that may occur in many different operating regimes. It is related to high levels of torsional vibration inside the gearbox, which induce impacts between the teeth of the unloaded gear pairs, producing undesirable noise. The aim of using the CPVA on this system is to reduce the level of torsional vibration, mainly in the gearbox, so that the rattle noise becomes less relevant on the subjective analysis.

As explained in earlier sections of this work, high levels of vibration may be induced mainly by intense torsional vibration on the flywheel or by system amplification, being the latter the most usual. Given all the operating regimes, the one that makes rattle noise more evident is the drive condition, because it is the case in which the engine produces the highest levels of torsional vibration and it is possible to cross critical speeds very slowly, if there is any.

Hence, the drive condition is the operating regime chosen to be analyzed throughout this work. In this section, the measurements that are going to be presented were carried out aiming to expose the main reasons why rattle noise occurs. With these pieces of information, it will be possible to develop a representative model of the torsional dynamics of the vehicle and to tune the CPVA to achieve the best performance.

Four sets of measurements have been performed, and they are referred to as Run 1 to 4. On each set of measurements, a different clutch disk was used, and their characteristics are shown in Table 2.2.

The disk used on Run 2 had lower drive stiffness than the default value for this application and the lowest possible friction torque. The disk used on Run 1 also had the lowest amount of friction torque, but its drive stiffness was the default for this application. The combination of two disks with different stiffnesses and the lowest possible amount of energy dissipation capability is used to highlight system amplification on the measurements. This makes it easier to spot critical speeds and, as the drive stiffness of the clutch disk is a known parameter, these measurements can also be used for model updating.

Table 2.2: Torsional characteristics of clutch disks used on recognition measurements.

Run	Drive Stiffness [Nm/°]	Drive Friction [Nm]
1	393.9	21.9
2	318.8	15.2
3	386.3	77.0
4	379.8	194.9

The disks used on Run 3 and 4 have the default value of drive stiffness. The difference between them is that the one used on Run 3 has the lowest recommended amount of friction torque, while the other one has the maximum recommended friction torque. These values are usually tested because on the design of the clutch disk this parameter is prescribed as a range of values. This happens because the properties of the device that provides friction torque, inside the clutch disk, vary along time because of wear, thermal loads and due to stabilization of the friction surface. Furthermore, the necessary tolerances to manufacture a disk with a single value of friction would be so tight that it would make the process too expensive. Hence, the designers have to ensure that, during the clutch disk's service life, the friction torque must lie inside the prescribed range. Additionally, when the friction torque is low, it is known that some amplification conditions can still be spotted. On the other hand, if it is excessively high, vibration attenuation on high frequencies can be affected. Hence the need for testing these configurations.

In order to measure torsional vibrations, proximity sensors are placed close to gears. As the teeth crosses its magnetic field, it generates an oscillatory tension signal, and the instantaneous frequency of this signal is the teeth crossing frequency. This signal is used as input to a comparator circuit. Then, if the input signal is above a certain voltage, the comparator's output is a constant nonzero tension signal, and zero otherwise. The output from the comparator is acquired by a digital acquisition system from Rotec GmbH with 10 GHz of clock frequency.

For this reason, the acquired signals have synchronous sampling, instead of a constant sampling rate. Furthermore, the measurement points can be actual gears, which is the case of the flywheel and gearbox input, or gears manufactured for measurement purposes only, which is the case of the gearbox's output and the input of both differentials. On the left image of Fig. 2.4, it is possible to see the link between a cardan joint, at the end of the longest

propeller shaft, and the output of the gearbox. Between these parts there is a gear with short teeth that is not used to transmit torque. This is one of the gears used for measurement purposes only, and it is not an original part of the vehicle. At the left of the auxiliary lever there is a screwed cylindrical part which has one end close to the teeth of the aforementioned gear and has a white wire on the other end. This is one of the proximity sensors used for the measurements.

The layout of the gearbox is shown in Fig. 2.12. It is basically a four speed transmission which has a splitter group on its input and a range change group on its output, resulting in 16 speeds forward plus two reverses. The gear used for the measurements is the gear K2, indicated in the figure. In order to place the proximity sensor near this gear, a hole was drilled on the gearbox housing. This modification did not affect structural integrity or acoustic behavior of the system.

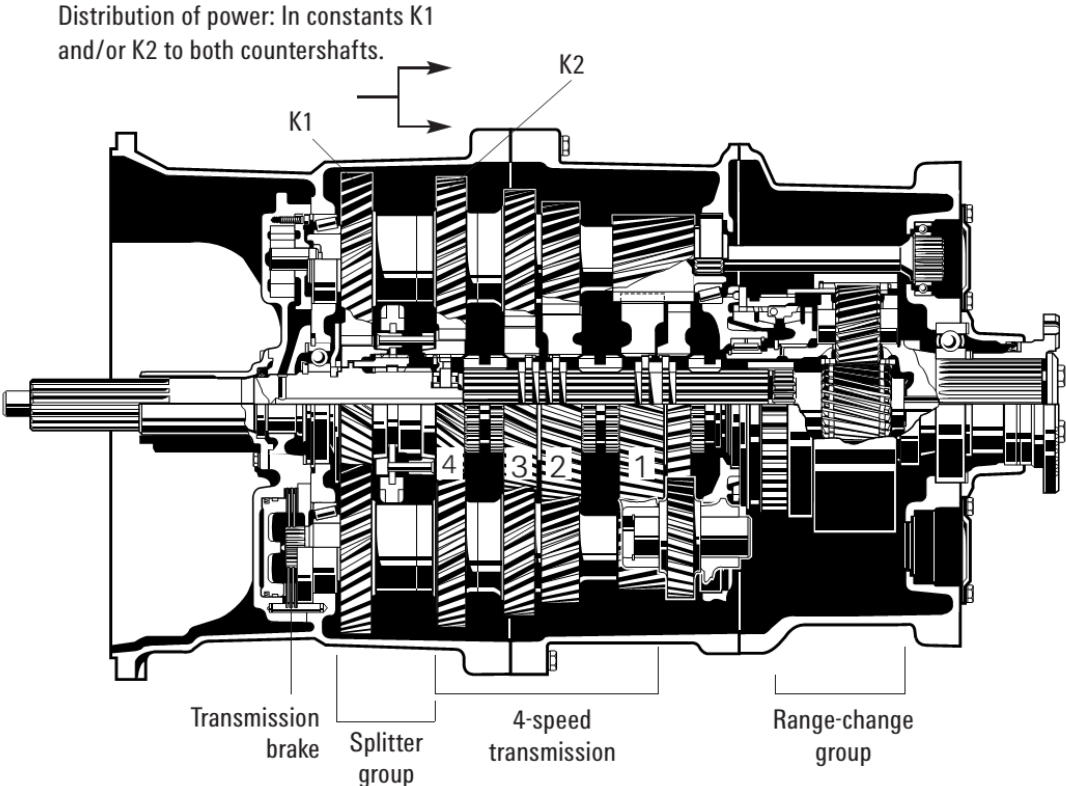


Figure 2.12: Layout of the ZF 16AS 2631 TO gearbox.

Five measurement points were chosen: the flywheel, the gearbox’s input, the gearbox’s output, the front differential’s input and the rear differential’s input. Measurement noise

was found in some of the measurements on the channel of the gearbox’s output, and for this reason, results from this signal will be suppressed in some graphics. However, it did not intervene the conclusions to be presented in this work.

The results of the measurements are presented below in the following way: for each gear, from the 7th to the 14th , the third order of the angular acceleration of each channel of Run 1 and Run 2 are compared. In the cases where it applies, the 6th order is also exhibited and compared. Then, the same procedure is adopted for Runs 3 and 4.

2.3.1 Analysis of the Torsional Behavior at 7th Gear

The results shown in this section have been obtained in a drive rattle test at 7th gear. The results for Run 1 and 2 are shown in Figs. 2.13 and 2.14 respectively. The amplitude of vibration of the flywheel is the black curve, and remains around 500 rad/s² in the whole range of engine speeds.

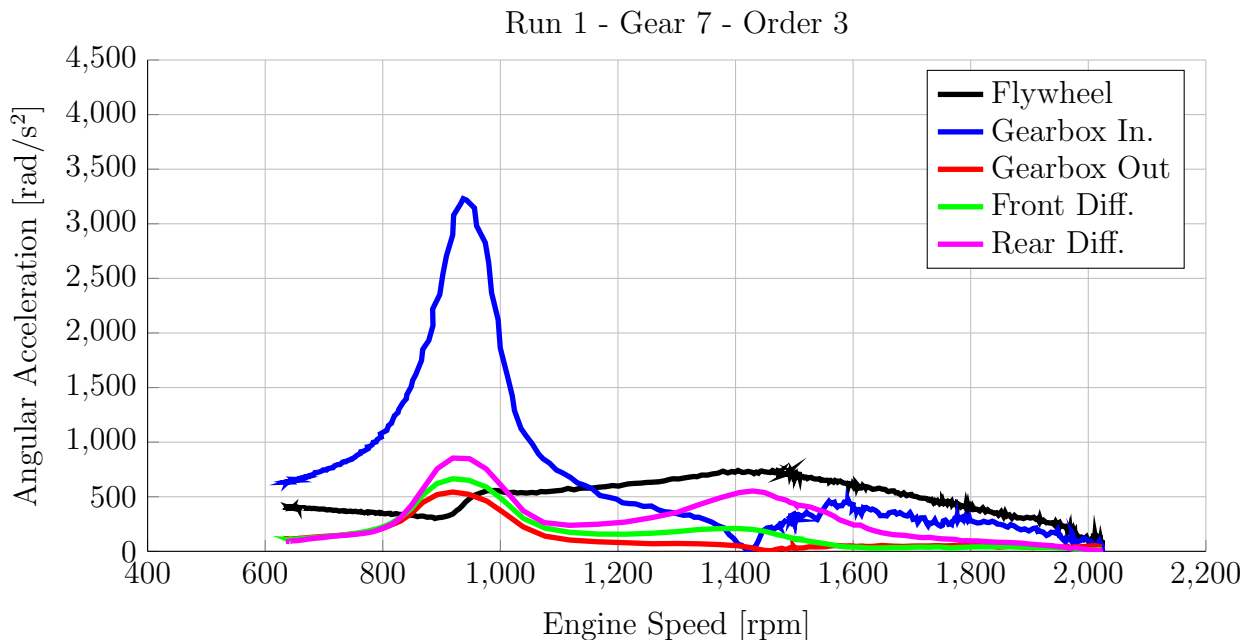


Figure 2.13: Results of the 3rd order obtained in Run 1 at 7th gear.

The first important feature to be spotted in both graphics is the huge amplification that

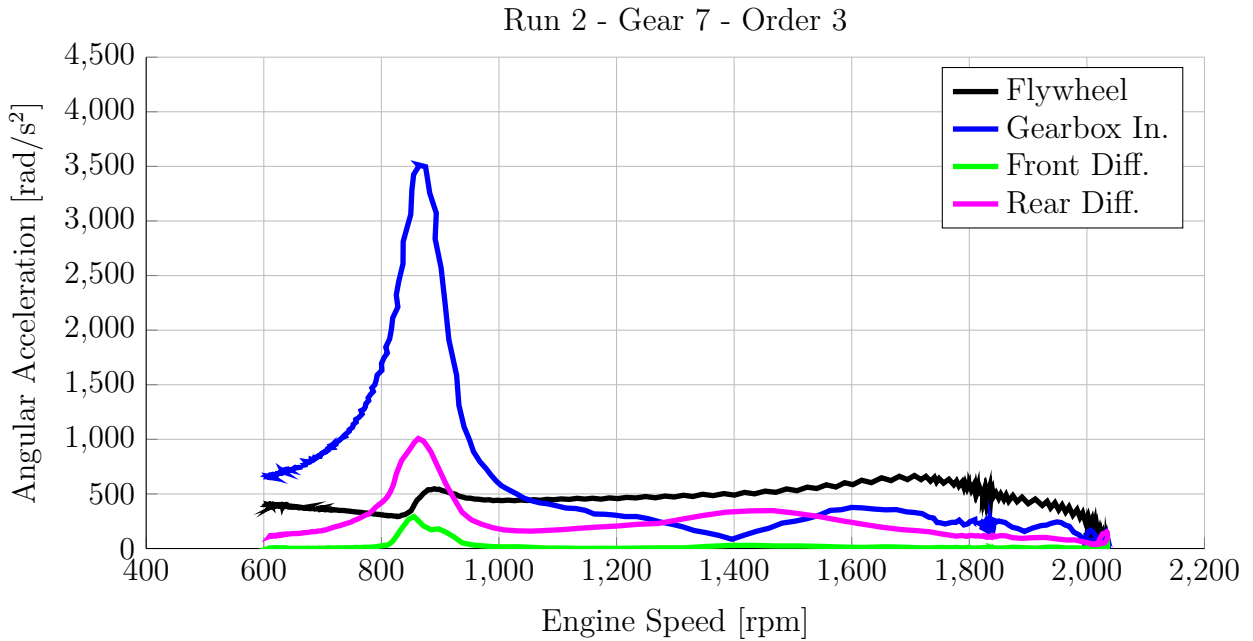


Figure 2.14: Results of the 3rd order obtained in Run 2 at 7th gear.

occurs between 700 and 1,100 rpm, mainly on the gearbox input. This happens because the disks used for Run 1 and 2 have minimum friction torque, and hence system amplifications are able to reach high amplitudes. It is shown in the work of Steinel (2000) and Drexel (1999) that, in most cases, linear models of powertrain have a mode which has the highest amplitude of vibration on the gearbox and is highly influenced by the energy dissipation capability of the clutch disk. Therefore, this amplification was expected to occur.

The frequency at which the peak of this amplification occurs is also very important. In Run 1, the disk used had default stiffness while in Run 2 the drive stiffness was nearly 16% lower than the design specification. For this reason, the peak found in Fig. 2.13 is around 950 rpm while the one found in Fig. 2.14 is close to 850 rpm. In the works of Drexel (1999) and Steinel (2000), it is also shown that the torsional stiffness of the clutch disk can influence significantly the natural frequency of the mode related to rattle noise.

The signals from the gearbox output and both differentials also present amplification in the same range of the gearbox input, but with relatively lower amplitude. Regarding the gearbox output signal, noise was found in Run 2, and hence this signal was omitted.

In Figs. 2.13 and 2.14 it is possible to verify that, for this order, the rear differential vibrates with greater amplitude than the front one. In the first graphic, specifically, it is possible to spot a region between 1,300 and 1,500 rpm where the gearbox seems to vibrate very little, and some amplification dominates the dynamics of the differentials. Subjectively, no objectionable noise was found in this range. This behavior seems to repeat on Run 2.

The sixth order from the same measurements is shown in Figs. 2.15 and 2.16.

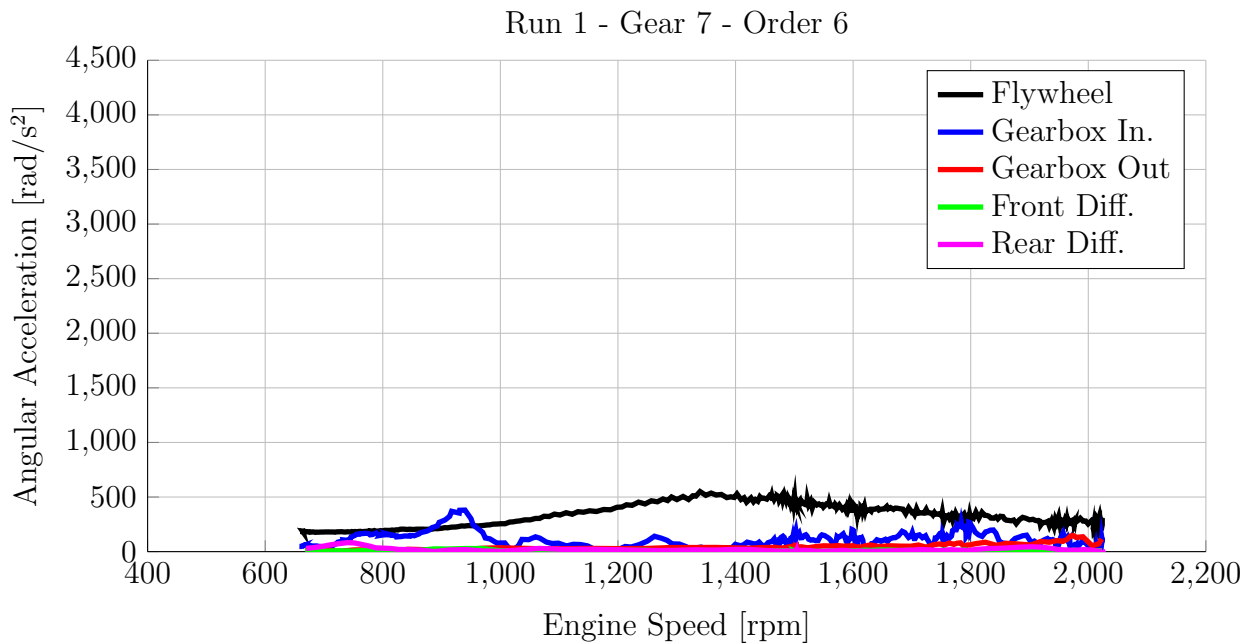


Figure 2.15: Results of the 6th order obtained in Run 1 at 7th gear.

The amplitude of the 6th order at the flywheel is very close to the one found in the 3rd order for the whole range of speeds. This was expected, because as previously explained, it seems to be a trend on Euro V engines and above. Although the excitation level is still significant, both Figs. 2.15 and 2.16 shown that this system is not sensitive to 6th order excitation. In all the forthcoming cases, if the behavior of the system in this order is the same, these graphics are going to be omitted.

All the relevant features of Runs 1 and 2 for the 7th gear have been presented. The 3rd order results for Runs 3 and 4 are shown in Figs. 2.17 and 2.18, respectively.

Although the clutch disk used in Run 3 already had a significant amount of friction

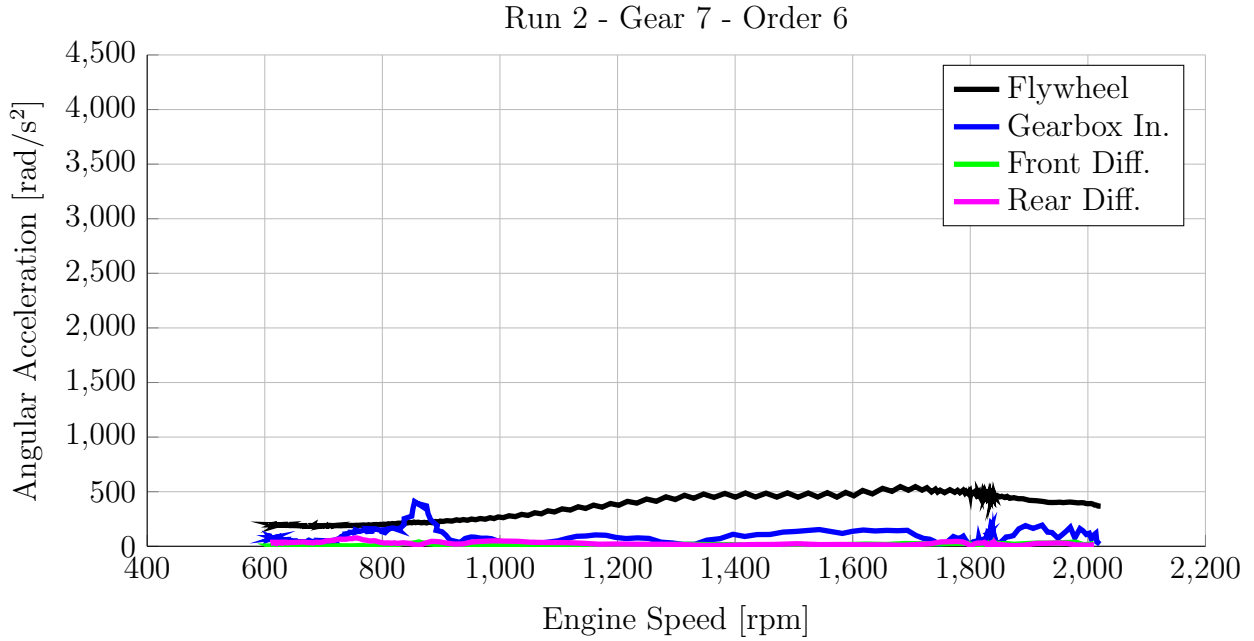


Figure 2.16: Results of the 6th order obtained in Run 2 at 7th gear.

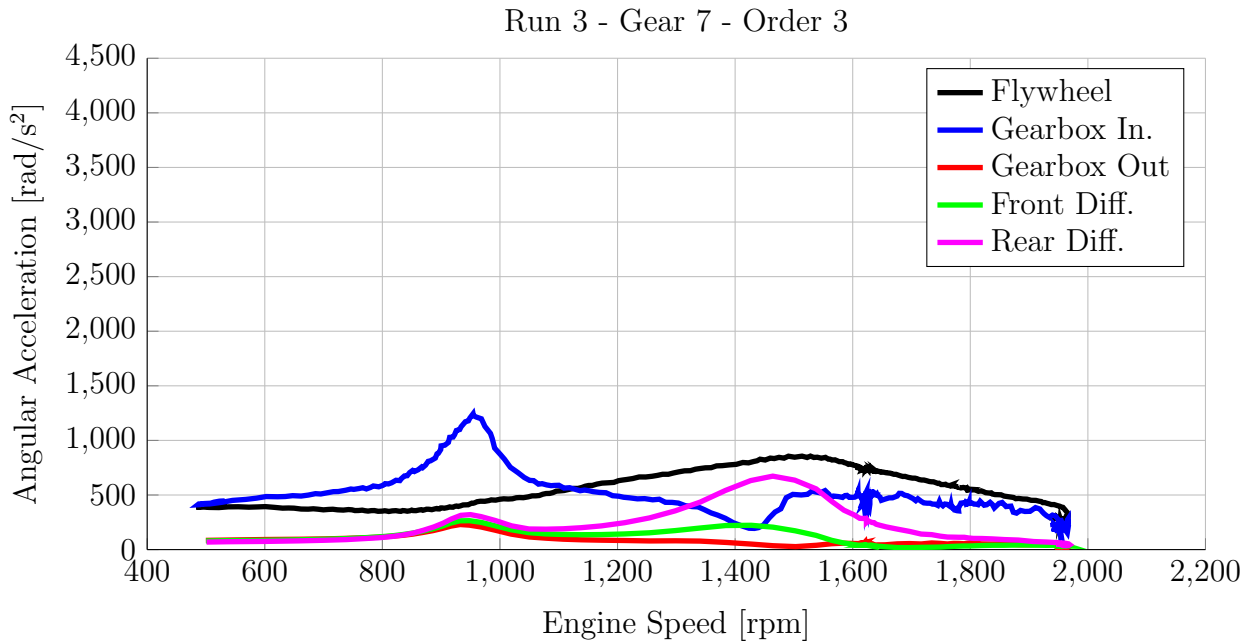


Figure 2.17: Results of the 3rd order obtained in Run 3 at 7th gear.

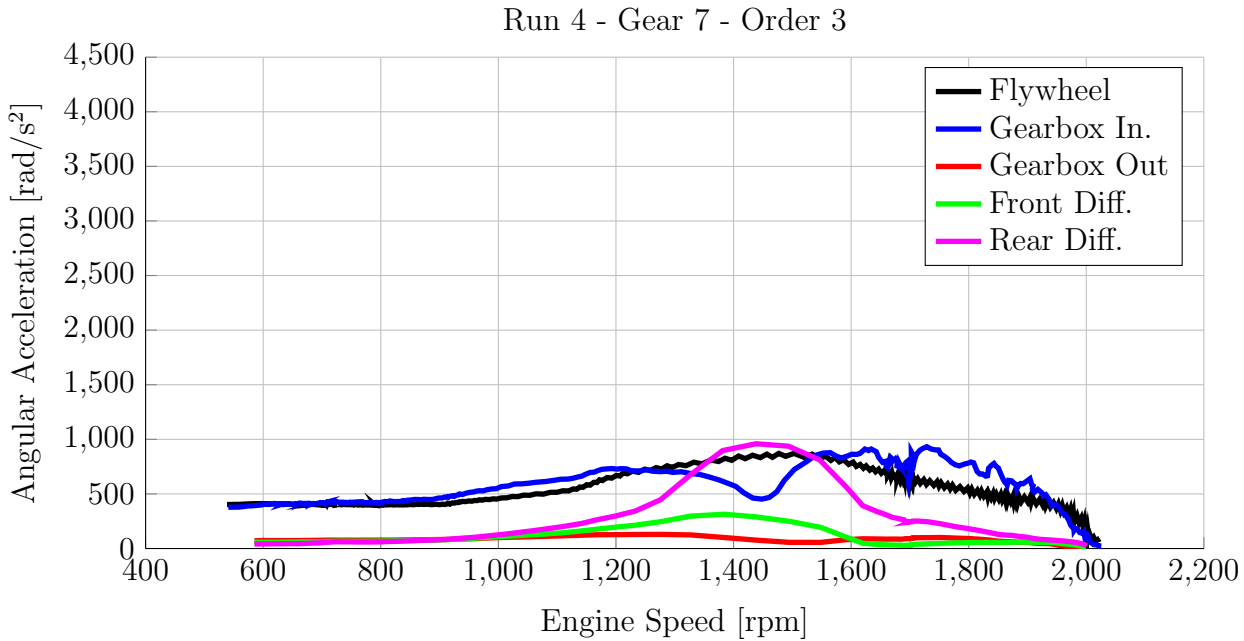


Figure 2.18: Results of the 3rd order obtained in Run 4 at 7th gear.

torque, it was shown not to be enough to control the amplification exhibited by the system at 950 rpm. However, the amount of friction torque in Run 4 successfully controlled this amplification. On the other hand, comparing Figs. 2.17 and 2.18 around 1,500 rpm, it is possible to observe that the more friction torque the clutch disk has, the more the amplification on the differentials becomes noticeable. At the same time, for higher engine speeds, the gearbox input tends to vibrate more than in cases where the friction torque was lower. During the tests, the subjective evaluators felt a great decrease on the rattle noise around 1000 rpm and no significant worsening at higher engine speeds.

There are also important features to be exposed on the 6th order found in these two Runs. They are shown in Figs. 2.19 and 2.20

Figure 2.19 shows that there is a little increase on the amplitude of vibration of the gearbox input with the amount of friction torque used on the disk for Run 3. Even though it happened, such increase was not significant enough to overcome the level of vibration of the flywheel or cause rattle noise to occur.

In Fig. 2.20, however, it is possible to see that the amount of friction torque on the

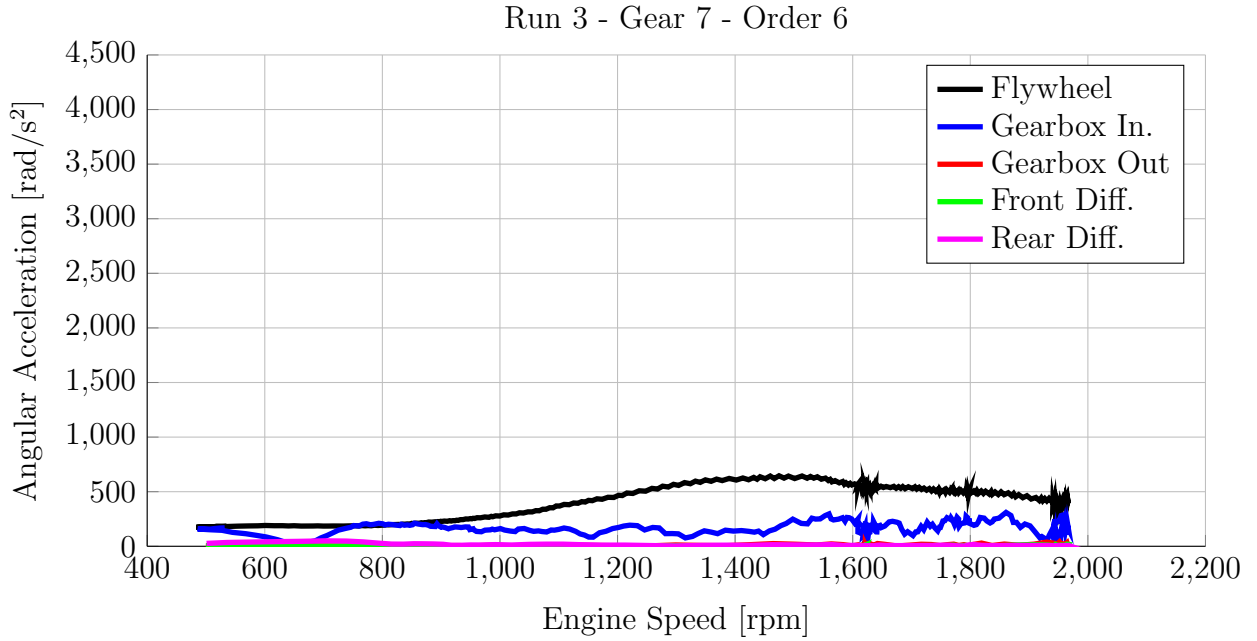


Figure 2.19: Results of the 6th order obtained in Run 3 at 7th gear.

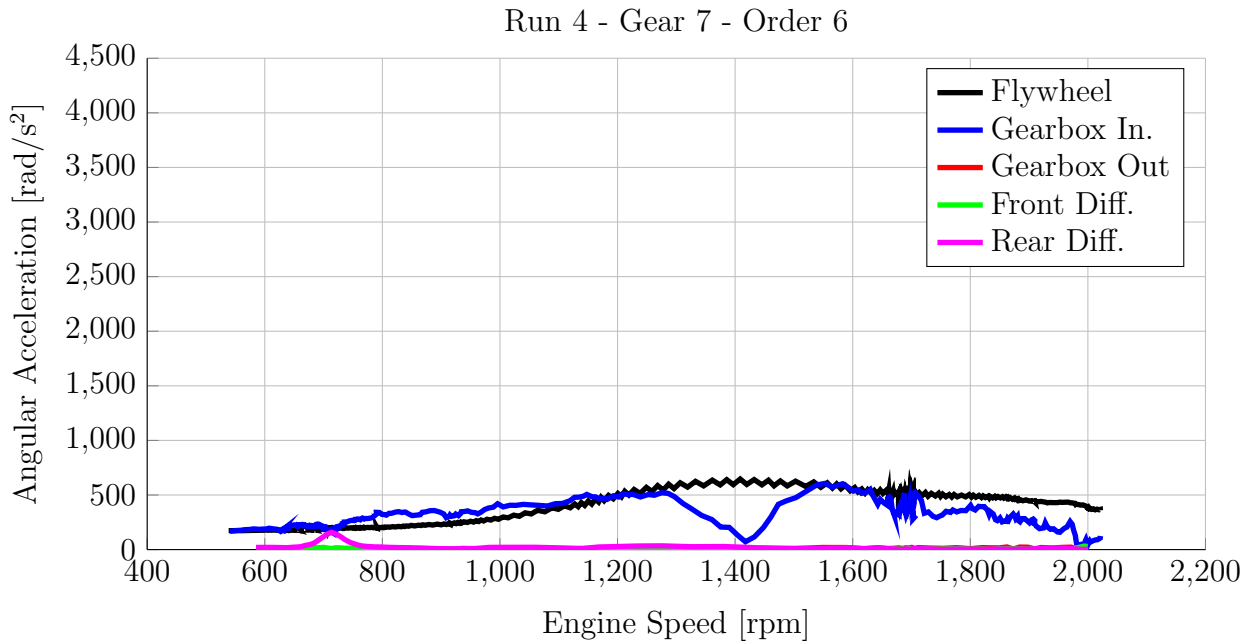


Figure 2.20: Results of the 6th order obtained in Run 4 at 7th gear.

disk caused the 6th order of the gearbox input to have nearly the same amplitude of the flywheel in almost the entire range of speeds. It just did not happen near 1,400 rpm, where the vibration at the gearbox suddenly ceases. Although this behavior is of academic interest and will be explained later in this work, it is not relevant in terms of acoustics.

These are the most relevant features found on the measurements performed using the 7th gear. All the forthcoming results and conclusions from measurements will be an extension of the ones shown in this section.

2.3.2 Analysis of the Torsional Behavior at 8th Gear

The next results to be shown are the 3rd order of the angular acceleration of the measurement points obtained in Runs 1 and 2 at 8th gear. These graphics are shown in Figs. 2.21 and 2.22.

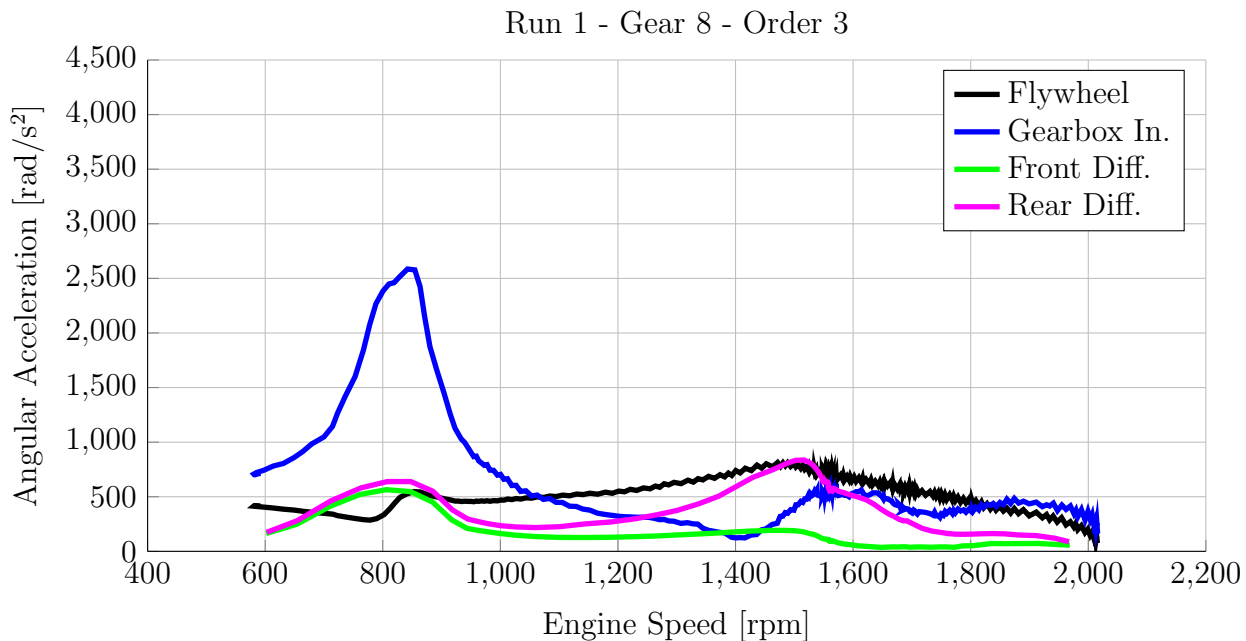


Figure 2.21: Results of the 3rd order obtained in Run 1 at 8th gear.

Regarding the first amplification, in Run 1 it happens around 800 rpm while in Run 2 it happens around 750 rpm. In the latter it is not possible to distinguish whether there are two

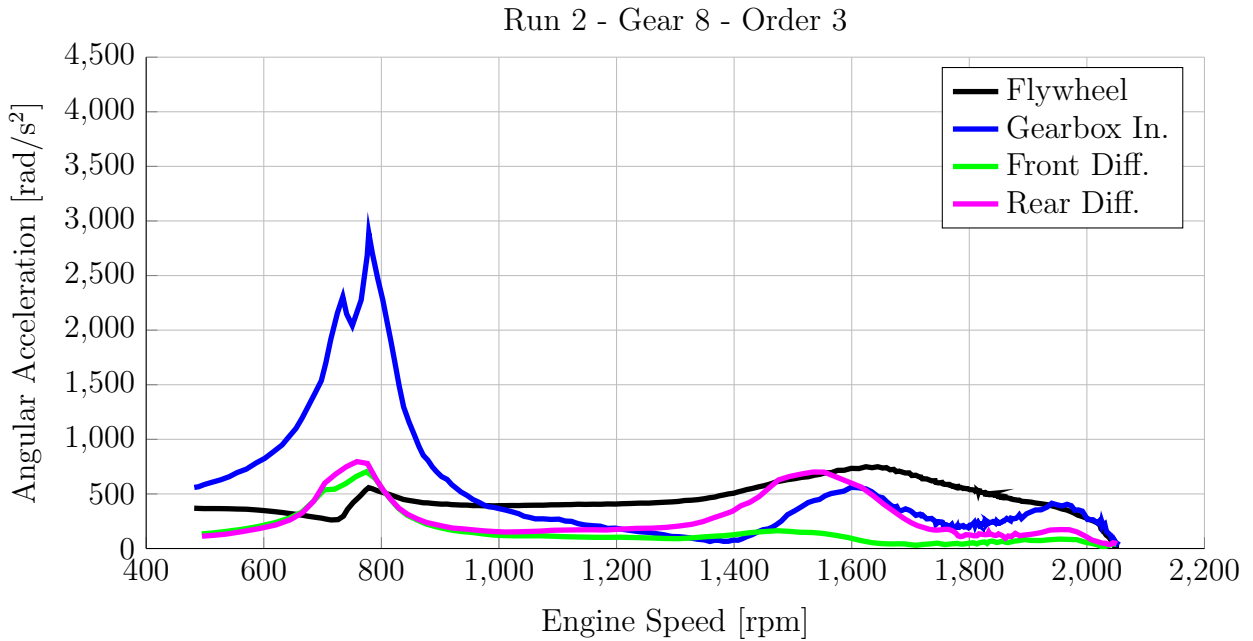


Figure 2.22: Results of the 3rd order obtained in Run 2 at 8th gear.

close peaks or if this distortion is caused by the shape of the excitation. At this frequency, the differentials seem to vibrate much more than the gearbox output, yet the latter signal had to be omitted for Run 2 because of measurement noise.

In both runs it is possible to spot some amplification near 1,500 rpm. In Run 1 it is possible to see that there is some amplitude of vibration on the front differential and an even greater amplitude on the rear differential. The same behavior is found on the results from Run 2. Finally, there seems to be another amplification around 1,900 rpm, which is a little more visible in Fig. 2.22, although it is still not possible to assure whether it is or not a system amplification based on these results.

In the 6th order results for Runs 1 and 2 there was no important system amplification. The results were very close to what was found using the 7th gear, and hence these results are not going to be shown here. The results for Runs 3 and 4 are shown in Figs. 2.23 and 2.24.

In Run 3, the amplitude found on the gearbox input was even greater than the amplitude found in Run 1, for the same gear. Once it is known that the clutch disk used for Run 3 has greater energy dissipation capability, this difference is explained by the fact that the tests

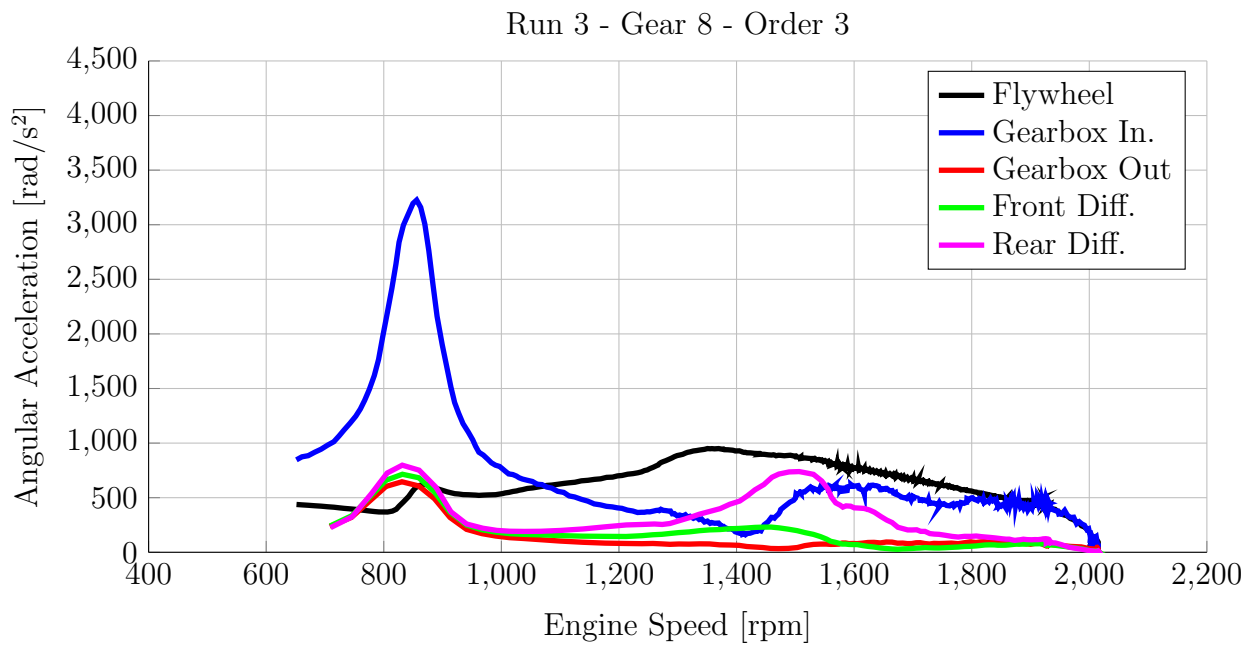


Figure 2.23: Results of the 3rd order obtained in Run 3 at 8th gear.

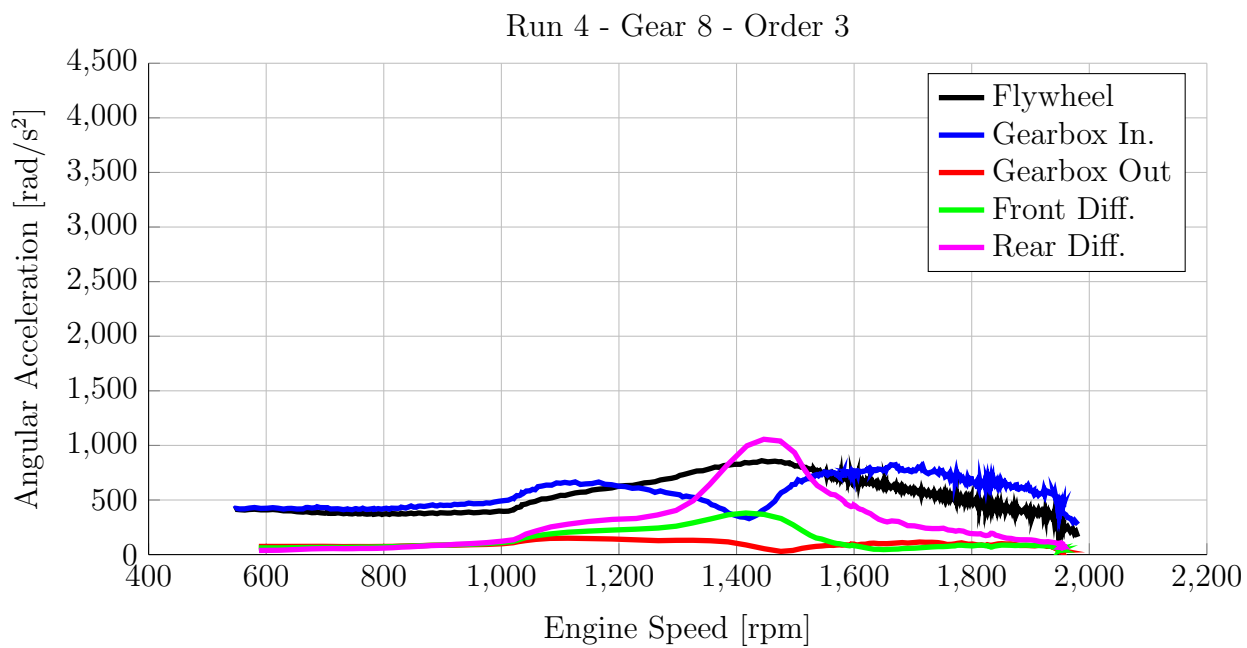


Figure 2.24: Results of the 3rd order obtained in Run 4 at 8th gear.

may not have good repeatability in a strict sense. It does not mean that in different tests the vehicle would have behaved in totally different ways. If there is a system amplification in some range of engine speeds, it will always be possible to detect it in the measurements and the noise produced in this critical range will be subjectively identical. However, the amplitude of the peak of acceleration is strongly influenced by the driver's capability of controlling the vehicle load, which is a very difficult task when testing vehicles with elevated levels of torque, as it is the case of the vehicle under investigation.

An important difference between Runs 1 and 3 is on the amplitude of the gearbox output. While in Run 1 the gearbox output vibrated with very little amplitude at the amplification, in Run 3, its amplitude was similar to the one found in both differentials.

In Run 4, once more the amount of friction torque in the clutch disk was able to control the main resonance, resulting in no significant amplification up to 1,300 rpm. However, once more the amplification found near 1,500 rpm could be verified. Besides, it became more intense with more friction torque at the clutch disk. Once more, in this range it is possible to see that the gearbox output vibrates very little, while the front differential has a greater amplitude of vibration and the greatest intensity is found on the rear differential. Once more, the subjective evaluations revealed no relevant rattling noise in this range.

Regarding the 6th order, the only result that is qualitatively different from the results found using the 7th gear are the ones from Run 4, shown in Fig. 2.25.

These results show that, although the amount of friction torque is elevated on the clutch disk used for this run, the system was still mostly not sensitive to 6th order excitation. A small amplification is found near 700 rpm, and it is exactly the same one found near 1,500 rpm in the 3rd order. No other important feature was found in the results for the measurements performed at 8th gear.

2.3.3 Analysis of the Torsional Behavior at 9th Gear

The results shown in this section have been obtained on tests at the 9th gear. Figures 2.26 and 2.27 contain the results for Runs 1 and 2, respectively. In both of these 2 runs, the signal from the gearbox output was corrupted by noise, therefore it is suppressed in these

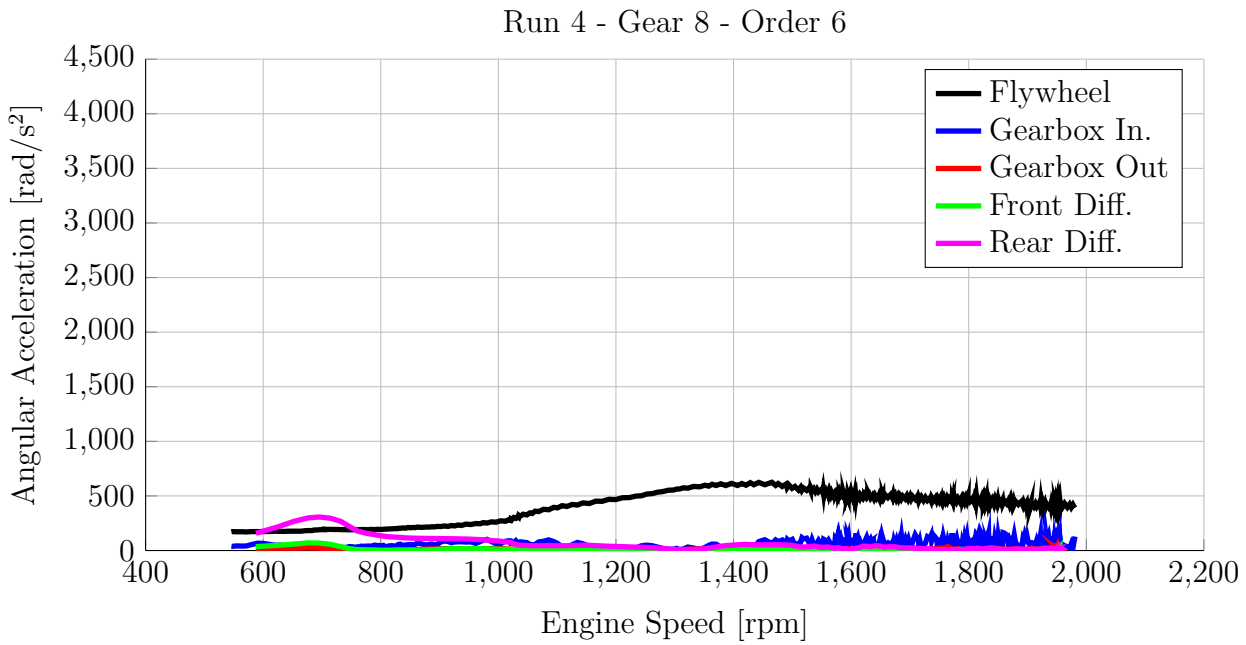


Figure 2.25: Results of the 6th order obtained in Run 4 at 8th gear.

graphics.

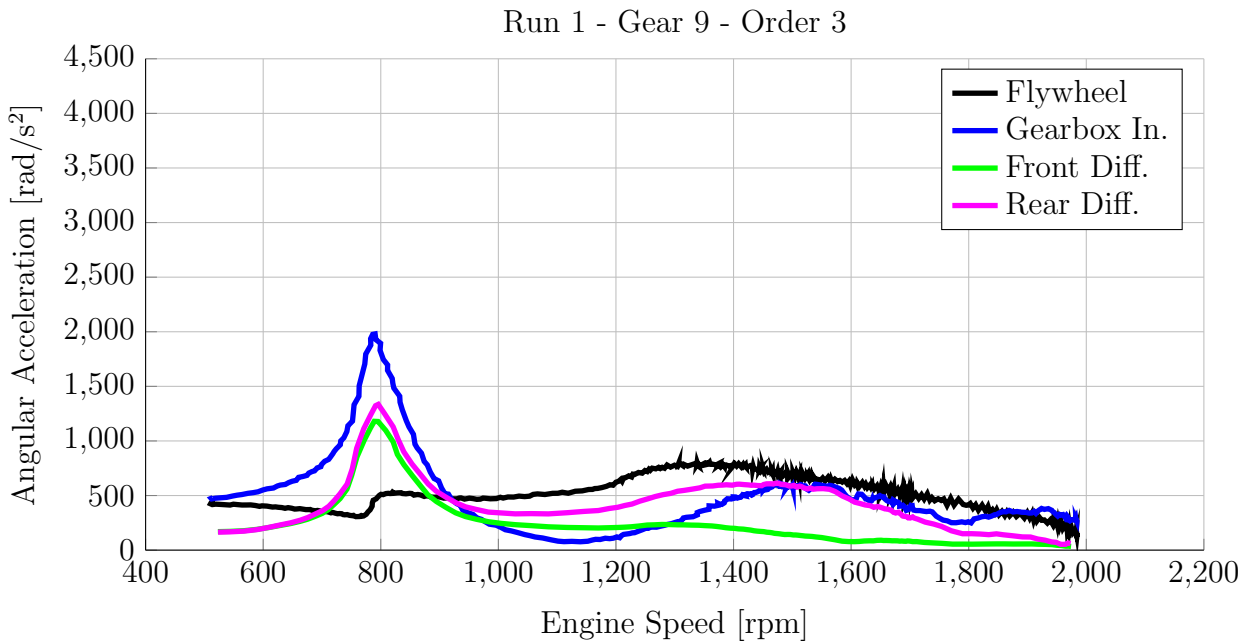


Figure 2.26: Results of the 3rd order obtained in Run 1 at 9th gear.

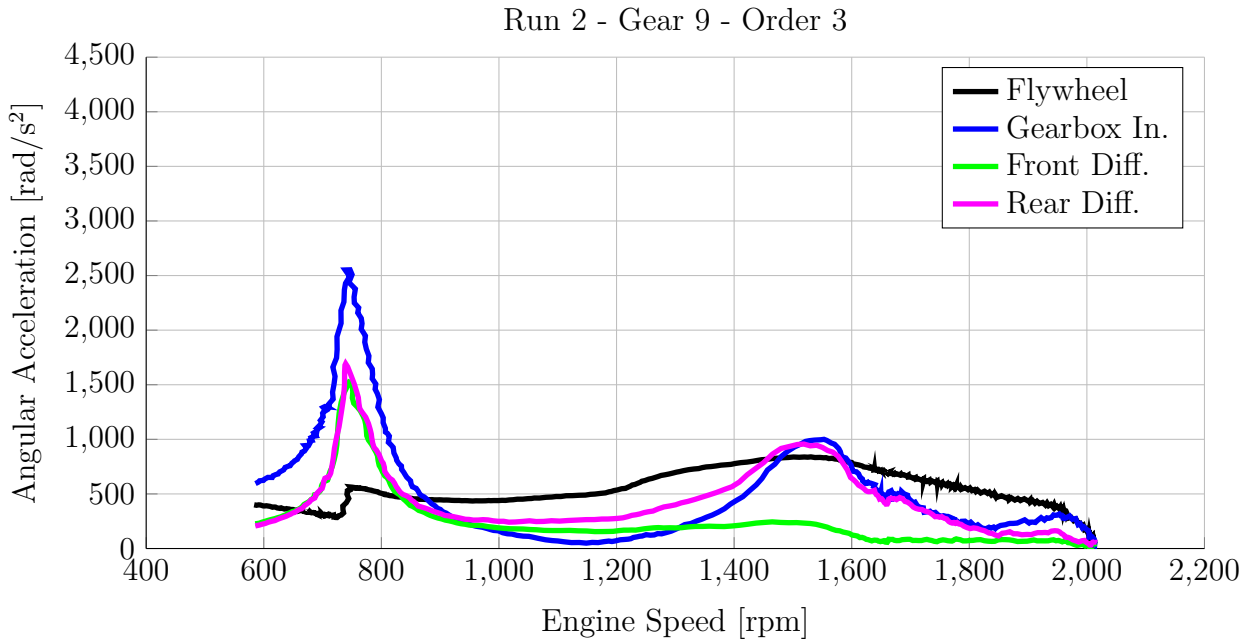


Figure 2.27: Results of the 3rd order obtained in Run 2 at 9th gear.

When at the 7th and 8th gears, in the first amplification in Run 1, between 800 and 1,000 rpm, the amplitude of the gearbox input was much higher than the amplitude of the differentials. At the 9th gear, however, this amplitude in Run 1 reached a maximum of 2,000 rad/s², while the peak amplitude of the differentials raised to approximately 1,250 rad/s². Both peaks occurred at 800 rpm. In Run 2 the same trend can be observed, but the peaks occurred at 750 rpm due to the lower torsional stiffness of the clutch disk used in this run.

The second amplification found between 1,400 and 1,600 rpm could not be identified on the results from Run 1. On Run 2, however, this amplification becomes evident, but in this case, differently from the previous ones, both the rear differential and the gearbox input have similar amplitudes, while the front differential vibrates with lower intensity.

The 6th order results for Runs 1 and 2 do not exhibit any significant amplification, and hence these graphics are going to be suppressed. The 3rd order results for Runs 3 and 4 are shown in Figs. 2.28 and 2.29, respectively.

The amount of friction torque in the clutch disk used for Run 3 was once more not enough to control the first resonance, yet the peak amplitude of the gearbox input was

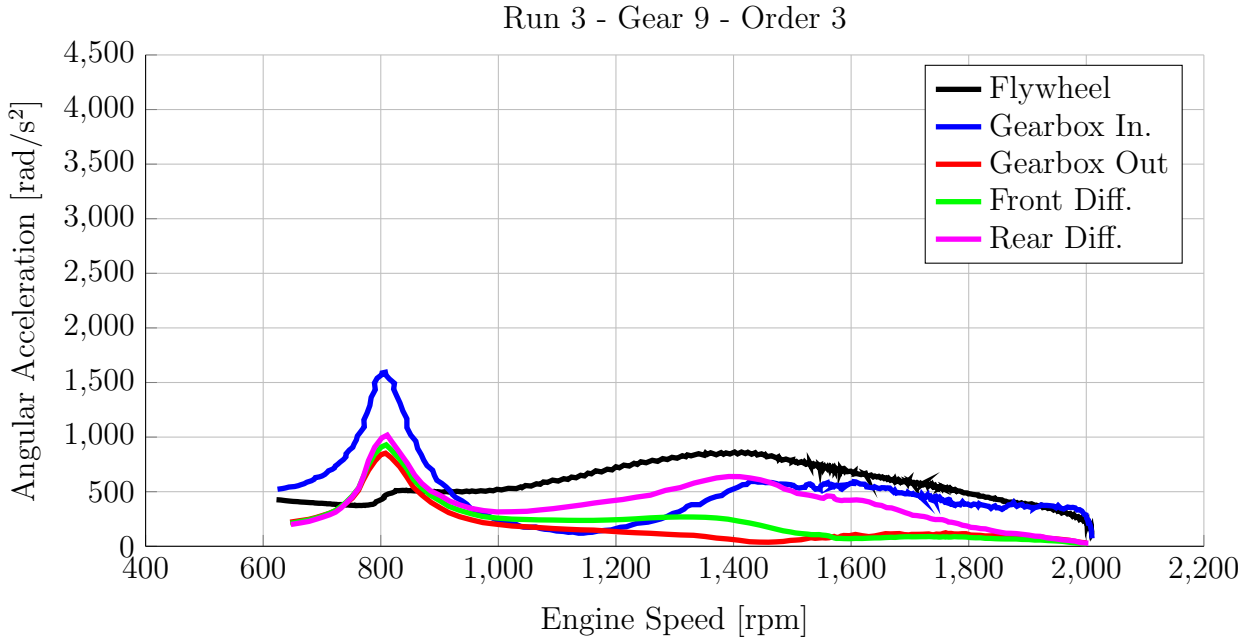


Figure 2.28: Results of the 3rd order obtained in Run 3 at 9th gear.

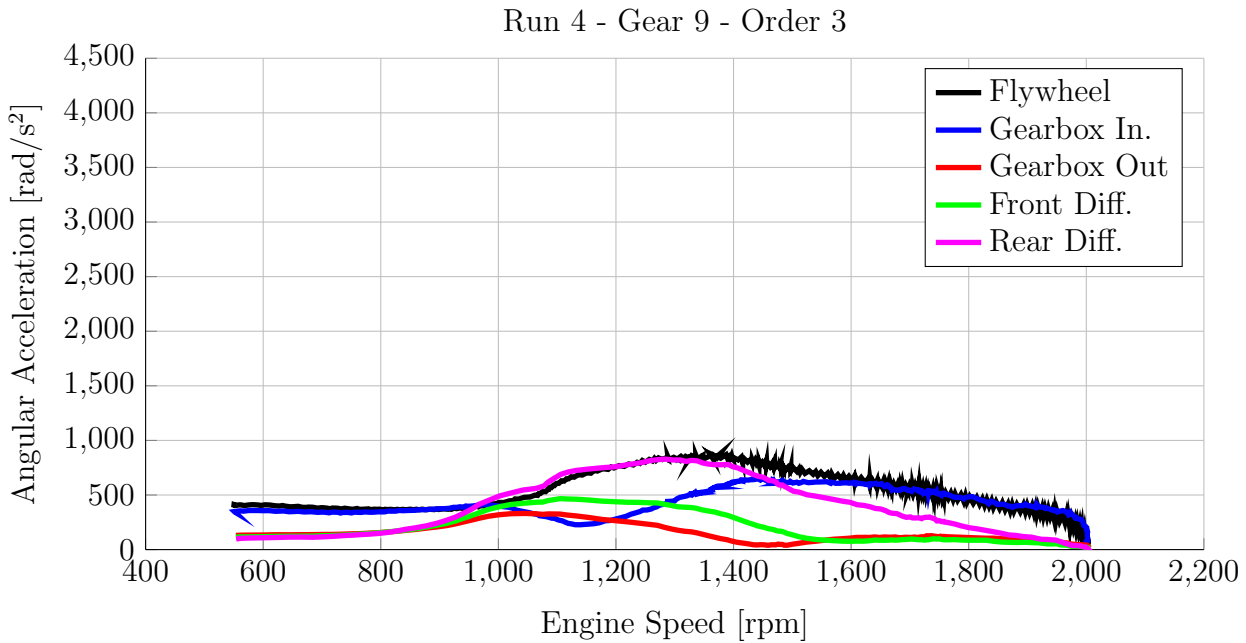


Figure 2.29: Results of the 3rd order obtained in Run 4 at 9th gear.

lowered to 1,500 rad/s². It is not possible to spot an amplification near 1,400 rpm, but the behavior of the gearbox output and differentials is the same found in previous cases: while the gearbox output vibrates very little, there is some amplitude on the front differential and the greatest intensity is found on the rear differential.

Major differences are found on Run 4, in which it is possible to see that the amplitude of vibration of the rear differential is very close to the amplitude of excitation from 900 rpm on. There is no significant difference on the amplitudes of the other measurement points when compared to previously presented tests. The 6th order results for this gear on Runs 3 and 4 were similar to the ones found when using the 7th gear, therefore these results will be suppressed.

The qualitative differences found on this gear, related to the previous ones, mainly at the first amplification range, are explained by the fact that from the 1st to the 8th gears the range-change group is set to the position L (Low), and from the 9th to the 16th gears, it is set to the position H (High), what alters the dynamic behavior of the system⁴.

2.3.4 Analysis of the Torsional Behavior at 10th to 14th Gears

The torsional behavior of the powertrain for gears from the 10th to the 14th was qualitatively similar to the behavior found at the tests using the 9th gear. The only differences lied in the first amplification range. As the gear increased, the engine speed at which the amplification would occur decreased. Also, the amplitude at the rear differential increased from lower to higher gears, when compared to the amplitude at the gearbox input. These trends can be seen in Figs. from 2.30 to 2.34, where the 3rd order results from Run 1 are shown for these gears, although in Fig. 2.34 the first amplification is not well represented because it occurs too close to the engine idle speed.

With these measurements it is now possible to understand the behavior of this powertrain at drive condition when gears from the 7th to the 14th are selected. The next step is to build a mathematical model that is able to represent the torsional dynamics of such system.

⁴The powerflow diagram of the gearbox, extracted from the manufacturer's maintenance manual is shown in Appendix A.1.

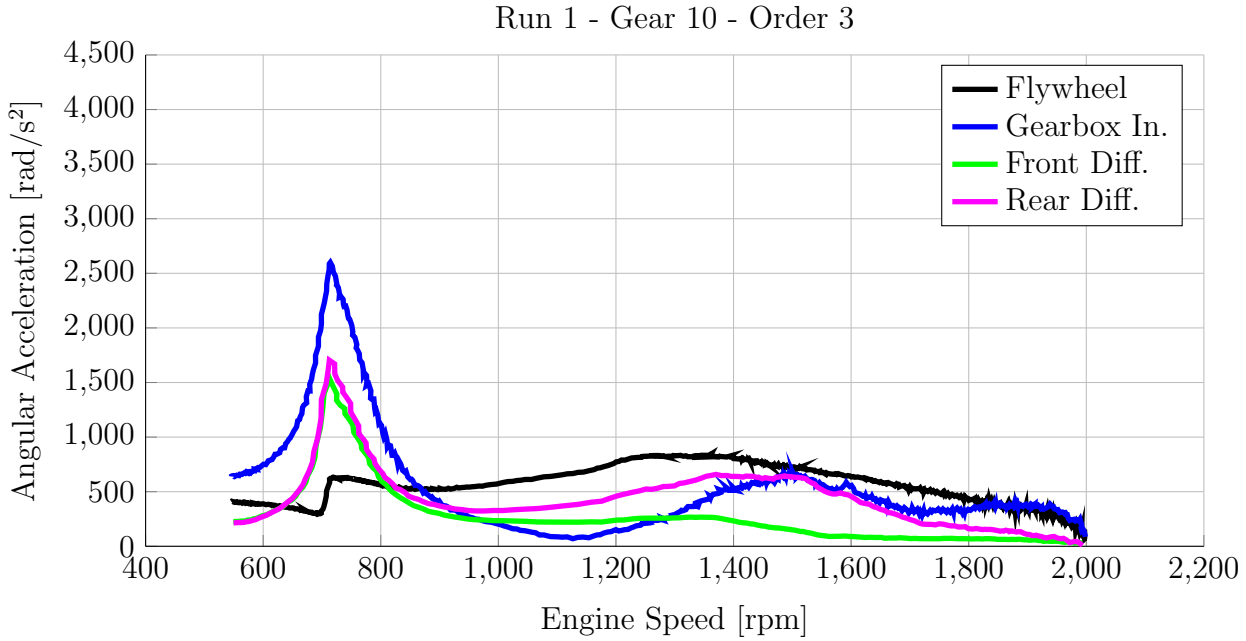


Figure 2.30: Results of the 3rd order obtained in Run 1 at 10th gear.

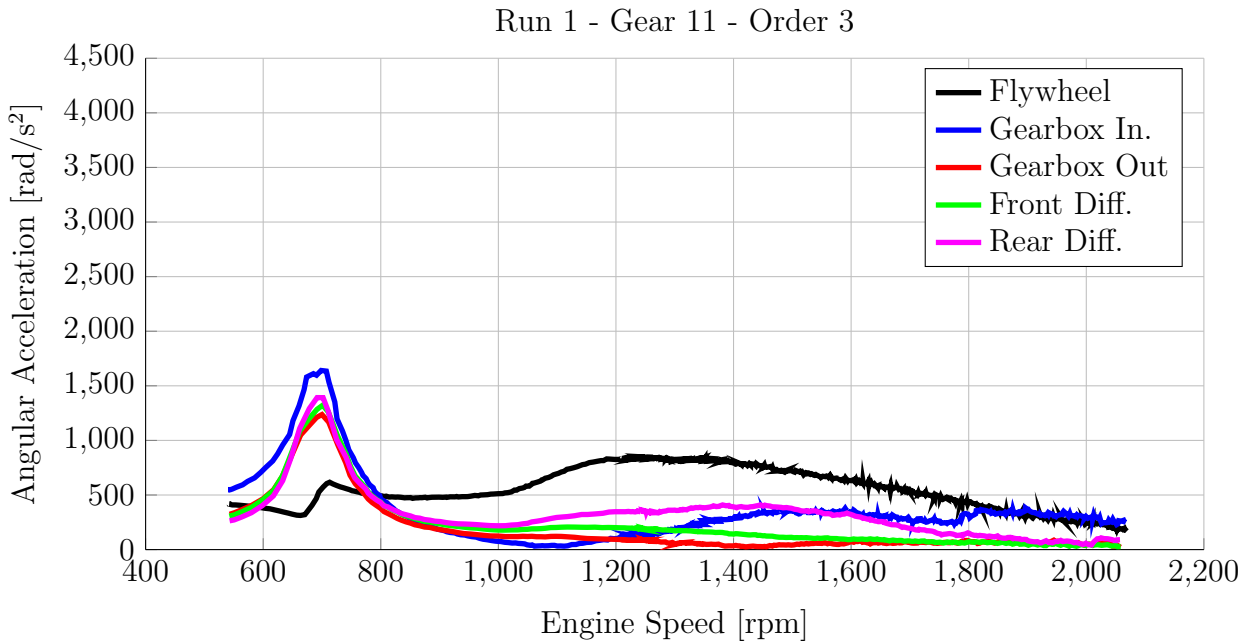


Figure 2.31: Results of the 3rd order obtained in Run 1 at 11th gear.

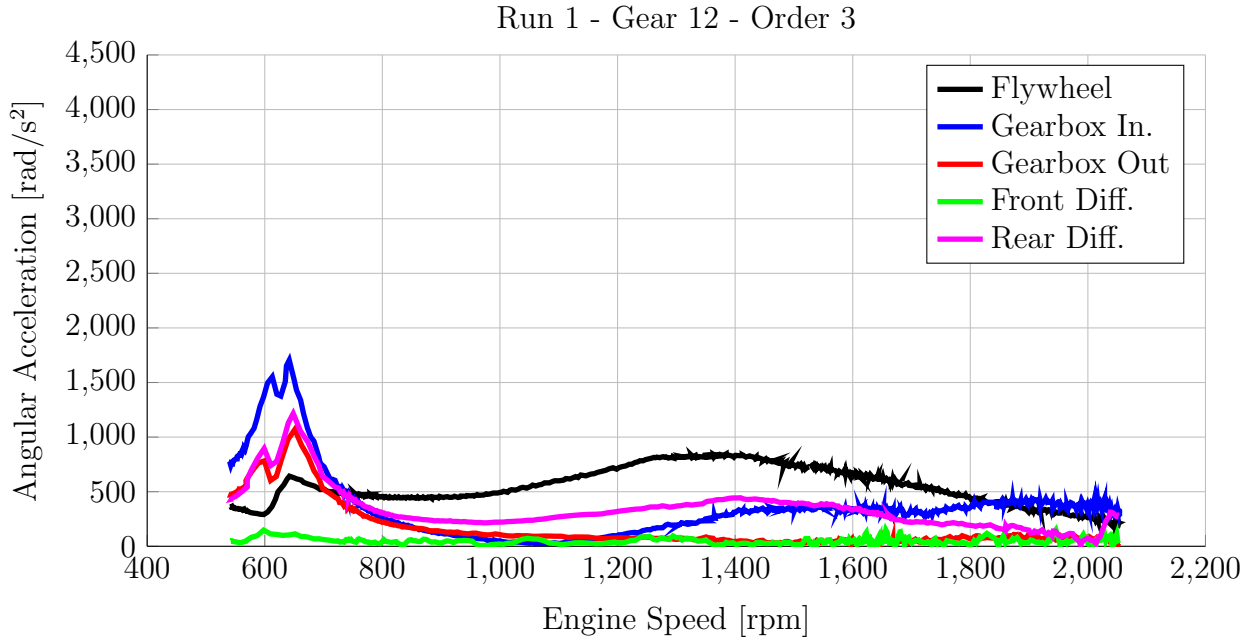


Figure 2.32: Results of the 3rd order obtained in Run 1 at 12th gear.

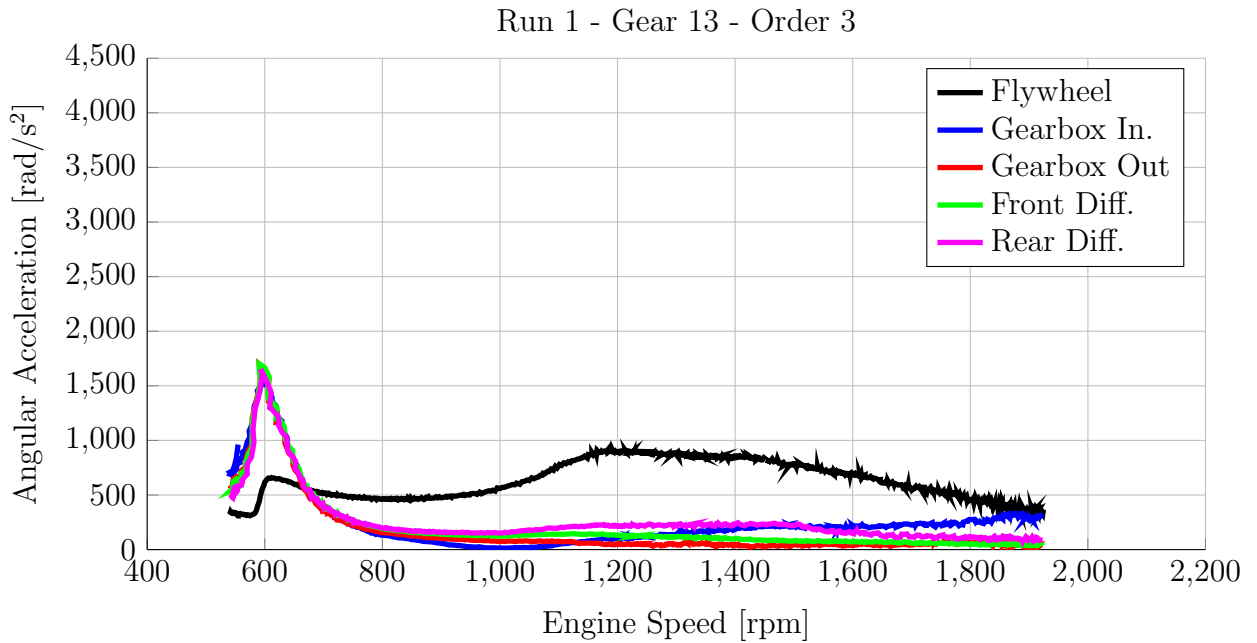


Figure 2.33: Results of the 3rd order obtained in Run 1 at 13th gear.

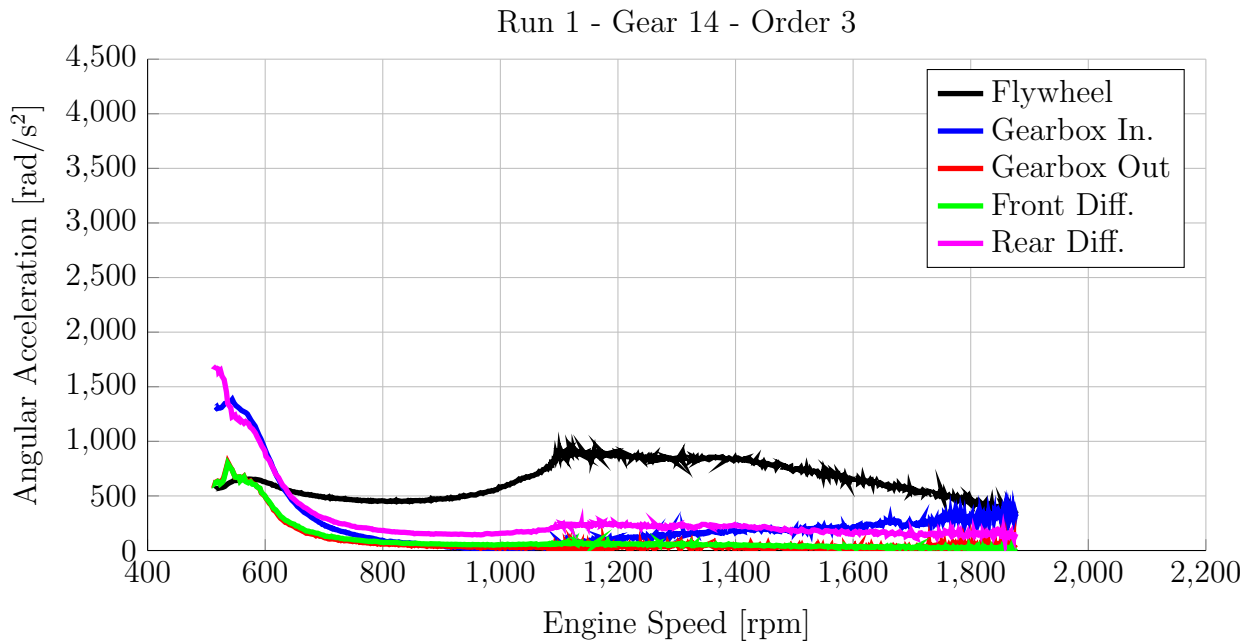


Figure 2.34: Results of the 3rd order obtained in Run 1 at 14th gear.

2.4 Part IV: Mathematical Modeling and Model Validation

At this stage of the investigation, much is known about the order content in torque provided by the engine, the dynamic behavior of the system and also important parameters that were not available at first. It is now possible to build a mathematical model that is able to represent the dynamics of the powertrain under investigation properly, so that the CPVA to be installed on it can be designed and virtually tested.

In this section, two models are going to be built for the powertrain, being the first for the condition when the eighth gear is shifted, and the second for when the ninth gear is shifted. These two gears have been chosen because they represent extremely different configurations in the gearbox. The fact is that one design of pendulum must be robust enough to diminish vibration no matter what gear is selected. However, it is shown in Chapter 3 that the tuning of the pendulum depends only on geometrical parameters that do not change when different gears are shifted. Hence, the tests with two different models aim at showing that the pendulum must work for different conditions.

The drive rattle measurements play an important role on the modeling process, because the results provide important information to update or validate the model. The first feature to be taken into account is that, although several tests were performed in different conditions, such as different gears, slightly different road surfaces, different clutch disks and so on, the vibration generated by the engine has shown no relevant difference. This can be seen in Figs. 2.35 and 2.36.

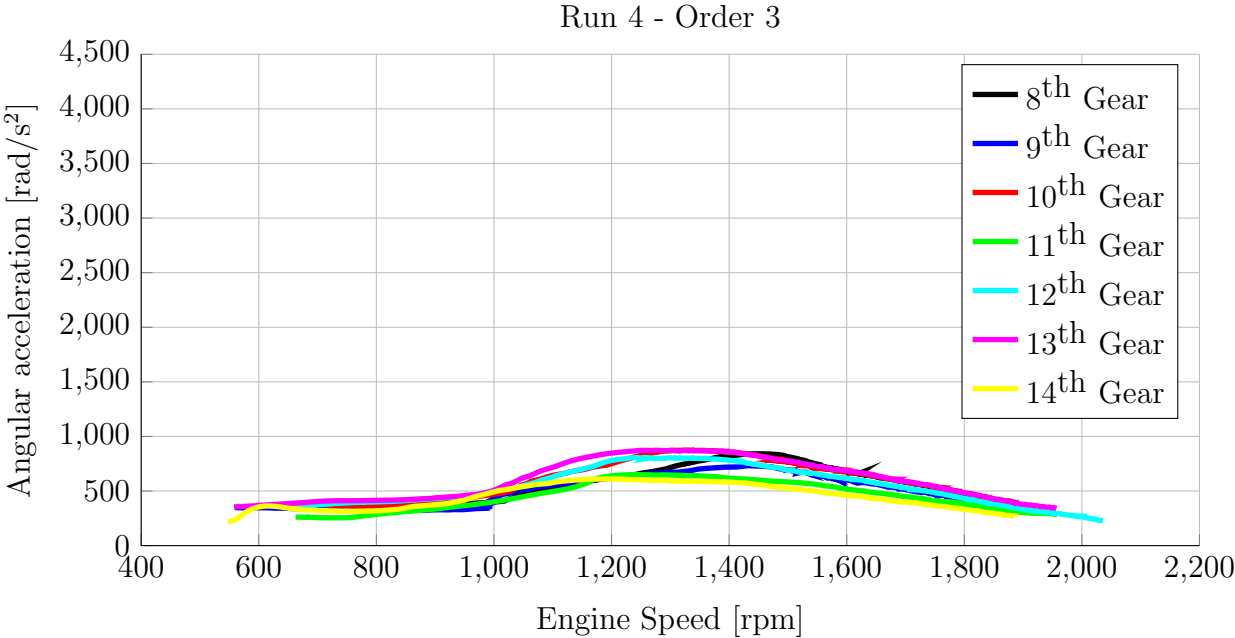


Figure 2.35: Angular acceleration of the flywheel at third order for different gears.

Regarding the third order, the greatest difference between the flywheel acceleration on different tests is found between 1,100 and 1,500 rpm. Yet there seems to be a difference of nearly 300 rad/s², from practical experience it is known that this difference is not capable of generating noticeable subjective change on the acoustic behavior of the powertrain, specially in this range. Furthermore, the critical speeds that could induce gear rattle lie between 600 and 850 rpm. In this range, the engine behaved equivalently in all tests.

The sixth order angular acceleration at the flywheel has shown an even more uniform behavior than the one found in third order. Besides, it was not possible to detect any noise or undesired amplification on the tests that could have been caused by the sixth order content.

These results have an important impact on the modeling of the powertrain. Once the

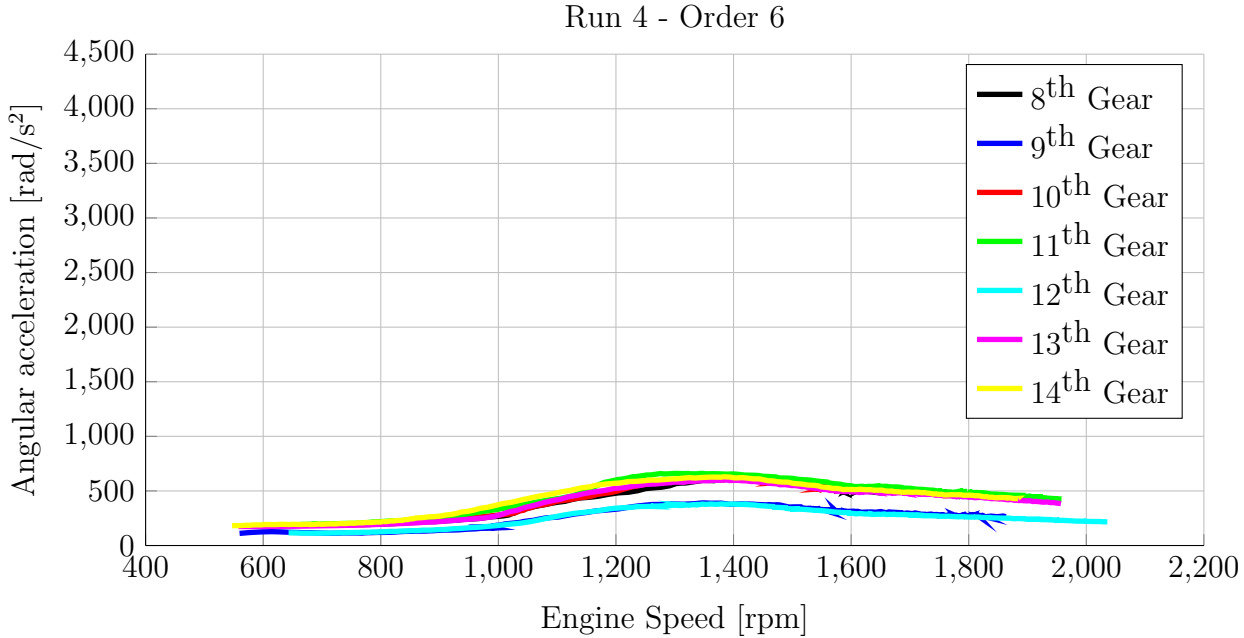


Figure 2.36: Angular acceleration of the flywheel at sixth order for different gears.

dynamics of the powertrain is not significantly relevant to cause change on the dynamic behavior of the flywheel, it means that if measurements of the torsional behavior of the flywheel are available, the angular displacement, speed and acceleration of the flywheel can be imposed on the model. The direct consequence is that it is not necessary to estimate the inertia of the flywheel, the clutch cover, pressure plate and the part of the clutch disk which remains stuck to the flywheel during the tests.

Evidently, there is a part on the dynamics of the flywheel that is influenced by the dynamics of the powertrain. It becomes more evident when studying low frequency phenomena, such as *shuffle*, as in the work of Simionatto (2011). For this phenomenon, which happens usually between 2 and 8 Hz, the motion of the flywheel is extremely relevant. For higher frequencies, however, as the flywheel is a huge inertia, in comparison to the other components of the system, it isolates the engine dynamics from the powertrain dynamics and vice versa, acting as a low pass filter.

The reduced need for data in order to perform torsional simulation of powertrains, yet at the cost of some simplifications, can be considered an advantage. This happens because the parts that compose a powertrain are usually produced by different industries which strug-

gle to protect their knowledge. Yet a system approach is the only way to deal with torsional vibrations in these systems, many of the necessary data to make a detailed approach are simply not made available by the manufacturers, for being considered confidential information. This is also the case of the gearbox in the vehicle under investigation.

The manufacturers of this gearbox only allowed the access to some information about their product. Among the information they could provide, the only data that were relevant for the simulation of the powertrain were the gear ratios and the equivalent inertia of the gearbox at each gear, taking the input shaft as reference. Once the calculations of the inertias does not take into account any possible deformation of the shafts of the gearbox, the use of these data imply that the transmission, in this model, is considered to be a rigid body.

In Figs. from 2.13 to 2.34, where the results of torsional vibration experiments are shown, in the graphics where there are both the gearbox input (blue) and output (red) signals, it is possible to see that the transmission cannot be considered a rigid body in the whole range of engine speeds. However, for rotating speeds up to 1000 rpm, this is a good approximation, i.e., it behaves as a rigid body in the rattle noise range.

The fact that the gearbox behaves as a rigid body in this range is known. It is found on the works of Miyasato (2011), Miyasato *et al.* (2011a), Miyasato *et al.* (2011b), Miyasato *et al.* (2013) and Lemes (2015 *planned*). Therefore, it is expected that the gear rattle phenomenon is well represented by this model. Yet this is not the best approximation for higher frequencies, in this range the amplitude of vibration of the differentials is much more significant than the amplitude of vibration of the gearbox output. Hence, good results are still expected for the second amplification range, between 1400 and 1600 rpm.

The modeling technique is also worth mentioning. The powertrain, apart from some nonlinearities, can be modeled through inertia, damping and stiffness matrices, i.e. it can be represented by a second order linear model, similarly to what is done in structural dynamics. The difference, however, is that even these linear matrices may account for kinematic constraints, like gearings, and this may complicate the visualization of the mode shapes.

One way to eliminate the gear ratios is to simply apply a coordinate transformation on the mode shape, so that the gear ratios are eliminated. This method is valid but it does not apply to the case of this work, because some of the data, such as the equivalent inertia of the gearbox, has been calculated taking as a reference the input shaft. There is

another method, however, shown in the work of Ligier *et al.* (2002), in which the inertias and stiffnesses of the powertrain components are calculated in such a way that the eigenfrequencies of the equivalent system are equal to the ones from the original one, and the mode shapes are the same that would have been obtained from the original system, after making the coordinate transformation in order to eliminate the gearing effects. This method is introduced in Appendix A.2.

The inertia of the differentials has been made available in the same way of the gearbox, i.e. the manufacturers provided an equivalent inertia taking the input shaft as reference. Once the differentials do not have inner shafts, they can be considered as rigid bodies in the whole working range. The inertia of the wheels and of the vehicle have been estimated. Yet the estimation was performed carefully, these parameters have shown not to influence the eigenfrequencies of interest.

Regarding the stiffness of the components of the powertrain, all of them have been measured with relatively high precision, except for the torsional stiffness of the tires. As shown in the work of Drexl (1999), this parameter influences a mode whose eigenfrequency is below the eigenfrequency related to rattle noise. Apart from being below the idle speed of the vehicle, this mode is usually very damped and hence not very influential for this analysis.

In fact, there is a lot of knowledge and experience on the torsional modeling and simulation of commercial vehicle powertrains. This is due to the fact that, yet different, they exhibit some similarities that make their dynamic behavior very alike. Subjectively, it is possible to notice that in some vehicles the presence of rattle noise, for instance, is more critical than in others. However, apart from the torsional dynamics, the acoustic sensitivity and sound insulation play very important roles on the propagation and isolation of noise, respectively.

As has already been mentioned, the inertias and stiffnesses available are enough to model the powertrain and obtain a good estimation of its eigenfrequencies and mode shapes, with a conservative model. However, this model is still not representative for calculating the final amplitudes of response for the main orders of vibration. This happens because, apart from the inner friction on the clutch disk, there are other sources of energy dissipation, such as oil in the gearbox and differentials, roller bearings, hysteresis of shafts and others, which are the key to determine the amplitude of vibration of the several parts of the powertrain, specially at amplification conditions, which must be well represented in order to make good

simulation of the behavior and performance of the CPVA.

The model of energy dissipation for the powertrain can be very complicated to describe, and the models that are available usually represent a single source of energy dissipation (usually drag torque in the gearbox) for very specific conditions. Furthermore they depend on several parameters which are usually not available. On the other hand, energy dissipation is usually avoided in the powertrain, because it leads directly to efficiency loss and increased fuel consumption. Hence, usually the greatest source of energy dissipation is the friction in the clutch disk, yet the other sources cannot be considered negligible.

One of the first attempts of representing the energy dissipation on the powertrain would be to simply neglect all the other energy dissipating features and consider that there is only dry friction in the clutch disk. The disadvantage of doing so is that the Coulomb friction is not capable of keeping the amplitude of the system from growing indefinitely on resonant conditions. Hence, when amplifications are reached, the model would not be representative (Duque *et al.* (2004)). Additionally, the friction in the clutch disk is sensitive to wear, temperature, relative speed and other factors, what makes of the choice of Coulomb friction only a too simplistic approach.

A simple approach for representing energy dissipation in such systems, which has brought good results in practice, is proposed in this work. It makes use of the tests with clutch disks whose inner friction is as low as possible, and the task is to represent the energy dissipation in the powertrain for low and high levels of friction in the clutch disk.

The first part of this procedure is to perform measurements using a clutch disk with minimal inner friction. From this procedure it will not only be possible to obtain the angular displacement, speed and acceleration to be imposed on the model, but also to obtain the levels of vibration of each measurement point of the powertrain over the whole range. These are referred to as “measurement curves”.

The second step is to build a conservative model of the powertrain which is capable of representing the eigenfrequencies as well as possible. Even if all the inertia and stiffness data are available, sometimes it is necessary to adjust some parameters to attenuate the effect of some simplifications.

The third step is to diagonalize this linear conservative model and to insert a damping

factor for each mode separately. The calculation of the damping factors is done through least squares minimization, and the cost function is the difference of the amplitudes from the measurement curves and from the simulated ones.

The use of this kind of damping is not usually recommended. For torsional powertrain dynamics, however, this model is very representative. This happens because, apart from the friction in the clutch disk, there is too few energy dissipation in the rest of the powertrain. Because of this, in tests with clutch disks with low friction, it is possible to observe that the phase between the measurement points is very close to 0° or 180° . This effect can be seen in Fig. 2.37.

In Fig. 2.37 are plotted the oscillating parts of the angular speeds in the time domain of the five measurement points. In the upper graphic, the system had still not passed through the gear rattle amplification, while in the lower one, the system had just passed through it. If the system were to vibrate with phases different from 0° or 180° , then it would be easier to spot it in these conditions. However, yet it is not possible to tell precisely how much the phase between the measurement points is, it is evident that they are close to the two theoretical values.

This makes of the classical damping a good candidate to represent the small amount of energy dissipation there is in this system, when the clutch disk's energy dissipation capability is reduced to its minimum. If the powertrain has to be simulated with higher amount of friction in the clutch disk, the procedure is then to insert dry friction on it in order to complement the amount that is not represented by the classical damping.

For instance, if one has to simulate a powertrain with $200Nm$ of friction torque in the clutch disk, and a real clutch disk with a minimum of $10Nm$ of friction is available, the first step is to perform measurements with the $10Nm$ disk. Then, they have to adjust a conservative model and perform the optimization with classical damping, so that it represents all the intrinsic losses of the powertrain plus the $10Nm$ of friction torque. Finally, they have to include the remaining $190Nm$ of dry friction in the clutch disk and then perform the simulation.

With all these considerations, it is now possible to build a model that represents the dynamics of the powertrain under investigation. This model is shown in the next section.

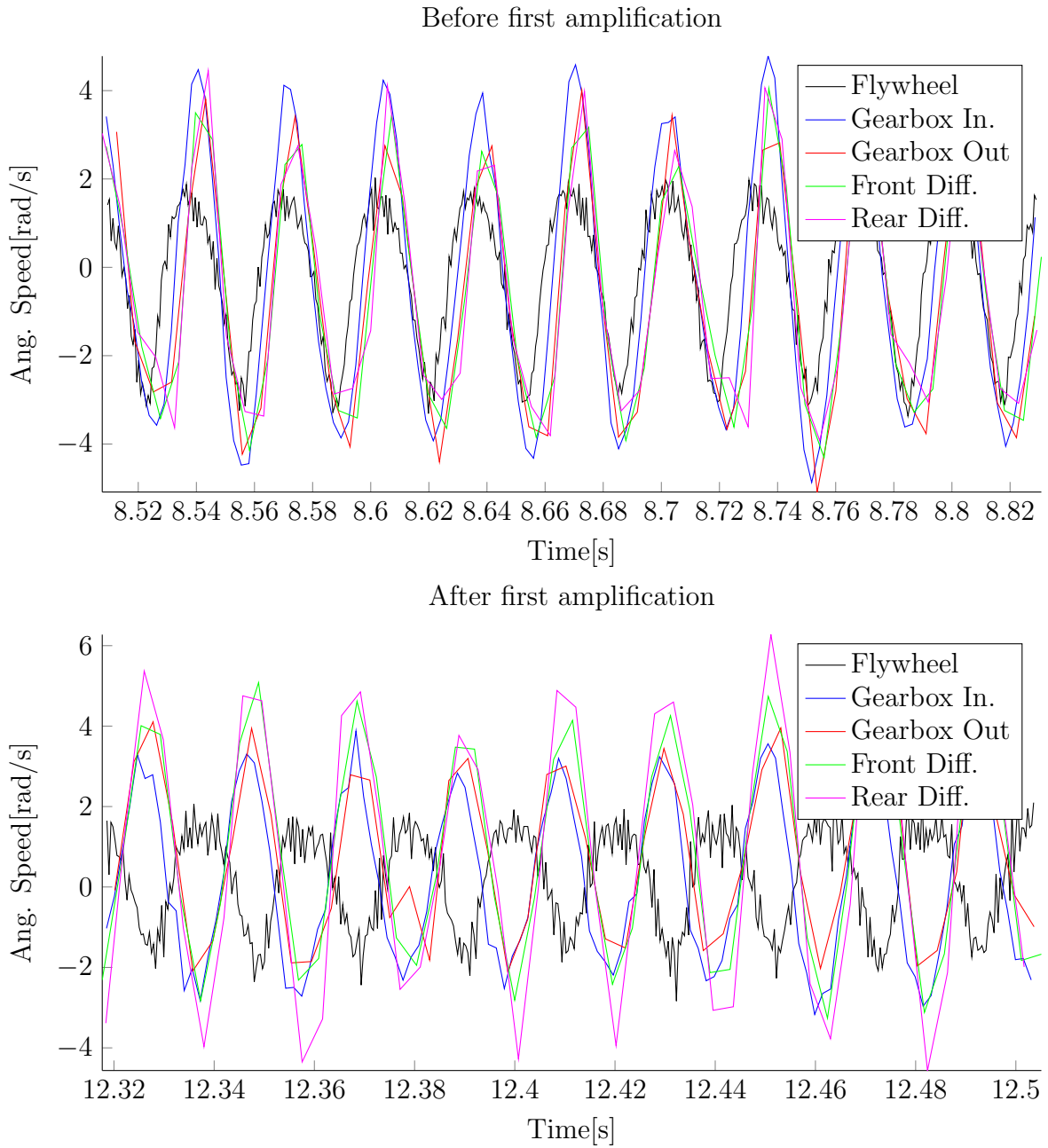


Figure 2.37: Time response of the measurement points immediately before and after the first amplification (Run 1 - 8th gear).

2.4.1 Development of Linear Conservative Model of the Powertrain

An important feature to consider on the modeling of powertrains is the balance between stiffnesses and inertias. If each shaft is modeled as a stiffness and each rotor (a gear or a disk) is modeled as an inertia, there is a huge chance that the resulting model will have many degrees of freedom, and more importantly, eigenfrequencies that are far from what is observed in practice.

The eigenfrequencies for this application are expected to be all below 200Hz. If there is an extremely high eigenfrequency, it means that there must be more degrees of freedom than the necessary to represent the powertrain in its operating range. At this point, reasonable kinematic constraints are a good choice to reduce the model and obtain a smaller and still representative one. As a matter of fact, frequency range model reduction is also a good technique, and in general leads to the same results.

Taking into consideration that the technique presented on Appendix A.2 was used, the idealization of the powertrain is shown in Fig. 2.38.

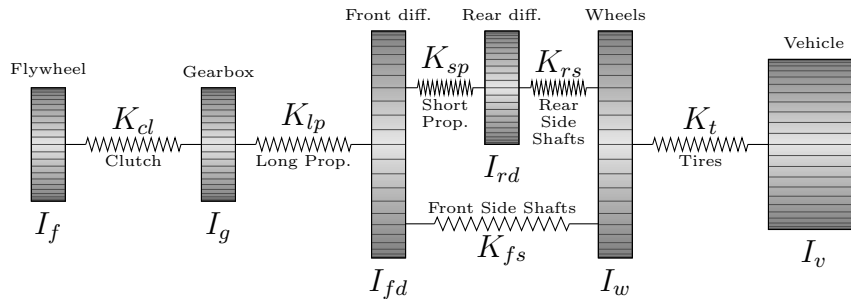


Figure 2.38: Idealization of the powertrain.

The flywheel is represented in the model shown in Fig. 2.38, but as it has already been mentioned, its motion is going to be imposed. The link between the flywheel and the gearbox is a linear torsional spring that represents the drive stiffness of the clutch disk. It can be represented as a linear spring because, during the tests, although the stiffness of the clutch disk has multiple stages, the vehicle operated only at the drive stiffness.

The gearbox is accounted for as a single inertia. In this inertia there is also part of the inertia of the long propeller shaft, which links the gearbox to the front differential and is

represented by a torsional spring. It must be reinforced here that the gearings have already been accounted for due to the modeling technique that has been used, and hence they do not need to be represented in this illustration.

The front differential is linked to the rear differential through the stiffness that represents the short propeller shaft and also to a single inertia, that represent the wheels, through a stiffness that represents the combined stiffness of the front side shafts. The rear differential is also linked to the inertia that represents the wheels through a stiffness that represents the combined stiffness of the rear side shafts. The combined stiffnesses of the side shafts and the wheels represented by a single inertia are all due to a kinematic constraint better explained in the following.

One must notice that this vehicle has four driving wheels, each one connected to a side shaft of slightly different stiffness. The presence of these bodies on the model would lead to some modes with near eigenfrequencies but few physical meaning (e.g. wheels going to opposite directions while the rest of the powertrain does not move). Furthermore, these modes are hardly excitable by an oscillating torque that acts on the flywheel.

In order to eliminate this undesired feature, it is considered that the vehicle moves on a straight line and that the deformation of the chassis is negligible, so that the wheels move together as if they were a single body, the aforementioned kinematic constraint. This simplification allows the wheels to be represented by a single inertia and the side shafts from each differential to be represented by a single stiffness. Also, as the vehicle is moving on a straight line, only the final ratio of the differential gear has to be considered, i.e. the bevel gear remains locked.

The wheels are connected to the inertia that represents the vehicle through the torsional stiffness of the tires. The latter inertia is calculated by simply multiplying the mass of the vehicle by the square of the dynamic radius of the driving wheels, as shown in the work of Simionatto (2011).

With this model, it is now possible to compare its response to the measurements in order to calculate an equivalent amount of modal damping, which represents all the inner energy losses of the powertrain. This is an essential step in order to obtain a representative model, and it is performed on the next section.

2.4.2 Calculation of Equivalent Damping for the Linear Model of the Powertrain

The goal to be achieved in this section is to calculate an equivalent amount of (linear) damping in order to make the linear model of the powertrain more representative. To do so, it was chosen to attribute a modal damping ratio to every one of the modes of the system, in the following way: let a linear time-invariant conservative system be represented in the form:

$$\mathbf{M}\ddot{\mathbf{x}} + \mathbf{K}\mathbf{x} = \mathbf{f}(t) \quad (2.1)$$

Also let the modal matrix⁵ of such system be named Φ and a diagonal matrix where every nonzero element is an eigenfrequency of the system be named ω_i . Using the coordinate transformation $\mathbf{x} = \Phi\mathbf{q}$, where \mathbf{q} is the vector of generalized coordinates, it is possible to diagonalize Eq. (2.1) as follows:

$$\begin{aligned} \Phi^T \mathbf{M} \Phi \ddot{\mathbf{q}} + \Phi^T \mathbf{K} \Phi \mathbf{q} &= \Phi^T \mathbf{f}(t) \\ \ddot{\mathbf{q}} + \omega_i^2 \mathbf{q} &= \Phi^T \mathbf{f}(t) \end{aligned} \quad (2.2)$$

The next step is to define a diagonal matrix which has a modal damping ratio at each element of its diagonal, called ζ_i . With this matrix it is possible to insert damping on Eq. (2.2) as follows:

$$\ddot{\mathbf{q}} + 2\zeta_i \omega_i \dot{\mathbf{q}} + \omega_i^2 \mathbf{q} = \Phi^T \mathbf{f}(t) \quad (2.3)$$

Now, using the transformation $\mathbf{q} = \Phi^{-1}\mathbf{x}$, it is possible to go back to the physical coordinates and obtain an equation with a damping matrix, such as:

$$\mathbf{M}\ddot{\mathbf{x}} + \mathbf{C}\dot{\mathbf{x}} + \mathbf{K}\mathbf{x} = \mathbf{f}(t) \quad (2.4)$$

,being \mathbf{C} given by:

$$\mathbf{C} = 2(\Phi^T)^{-1} \zeta_i \omega_i \Phi^{-1} \quad (2.5)$$

It is known that the system represented on Eq. (2.4) is not always diagonalizable. It is only possible to diagonalize it for some special forms of the matrix \mathbf{C} . In these cases, this

⁵In this case it is normalized by the mass matrix.

type of damping is called *classical damping*⁶, and it has some drawbacks to be mentioned.

A direct consequence to the fact that the system is diagonalizable is that the mode shapes of the dissipative system are exactly equal to the ones from the conservative system. It means that the phase of the degrees of freedom is constrained to be either 0 or 180° regardless of the amount of damping. For many applications, this constraint does not apply, and hence results are poor.

In this work, however, this constraint represents well what happens in the system, specially considering the fact that for the test of interest, energy dissipation was as low as possible for this system. An example of the phase between the degrees of freedom for critical conditions is shown in Fig. 2.37. The graphics in this figure shows the time response of the system right before and right after the first amplification. If there was to be some phase far from 0 or 180°, it should be more visible in these conditions.

Yet the modal damping approach is not the best model of damping, it has shown to bring good results to linear powertrain modeling, leading to good representativeness of the models, once the damping ratios have been calculated. In order to calculate them, the motion of the flywheel was imposed⁷ on the model, and then the amplitude of the angular acceleration of the model was simulated and compared to the measurements. The square of the difference between the simulation and the measurement was used as a cost function for the nonlinear least squares problem of finding the damping ratios that minimize it. The least squares method used to solve this problem was the “trust region reflective”, available in Matlab 2010® as the routine `lsqnonlin`.

The results for the 8th gear model are shown in Fig. 2.39. In the upper graphic are shown the 3rd order amplitudes of the measured angular acceleration, while in the lower one are shown the same results, but simulated instead of measured.

In the range of measurement, there are two relevant modes, one of them near 40Hz and the other near 74Hz. The first one is related to the gear rattle phenomenon, and the damping ratio calculated to it is of 6.9%. This mode shape is represented in Fig. 2.40 in two ways. The graphic entitled “Physical mode” shows the mode from the physical system, considering the gear ratios. In this graphic one can observe the real amplitudes found in

⁶Proportional damping is one type of classical damping, but there are others.

⁷In order to impose the motion of the flywheel, a simple yet generic procedure is proposed. It is shown in details in Appendix A.3.

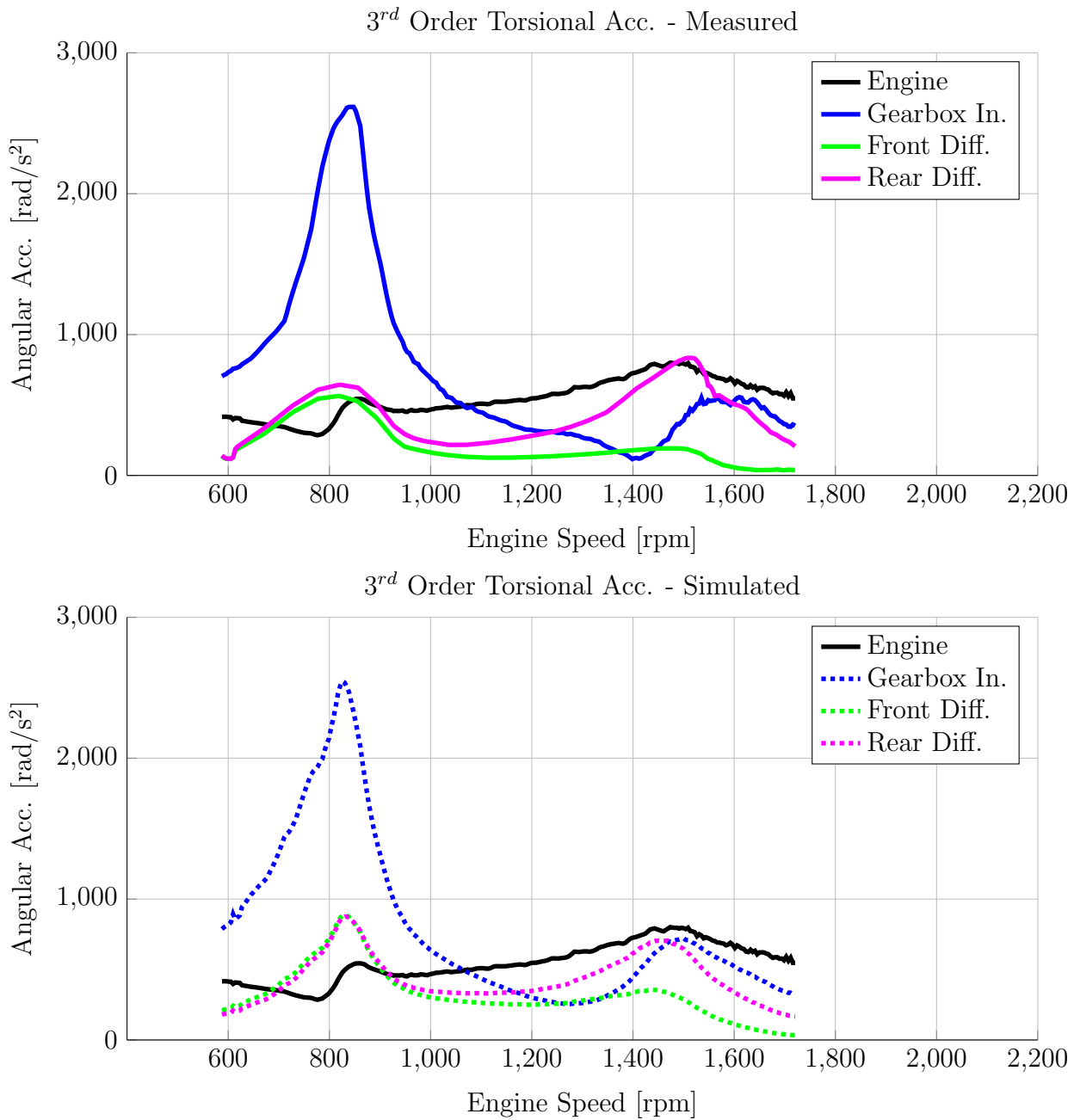


Figure 2.39: Measured and simulated amplitude responses for 8th gear - Run 1.

this mode shape in the real system. However, once it considers the gearings, it is difficult to know if the difference of amplitude between two degrees of freedom is because some element is being deflected or if it is just because of the gear ratio. In order to visualize this, it is better to analyze the graphic entitled “Mode w/o gearings”, where gearings are suppressed and then it is possible to visualize the deflection of the elements only. However, it does not

represent the physical amplitudes of vibration at that mode.

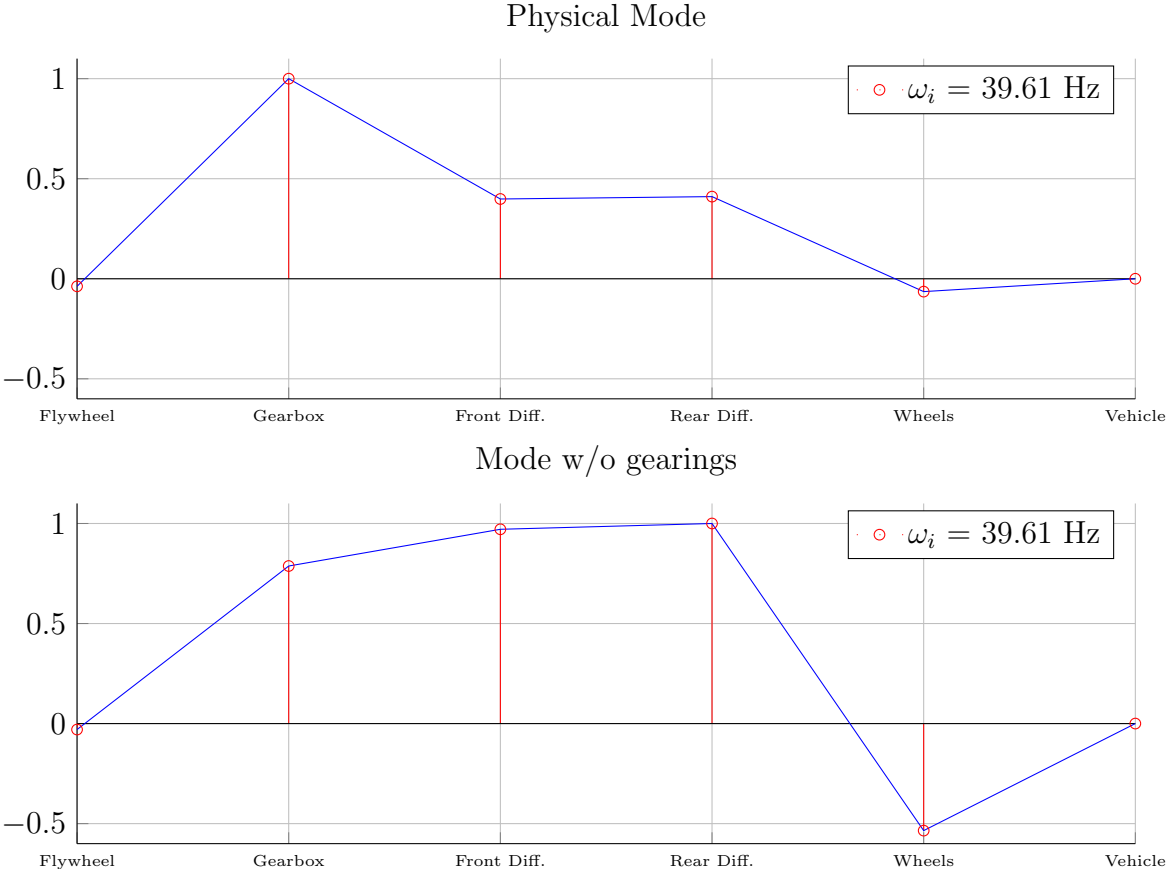


Figure 2.40: Physical mode and mode without gearings for gear rattle at 8th gear.

Regarding the first amplification, the simulated peak amplitude of the gearbox approached well the measured one (the blue curves in Fig. 2.39), while the peak amplitude at the differentials is slightly higher than the one found in the measurements. This must happen due to the fact that the theoretical mode shape differs a little from what is found in the experiment, because of simplifications, and also because the damping model chosen may not be accurate for that configuration. Also, the engine speed is varied under a *quasi-static* hypothesis, which is difficult to assure. Therefore, given the small difference between the amplitudes and the factors that could have caused it, it is possible to conclude that this model represents well the dynamics of the powertrain in the first amplification.

The second amplification is related to a mode shape shown in Fig. 2.41, and its damping ratio is of 8.2% in the model. The second amplification itself is not related to any noise or vibration that could possibly be subjectively evaluated as a problem, in this vehicle. As it

is possible to see in Fig. 2.41, it is related to a mode where the shafts twist, and twisting usually does not cause strong teeth impact. Nevertheless, both amplitudes of the gearbox and of the differentials are well represented, and match the relationships found in the mode shape.

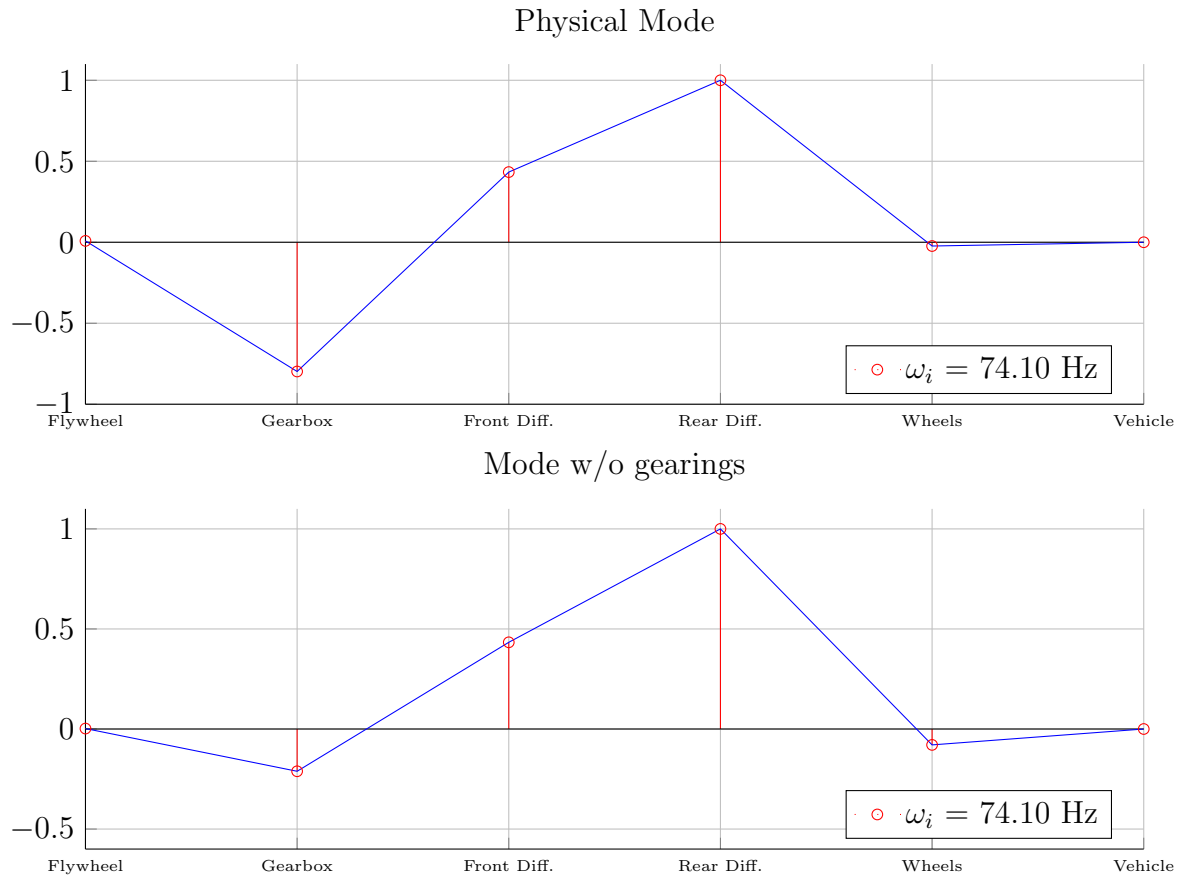


Figure 2.41: Physical mode and mode without gearings for second amplification at 8th gear.

Hence, the model proposed for the powertrain at the eighth gear is considered representative and is going to be used for further simulations. The results for the simulation of the powertrain at the ninth gear are shown in Fig. 2.42.

The mode shape related to the first amplification, around 800 rpm is shown in Fig. 2.43. Yet the amplitude found on the differentials is smaller in the simulation, compared to the experiment, the same ratio of the simulated is found on the rattle mode shown in this picture. Hence, this difference of amplitudes is due to some simplification, possibly for considering the gearbox as a rigid body. Even though, the amplitude at the gearbox is well represented, and this is important because high amplitudes in the gearbox may lead to undesirable rattle

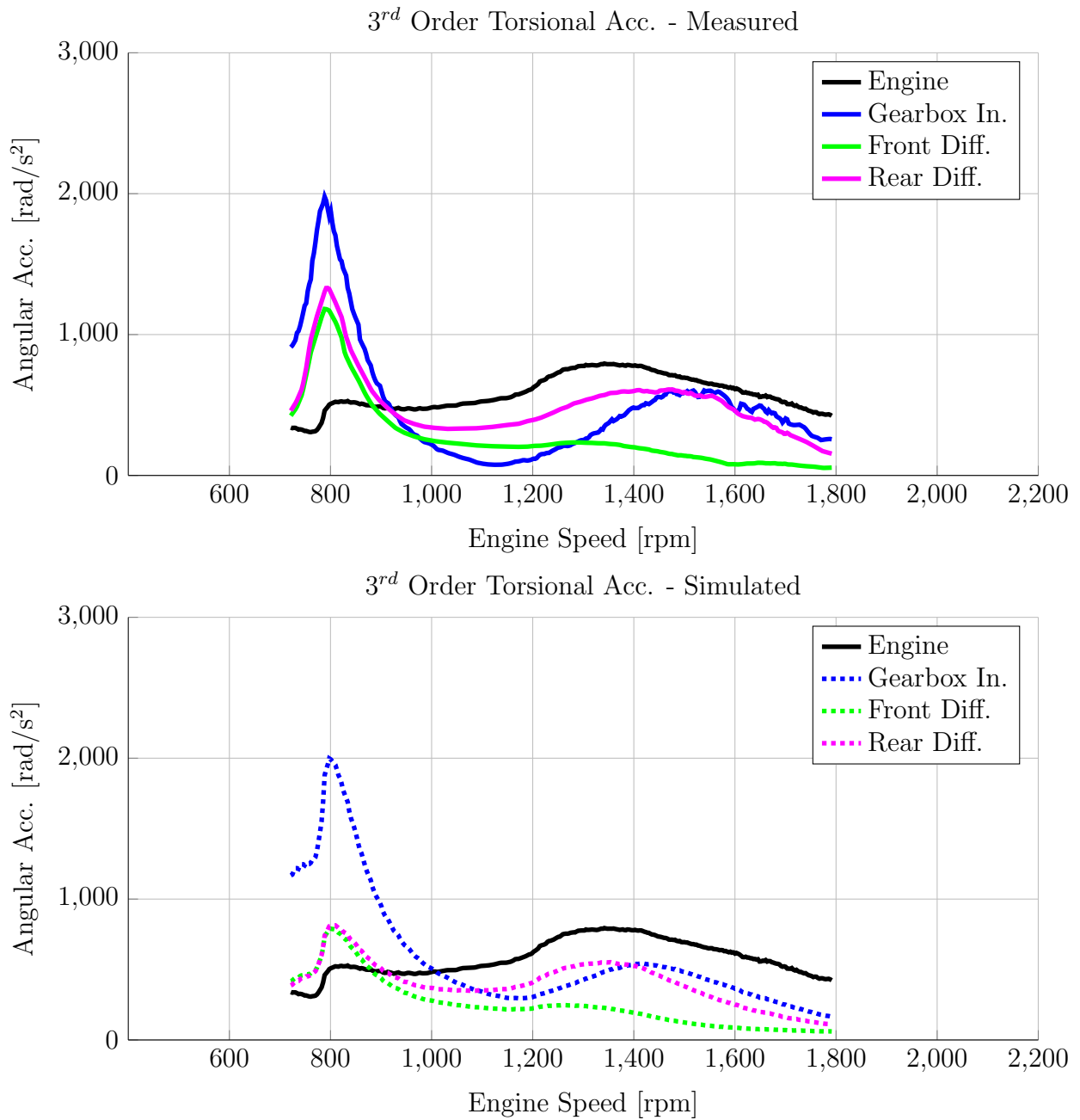


Figure 2.42: Measured and simulated amplitude responses for 9th gear - Run 1.

noise. The damping ratio calculated for this mode is of 9.9%.

The second amplification is related to a mode shape whose natural frequency is near $71Hz$. The calculated damping ratio is of 14.2% and the mode shape is shown in Fig. 2.44. In this case all the amplitudes have been well represented by the theoretical model. The

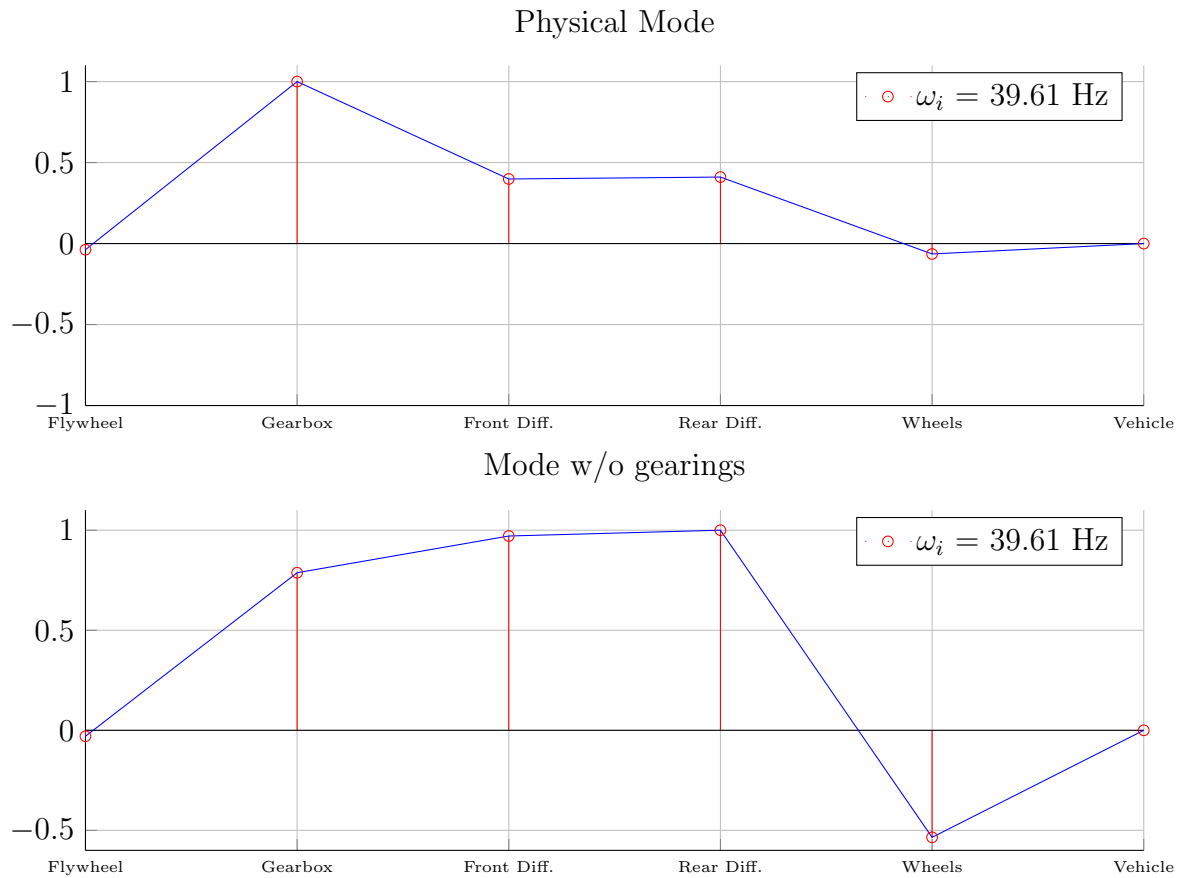


Figure 2.43: Physical mode and mode without gearings for gear rattle at 9th gear.

amplitude of the gearbox is a little underestimated above 1,500 rpm, but at this engine speed gear rattle is subjectively not present.

Therefore, the ninth gear model is also considered representative for the tests with the CPVA, and is going to be used for further simulations. The goal of this chapter, which was to recognize the powertrain and build representative models for further simulations has been achieved. In the next chapter, the reader will find theoretical aspects regarding passive vibration absorbers, mainly of the centrifugal pendulum type.

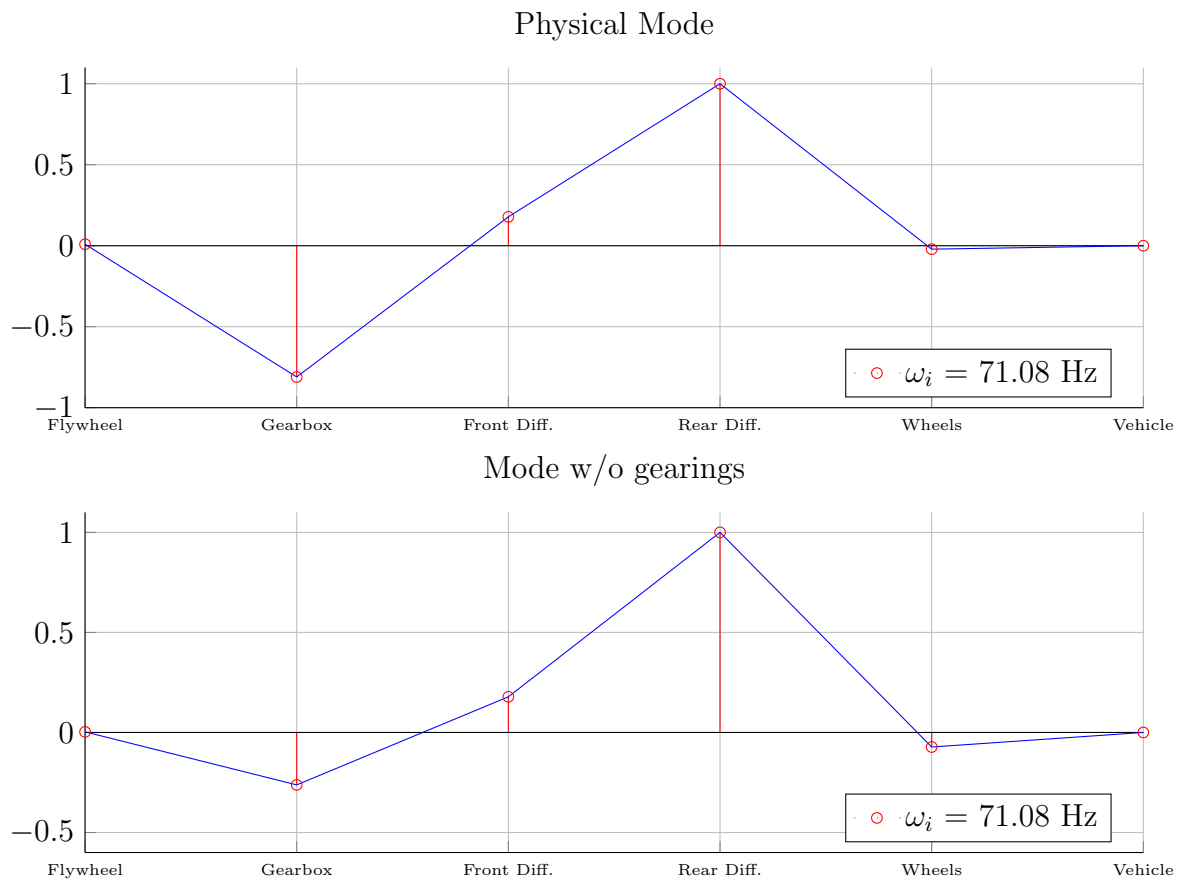


Figure 2.44: Physical mode and mode without gearings for second amplification at 9th gear.

3 Theoretical Aspects of Passive Vibration Absorbers

Passive Vibration Absorbers are auxiliary devices designed to be linked to a specific structure in a way that the dynamic behavior of the new system (original structure with the vibration absorber) becomes more favorable to its desired operating regime.

Although passive absorbers are designed to improve the system's performance in terms of vibration, care must be taken when selecting the type of vibration absorber to be used. Depending on its working principle, some types of vibration absorbers may be considered more appropriate for specific applications. However, the tuning of its parameters must also take into account the operating regime of the carrier structure, once there are also some drawbacks to be considered.

In the case being studied in this work, the goal is to install a centrifugal pendulum vibration absorber (CPVA) in an automotive powertrain in order to reduce the torsional vibration of the system, avoiding impact noises in the gearbox. Once the type of vibration absorber has already been selected, it is necessary to perform a deep and progressive theoretical investigation in order to understand its dynamic behavior and also to come up with parameter tuning techniques.

For this reason, this chapter starts with a brief review of the well-known theory of tuned mass dampers (TMD). This is due to the fact that some of the dynamic features of the CPVA bear some resemblance with the ones found in TMDs, what makes of it a good starting point.

3.1 Review on Tuned Mass Dampers

The theory regarding tuned mass damper absorbers is based on a carrier structure with one degree of freedom, to which a TMD is installed. Both structure and absorber are conservative. A schematic representation is found in Fig. 3.1.

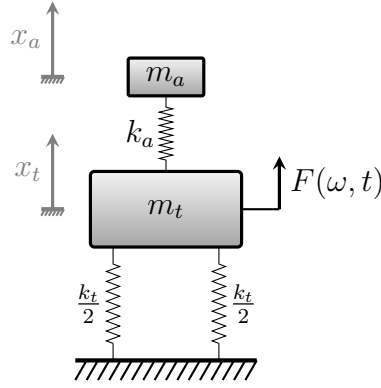


Figure 3.1: A one degree of freedom carrier structure with a TMD.

In this case, both of the degrees of freedom are chosen to be absolute, and both origins are at the static equilibrium positions of the respective inertias. Therefore, $x_a(t)$ is the vertical displacement of the center of mass of the TMD and $x_t(t)$ is the vertical displacement of the mass of the carrier structure, both positive upwards. The mass and stiffness of the carrier structure are given by m_t and k_t while the same parameters for the absorber are m_a and k_a . Finally, the carrier structure is subjected to a sinusoidal effort $F(\omega, t)$.

The equations of motion for this system are given by:

$$\begin{bmatrix} m_t & 0 \\ 0 & m_a \end{bmatrix} \begin{Bmatrix} \ddot{x}_t \\ \ddot{x}_a \end{Bmatrix} + \begin{bmatrix} k_t + k_a & -k_a \\ -k_a & k_a \end{bmatrix} \begin{Bmatrix} x_t \\ x_a \end{Bmatrix} = \begin{Bmatrix} F(\omega, t) \\ 0 \end{Bmatrix} \quad (3.1)$$

The parameters of the equations of motion as shown in Eq. (3.1) are the physical ones, and carrying analyses through these would lead to unintelligible results, once they are neither independent nor dimensionless. Considering the relationships given below,

$$\omega_a = \sqrt{\frac{k_a}{m_a}}; \quad \omega_t = \sqrt{\frac{k_t}{m_t}}; \quad \mu = \frac{m_a}{m_t}; \quad \beta = \frac{\omega_a}{\omega_t}; \quad \tau = \omega_t t; \quad \frac{\partial x_i}{\partial \tau} = x'_i \quad (i = a, t); \quad r = \frac{\omega}{\omega_t}$$

where:

ω_a is the natural frequency of the TMD,

ω_t is the original natural frequency of the carrier structure,

μ is the mass ratio,

β is the natural frequency ratio,

τ is the dimensionless time,
 r is the frequency ratio.

then the equations of motion reduce to:

$$\begin{Bmatrix} x_t'' \\ x_a'' \end{Bmatrix} + \begin{bmatrix} 1 + \beta^2 \mu & -\beta^2 \mu \\ -\beta^2 & \beta^2 \end{bmatrix} \begin{Bmatrix} x_t \\ x_a \end{Bmatrix} = \begin{Bmatrix} \frac{F(r,\tau)}{k_t} \\ 0 \end{Bmatrix} \quad (3.2)$$

Although the right hand side of Eq. (3.2) still depend on a physical parameter, it is merely a scaling factor for the force, which is now represented in the dimensionless time τ . The eigenvalues, eigenvectors and eigenfrequencies, however, are functions of the aforementioned dimensionless parameters β and μ .

For being a conservative system, its eigenvalues are of the form:

$$s_{1,2} = \pm jr_{1,2} \quad , \quad r_{1,2} \in \mathbb{R} \quad (3.3)$$

where r_i is the i -th eigenfrequency of the system on the dimensionless time scale, and is given by:

$$r_{1,2}^2 = \frac{1}{2} \left(1 + \beta^2(1 + \mu) \mp \sqrt{(1 + \beta^2(1 + \mu))^2 - 4\beta^2} \right) \quad (3.4)$$

The first feature to check is for which values of the dimensionless parameters, the term inside the square root is real and nonnegative. It is proven¹ that this is true for $\beta \in \mathbb{R}$ and $\mu \in \mathbb{R}_+$. It is also proven² that the square of each dimensionless eigenfrequency is a real nonnegative number. Both facts indicate that for any value of mass and stiffness, the system will have two real dimensionless eigenfrequencies (r_1 and r_2), and hence two eigenfrequencies in the time domain.

An important feature regarding the value of the dimensionless eigenfrequencies³ is that the smallest one is always less than or equal to β , while the greatest one is always greater than or equal to β . Besides, they will only be equal to β for non physical conditions (e.g. $\beta = 0$ or $\mu = 0$).

¹Proof is shown in Appendix B.1

²Proof is shown in Appendix B.2

³Proofs are shown in Appendix B.3 and Appendix B.4.

From the design point of view, once there is a frequency gap between the dimensionless eigenfrequencies, it is important to know how this gap behaves for different values of β and μ . One must notice that while the original system had one eigenfrequency, the new one with the tuned mass damper has two. Typically, the TMD design is such that the operating range of the system lies inside this frequency gap, for reasons that are better explained when the steady state response of the system is analyzed.

For a fixed value of μ , the value of the dimensionless frequency gap as a function of β is shown in Fig. 3.2.

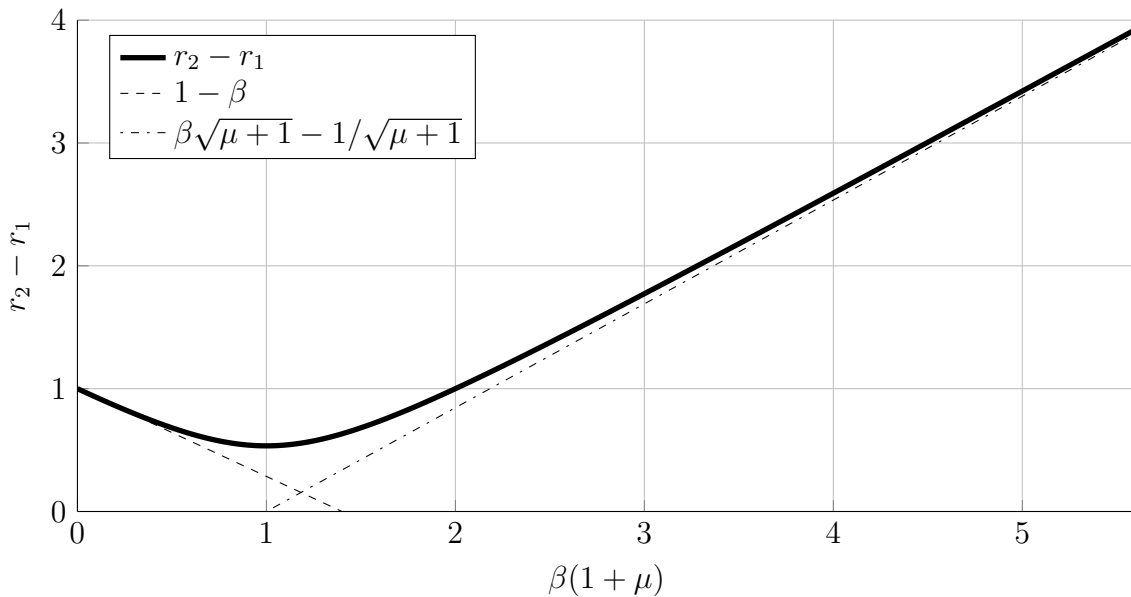


Figure 3.2: Dimensionless frequency gap as a function of β .

It is possible to see⁴ that it starts at the value of 1 with a slope of -1 and reaches a minimum at $\beta = 1/(\mu + 1)$. From this point on, as β tends to the infinity, the gap follows the asymptote:

$$\lim_{\beta \rightarrow \infty} (r_2 - r_1) \rightarrow \beta\sqrt{\mu + 1} - \frac{1}{\sqrt{\mu + 1}} \quad (3.5)$$

For a fixed value of β , the value of the dimensionless frequency gap as a function of μ is shown in Fig. 3.3.

⁴Proof is shown in Appendix B.5

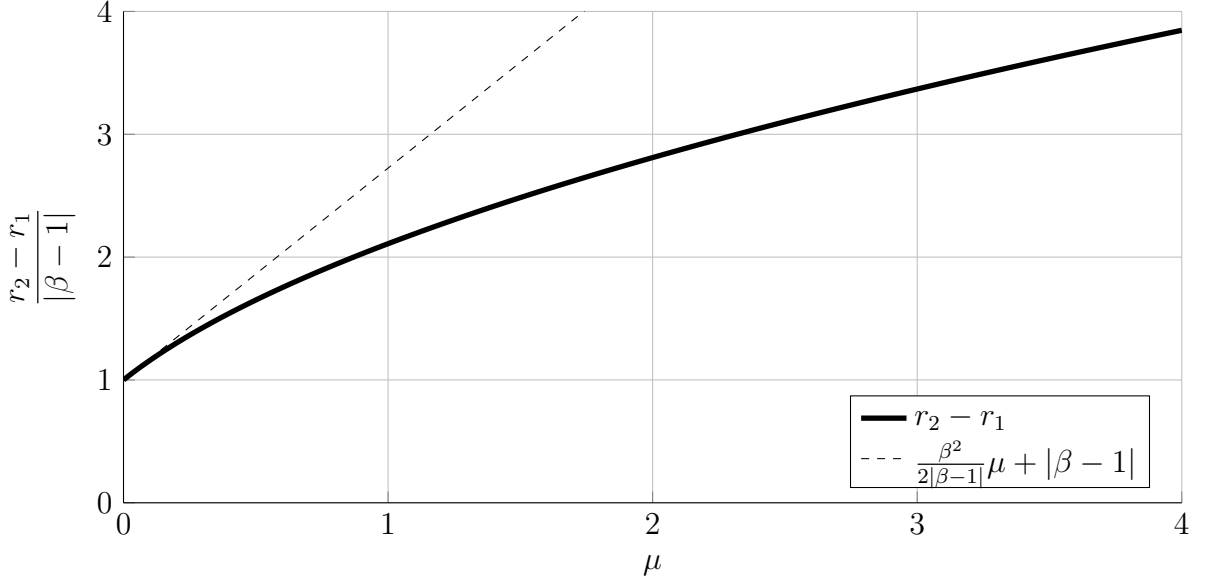


Figure 3.3: Dimensionless frequency gap as a function of μ .

For small values of μ , which is often desirable, the curve follows the asymptote⁵:

$$\lim_{\mu \rightarrow 0} (r_2 - r_1) \rightarrow \frac{\beta^2}{2|\beta - 1|} \mu + |\beta - 1| \quad (3.6)$$

For greater values of μ , however, no asymptotic behavior is found.

Further analyses on the mode shapes of this simple system are chosen not to be carried out, because the conclusions in this case wouldn't be relevant for this work. There are important results to be shown regarding the steady state response of this system, though. The normalized frequency response function of this system for the carrier structure is given by:

$$\frac{|x_t(\tau)|}{|F(r, \tau)|/k_t} = \frac{\beta^2 - r^2}{r^4 - r^2(1 + \beta^2(1 + \mu)) + \beta^2} \quad (3.7)$$

A straightforward conclusion to draw from Eq. (3.7) is that the amplitude of vibration of the carrier structure vanishes when $r = \beta$. This is the only value for which it happens, because r is considered positive for this analysis and the denominator of this fraction is a biquadratic polynomial in r with finite coefficients, and hence it will only tend to the infinity if $r \rightarrow \infty$. The value of the denominator goes to zero when $r = r_1$ or $r = r_2$, because the

⁵Proof is shown in Appendix B.6

system under investigation has no damping, and at resonance condition the amplitude of the response must increase indefinitely.

It is also important to consider the normalized frequency response function for the absorber mass, shown in Eq. (3.8).

$$\frac{|x_a(\tau)|}{|F(r, \tau)|/k_t} = \frac{\beta^2}{r^4 - r^2(1 + \beta^2(1 + \mu)) + \beta^2} \quad (3.8)$$

In this case there is no real value for r at which the absorber would not vibrate. Furthermore, both resonant conditions are also present in the motion of this body. Yet these facts must be carefully considered, it is of great importance to understand what happens to the vibration absorber when the carrier mass does not vibrate (i.e. $r = \beta$). In this case, the normalized frequency response function is given by:

$$\frac{|x_a(\tau)|}{|F(\beta, \tau)|/k_t} = \frac{-1}{\beta^2\mu} \quad (3.9)$$

This equation brings useful information about the amplitude of vibration of the tuned mass damper, which is usually limited. If this amplitude is to be reduced, the designer has two options: either β should be increased, which is less usual, or μ should be increased. The increase of the latter parameter not only leads to reduction of the amplitude of vibration of the TMD, but also widens the frequency range for which the carrier mass would vibrate with lower amplitudes. However, it is usually done through the increase of the inertia of the vibration absorber, which must also be limited.

At this point, a brief yet useful review on tuned mass dampers has been introduced. On the next section, theoretical aspects of a one degree of freedom with multiple tuned mass dampers will be introduced.

3.2 Dynamics of a system with multiple tuned mass dampers

Tuned mass dampers are a good practical solution for many applications in engineering. For some of them, generally in Civil Engineering, where inertias are huge and vibration must

be controlled, if one single TMD were to be used, its inertia would be tremendous, making it difficult to build⁶. An alternate solution to this problem is to use several tuned mass dampers, all of them tuned to the same frequency. An example of such application is shown in Fig. 3.4.

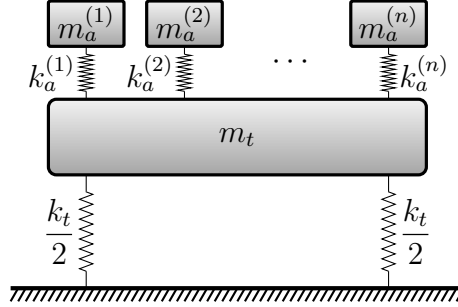


Figure 3.4: One degree of freedom structure with n tuned mass dampers.

For the sake of simplicity, all the tuned mass dampers are considered conservative, and the parameter μ is also the same for each absorber. The goal of this analysis is to demonstrate what happens to the dynamics of the system if multiple TMDs are chosen to be used, and hence it was decided not to account for mistuning at this point. Therefore, if the mass of each TMD is called $m_a^{(p)} = m_a$, its stiffness is called $k_a^{(p)} = k_a$ and its absolute vertical displacement is given by $x_a^{(p)}(t)$, with $p \in \{1, \dots, n\}$, then the equations of motion are given by:

$$m_t \ddot{x}_t + k_t x_t + \sum_{p=1}^n k_a (x_t - x_a^{(p)}) = F(\omega, t) \quad (3.10)$$

$$m_a \ddot{x}_a^{(p)} + k_a (x_a^{(p)} - x_t) = 0 \quad , \quad p \in \{1, \dots, n\} \quad (3.11)$$

Once the system is undamped, it suffices to calculate the steady state response of the system in order to compare it with the previous case, where a single TMD was used. It will bring the information about the eigenfrequencies and vanishing frequencies for the carrier mass. In this case, it is given by⁷:

$$\frac{|x_t(\tau)|}{|F(r, \tau)|/k_t} = \frac{\beta^2 - r^2}{r^4 - r^2(1 + \beta^2(1 + n\mu)) + \beta^2} \quad (3.12)$$

⁶There are some successful applications, however, where a single TMD is still chosen to be used, which is the case of the Taipei Tower, in Taiwan

⁷Proof is shown in Appendix B.7

where β is the ratio between the eigenfrequency of each TMD isolated from the carrier structure and the eigenfrequency of the original structure, and μ is the ratio between the mass of a single absorber and the mass of the carrier structure.

Comparing Eq. (3.12) to Eq. (3.7) makes clear that, in this case, the use of multiple TMDs brings exactly the same effect of using a single absorber with a larger inertia. Therefore, all the conclusions from the previous analysis are valid for this case. If, on the other hand, the carrier structure has more degrees of freedom, further analyses must be carried out in order to understand the several effects of using multiple tuned mass dampers.

3.3 Centrifugal Pendulum Vibration Absorber: a thorough analysis

The main goal of this work is to use a centrifugal pendulum vibration absorber (CPVA) in order to control torsional vibration in a vehicular powertrain. Therefore, it is of utmost importance to perform a very deep theoretical analysis in order to exhibit every single aspect of the dynamic behavior of such device and also of the torsional system containing it.

For this reason, this section is going to be divided as follows: on the first part linear analysis is performed on a system composed of a disk spinning at constant speed and a pendulum attached to this disk, which is free to oscillate. This analysis is divided in two parts: the first one neglecting gravity and the second one taking it into consideration.

On the next part, a system with two disks is analyzed. One of them spins at constant speed and is linked to a second one, which is free to oscillate, through a linear torsional spring. The latter rotor also has a pendulum attached to it. Linear analyses are performed firstly without gravity and then considering it. All these linear analyses are performed considering a circular path for the pendulum, because the features from non-circular paths vanish after linearization.

For this reason, on the third part of this section, general paths are considered and non-linear analyses are performed on the same systems which have been previously analyzed after linearization. On this part, firstly a mathematical procedure for calculating the coefficients of the power series that represents the path under consideration is shown. This procedure allows the nonlinear analysis to be performed. Then, the method used for calculating the

approximate solutions for the nonlinear problems is shown. Finally, the same systems with one and two disks are analyzed and stability and detuning due to the presence of gravity and external excitation are assessed.

3.3.1 Single torsional disk with a Circular Path CPVA

In this section a single torsional disk with a circular path centrifugal pendulum vibration absorber is modeled and analyzed. The schematic representation of this system is shown in Fig. 3.5. The angular displacement of the carrier disk is represented by the absolute degree of freedom θ_t , while the angular displacement of the pendulum bob is represented by the degree of freedom θ_a , which is relative to θ_t .

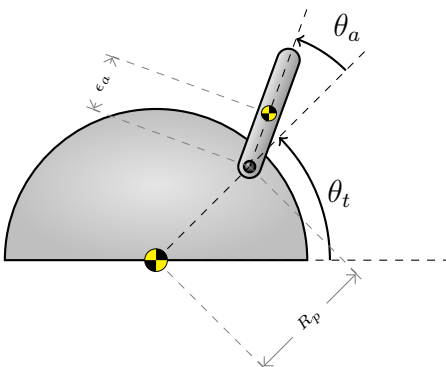


Figure 3.5: Scheme of a single torsional disk with a CPVA attached to it.

The distance between the geometric center of the carrier disk and the point to which the pendulum is pinned is R_p . The polar moments of inertia of the disk and the pendulum about their own centers of mass are I_t and I_a , respectively. The distance between the point at which the pendulum bob is pinned and its center of mass is ϵ_a , and its mass is m_a . There is an important detail about this system: in vehicle applications, the shafts are usually placed horizontally, and hence, the disks are in the vertical position, which means that the acceleration of gravity (g) is always parallel to the plane defined by the carrier disk. For this reason, in this problem the influence of the gravity must be accounted for.

With these parameters it is possible to calculate the equations of motion ⁸, which are

⁸Derivation is shown in Appendix B.8

given by:

$$\begin{aligned} (I_t + m_a R_p^2 + m_a R_p \epsilon_a \cos \theta_a) \ddot{\theta}_t + m_a R_p \epsilon_a (\ddot{\theta}_a + \ddot{\theta}_t) \cos \theta_a + \dots \\ - m_a R_p \epsilon_a (\dot{\theta}_t + \dot{\theta}_a)^2 \sin \theta_a + m_a R_p g \cos \theta_t = 0 \end{aligned} \quad (3.13)$$

for the motion of the disk and:

$$(I_a + m_a \epsilon_a^2) \ddot{\theta}_a + (I_a + m_a \epsilon_a^2 + m_a \epsilon_a R_p \cos \theta_a) \ddot{\theta}_t + m_a \epsilon_a R_p \dot{\theta}_t^2 \sin \theta_a + m_a \epsilon_a g \cos(\theta_t + \theta_a) = 0 \quad (3.14)$$

for the motion of the pendulum bob.

As they are, the equations of motion describe a nonlinear autonomous system, and they contain all the terms without any simplification. The first analysis to be performed is for the condition where the carrier disk spins at constant speed and gravity is neglected.

3.3.1.1 Linear analysis at constant angular speed and zero gravity

In this case, the degree of freedom θ_t is going to be imposed, and then Eq. (3.13) is of no use. As the system now has only one degree of freedom (θ_a), only Eq. (3.14) is necessary to describe its dynamics. However, the degree of freedom θ_t must be replaced by the appropriate time-dependent expression so that the disk spins at constant angular speed. Hence, θ_t and its derivatives are replaced by:

$$\theta_t = \Omega t + \delta; \quad \dot{\theta}_t = \Omega; \quad \ddot{\theta}_t = 0 \quad (3.15)$$

where Ω is the constant angular speed of the disk and δ is an angle reference.

Regarding the acceleration of gravity, the consideration of such terms will lead to important consequences. However, relevant conclusions are drawn in the analysis without these terms, and hence they are chosen to be neglected at this point, and considered in further steps.

With all these considerations, Eq. (3.14) reduces to:

$$(I_a + m_a \epsilon_a^2) \ddot{\theta}_a + m_a \epsilon_a R_p \Omega^2 \sin \theta_a = 0 \quad (3.16)$$

Considering that the angle θ_a is small, which is desirable, then it is possible to linearize this equation, resulting in:

$$(I_a + m_a \epsilon_a^2) \ddot{\theta}_a + m_a \epsilon_a R_p \Omega^2 \theta_a = 0 \quad (3.17)$$

Once this equation is linear, homogeneous, time invariant and has positive coefficients, the response from this system is bounded if the initial conditions are so. Also, in case of harmonic excitation, in all conditions but resonance the system response is also bounded. Through simple eigenvalue analysis, the eigenfrequency of the system for this case is given by:

$$\omega_a = \sqrt{\frac{m_a \epsilon_a R_p \Omega^2}{I_a + m_a \epsilon_a^2}} = \Omega \sqrt{\frac{\epsilon_a R_p}{r_{ga}^2 + \epsilon_a^2}} = \Omega v \quad (3.18)$$

where r_{ga} is the radius of gyration of the pendulum bob.

Equation (3.18) brings important facts to be kept in mind in the analysis of systems with centrifugal pendulums: firstly, the eigenfrequency of the pendulum, when attached to a system spinning at constant speed, varies linearly with the angular frequency, according to a constant (v). Secondly, this constant depends only on the geometry of the pendulum (ϵ_a , r_{ga}) and the distance between the point where it is pinned on the disk and the center of mass of the latter (R_p). It does not depend on the inertia or mass of the pendulum bob.

These conclusions bring some qualitative aspects of the behavior of the pendulum bob when its swing angle is small and when no gravitational terms are considered. On the next analysis, the acceleration of gravity is taken into account for small swing angles of the pendulum bob and constant angular speed.

3.3.1.2 Linear analysis at constant angular speed considering gravitational terms

In this case, as in the previous one, the angle θ_a is considered small and the degree of freedom θ_i is going to be imposed using the same constraints as in Eq. (3.15). The only difference is that at this point, gravity is not neglected. Hence, this time Eq. (3.14) reduces to:

$$(I_a + m_a \epsilon_a^2) \ddot{\theta}_a + m_a \epsilon_a (R_p \Omega^2 - g \sin(\Omega t + \delta)) \theta_a = -m_a \epsilon_a g \cos(\Omega t + \delta) \quad (3.19)$$

It now refers to a non-homogeneous linear time varying system, and at this point new concerns arise about the system stability, which in this work is directly related to the boundedness of its solutions.

It is important to mention at this point that, although parameters are time-varying and there is excitation already, linearity still holds, and hence zero-state and zero-input responses can be analyzed separately before boundedness properties are stated.

It is also of great importance to carry analyses using dimensionless parameters. For this reason, Eq. (3.19) must be rewritten considering some rearrangements and also time scaling, which at this point deserve some special attention. The relationship between physical time and dimensionless time in this case is given by:

$$\Omega t + \delta = \tau + \pi/2 \tag{3.20}$$

The constant terms δ and $\pi/2$ are chosen so that the final equation is in a convenient form, but they do not imply in loss of generality in any sense. When the change of variables is performed, it is important not only to change the functions of t for proper functions of τ , but also to replace the derivatives, which were originally with respect to t , to the proper ones, with respect to τ . This can be done through the chain rule relationship shown below:

$$\dot{\theta}_a(\tau(t)) = \frac{d}{dt}(\theta_a(\tau(t))) = \frac{\partial}{\partial \tau}(\theta_a(\tau)) \frac{d\tau}{dt} = \theta'_a(\tau)\Omega \tag{3.21}$$

where Ω comes from the Eq. (3.20).

When the change of independent variables is performed, the resulting equation represents the dynamics of the system in the dimensionless time-scale τ , which happens to have a physical meaning in this case: once the left-hand side of Eq. (3.20) represents the time evolution of the angular displacement of the carrier disk, the dimensionless time τ represents an angle, i.e., the system goes from time-domain to the angular domain representation.

Considering this, Eq. (3.19) reduces to:

$$\theta''_a + (\kappa + \eta \cos \tau) \theta_a = \eta \sin \tau \tag{3.22}$$

where κ and η are given by:

$$\kappa = \frac{m_a \epsilon_a R_p}{I_a + m_a \epsilon_a^2} = v^2; \quad \eta = \frac{-m_a \epsilon_a g}{(I_a + m_a \epsilon_a^2) \Omega^2} = \frac{-v^2 g}{R_p \Omega^2} \quad (3.23)$$

The homogeneous part of Eq. (3.22) is precisely the homogeneous Mathieu equation, which is a special case of Hill's equation, first published in the work of Hill (1886)⁹. Hill studied equations of the form:

$$\frac{d^2 y(\tau)}{d\tau^2} + f(\tau)y(\tau) = 0 \quad (3.24)$$

where $f(\tau)$ is a periodic function.

The solution of such equation can be expressed in terms of Hill's (or infinite) determinants, or by the Floquet theory, which is devoted to the study of linear time-varying systems with periodic coefficients.

The Mathieu equation is a special case of Hill's equation, where the function $f(\tau)$ is given by the sum of a sinusoidal function of period 2π in τ with a constant. In order to infer the stability of the homogeneous solution of this equation, it is necessary to observe the following concept from Floquet theory¹⁰: it is not true that all homogeneous solutions θ_a of Eq. (3.22) are periodic. However, it is true that these solutions can be written in the form:

$$\theta_a(\tau) = e^{\alpha\tau} \varphi(\tau) \quad (3.25)$$

where $\varphi(\tau)$ is periodic with period 2π and α is not necessarily real. The value of α is strictly related to the boundedness of the solution, i.e. if $\Re[\alpha] \leq 0$, the solution is bounded. For the case where the latter equality holds, if $e^{2\pi\alpha} = 1$ (i.e. $\alpha = n \mid n \in \mathbb{Z}$), then the solution θ_a is 2π -periodic, and if $e^{2\pi\alpha} = -1$ (i.e. $\alpha = j/2 + n \mid n \in \mathbb{Z}$), then θ_a is 4π -periodic.

The stability character of the solutions of Eq. (3.22), i.e. the value of α , is exclusively defined by the parameters κ and η , and it is not influenced by the initial conditions. If a pair (κ, η) leads to a stable solution, these values are called *stable values*. If, on the other hand, it would lead to an unstable solution, the values are called *unstable values*. Finally, if the pair results in at least one periodic solution, they are called *transition values*. The other solution

⁹It was named after G. W. Hill and was firstly used to infer lunar stability. However, it has been used on the modeling of quadrupole mass spectrometer, as the one dimensional Schrödinger equation of an electron in a crystal and in accelerator physics, among other applications.

¹⁰A brief introduction to this theory applied to one-degree-of-freedom systems is shown in Appendix B.9.

is usually unstable (because the roots are repeated), but this point is at the limit of stability.

According to Haupt (1918), in a κ, η -plane, the points that define a purely periodic solution ($|e^{2\pi\alpha}| = 1$) are the stability limits of the system, i.e. they separate stable and unstable regions of the plane. Hence, in order to infer stability, it suffices to calculate the transition values, which lead to periodic homogeneous solutions. The proposed solution must be a 4π -periodic Fourier series, because includes 4π -periodic and 2π -periodic terms, both mentioned by Floquet theory. It is then written in the following form:

$$\theta_a(\tau) = a_0 + \sum_{n=1}^{\infty} a_n \cos\left(\frac{n\tau}{2}\right) + b_n \sin\left(\frac{n\tau}{2}\right) \quad (3.26)$$

Using this solution to calculate the homogeneous response of Eq. (3.22) leads to the following recurrence relations:

- For n even:

$$\begin{array}{l} \text{For } n = 0 \\ \kappa a_0 + \frac{\eta}{2} a_2 = 0 \\ \hline \text{For } n = 2 \\ \left\{ \begin{array}{l} \left(\kappa - \frac{2^2}{4}\right) a_2 + \eta \left(a_0 + \frac{a_4}{2}\right) = 0 \\ \left(\kappa - \frac{2^2}{4}\right) b_2 + \eta \left(\frac{b_4}{2}\right) = 0 \end{array} \right. \\ \hline \text{For } n \geq 4 \\ \left\{ \begin{array}{l} \left(\kappa - \frac{n^2}{4}\right) a_n + \frac{\eta}{2} (a_{n-2} + a_{n+2}) = 0 \\ \left(\kappa - \frac{n^2}{4}\right) b_n + \frac{\eta}{2} (b_{n-2} + b_{n+2}) = 0 \end{array} \right. \end{array} \quad (3.27)$$

- For n odd:

$$\begin{array}{l} \text{For } n = 1 \\ \left\{ \begin{array}{l} \left(\kappa - \frac{1^2}{4}\right) a_1 + \frac{\eta}{2} (a_1 + a_3) = 0 \\ \left(\kappa - \frac{1^2}{4}\right) b_1 + \frac{\eta}{2} (b_3 - b_1) = 0 \end{array} \right. \\ \hline \text{For } n \geq 3 \\ \left\{ \begin{array}{l} \left(\kappa - \frac{n^2}{4}\right) a_n + \frac{\eta}{2} (a_{n-2} + a_{n+2}) = 0 \\ \left(\kappa - \frac{n^2}{4}\right) b_n + \frac{\eta}{2} (b_{n-2} + b_{n+2}) = 0 \end{array} \right. \end{array} \quad (3.28)$$

One may notice that equations for even and odd values of n are uncoupled. This happens because the 2π -periodic part of the solution is represented by the even terms of the Fourier series, while the odd ones represent the 4π -periodic part.

As there are infinite recurrence relations and all of them are homogeneous, the calculation of the coefficients a_i and b_i involve the solution of an infinite homogeneous algebraic system of equations. Nontrivial solutions are found through setting the determinant of the infinite matrix that represents this system to zero, which provides relationships between η and κ . These relationships are the loci formed exclusively by transition values on the κ, η -plane. Such class of determinants is called Hill's determinants.

With these loci, it suffices to find points for which the solution is stable (for example, if $\eta = 0$, the system would be linear and time invariant, and stability inference is direct). When such point is found, all the points in its neighborhood will also be stable values until some loci from Hill's determinant is reached. From this point on, the stability character is reversed, and so forth. This is better shown in Fig. 3.6. The values in blue are stable, while the ones in white are unstable and the ones in black are transition values.

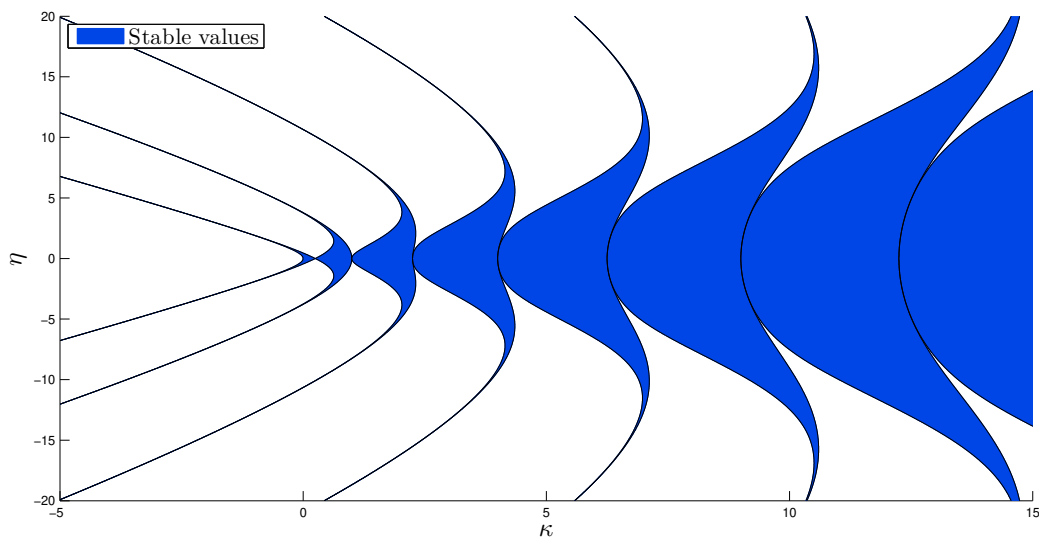


Figure 3.6: Stability diagram for homogeneous Mathieu equation.

Once the parameters η and κ are calculated in terms of the physical parameters of the system, it is now possible to obtain important information about some characteristics of the

pendulum bob and its assembly that would contribute for greater stability. The term *stability* in this case refers to the fact that the equilibrium position of the pendulum bob must be the one at which its tip points outwards, related to the carrier disk, and also to the fact that the pendulum must swing only (in a small angle), and not rotate completely, otherwise the nonlinearity would be too strong.

From the diagram in Fig. 3.6, it is readily noticeable that in order to increase the chances of obtaining a stable response, one must design a pendulum with positive and high values for κ and small values for $|\eta|$. From Eq. (3.23), it is possible to conclude that, the higher the parameter v , which is directly related to the natural frequency of the pendulum, the higher is the chance of obtaining a stable pendulum. On the other hand, if v is too large, then the absolute value of η would increase and the chances of obtaining stable behavior would decrease. According to the latter parameter, once the acceleration of gravity in this work is constant, then the pendulum should be installed in a position R_p as far as possible from the center of the carrier disk. Furthermore, as Ω increases, the chances of obtaining stable behavior increase significantly. It means that, in practice, the lower the ratio between the acceleration of gravity (g) and the mean centripetal acceleration ($\Omega^2 R_p$), the better.

These conclusions are valid for the homogeneous response of Eq. (3.22). Once the equation is linear, then these conclusions will hold independently from the input that acts on the system. However, it is still necessary to infer stability for the response to the input in Eq. (3.22), and the stability of this system will obviously hold if and only if the zero state and zero input responses are simultaneously bounded.

In order to address this problem, useful information is found on the work by Slane and Tragesser (2011). The authors propose an extension to the Floquet theory¹¹, that originally dealt only with homogeneous systems, making it possible to analyze nonautonomous ones. This extension is valid if the input is periodic with the same period of the system's coefficients, which is precisely the case of Eq. (3.22). Table 3.1 summarizes the results for the both cases.

It is clear from the results shown in this table that the response of the pendulum will be stable when all the multipliers lie inside the unit circle and when multipliers on the unit circle are not 1 but are semisimple. The first case refers to a naturally stable system while the second one refers to a system whose response is periodic and not at resonance. When the

¹¹The comprehension of such extension requires knowledge of the general Floquet theory. Hence, the general theory is shown in Appendix B.10 and its extension on Appendix B.11

Table 3.1: Stability results from general and extended Floquet theory for homogeneous and inhomogeneous systems.

Magnitude of Largest Floquet Multiplier ($\rho[\sigma_i]$)	Homogeneous Stability	Inhomogeneous Stability
$\rho[\sigma_i] < 1$ Semisimple	Asymptotic stability	Bounded
$\rho[\sigma_i] = 1$ One is the only multiplier on the unit circle and is semisimple	Lyapunov stability	Unbounded
$\rho[\sigma_i] = 1$ Multipliers, other than one, on the unit circle are semisimple	Lyapunov stability	Bounded
$\rho[\sigma_i] = 1$ Multiple eigenvalues not semisimple	Unstable	Unbounded
$\rho[\sigma_i] > 1$ Multipliers outside the unit circle	Unstable	Unbounded

multiplier is precisely 1, the system is at resonance. Multiple and not semisimple multipliers on the unit circle or multipliers outside the unit circle are natural the causes of instability¹².

A direct consequence of the results brought by Slane and Tragesser (2011) is that the blue area in the diagram shown in Fig. 3.6, that indicates stable behavior for the homogeneous solution, is also valid for inhomogeneous systems whose input is periodic with the same period of the system's coefficients, i.e. if the parameters η and κ are stable values, then the response of the pendulum will be bounded for the case where the carrier disk spins at constant angular speed.

At this point, all the relevant aspects of the dynamics of a system composed by a

¹²The multipliers σ_i are eigenvalues of a special matrix defined in Appendix B.10. The algebraic multiplicity of an eigenvalue is the number of times it is repeated as a root of the characteristic polynomial defined by that matrix. The geometrical multiplicity of an eigenvalue is the number of linearly independent eigenvectors associated to it. A simple eigenvalue has both multiplicities equal to one, while a semisimple eigenvalue is an eigenvalue whose algebraic and geometric multiplicities are equal. A simple eigenvalue is always semisimple, but not conversely.

pendulum bob attached to a carrier disk spinning at constant speed for this work have been presented. The discussion will now focus on systems with more spinning disks that are allowed not only to spin at constant speed but also to oscillate with small amplitudes.

3.3.2 Elastic two-disk system with a Circular Path CPVA

In the previous section a single disk spinning at constant rotating speed with a CPVA attached to it is analyzed. The next step of the analysis would be to allow the disk to spin at constant speed and also to oscillate with small amplitudes. However, this analysis would be really close to the one which considers a system with two elastically coupled disks where one of them spins at constant speed, the other is allowed to oscillate torsionally while spinning at the same constant speed of the first one, and also has a CPVA attached to it. Therefore, it was chosen to present the relevant aspects of both analyses making use of the latter system only. Its schematic representation is shown in Fig. 3.7.

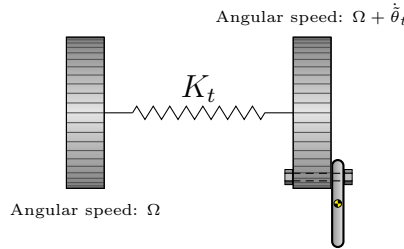


Figure 3.7: Two elastically coupled disks, one of them with a CPVA.

As there are two disks and one of them has a pendulum, then this system would have three degrees of freedom. However, it is imposed that the disk without the CPVA must rotate at constant rotating speed Ω . Consequently, there will be only two equations of motion: one for the dynamics of the carrier disk and another for the torsional dynamics of the pendulum bob. They are:

$$\begin{aligned} (I_t + m_a R_p^2 + m_a R_p \epsilon_a \cos \theta_a) \ddot{\theta}_t + m_a R_p \epsilon_a \ddot{\theta}_a \cos \theta_a - m_a R_p \epsilon_a (\dot{\theta}_t + \dot{\theta}_a)^2 \sin \theta_a + \dots \\ \dots + m_a R_p g \cos \theta_t + K_t (\theta_t - \Omega t - \delta) = 0 \end{aligned} \quad (3.29)$$

and:

$$(I_a + m_a \epsilon_a^2) \ddot{\theta}_a + (I_a + m_a \epsilon_a^2 + m_a \epsilon_a R_p \cos \theta_a) \ddot{\theta}_t + m_a \epsilon_a R_p \dot{\theta}_t^2 \sin \theta_a + m_a \epsilon_a g \cos(\theta_t + \theta_a) = 0 \quad (3.30)$$

respectively.

One must notice that Eq. (3.30) is identical to Eq. (3.14), while the only difference between Eq. (3.29) and Eq. (3.13) is the term $K_t \theta_t$. The next step is to perform an analysis which allows the carrier disk to have an angular speed with small fluctuations.

3.3.2.1 Linear analysis with zero gravity and small oscillations on the carrier disk's angular speed

For this analysis, gravitational terms are neglected and the carrier disk is allowed to have oscillating angular speed, given that such oscillation is small enough so that a linear system would still be able to describe most of the system's dynamics. Additionally, the swing angle of the pendulum bob is also considered to be small. Mathematically, it is represented as follows:

$$\theta_t = \Omega t + \delta + \tilde{\theta}_t; \quad \tilde{\theta}_t \rightarrow 0; \quad \theta_a \rightarrow 0$$

with δ and Ω constants.

After linearizing Eqs. (3.29) and (3.30) and replacing the terms described in the constraints above, it is possible to find the following set of equations of motion:

$$\begin{bmatrix} I_t + m_a R_p^2 + m_a R_p \epsilon_a & m_a R_p \epsilon_a \\ I_a + m_a \epsilon_a^2 + m_a R_p \epsilon_a & I_a + m_a \epsilon_a^2 \end{bmatrix} \begin{Bmatrix} \ddot{\tilde{\theta}}_t \\ \ddot{\theta}_a \end{Bmatrix} + \begin{bmatrix} K_t & -m_a \epsilon_a R_p \Omega^2 \\ 0 & m_a \epsilon_a R_p \Omega^2 \end{bmatrix} \begin{Bmatrix} \tilde{\theta}_t \\ \theta_a \end{Bmatrix} = \begin{Bmatrix} 0 \\ 0 \end{Bmatrix} \quad (3.31)$$

After introducing the dimensionless parameters shown below:

$$a = \frac{I_t + m_a R_p \epsilon_a + m_a R_p^2}{I_t}; \quad b = \frac{I_a + m_a \epsilon_a^2}{I_a}; \quad \mu = \frac{I_a + m_a \epsilon_a^2}{I_t + m_a R_p^2 + m_a R_p \epsilon_a} = \frac{b I_a}{a I_t};$$

$$p = \frac{\epsilon_a}{R_p}; \quad v = \sqrt{\frac{b-1}{bp}}; \quad \omega_t = \sqrt{\frac{K_t}{I_t}}; \quad \omega_a = v \Omega; \quad \beta = \frac{\omega_a}{\omega_t}; \quad \tau = \Omega t + \delta;$$

$$\dot{f}(\tau) = \frac{d}{dt}f(\tau(t)) = \Omega \frac{\partial}{\partial \tau}f(\tau) = \Omega f'(\tau)$$

the equations of motion become:

$$\begin{bmatrix} \mu^{-1} & v^2 \\ 1 + v^2 & 1 \end{bmatrix} \begin{Bmatrix} \tilde{\theta}_t'' \\ \theta_a'' \end{Bmatrix} + \begin{bmatrix} \frac{v^2}{\beta^2 \mu a} & -v^2 \\ 0 & v^2 \end{bmatrix} \begin{Bmatrix} \tilde{\theta}_t \\ \theta_a \end{Bmatrix} = \begin{Bmatrix} 0 \\ 0 \end{Bmatrix} \quad (3.32)$$

As there is no excitation or gravitational terms, this system of equations is homogeneous, and hence its eigenproblem must be analyzed. The square of the eigenvalues of this system is given by:

$$s_{1,2}^2 = \frac{v^2}{2q} \left(- \left(\frac{1-q}{v^2} + 1 + \frac{1}{\beta^2 a} \right) \pm \sqrt{\left(\frac{1-q}{v^2} + 1 + \frac{1}{\beta^2 a} \right)^2 - \frac{4q}{\beta^2 a}} \right) \quad (3.33)$$

where q is given by:

$$q = 1 - \mu v^2 (v^2 + 1) \quad (3.34)$$

The first thing to check is whether the eigenvalues of the system are purely imaginary (i.e. if their squares are always negative) or not. Once there is no energy dissipation involved, if s_i^2 is anything other than a real negative number, this could be an evidence of instability. The only constraint that must be obeyed¹³ so that the response of this system remains bounded is that $\mu \leq 1/v^2(v^2 + 1)$, which draws a direct relationship between the natural frequency of the pendulum and the inertia added to the system.

The eigenvalues of the system will then be of the following form:

$$s_{1,2} = \pm j \chi_{1,2}$$

where it is emphasized that χ_i are eigenfrequencies in the dimensionless time τ , and not in the physical time t . It is important to mention that the relationship between an eigenfrequency on the physical time domain (ω_i) and its corresponding in the dimensionless time domain (χ_i) is $\omega_i = \Omega \chi_i$. In order to avoid ambiguity, once the physical meaning of the dimensionless time τ is an angle, then, from this point on, the eigenfrequencies in the physical time domain will be referred to as *eigenfrequencies*, while the eigenfrequencies in the dimensionless time domain will be referred to as *eigen-orders*.

¹³Proof shown in Appendix B.12

The eigen-orders of this systems are then given by:

$$\chi_{1,2} = \frac{v}{\sqrt{2q}} \left(\left(\frac{1-q}{v^2} + 1 + \frac{1}{\beta^2 a} \right) \mp \sqrt{\left(\frac{1-q}{v^2} + 1 + \frac{1}{\beta^2 a} \right)^2 - \frac{4q}{\beta^2 a}} \right)^{1/2} \quad (3.35)$$

where χ_1 refers to the smallest eigen-order while χ_2 refers to the largest.

Among all the dimensionless parameters involved in the calculation of $\chi_{1,2}$, the only one that varies with Ω is β . Hence, the eigen-orders of this system must also vary with the rotating speed. This behavior is of great interest for the design of the pendulum absorber, and must be analyzed carefully.

Figure 3.8 shows the behavior of the eigen-orders ($\chi_{1,2}$) of the system along its rotating speed. The lowest eigen-order (χ_1) is represented by the blue curve. It tends to v when the rotating speed tends to zero, and for high values of Ω , χ_1 tends asymptotically to zero¹⁴. The highest eigen-order (χ_2) is represented by the red curve. It tends to the infinity as Ω tends to zero, and when the rotating speed reaches higher values, χ_2 tends asymptotically¹⁵ to $\sqrt{\frac{1-q+v^2}{q}}$.

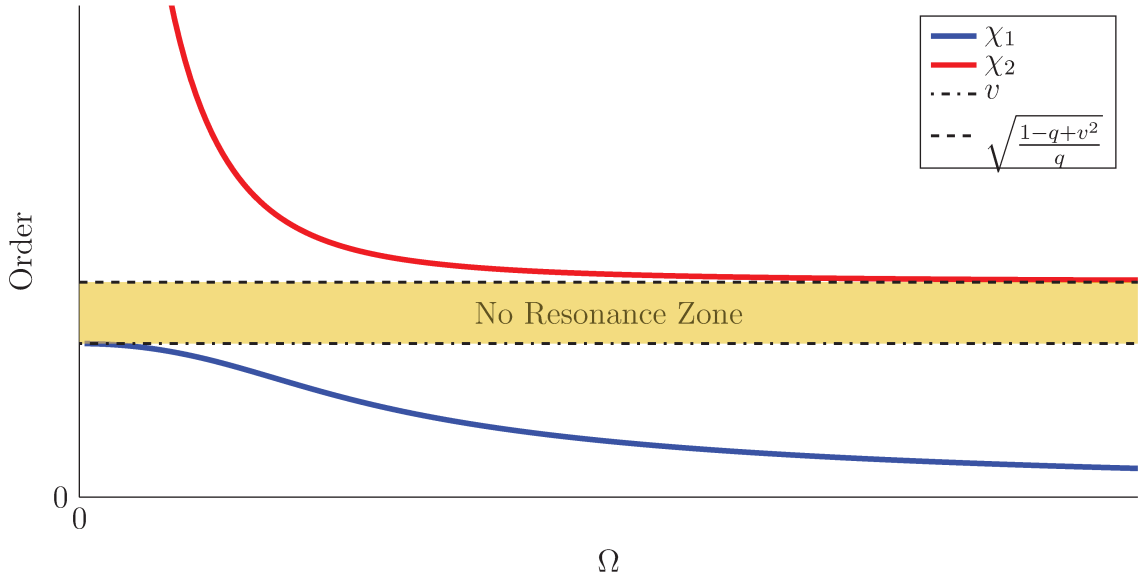


Figure 3.8: Eigen-orders of a two disk system with a CPVA.

¹⁴For detailed proof of the asymptotic behavior of χ_1 , refer to Appendix B.13

¹⁵For detailed proof of the asymptotic behavior of χ_2 , refer to Appendix B.14

The most important feature, however, is the fact that the lowest eigen-order is always¹⁶ lower than v while the greatest one is always¹⁷ greater than $\sqrt{\frac{1-q+v^2}{q}}$. This creates a gap, shown as a yellow horizontal stripe in Fig. 3.8 where no resonance is found. This is extremely important, because as this graphic is shown in an $\text{Order} \times \Omega$ -plane, any excitation whose frequency is a multiple of the rotating speed of the system would be represented as a horizontal line. If this line lies inside the no resonance zone, then this part of the excitation would not excite any resonance of this system.

It is also possible to see this behavior on the graphics shown in Fig. 3.9. It is represented on a $\text{Frequency} \times \Omega$ -plane, and the blue and red lines are the lowest and the greatest eigenfrequencies respectively. An excitation whose frequency is a multiple of the rotating speed would be represented in this graphic as a sloped line that crosses the origin. Once again, if such part of the excitation is represented by a line that lies inside the yellow zone, then it would cross no natural frequency. The bounding lines of this zone are the asymptotes for ω_1 as the rotating speed tends to zero and for ω_2 as Ω tends to the infinity, as shown in the work of Simionatto *et al.* (2013).

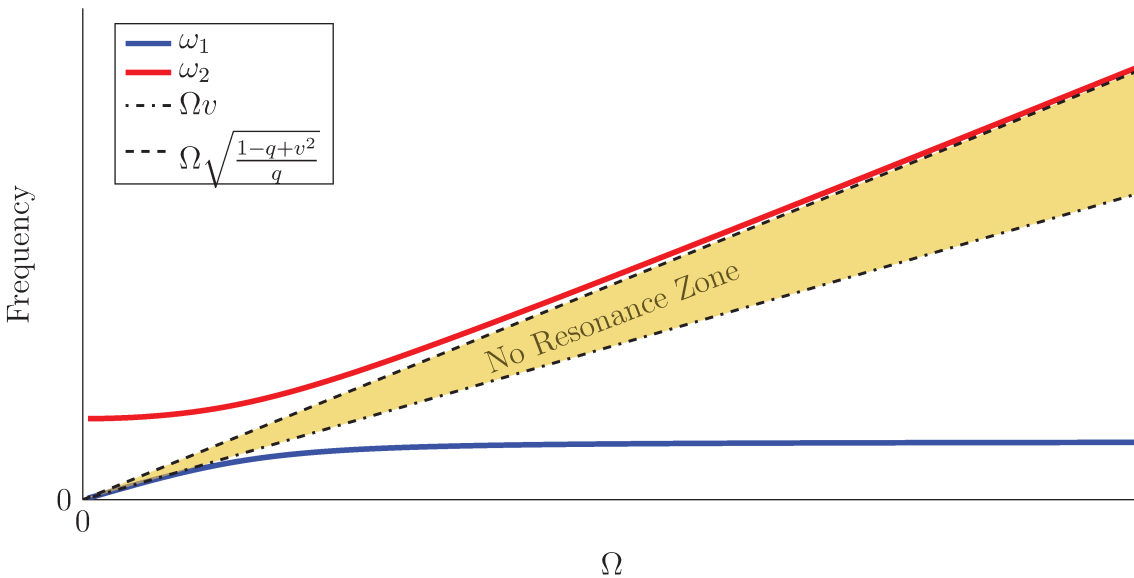


Figure 3.9: Eigenfrequencies of a two disk system with a CPVA.

There are many sources in the bibliography, such as Wilson (1941), Olson *et al.* (2005), Olson and Shaw (2008), Olson and Shaw (2009), Gozen *et al.* (2012) and Shaw *et al.* (2014), which mention the existence of the no resonance zone. The first one is a rather general work

¹⁶Proven in Appendix B.15.

¹⁷Proven in Appendix B.16.

while the latter five are focused on rotating blade array dynamics.

The work of Wilson (1941) deserves special attention because it brings a method for tuning the CPVA based on the existence of such zone. This method is called *Inertia Tuning* and is going to be presented in chapter 4. Another important aspect is brought by the work from Gozen *et al.* (2012). Instead of a no-resonance zone, the authors were able to find a resonance suppression zone, i.e. while some resonances would be out of the zone created by the CPVA, others would still cross such zone, so that they could still be excited by excitations lying on it. The reason why the existence of this zone is of great importance for the professionals who aim at reducing NVH issues related to torsional vibrations, such as rattle noise, lies on the nature of generation of impact-induced noise.

From practical experience and literature, as seen on the works of Seaman *et al.* (1984) and Steinel (2000), it is known that undesirable levels of noise are achieved when the torsional vibration in the gearbox is above a certain limit which differs from one transmission to another. In the operating regime studied in this work, once the engine torque oscillation is not critical, the main factor that would increase torsional vibration in the gearbox is system amplification, which is closely related to resonance. Hence, if there is a way to suppress the most relevant resonances, then the system would be less prone to produce rattle noise.

It is also important to understand the behavior of the modes of this system, once they also vary with the rotating speed. As the system has only two degrees of freedom, if the modes are normalized so that the first component is always unitary, then the second one, which is a ratio, is capable of representing that mode. More precisely, it is the ratio between the torsional amplitude of the carrier disk and the angular amplitude of the pendulum bob, and it is given by:

$$\Gamma_{1,2} = \frac{\tilde{\Theta}_{t(1,2)}}{\Theta_{a(1,2)}} = \frac{-(s_{1,2}^2 + v^2)}{s_{1,2}^2(v^2 + 1)} \quad (3.36)$$

where $\tilde{\Theta}_{t(i)}$ and $\Theta_{a(i)}$ are the amplitudes of the carrier disk and the pendulum bob at the i -th mode, respectively. These ratios are represented in Fig. 3.10.

In mode 1, represented by the blue line in Fig. 3.10, both carrier disk and pendulum bob are in phase, and as the rotating speed increases, the amplitude of the pendulum bob tends to decrease when compared to the amplitude of the carrier disk. Also, it tends to zero for lower speeds. In mode 2, the red line in Fig. 3.10, the carrier disk and the pendulum bob are opposite in phase, and as the rotating speed increases, the ratio Γ_2 tends to $(q-1)/(1-q+v^2)$,

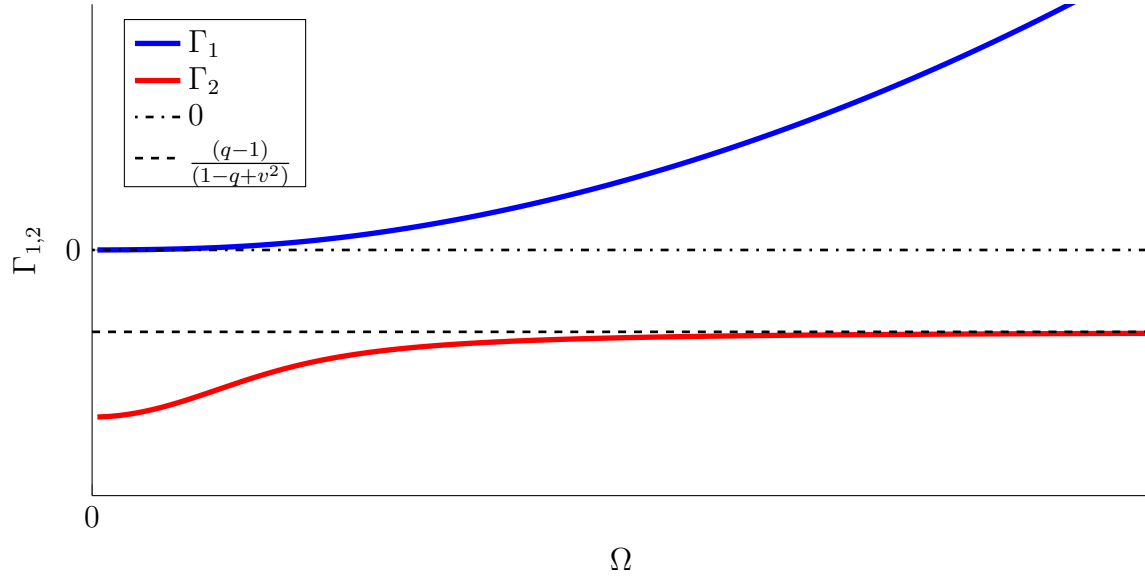


Figure 3.10: Modal ratios of a two disk system with a CPVA.

which means that for this mode, if the amplitude of the carrier disk is limited, so is the amplitude of the pendulum bob.

With these information, the analysis of the homogeneous response of this system, apart from gravitational terms is complete. As there is no excitation in this system, a hypothetical oscillating torque ($T(n\Omega, t)$) is assumed to be acting on the carrier mass. Its oscillates at the n -th order of the rotating speed and can be included on Eq. (3.32) as follows:

$$\begin{bmatrix} \mu^{-1} & v^2 \\ 1 + v^2 & 1 \end{bmatrix} \begin{Bmatrix} \tilde{\theta}_t'' \\ \theta_a'' \end{Bmatrix} + \begin{bmatrix} \frac{v^2}{\beta^2 \mu a} & -v^2 \\ 0 & v^2 \end{bmatrix} \begin{Bmatrix} \tilde{\theta}_t \\ \theta_a \end{Bmatrix} = \begin{Bmatrix} \frac{T(n, \tau)}{\Omega^2 b I_a} \\ 0 \end{Bmatrix} \quad (3.37)$$

Although in the time domain, such excitation would have variable frequency, in the angle domain its frequency is constant, and hence $T(n, \tau)$ is a sinusoidal function. The calculation of the steady state response of the system in Eq. (3.37) for any order n results in the *order response functions* (ORF), which are basically the frequency response functions of this system in the order domain. Their normalized forms are given by:

$$\frac{|\tilde{\theta}_t|}{\frac{|T(n, \tau)|}{\Omega^2 b I_a}} = \frac{\mu(v^2 - n^2)}{n^4 q - n^2 v^2 \left(\frac{1-q}{v^2} + 1 + \frac{1}{\beta^2 a} \right) + \frac{v^4}{\beta^2 a}} \quad (3.38)$$

for the carrier disk and:

$$\frac{|\theta_a|}{\frac{|T(n,\tau)|}{\Omega^2 b I_a}} = \frac{\mu n^2 (v^2 + 1)}{n^4 q - n^2 v^2 \left(\frac{1-q}{v^2} + 1 + \frac{1}{\beta^2 a} \right) + \frac{v^4}{\beta^2 a}} \quad (3.39)$$

for the pendulum bob.

The formulae shown in Eqs. (3.38) and (3.39) are represented in Fig. 3.11. The normalized amplitude of the carrier disk starts at $\mu\beta^2 a/v^2$ for low values of n , and has major amplifications at the eigen-orders χ_1 and χ_2 . It has a zero at $n = v$ and the no resonance zone starts at this point and ends at the point where the line $\mu\beta^2 a/v^2$ crosses the ORF, at $n = \sqrt{\frac{1-q+v^2}{q}}$. The normalized amplitude of the pendulum bob starts at zero and has two major amplifications at the eigen-orders χ_1 and χ_2 . More importantly, the pendulum bob's normalized amplitude has no other zero but the one at $n = 0$. Hence, the pendulum responds to any order of excitation of this system.

The graphics shown in Fig. 3.11 have been calculated for a given value of Ω which would improve the visualization of all the features shown. It has already been shown in Fig. 3.8 that χ_1 tends to v for low rotating speeds and to zero for the high ones, while χ_2 tends to infinity if Ω is low and approaches $\sqrt{\frac{1-q+v^2}{q}}$ for increasing values of Ω . From Eq. (3.38), it is evident that the amplitude of the carrier disk will be zero whenever $n = v$, independently of the rotating speed.

3.3.2.2 Linear analysis considering gravity and small oscillations on the carrier disk's angular speed

Differently from the analysis performed in the previous section, in this case the gravitational terms are included. The amplitude of vibration of the carrier disk is still considered small, and so is the amplitude of vibration of the pendulum bob.

Once the gravitational terms are considered, a new dimensionless parameter must be defined. It is:

$$g_\epsilon = \frac{g}{\Omega^2 \epsilon_a}$$

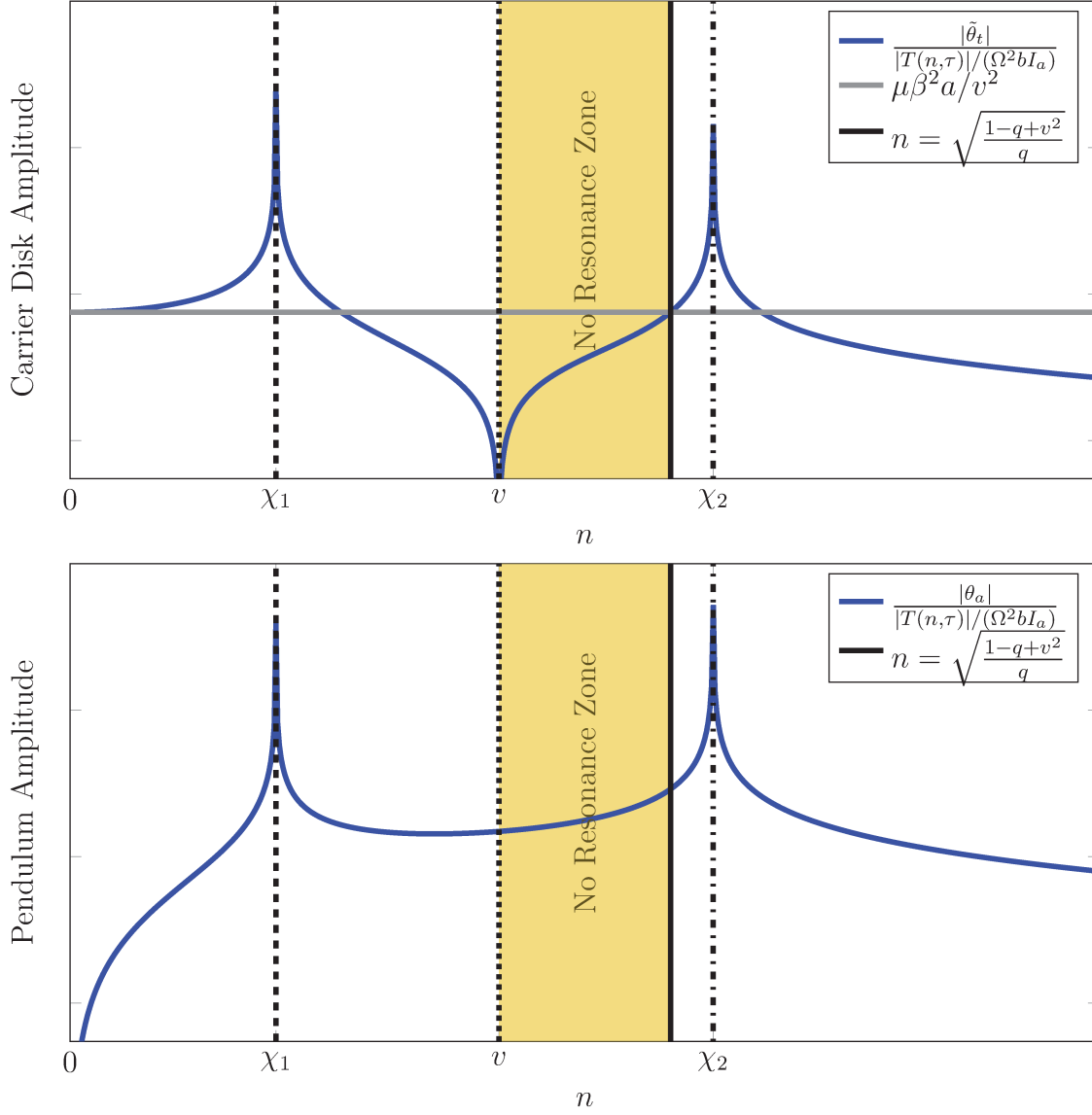


Figure 3.11: Order Response Function of carrier disk.

The equations of motion for this case become:

$$\begin{aligned}
 & \begin{bmatrix} \mu^{-1} & v^2 \\ 1+v^2 & 1 \end{bmatrix} \begin{Bmatrix} \tilde{\theta}_t'' \\ \theta_a'' \end{Bmatrix} + \dots \\
 & \dots + \left(\begin{bmatrix} \frac{v^2}{\beta^2 \mu a} & -v^2 \\ 0 & v^2 \end{bmatrix} - \begin{bmatrix} 1 & 0 \\ p & p \end{bmatrix} g_\epsilon v^2 \sin \tau \right) \begin{Bmatrix} \tilde{\theta}_t \\ \theta_a \end{Bmatrix} = - \begin{Bmatrix} 1 \\ p \end{Bmatrix} g_\epsilon v^2 \cos \tau
 \end{aligned} \tag{3.40}$$

The system is still linear, but it has time varying coefficients, which are 2π -periodic in the angle domain. There are some special cases in which it is possible to find a closed formula for the response of this system. This case, however, does not fit into this category. Hence, the Floquet theory must be used.

It is important to mention that the analysis to be performed in this case, where gravitational terms are considered, focuses on asserting whether these terms are capable of making the pendulum unstable or not. From previous analyses, it was shown that for certain combinations of parameters, the behavior of the pendulum could be unstable. In that case, however, the carrier disk was not allowed to vibrate.

In order to apply the Floquet theory, once the system does not have an analytical solution, the monodromy matrix¹⁸ was calculated using the numerical integrator `ode45`¹⁹ available in Matlab R2010a®. The integrator's parameters have been set to optimize precision of the results. The monodromy matrix was calculated using the homogeneous part of Eq. (3.40) only. Extension of these results to the non-homogeneous case is done through the results from the work of Slane and Tragesser (2011).

These matrices were calculated based on different values for the rotating speed of the system (Ω) and the tuning parameter of the pendulum v . For each point (Ω, v) , the monodromy matrix was calculated up to $\tau = 2\pi$, as required by the Floquet Theory, and then the eigenvalues of this matrix were computed. The maximum absolute value of the eigenvalues found for each point (Ω, v) is shown in Fig. 3.12.

In this graphic, the system will be stable (i.e. has a bounded response) on the dark blue points. For low rotating speeds, there is a region at the left of the graphic where the system is likely to be unstable. Above a certain rotating speed, the centripetal forces become much more relevant than the gravitational forces, and from this point on the system is stable up to a certain value of v . There is a well defined line on the top of Fig. 3.12, where the system turns from stable to unstable. This happens because the parameter v reaches a value where the constraint $\mu \leq 1/v^2(v^2 + 1)$ cannot be obeyed. Hence, the parameter q will be negative and consequently the system will be unstable.

¹⁸Defined in Appendix B.10.

¹⁹Further information about this integrator can be found in the work of Dormand and Prince (1980). In this work, this integrator is referred to as RK5(4)7M.

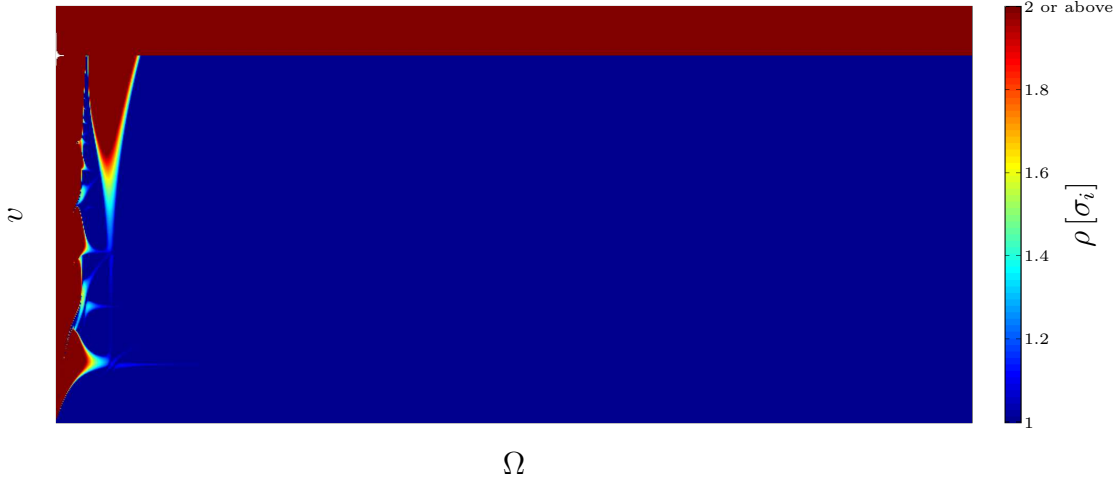


Figure 3.12: Maximum absolute value of the eigenvalues of the system for several (Ω, ν) points.

3.3.3 Systems with General Path CPVA

All the analyses carried so far in this chapter were performed on linear systems with a Circular Path CPVA. Nonlinear analyses were chosen not to be presented in the previous sections because pendulums with other than circular paths are an extension of the pendulums of the first kind. Hence, the results of the linear and nonlinear analyses shown for the general path pendulums apply for the circular path ones, and this eliminates the need for performing these analyses on previous sections.

Basically, all the inertia and distance parameters are the same from the previous analyses. The only parameter that is not going to be used directly is ϵ_a , because the pendulum's path is not necessarily circular. Its radius is actually a function of the pendulum bob's swing angle θ_a , called $r_a(\theta_a)$ and expressed in terms of a power series:

$$r_a(\theta_a) = \bar{\alpha}_0 + \sum_{k=1}^{\infty} \bar{\alpha}_k \theta_a^k \quad (3.41)$$

One must notice that if $\bar{\alpha}_k = 0 \mid k \in \mathbb{Z}_+^*$ and $\bar{\alpha}_0 = \epsilon_a$, then the path is circular. The

equations of motion for such system are²⁰:

$$\begin{aligned}
& (I_t + m_a R_p^2) \ddot{\theta}_t + m_a R_p \frac{d^2 r_a(\theta_a)}{d\theta_a^2} (\dot{\theta}_a^2 \sin \theta_a) + \dots \\
& + m_a R_p \frac{dr_a(\theta_a)}{d\theta_a} \left(\ddot{\theta}_a \sin \theta_a + 2\dot{\theta}_a (\dot{\theta}_a + \dot{\theta}_t) \cos \theta_a \right) + \dots \\
& + m_a R_p r_a(\theta_a) \left((\ddot{\theta}_a + \ddot{\theta}_t) \cos \theta_a - (\dot{\theta}_a + \dot{\theta}_t)^2 \sin \theta_a \right) + m_a R_p g \cos \theta_t = 0
\end{aligned} \tag{3.42}$$

for the disk and:

$$\begin{aligned}
& (I_a + m_a r_a^2(\theta_a)) (\ddot{\theta}_a + \ddot{\theta}_t) + 2m_a \frac{dr_a(\theta_a)}{d\theta_a} r_a(\theta_a) \dot{\theta}_a (\dot{\theta}_a + \dot{\theta}_t) + \dots \\
& + m_a r_a(\theta_a) \left(R_p (\ddot{\theta}_t \cos \theta_a + \dot{\theta}_t^2 \sin \theta_a) + g \cos(\theta_t + \theta_a) \right) = 0
\end{aligned} \tag{3.43}$$

for the pendulum.

The difference between these equations of motion and Eqs. (3.13) and (3.14) are the terms multiplied by the first and second derivatives of $r_a(\theta_a)$ with respect to θ_a . Among them are the terms related to the Coriolis acceleration, which were not present before because of the constant radius of the pendulum's path.

At this point a series of works has to be mentioned. They are the works from: Denman (1992), Chao *et al.* (1997), Lee and Shaw (1997), Chao and Shaw (2000), Alsuwayian and Shaw (2002), Alsuwayian and Shaw (2003), Haddow and Shaw (2003), Nester *et al.* (2003), Nester *et al.* (2004), Olson *et al.* (2005), Olson and Shaw (2008), Olson and Shaw (2009) and Gozen *et al.* (2012). In all of these works, the degrees of freedom used to model the pendulum dynamics are different from what is done in the present thesis.

All these authors have chosen to describe the motion of the pendulum's center of mass using an arc-length coordinate. This coordinate is zero at the vertex of the pendulum's path and describes the distance run by the center of mass of the pendulum bob along this path. For this reason, it requires the path to be symmetric and also the radius of curvature of the path has to be described as a function of the arc-length variable. The use of this formulation allows one to simulate a family of circular, cycloid and epicycloid paths through the variation of a single parameter, and is brought by Denman (1992). The formula is shown in Eq. (3.44).

$$\rho_i = \sqrt{\rho_{i0}^2 - \lambda^2 S_i^2} \tag{3.44}$$

²⁰Derivations are shown in Appendix B.17

Equation (3.44) is shown as it is in the work of Alsuwayian and Shaw (2002). The variable ρ_i is the radius of curvature of the i -th pendulum at a given position S_i , which is the arc-length of the path described by the center of mass of the pendulum bob. The constant ρ_{i0} is the radius of curvature of the path at its vertex and λ is the parameter to be varied. For $\lambda = 0$, the path is circular, while for $\lambda = 1$ it is cycloidal and for $\lambda = \sqrt{\tilde{n}_i^2/(\tilde{n}_i^2 + 1)}$ it is an epicycloidal of order \tilde{n}_i . The relationship between this parameter and the parameters used in the present thesis is: $\tilde{n}_i = 1/\sqrt{p}$.

In their work, the authors mention that this parameter sets the eigen-order of the pendulum to be \tilde{n}_i . Comparing their results to the ones found in the present thesis, it is not possible to confirm this statement, once the tuning parameter found is shown to be v , which depends on p and b , while \tilde{n}_i depends only on p .

There are, however, some disadvantages to be mentioned. The first one is that if the pendulum's path is not on the family mentioned above, then this formulation will not handle it conveniently. Secondly, the direct result from simulations is an arc-length and not the pendulum's swing angle, which is an important feature to be analyzed as mentioned by Wilson (1941). Thirdly, it restricts the path to be symmetric. For this reason, in the present thesis the dynamics of the pendulum is described by the angle θ_a and the radius of the path is given by the function $r_a(\theta_a)$. In order to ease further calculations and analysis and make this work more general, the function $r_a(\theta_a)$ is defined in the following way:

$$r_a(\theta_a) = \epsilon_a f_a(\theta_a) \quad \left| \quad f_a(\theta_a) = 1 + \sum_{k=1}^{\infty} \alpha_k \theta_a^k \quad (3.45)$$

The function $f_a(\theta_a)$ is a shape function for the path of the pendulum. Once it can be defined as a power series, any path can be handled with the same formulation. Besides, this function is dimensionless, and hence it does not depend on parameters of the system to be calculated. It means that, if for instance one wants to test a system with a cycloidal path pendulum, the function $f_a(\theta_a)$ will be exactly the same for any system. Another advantage is that it makes possible to run optimization routines in order to find paths that bring specific features to the dynamics of the pendulum.

Although pendulum paths are usually symmetric about their vertexes, it does not assure that the pendulum's trajectory is symmetric. In the case being studied in this work, the pendulum is going to be installed in a rotor that is subjected to both small oscillations

and changes on its mean rotating speeds. The angular acceleration that induces the change on the mean speed of the rotor has a very low frequency content. However, it forces the pendulum to oscillate about a point which is not the vertex of the path. Hence, in case of non-circular paths there will be some extra terms in the equation of motion that represent this non-symmetry which may detune or harm stability of the pendulum. Detuning terms also appear when using circular paths.

In order to illustrate this concept, the rotor of the system studied in this section is thought to be spinning at a speed Ω while it accelerates in such a way that the pendulum is forced to oscillate about an angle $\theta_a = \iota$. If $\theta_a = \tilde{\theta}_a + \iota$ and $\tilde{\theta}_a$ is very small, then it is possible to linearize Eq. (3.43) about this point. The dimensionless linearized equation that describes the motion of the pendulum bob is given by:

$$\begin{aligned} & \left(\frac{1}{b} + \left(1 - \frac{1}{b} \right) f_a^2(\iota) \right) \tilde{\theta}_a'' + 2 \left(1 - \frac{1}{b} \right) \frac{df_a}{d\theta_a}(\iota) f_a(\iota) \tilde{\theta}_a' + \dots \\ & + v^2 \left(\frac{df_a}{d\theta_a}(\iota) \sin \iota + f_a(\iota) \cos \iota \right) \tilde{\theta}_a = 0 \end{aligned} \quad (3.46)$$

where constant terms have been neglected.

If the path is circular, then $f_a(\iota) = 1$ and $\frac{df_a}{d\theta_a}(\iota) = 0$. This reduces Eq. (3.46) to:

$$\tilde{\theta}_a'' + v^2 \cos(\iota) \tilde{\theta}_a = 0 \quad (3.47)$$

The difference between this equation and Eq. (3.17) is that the eigen-order for this case is $v\sqrt{\cos(\iota)}$ and not v as previously demonstrated. The term $\sqrt{\cos(\iota)}$ is then a detuning term.

If the path is not circular, Eq. (3.46) has to be analyzed more carefully. Regarding the inertial term, b is real and greater than one, and $f_a(\iota)$ is also always real and greater than one, because on the work of Olson and Shaw (2008) it is shown that the performance of the pendulum is improved if the path is softening, what requires $f_a(\iota)$ to be greater than one. Hence, the inertia of this system is always positive. If the path is symmetric about its vertex, then $\frac{df_a}{d\theta_a}(\iota)$ is an odd function, and when multiplied by $\sin(\iota)$, the result is an even nonnegative function. If $-\pi/2 \leq \iota \leq \pi/2$, then the product $f_a(\iota) \cos \iota$ is also positive, and hence the stiffness term is always positive.

The same, however, cannot be said about the term that multiplies $\tilde{\theta}'_a$. The shape function $f_a(\iota)$ is even and continuous and has continuous derivatives. Hence, the derivative of this function for $\iota = 0$ is zero, and it is an odd function. Therefore, if ι is negative, this term is negative and the motion of the pendulum bob is unstable in this example. Of course the stability of the pendulum itself depends on other parameters that have not been considered in this illustrative example.

The shape of the pendulum's path is then a crucial parameter to determine its tuning and stability for large amplitude motion or nonzero equilibrium position. In the work of Alsuwayian and Shaw (2002), the authors analyze the stability of general path CPVAs focusing on the three most classical paths: the circular, the cycloidal and the epicycloidal or tautochronic. Among their conclusions are the facts that for large amplitude motions, paths other than circular have not shown significant improvements. Furthermore, the authors make the point that for any path considered, small amplitude motions always lead to less detuning, better stability and better performance.

According to Wilson (1941) and all the subsequent works in this area, the higher the effective inertia of the pendulum and the higher the radius at which it is installed, the smaller is the pendulum swing angle. However, both of these parameters would increase the inertia of the input shaft of the gearbox, leading to worse shiftability or increased wear of the synchronizers. Hence, it is desirable to obtain a pendulum with good performance that would add the least possible inertia to the input shaft, and at this point non-circular paths are desirable.

Before heading to the shape function for other paths, it is important to present a mathematical procedure that is fundamental for the calculation of the coefficients of $f_a(\theta_a)$. Because it is defined as a power series, it is necessary to calculate its coefficients using Taylor Series approach, what means that, if the resulting polynomial is to be truncated at a given order n , then the n -th derivative of the function $f_a(\theta_a)$ must be calculated, and this brings some mathematical difficulties to be dealt with.

It is usually difficult to describe cycloids or epicycloids as a function of the angle θ_a . It is more convenient to describe these paths using a rolling angle θ_r , which is defined differently for each of them. However, it is always possible to describe a point $(x_p(\theta_r), y_p(\theta_r))$ as a function of the rolling angle and also to write the angle θ_a as a (usually non-invertible) function of θ_r , i.e. $\theta_a = \theta_a(\theta_r)$.

The radius of the path $r_a(\theta_a)$ is now written as a function of the rolling angle. Therefore, $r_a(\theta_a) = r_a(\theta_r(\theta_a)) = \sqrt{x_p(\theta_r)^2 + y_p(\theta_r)^2}$. In order to differentiate this function with respect to θ_a , the chain rule must be applied, leading to the following relationship:

$$\frac{d}{d\theta_a} (r_a(\theta_r(\theta_a))) = \frac{\partial r_a}{\partial \theta_r} \frac{d\theta_r}{d\theta_a} \quad (3.48)$$

The partial derivative from Eq. (3.48) is easily obtained, because x_p and y_p are direct functions of θ_r . The latter derivative is obtained implicitly from the relationship between θ_a and θ_r . This relationship can always be defined as:

$$\theta_a = \arctan \left(\frac{x_p(\theta_r)}{y_p(\theta_r)} \right) \quad (3.49)$$

Through performing implicit differentiation with respect to θ_r , it is possible to find the desired derivative, given by:

$$\frac{d\theta_r}{d\theta_a} = \frac{r_a^2(\theta_r(\theta_a))}{\frac{dx_p}{d\theta_r} y_p - \frac{dy_p}{d\theta_r} x_p} \quad (3.50)$$

The partial derivative on Eq. (3.48) is directly calculated, and it is given by:

$$\frac{\partial r_a}{\partial \theta_r} = \frac{1}{r_a} \left(\frac{dx_p}{d\theta_r} x_p + \frac{dy_p}{d\theta_r} y_p \right) \quad (3.51)$$

Combining Eqs. (3.50) and (3.51) makes possible to write an analytical expression for the result of Eq. (3.48):

$$\frac{d}{d\theta_a} (r_a(\theta_r(\theta_a))) = \left(\frac{\frac{dx_p}{d\theta_r} x_p + \frac{dy_p}{d\theta_r} y_p}{\frac{dx_p}{d\theta_r} y_p - \frac{dy_p}{d\theta_r} x_p} \right) r_a(\theta_r(\theta_a)) = g(\theta_r(\theta_a)) r_a(\theta_r(\theta_a)) \quad (3.52)$$

The most important fact about this procedure is that the derivative of $r_a(\theta_r(\theta_a))$ with respect to θ_a is, for any path, the product between a given function and $r_a(\theta_r(\theta_a))$. This fact eases the calculation of the coefficients on the following way: given the function $r_a(\theta_r(\theta_a))$, its first derivative with respect to θ_a is given by $g(\theta_r(\theta_a)) r_a(\theta_r(\theta_a))$. The second derivative of

$r_a(\theta_r(\theta_a))$ with respect to θ_a is then given by:

$$\begin{aligned} \frac{d^2 r_a(\theta_r(\theta_a))}{d\theta_a^2} &= \frac{\partial g(\theta_r(\theta_a))}{\partial \theta_r} \frac{d\theta_r}{d\theta_a} r_a(\theta_r(\theta_a)) + g(\theta_r(\theta_a)) \frac{dr_a(\theta_r(\theta_a))}{d\theta_a} \\ &= \left(\frac{\partial g(\theta_r(\theta_a))}{\partial \theta_r} \frac{d\theta_r}{d\theta_a} + g^2(\theta_r(\theta_a)) \right) r_a(\theta_r(\theta_a)) \end{aligned} \quad (3.53)$$

i.e., if the derivative of $r_a(\theta_r(\theta_a))$ is a product between this function and another one, namely $g(\theta_r)$, then all the higher derivatives of this functions will be products between $r_a(\theta_a)$ and functions of $g(\theta_r)$ and its derivatives. Consequently, in order to calculate the derivatives of $r_a(\theta_r(\theta_a))$, it is only necessary to calculate the derivatives of $g(\theta_r)$. The expressions for the first up to the eighth derivatives of $r_a(\theta_r(\theta_a))$ in terms of $g(\theta_r)$ and its derivatives are shown in Appendix B.18.

Although the calculations may still be tiresome, the function $g(\theta_r(\theta_a))$ is essentially composed by the functions $x_p(\theta_r)$ and $y_p(\theta_r)$, which are simple functions, whose derivatives are rather easy to calculate. Therefore, in order to define the derivatives of $r_a(\theta_r(\theta_a))$ or $f_a(\theta_a)$, it suffices to define $g(\theta_r(\theta_a))$, i.e., it suffices to define the functions $x_p(\theta_r)$ and $y_p(\theta_r)$.

The problem of writing the radius of the path as a power series is then overcome. One must notice that, an outstanding feature from this procedure is that, although it is not possible to write $r_a(\theta_a)$ analytically, the power series $f_a(\theta_a)$ is written as a function of θ_a directly, eliminating the need for calculating $\theta_r(\theta_a)$ numerically, once this function is not invertible.

3.3.3.1 Shape function for the cycloidal path

The cycloid is a curve generated by the path of a point at the edge of a circle which rolls on a straight line without slippage. It was first formally studied by Galileo Galilei and for causing lots of quarrels between 17th century mathematicians, it is sometimes referred to as “The Helen of Geometers”. Apart from lots of history of Mathematics, in 1696 the swiss mathematician John Bernoulli found this curve as a solution to the brachistochrone problem, whose aim was to find the expression of the path on which a particle would slide, under the influence of the gravity, from a point A to a lower point B , not immediately below A , in the shortest time.

Before the results achieved by Bernoulli, the dutch physicist and horologist Christiaan Huygens, the inventor of pendulum clock, had had some problems on the synchronism of his clocks, because he was able to detect that, as the amplitude of his pendulum decreased, its frequency of oscillation would also change. This fact led to the isochrone problem, whose goal was to find a path for which the period of oscillation of the pendulum would be the same, regardless of its amplitude. Huygens found the solution to this problem as being the cycloidal path.

These facts motivated the use of this path on the problem being studied in this work. Figure 3.13 shows the geometric features that are necessary to generate the cycloidal path.

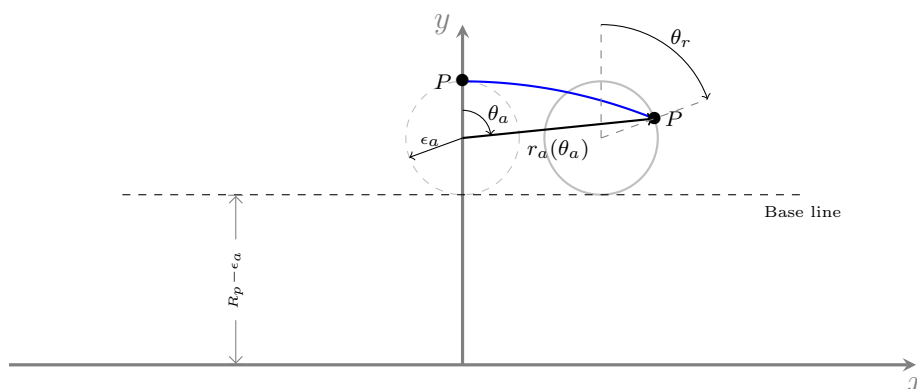


Figure 3.13: Geometry for the generation of the cycloidal path.

The position of the point P, on the edge of the rolling circle, can be described by the functions $x_p(\theta_r)$ and $y_p(\theta_r)$, being the first the position of this point along the x -axis and the latter the position of this point along the y -axis, considering that its origin is at the center of the rolling circle when it is at the position $x = 0$. These functions are defined as follows:

$$x_p(\theta_r) = \epsilon_a(\theta_r + \sin \theta_r) \quad (3.54)$$

$$y_p(\theta_r) = \epsilon_a \cos \theta_r \quad (3.55)$$

Also, the implicit relationship between θ_a and θ_r is:

$$\theta_a = \arctan \left(\frac{x_p(\theta_r)}{y_p(\theta_r)} \right) = \arctan \left(\frac{\theta_r + \sin \theta_r}{\cos \theta_r} \right) \quad (3.56)$$

This relationship is graphically represented in Fig. 3.14. It has some important features to be mentioned: firstly, it has no local minima on this interval, what makes it an invertible function within this domain. Secondly, both angles are coincident at the boundaries of the domain. Thirdly and more importantly, $\theta_r(\theta_a = 0) = 0$. The last fact is important because this angle is going to be the center of the Taylor series to be computed. One must notice that although the center of the Taylor series is at $\theta_a = 0$, many of the functions are calculated in terms of $\theta_r(\theta_a)$. As $\theta_r(\theta_a = 0) = 0$ by definition, then there will be no error on the calculation of $\theta_r(\theta_a)$.

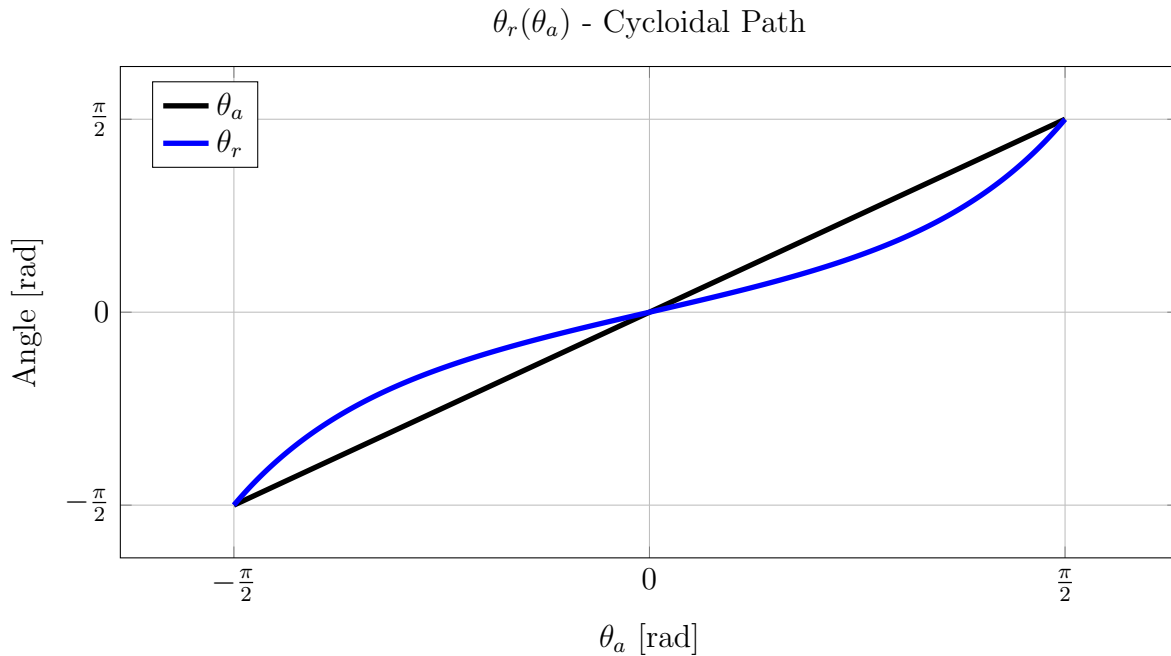


Figure 3.14: Graphical representation of the implicit relationship $\theta_r(\theta_a)$ for the cycloidal path.

With these definitions it is now possible to define the function $g(\theta_r)$. With this function it is possible to calculate the derivatives of $f_a(\theta_a)$ with respect to θ_a . For being an even function, the odd derivatives of $r_a(\theta_a)$ with respect to θ_a are null at $\theta_a = 0$, and consequently, so are the odd coefficients α_i , $i \in \{1, 3, 5, \dots\}$. The even derivatives of the radius of the path and the even coefficients²¹ of $f_a(\theta_a)$ are shown on the Table 3.2.

As previously mentioned, the coefficients of the function $f_a(\theta_a)$ do not depend on any parameter of the system. Obviously the power series must be truncated at a given order. For this reason, the following notation is going to be used: given that the whole series is defined

²¹Refer to Eq. (3.45).

Table 3.2: First coefficients of $f_a(\theta_a)$

k	0	1	2	3	4
$\epsilon_a^{-1} \frac{d^{2k}}{d\theta_a^{2k}} (r_a(\theta_r(\theta_a)))$	1	$\frac{3}{4}$	$\frac{35}{16}$	$\frac{1325}{128}$	$\frac{2199}{256}$
α_{2k}	1	$\frac{3}{8}$	$\frac{35}{384}$	$\frac{1325}{92160}$	$\frac{2199}{10321920}$

as:

$$f_a(\theta_a) = 1 + \sum_{k=1}^{\infty} \alpha_k \theta_a^k \quad (3.57)$$

then the truncated series is termed as:

$$f_a^{(n)}(\theta_a) = 1 + \sum_{k=1}^n \alpha_k \theta_a^k \quad , \quad n \in \mathbb{Z}_+^* \quad (3.58)$$

Once the first term of the shape function $f_a(\theta_a)$ is one, $f_a^{(0)}(\theta_a)$ is, for any path, the circular path that approaches it best. The even approximations from $f_a^{(2)}(\theta_a)$ to $f_a^{(8)}(\theta_a)$ are shown in Fig. 3.15. The thick black line represents the original cycloid, while the thin ones represent the truncated series approximations. The black dashed line represents the circular path²². In this picture it is evident that the circular path approaches the cycloidal path for a rather small amplitude of the swing angle of the pendulum. The second order approximation is more representative for an amplitude higher than the circular path, but it is still limited to a small angle. The fourth order approximation approaches the cycloid very well, while the two higher ones also do, and are almost superposed.

The percent error of the estimation is shown in Fig. 3.16, where only positive values of θ_a are shown because the curves are symmetric about the y axis. In this figure it becomes evident that the circular path approximation provides very much error. If the swing angle of the pendulum is of at most $\pm 15^\circ$, then the second order series would already be a good approximation. The eighth order polynomial does not bring great advantage over the sixth order one. Both provide less than 1% of error for swing angles up to $\pm 75^\circ$.

Concluding this section, one must notice that the geometric functions $x_p(\theta_r)$ and $y_p(\theta_r)$ do not depend on the distance R_p for the case of the cycloidal path. For this reason, the coefficients of $f_a(\theta_a)$ are purely numeric. Furthermore, once the series is centered at zero, all

²²It looks elliptical because the axes are in different scales.

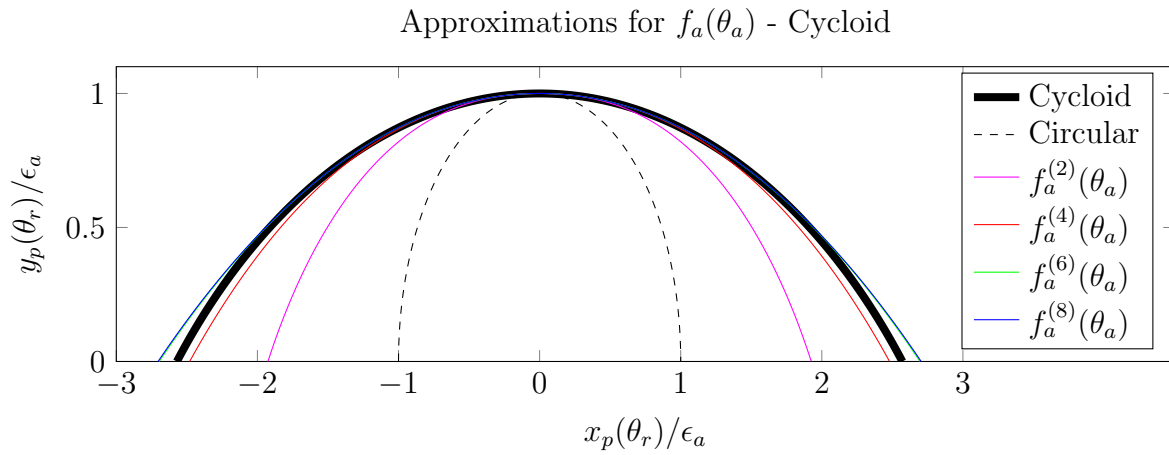


Figure 3.15: Second, 4th , 6th and 8th order approximations for the cycloidal path.

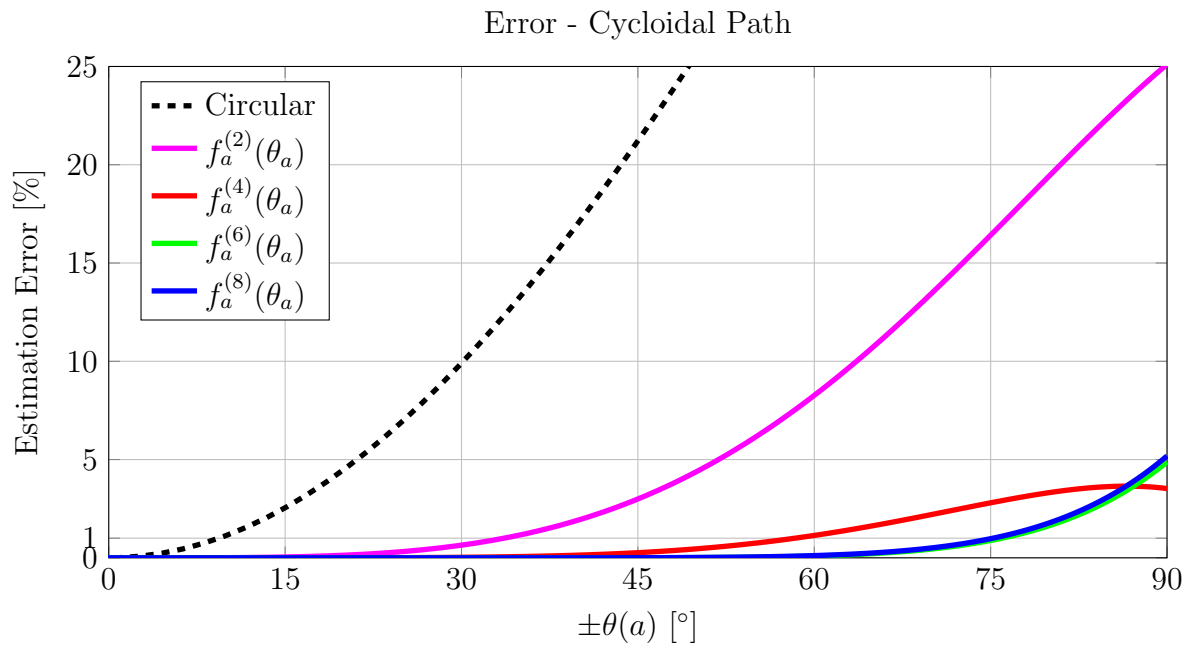


Figure 3.16: Percent estimation error for the 2nd , 4th , 6th and 8th order approximations for the cycloidal path.

the coefficients are rational numbers, therefore they can be defined precisely. On the next section, the shape function for the epicycloidal path is going to be defined.

3.3.3.2 Shape function for the epicycloidal path

An epicycloid is a curve generated by the path performed by a point on the edge of a circle that rolls, without slip, on the surface of another circle. The main motivation to adopt an epicycloidal path instead of a cycloid is related to the detuning of the pendulum.

For the case of a simple pendulum, whose base is fixed, under the acceleration of gravity, the *tautochronic*²³ path is a cycloid. However, if the gravitational field is represented by means of lines of field, then all the lines are going to be parallel, considering the application is close enough to the surface of the Earth.

When a centrifugal field is considered, i.e. the pendulum is installed on a rotor, then the lines of field are originated at the geometrical center of the rotor and point radially outwards. For small displacements, the effect of both accelerations is the same. However, for large displacements the effects differ, and the *tautochronic* path in this case is not a cycloid, it is an epicycloid (Wedin (2011)).

The geometrical features for the mathematical description of the epicycloid are shown in Fig. 3.17. Based on these variables, it is possible to write the geometric functions $x_p(\theta_r)$ and $y_p(\theta_r)$, which are given by:

$$x_p(\theta_r) = \epsilon_a \left(\frac{1}{p} \sin \left(\frac{\theta_r p}{1-p} \right) + \sin \theta_r \right) \quad (3.59)$$

$$y_p(\theta_r) = \epsilon_a \left(\frac{1}{p} \cos \left(\frac{\theta_r p}{1-p} \right) + \cos \theta_r - \frac{1}{p} \right) \quad (3.60)$$

As in the previous case, the angle θ_a is defined as:

$$\theta_a = \arctan \left(\frac{x_p(\theta_r)}{y_p(\theta_r)} \right) \quad (3.61)$$

²³The term *tautochronic* refers to a path that allows the pendulum to have the same period of oscillation, regardless of its amplitude.

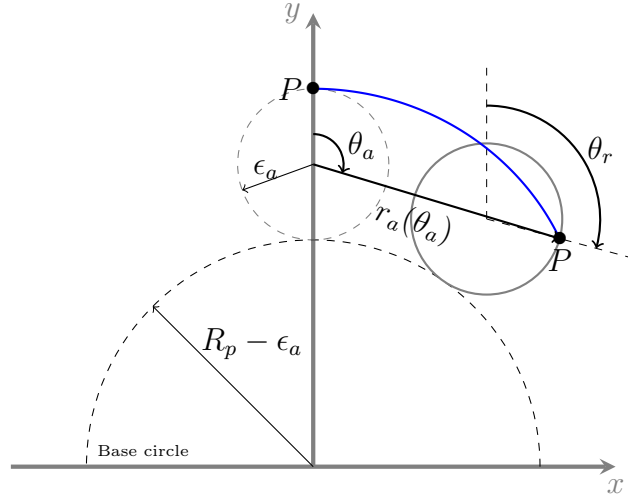


Figure 3.17: Geometry for the generation of the epicycloidal path.

Although this angle does not depend on any physical parameter but, of course, the angle θ_r , it depends on a dimensionless parameter p , which is given by $p = \epsilon_a/R_p$. This is in line with what is shown in the work of Alsuwayian and Shaw (2002). In their work, the authors describe the epicycloid in terms of a parameter \tilde{n}_i and say that it results in an epicycloid of the same order. This parameter is related to the parameter p from this work as follows: $\tilde{n}_i = 1/\sqrt{p}$. It is worth mentioning that this parameter is calculated at the project of the pendulum for low amplitudes. Once this parameter is defined, the path is defined.

Once again the relationship between the angles θ_r and θ_a is implicit. It is graphically represented for some values of p in Fig. 3.18 and it is also limited so that $-\pi/2 < \theta_a < \pi/2$. Although at the boundaries of the domain the values of θ_r and θ_a are not coincident, $\theta_r(\theta_a = 0) = 0$ regardless of the value of p by definition, which is important because this point is the center of the Taylor series to be calculated. Also, through Eqs. (3.59) and (3.60) it is easy to see that when $p \rightarrow 0$ the epicycloid tends to a cycloid.

For being a symmetric function about $\theta_a = 0$, all the odd coefficients of the polynomial $f_a(\theta_a)$ are null. The even coefficients are either real numbers or functions of p . For this reason, the derivatives of the function $r_a(\theta_r(\theta_a))$ are defined in the following way:

$$\epsilon_a^{-1} \frac{d^{2k}}{d\theta_a^{2k}} (r_a(\theta_r(\theta_a))) = E_{2k}(p) \quad , \quad k \in \mathbb{Z}_+ \quad (3.62)$$

$\theta_r(\theta_a)$ - Epicycloidal Path

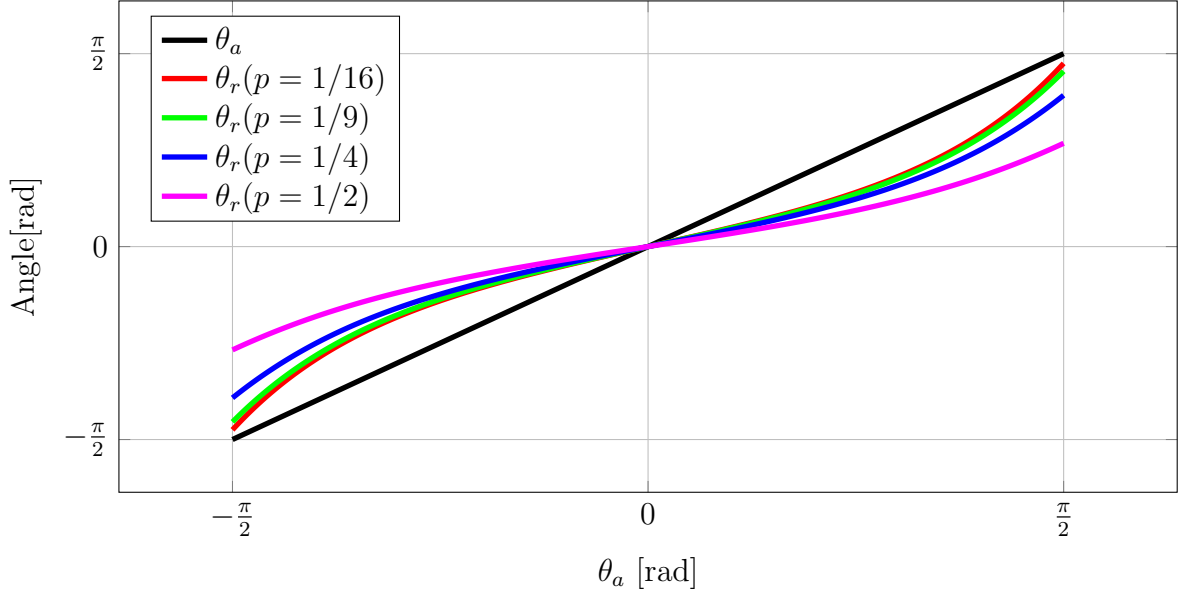


Figure 3.18: Graphical representation of the implicit relationship $\theta_r(\theta_a)$ for the epicycloidal path.

Therefore, the coefficients of the polynomial $f_a(\theta_a)$ become:

$$\alpha_{2k} = \frac{E_{2k}(p)}{(2k)!} \quad , \quad k \in \mathbb{Z}_+ \quad (3.63)$$

The functions from $E_0(p)$ to $E_8(p)$ are defined in Appendix B.19. One must notice that, if $p = 0$, then the coefficients are the same of the cycloid, and when $p = 1$, all the coefficients but $E_0(p)$ are null.

The forthcoming analyses are going to be performed assuming that $p = 1/4$. The results found for this value are also valid for smaller value of p . If $p = 0$, the epicycloid becomes a cycloid, which has already been analyzed in the previous section. Higher values for p are not usual in practice, because one of the design goals is to maximize R_p , which reduces the value of p . However, if $p = 1$, then the path becomes circular and the first term of the Taylor series is precisely the expression of the path. Hence, higher values of p , up to the unity, lead to smaller approximation error²⁴.

²⁴Values of p greater than the unity are of no practical use.

The approximations of the epicycloid up to the eighth order are shown in Fig. 3.19. As in the case of the cycloid, the circular path and the second order approximation provide good estimation of the path for small swing angles. The fourth order approximation provides a good estimation for the whole path, and the sixth and eighth order approximations also do. However, the two latter ones are almost superposed.

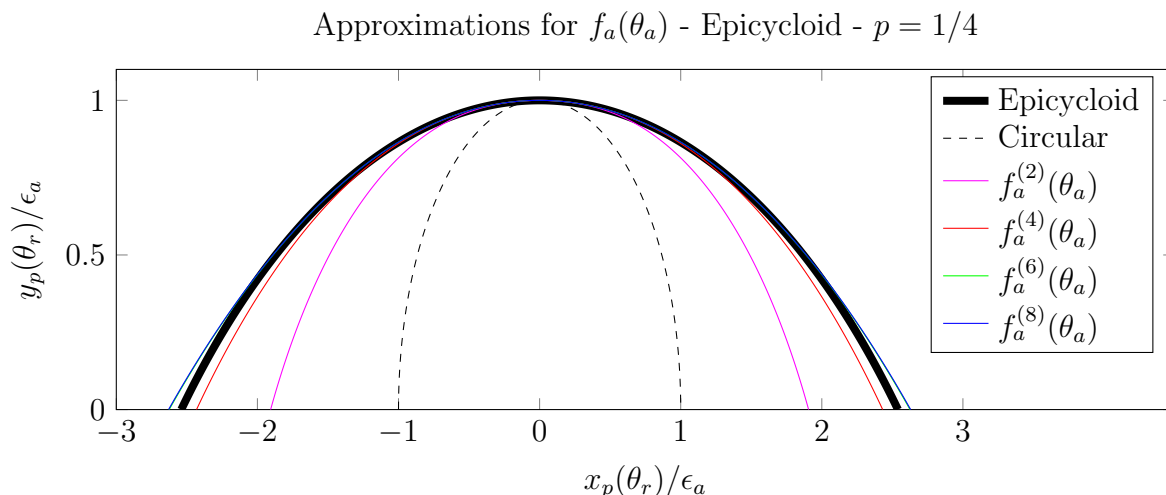


Figure 3.19: Second, 4th , 6th and 8th order approximations for the epicycloidal path.

The percent error of estimation of the epicycloidal path is shown in Fig. 3.20. The estimation error obtained is very close to what was obtained for the cycloidal path. If the swing angle is less than $\pm 45^\circ$, $f_a^{(4)}(\theta_a)$ is a good approximation. For swing angles below $\pm 75^\circ$, $f_a^{(6)}(\theta_a)$ is shown to provide less than 1% of error.

With these approximations it is possible to analyze the behavior of approximate solutions for the nonlinear equations of motion, in order to evaluate stability and performance of the pendulum with the cycloidal and epicycloidal paths. This is done in the following sections.

3.3.3.3 Multiple Scales Method

Before heading to the analysis of the nonlinear equations of motion, the method chosen to obtain the approximate solutions of the nonlinear equations of motion is presented. Additionally, the choice of this method instead of the most usual one in the recent works on

Error - Epicycloidal Path - $p = 1/4$

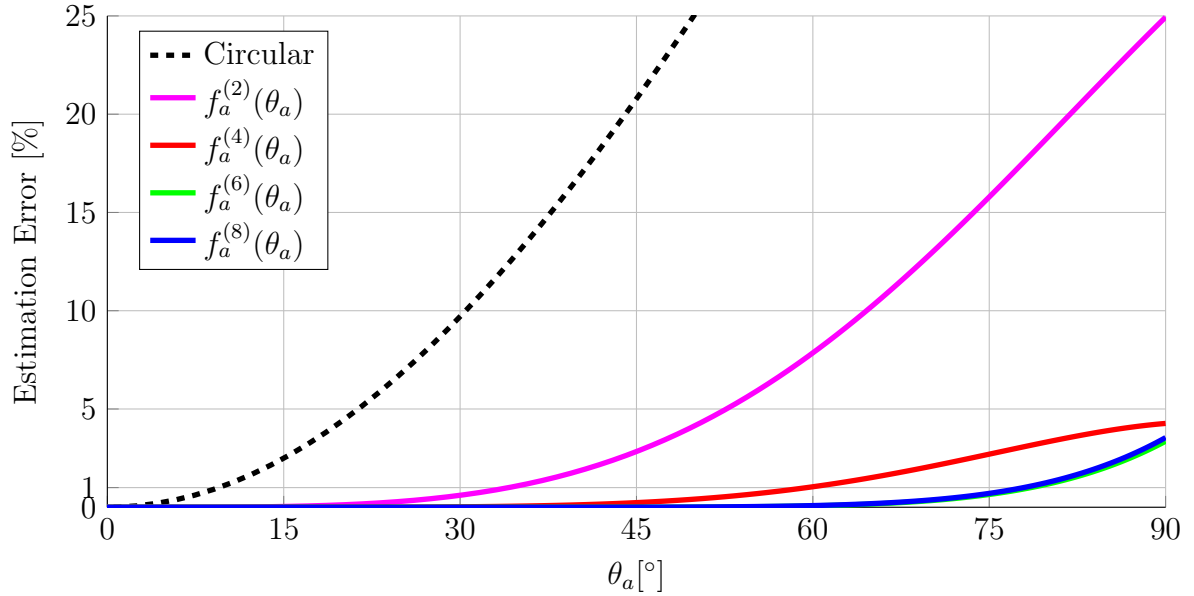


Figure 3.20: Percent estimation error for the 2nd, 4th, 6th and 8th order approximations for the epicycloidal path.

centrifugal pendulums is justified.

One of the main contributions of this work, on the study of centrifugal pendulum vibration absorbers, is to develop the equations of motion in terms of the spinning angle of the rotor and the swing angle of the pendulum. These coordinates have not been chosen by recent authors on this field because it leads to mathematical obstacles they could avoid by the choice of different coordinates.

Yet mathematically convenient, these coordinates do not allow for direct physical interpretation of the results. Furthermore, the same mathematical convenience may not be achieved, unless the path of the pendulums belongs to the family of circular-epicycloid-cycloid family.

The choice of angular coordinates is proposed to deal with these disadvantages. They lead directly to nonlinear equations of motion with trigonometrical functions of the coordinates, which is an obstacle, and also require the knowledge of the radius of the pendulum's path²⁵ in terms of the swing angle of the pendulum, which is usually not easy to describe

²⁵Not to be confused with the radius of curvature of the path.

mathematically.

The latter disadvantage has been overcome earlier in this chapter, where a mathematical procedure was developed and it was shown that it is possible to represent the radius of the path as a function of the swing angle with high degree of precision. The first one, however, demanded additional effort to be overcome.

In the recent works on centrifugal pendulum vibration absorbers, the convenient choice of coordinates led to equations of motion on the form:

$$z_i'' + n^2 z_i = \epsilon f(z_i, z_j, z_k, \dots, z_i', z_j', z_k', \dots; p) \quad (3.64)$$

, which makes them suitable for the application of Krylov-Bogoliubov technique or its variants, the former being usually referred to as the *Method of Averaging*.

This method belongs to the family of perturbation methods, and basically consists of proposing that the response for equations such as Eq. (3.64) is of the form:

$$z_i(\tau) = a(\tau) \cos(n\tau + \beta(\tau)) \quad (3.65)$$

, where, instead of being constant, $a(\tau)$ and $\beta(\tau)$ are slowly varying functions of τ , a given independent variable, usually a given dimensionless time scale.

Although this is a widespread method, it has shown to be limited, as in the work of Nayfeh (1981). Even in a very simple case, such as the linear oscillator, this method fails to compute the correction on the frequency response of free oscillation of the system. The generalized method of averaging or the Krylov-Bogoliubov-Mitropolsky method of averaging are able to handle this flaw, at the cost of an increased amount of algebra.

Even though a variant of the most usual method for obtaining approximated solutions for the nonlinear equations is more precise than what is being currently used, the latter methods also require the equations to be on the form of Eq. (3.64). The equations on this work, mainly Eqs. (3.42) and (3.43) can be manipulated to be represented in such form, but this would lead to a very complicated right hand side of the equation, because inertial terms are not constant. This is undesirable because this class of methods requires the right hand side to be integrated, and hence it should be simple to allow integrals to be solvable.

Regarding perturbation methods, one of the simplest ones is the straightforward expansion. In order to present a comprehensive explanation with direct examples, the Duffing equation is introduced:

$$\ddot{u} + u + \epsilon u^3 = 0 \quad (3.66)$$

, where the dot ($\dot{}$) represents differentiation with respect to t and ϵ is a small parameter.

In order to perform a straightforward expansion, the solution of this equation is proposed to be of the form:

$$u = u(t; \epsilon) = u_0(t) + \epsilon u_1(t) + \epsilon^2 u_2(t) + \dots \quad (3.67)$$

This expansion must be replaced on Eq. (3.66). One must notice that if $\epsilon = 0$, then the solution to Eq. (3.66) is $u_0 = a \cos(t + \beta)$ ²⁶. The other terms on the expansion are considered corrections to this first order approximation due to the presence of the nonlinearity.

The next step is to replace Eq. (3.67) into Eq. (3.66) and equal the coefficients of equal powers of ϵ on both sides. This procedure results in a set of linear differential equations to be solved:

$$\ddot{u}_0 + u_0 = 0 \quad (3.68)$$

$$\ddot{u}_1 + u_1 = -u_0^3 \quad (3.69)$$

$$\ddot{u}_2 + u_2 = -3u_1 u_0^2 \quad (3.70)$$

$$\ddot{u}_3 + u_3 = -3u_2 u_0^2 - 3u_0 u_1^2 \quad (3.71)$$

$$\vdots \quad \vdots$$

It is evident that this system can be solved iteratively. From Eq. (3.68) it is possible to obtain u_0 , which is used to calculate the response u_1 and so on. Once every single equation in this set has the same eigenvalues, the homogeneous response has to be calculated only for u_0 . For all the other terms, the inhomogeneous response is needed only.

²⁶In this case, a and β are not the parameters of the pendulum, but constants to be determined using initial conditions.

Beginning with the iterative process, the term u_0 is given by:

$$u_0(t) = a \cos(t + \beta) \quad (3.72)$$

For the solution of the next equation, u_0^3 must be calculated. This term is conveniently represented in the form:

$$u_0^3(t) = a^3 \cos^3(t + \beta) = \frac{a^3}{4} (\cos(3t + 3\beta) + 3 \cos(t + \beta)) \quad (3.73)$$

, which results in:

$$u_1(t) = -\frac{a^3}{32} \cos(3t + 3\beta) - \frac{3a^3}{8} t \sin(t + \beta) \quad (3.74)$$

The term $u_1(t)$ is composed of an oscillatory term ($\cos(3t + 3\beta)$) and an indefinitely growing one ($t \sin(t + \beta)$), usually referred to as *secular term* or *mixed secular term*. This denomination is derived from the French word *si ecle*, which means century. In astronomical applications, ϵ is very small and secular terms become noticeable only after very long times of the order of a century.

Equation (3.66) represents a weakly nonlinear unforced oscillator with no unstable equilibria, and hence secular terms are not physically representative. The only condition that could make the secular term vanish would be $a = 0$, leading to the trivial solution.

In this expansion, the correction terms should be smaller than the main one (u_0). Once this is consistent only if $t < O(\epsilon^{-1})$, the series is called nonuniform because it breaks down for a long time. This kind of expansion is usually referred to as *pedestrian expansion*.

In fact, it happens because the expansion does not account for a nonlinear frequency, i.e., corrections on the frequency of oscillation of the system due to the presence of nonlinearities. According to Nayfeh (1981), any expansion that does not account for this frequency correction is doomed to failure.

An expansion that takes this frequency correction into account is present in the method of Lindstedt-Poincar e. This method, however, is not suitable for systems with first order derivatives, as is the case of Eqs. (3.42) and (3.43). Therefore, a more general method based on the straightforward expansion must be used. One must notice that such expansion does

not demand the equations to be in any specific form.

This is the case of the *Multiple Scales Method*, which is going to be applied on Eq. (3.66). Firstly, the solution is thought to be of the form:

$$u(t; \epsilon) = u(t, \epsilon t, \epsilon^2 t, \dots; \epsilon) = u(T_0, T_1, T_2, \dots; \epsilon) \quad (3.75)$$

$$u(t; \epsilon) = u_0(T_0, T_1, T_2, \dots) + \epsilon u_1(T_0, T_1, T_2, \dots) + \epsilon^2 u_2(T_0, T_1, T_2, \dots) + \dots$$

The terms in the expansion are thought to depend on more than one time scale. As ϵ is a small parameter, t is a fast time scale while ϵt is a slower one and so on. Also, the time scales $T_n = \epsilon^n t$ are independent. Hence, differentiation with respect to time must now obey to the chain rule:

$$\frac{d}{dt} = \frac{\partial}{\partial T_0} + \epsilon \frac{\partial}{\partial T_1} + \epsilon^2 \frac{\partial}{\partial T_2} + \dots = \sum_{k=0}^{\infty} \epsilon^k \frac{\partial}{\partial T_k} \quad (3.76)$$

$$\frac{d^2}{dt^2} = \sum_{l=0}^{\infty} \epsilon^l \frac{\partial}{\partial T_l} \left(\sum_{k=0}^{\infty} \epsilon^k \frac{\partial}{\partial T_k} \right) \quad (3.77)$$

The next step is to replace Eqs. from (3.75) to (3.77) into Eq. (3.66) and equate the coefficients of like powers of ϵ on both sides. This leads to a set of partial differential equations to be solved:

$$\frac{\partial^2 u_0}{\partial T_0^2} + u_0 = 0 \quad (3.78)$$

$$\frac{\partial^2 u_1}{\partial T_0^2} + u_1 = -u_0^3 - 2 \frac{\partial^2 u_0}{\partial T_0 \partial T_1} \quad (3.79)$$

$$\frac{\partial^2 u_2}{\partial T_0^2} + u_2 = -3u_1 u_0^2 - 2 \frac{\partial^2 u_0}{\partial T_0 \partial T_2} - \frac{\partial^2 u_0}{\partial T_1^2} - 2 \frac{\partial^2 u_1}{\partial T_0 \partial T_1} \quad (3.80)$$

⋮ ⋮

Similarly to the case of the simple straightforward expansion, this set of equations can be solved iteratively. The difference is that, for being a set of partial differential equations, the task is now to define the dependence of the solution on each time scale as follows: the

solution for Eq. (3.78) is given by:

$$u_0(T_0, T_1, T_2, \dots) = a(T_1, T_2, \dots) \cos(T_0 + \beta(T_1, T_2, \dots)) \quad (3.81)$$

By solving the first equation it was possible to determine the dependence of u_0 on T_0 . For this reason, the functions a and β are constant on the time scale T_0 , but their dependence on the other time scales is still to be determined. Taking into account the knowledge of the term u_0 , it is possible to rewrite Eq. (3.79) on the more convenient form:

$$\frac{\partial^2 u_1}{\partial T_0^2} + u_1 = -\frac{a^3}{4} \cos(3T_0 + 3\beta) + \left(2a \frac{\partial \beta}{\partial T_1} - \frac{3a^3}{4}\right) \cos(T_0 + \beta) + 2 \frac{\partial a}{\partial T_1} \sin(T_0 + \beta) \quad (3.82)$$

The first term on the right-hand side of Eq. (3.82) is a uniform term, because it will lead to a bounded response. The other two terms are secular ones and must be eliminated. Unlike Eq. (3.74), the trivial solution is not the only alternative for eliminating secular terms, because in this case, different time scales have been considered. A simple analysis of Eq. (3.82) yields to the following conditions for the vanishing of secular terms:

$$\frac{\partial a}{\partial T_1} = 0 \quad (3.83)$$

$$2a \frac{\partial \beta}{\partial T_1} - \frac{3a^3}{4} = 0 \quad (3.84)$$

The first condition says that the amplitude a is constant on the time scale T_1 , and the second condition provides a first correction to the frequency of oscillation of the system in terms of the amplitude:

$$\beta(T_1, T_2, \dots) = \frac{3a^2}{8} T_1 + \beta_1(T_2, T_3, \dots) \quad (3.85)$$

, and the solution for the term u_1 is:

$$u_1(T_0, T_1, T_2, \dots) = -\frac{a^3(T_2, T_3, \dots)}{32} \cos(3T_0 + \frac{9a^2}{8} T_1 + 3\beta_1(T_2, T_3, \dots)) \quad (3.86)$$

If the process is stopped at the current order, then the approximate solution for Eq.

(3.66) is:

$$u(t; \epsilon) = a \cos(\varphi) - \epsilon \frac{a^3}{32} \cos(3\varphi) + O(\epsilon^2) \quad ; \quad \varphi = \left(1 + \epsilon \frac{3a^2}{8}\right)t + \beta_1 \quad (3.87)$$

The resulting series for this method is uniform, and the conditions for the elimination of secular terms allow for the calculus of corrections of frequencies, which is found on this example, and also amplitudes, to capture transient responses.

There are some cases where there is no explicit small parameter on the equations of motion. In these cases, the expansion of the response can be thought to be of the form:

$$u(T_0, T_1, T_2, \dots; \epsilon) = \epsilon u_0(T_0, T_1, \dots) + \epsilon^2 u_1(T_0, T_1, \dots) + \dots \quad (3.88)$$

, where ϵ , the small parameter, can be thought of as a bookkeeping parameter or a crutching device (Nayfeh (1981)), and can be equal to the unity if the amplitude is taken to be small.

Although this method transforms the problem of solving one nonlinear differential equation into solving a truncated set of linear partial differential equations, it still generates less algebra than the averaging methods, and leads to a complete uniform expansion. Therefore, the problem described on the beginning of this section, of having equations of motion on non usual forms is overcome by the choice of this method.

On the next section analyses are performed considering that the rotor spins at constant speed in order to infer stability of the pendulum.

3.3.3.4 Nonlinear analysis at constant angular speed and zero gravity

In this section, the multiple scales method is applied to the simplest case studied in this work: a pendulum absorber is installed on a rotor which spins at constant angular speed. The difference is that the path of the pendulum is a generic one, constrained to be symmetric with respect to its vertex.

The equation of motion that describes this problem is given by Eq. (3.43). It is defined in terms of the physical parameters of the system. However, because of the definition of $f_a(\theta_a)$, the same dimensionless parameters that were used on the linear analysis can be

used on the nonlinear one. Equation (3.43) is then written in terms of the dimensionless parameters²⁷:

$$(b^{-1} + v^2 p f_a^2(\theta_a))(\theta_a'' + \theta_t'') + 2v^2 p \frac{df_a(\theta_a)}{d\theta_a} f_a(\theta_a) \theta_a'(\theta_a' + \theta_t') + \dots \quad (3.89)$$

$$+ v^2 f_a(\theta_a)(\theta_t'' \cos(\theta_a) + \theta_t'^2 \sin(\theta_a)) + v^2 p g_\epsilon f_a(\theta_a) \cos(\theta_t + \theta_a) = 0$$

Due to the constraints imposed by the problem and to the dimensionless time scale being used $\tau = \omega t$, in this equation, $\theta_t'' = 0$, $\theta_t' = 1$, $\theta_t = \tau$ and $g_\epsilon = 0$. Hence, this equation becomes²⁸:

$$(1 + v^2 p (f_a^2(\theta_a) - 1)) \theta_a'' + 2v^2 p \frac{df_a(\theta_a)}{d\theta_a} f_a(\theta_a) \theta_a'(\theta_a' + 1) + v^2 f_a(\theta_a) \sin(\theta_a) = 0 \quad (3.90)$$

This equation is a function of the parameters v , p and the coefficients α_k , $k = 2, 4, 6, \dots$ of the shape function $f_a(\theta_a)$. Once there is no explicit small parameter on this equation, the expansion for the solution is proposed to be of the form:

$$\theta_a(t; \epsilon) = \sum_{k=1}^{\infty} \epsilon^k \theta_{ak}(T_1, T_2, T_3, \dots) \quad ; \quad T_i = \epsilon^{i-1} \tau \quad , \quad i \in \{1, 2, 3, \dots\} \quad (3.91)$$

The next step proposed by the method is to replace the expansion on Eq. (3.90) and equate the like powers of ϵ . For this equation to be suitable for such expansion, the trigonometric term $\sin(\theta_a)$ is expanded in its Taylor series. Then, it leads to the following set of partial differential equations:

$$\frac{\partial^2 \theta_{a1}}{\partial T_1^2} + v^2 \theta_{a1} = 0 \quad (3.92)$$

$$\frac{\partial^2 \theta_{a2}}{\partial T_1^2} + v^2 \theta_{a2} = -2 \frac{\partial^2 \theta_{a1}}{\partial T_1 \partial T_2} - 4\alpha_2 p v^2 \theta_{a1} \frac{\partial \theta_{a1}}{\partial T_1} \quad (3.93)$$

$$\begin{aligned} \frac{\partial^2 \theta_{a3}}{\partial T_1^2} + v^2 \theta_{a3} = & -2 \frac{\partial^2 \theta_{a1}}{\partial T_1 \partial T_3} - \frac{\partial^2 \theta_{a1}}{\partial T_2^2} - 2 \frac{\partial^2 \theta_{a2}}{\partial T_1 \partial T_2} + v^2 \left(\frac{1}{6} - \alpha_2 \right) \theta_{a1}^3 + \dots \\ & - 2\alpha_2 p v^2 \theta_{a1}^2 \frac{\partial^2 \theta_{a1}}{\partial T_1^2} - 4\alpha_2 p v^2 \theta_{a2} \frac{\partial \theta_{a1}}{\partial T_1} + \dots \end{aligned}$$

²⁷The prime denotes differentiation with respect to τ .

²⁸Notice that $b^{-1} + v^2 p = 1$.

$$-4\alpha_2pv^2\theta_{a1} \left(\left(\frac{\partial\theta_{a1}}{\partial T_1} \right)^2 + \frac{\partial\theta_{a1}}{\partial T_2} + \frac{\partial\theta_{a2}}{\partial T_1} \right) \quad (3.94)$$

⋮ ⋮

The solution of these equations has been calculated up to the third order. Considering powertrain applications, this is more than enough, taking into account that in such applications only the two most significant orders (i.e. the two first ones) are analyzed. The solution is then of the form:

$$\begin{aligned} \theta_a(\tau; \epsilon) = & \epsilon a \cos(\varphi) - \frac{2\epsilon^2 a^2 \alpha_2 p v}{3} \sin(2\varphi) + \dots \\ & - \frac{\epsilon^3 a^3}{192} (1 - 6\alpha_2 + 36\alpha_2 p v^2 + 96\alpha_2^2 p^2 v^2) \cos(3\varphi) + O(\epsilon^4) \end{aligned} \quad (3.95)$$

$$\varphi(\tau) = v \left(1 + \frac{\epsilon^2 a^2}{48} (-3 + 18\alpha_2 - 12\alpha_2 p v^2 - 32\alpha_2^2 p^2 v^2) \right) \tau + \beta(T_4, T_5, \dots) \quad (3.96)$$

There are some important features to be discussed about this solution. The first one is that the amplitude a is always multiplied by the parameter ϵ in any of the terms, i.e. there are always products of equal powers of these two constants ($\epsilon a, \epsilon^2 a^2, \epsilon^3 a^3, \dots$). This is a direct result of the proposed expansion. In this case, instead of determining the value of the amplitude a and the phase β through the initial conditions of the system, one must determine the value of the product ϵa and the phase β through the initial value problem.

Secondly, the first correction to the frequency of free-oscillation of the system ($\epsilon^2 a^2 v_c$) was found from the conditions for vanishing secular terms on the calculation of the third order term. Apart from all the parameters of the system, it also depends on the square of the amplitude of oscillation of the pendulum. However, this correction is a product between the square of the amplitude of oscillation of the system ($\epsilon^2 a^2$) and a function of the system parameters only (v_c). This factor is given by:

$$\frac{d\varphi}{d\tau} = v(1 + \epsilon^2 a^2 v_c) + O(\epsilon^4) \quad ; \quad v_c = \frac{1}{48} (-3 + 18\alpha_2 - 12\alpha_2 p v^2 - 32\alpha_2^2 p^2 v^2) \quad (3.97)$$

For the family of paths circular-epicycloid-cycloid, α_2 either a constant or a function of

p . In fact, α_2 can be represented as a direct function of p as:

$$\alpha_2(p) = -\frac{3(p-1)}{2(p-2)^2} \quad (3.98)$$

In this expression, if $p = 0$ the path is a cycloid, while if $p = 1$ the path is circular and if $0 < p < 1$ the path is an epicycloid. The parameter v_c is then a function of v and p :

$$v_c = \frac{-(18v^2 + 1)p^4 + (18v^2 - 1)p^3 + (24v^2 + 21)p^2 - (24v^2 + 40)p + 20}{16(p-2)^4} \quad (3.99)$$

Once detuning is caused by this term, at least up to order three, it is desirable that this term vanishes. Once v is a design parameter, and v and p can be varied independently, because v also depends on b , one should look for values of $p(v)$ so that the term v_c vanishes, avoiding third order detuning. As p usually lies on the range $0 < p \ll 1$, the denominator is a bounded value, and hence it is necessary to find the roots of the numerator of v_c . These roots $p_i(v), i \in 1, 2, 3, 4$ are shown in Fig. 3.21.

For being a 4th degree polynomial, its roots may have a very complicated closed formula. For small values of v , this polynomial has two real roots and a pair of complex conjugate roots. For values of v above approximately 2.256, the polynomial has four real roots. It is also possible to infer how these roots behave for high values of v . Dividing the numerator of v_c by v^2 and taking the limit with $v \rightarrow \infty$ leads to the following polynomial:

$$\lim_{v \rightarrow \infty} \frac{\text{num}(v_c)}{v^2} = -3p^4 + 3p^3 + 4p^2 - 4p = 0 \quad (3.100)$$

Through direct inspection, it is possible to state that 0 and 1 are roots of this polynomial. Hence, the other two roots can be calculated analytically, and they are $\pm \frac{2\sqrt{3}}{3}$. Therefore, for high values of v , the roots of v_c tend asymptotically to these four values, as shown in Fig. 3.21.

Due to the fact that p must be positive and much lower than one, the only root of this polynomial that brings realizable values for project is $p_1(v)$. Some values of this root for specific values of v are given on Appendix B.20.

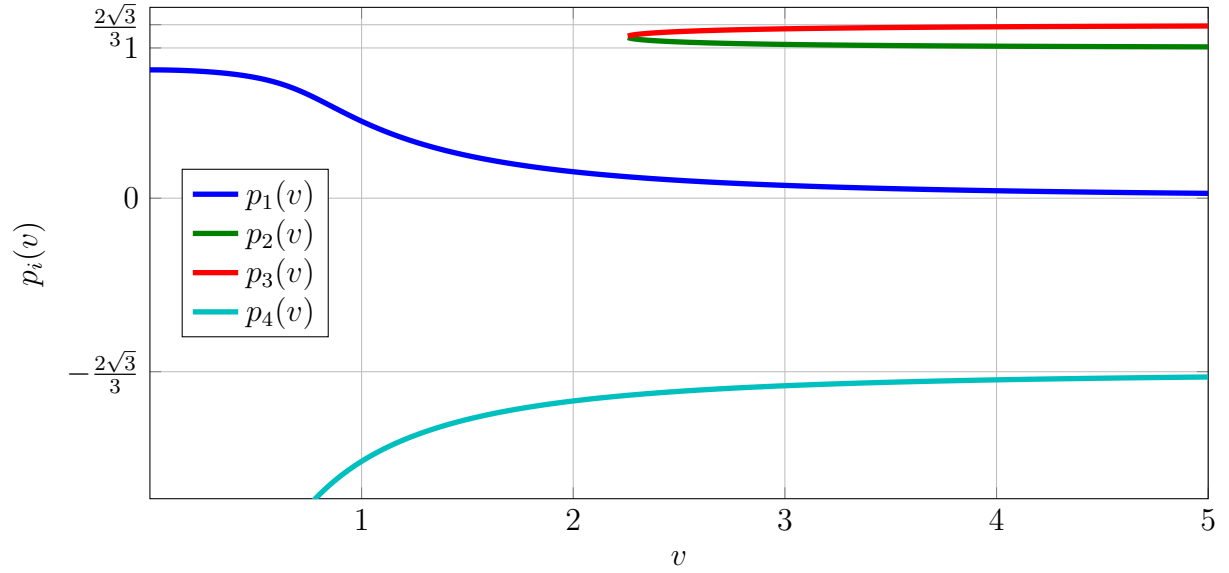


Figure 3.21: Roots of the numerator of v_c

The next step on this analysis is to include gravity in order to verify its influence on the frequency of oscillation and also on the stability of the system. This is done on the next section.

3.3.3.5 Nonlinear analysis at constant angular speed considering gravitational terms

The equation of motion that represents the problem considered on this section is Eq. (3.89) with $\theta_t'' = 0$, $\theta_t' = 1$ and $\theta_t = \tau$. In this case, evidently, the gravitational term is not neglected. However, it is represented on the system as a perturbation of the previous equation by introducing the parameter $g_\epsilon^{(0)} = g_\epsilon/\epsilon$. Hence, the equation of motion for this case reads:

$$(1 + v^2 p(f_a^2(\theta_a) - 1))\theta_a'' + 2v^2 p \frac{df_a(\theta_a)}{d\theta_a} f_a(\theta_a) \theta_a' (\theta_a' + 1) + v^2 f_a(\theta_a) \sin(\theta_a) + \dots + \epsilon v^2 p g_\epsilon^{(0)} f_a(\theta_a) (\cos(\tau) \cos(\theta_a) - \sin(\tau) \sin(\theta_a)) = 0 \quad (3.101)$$

Like the previous cases, the trigonometric functions of θ_a are expanded on their respec-

tive Taylor series forms. The proposed expansion for the solution is, once more:

$$\theta_a(t; \epsilon) = \sum_{k=1}^{\infty} \epsilon^k \theta_{ak}(T_1, T_2, T_3, \dots) \quad ; \quad T_i = \epsilon^{i-1} \tau \quad , \quad i \in \{1, 2, 3, \dots\} \quad (3.102)$$

Substituting Eq. (3.102) into Eq. (3.101) and equating the like powers of ϵ results in the following set of linear partial differential equations to be solved²⁹:

$$\frac{\partial^2 \theta_{a1}}{\partial T_1^2} + v^2 \theta_{a1} = -g_\epsilon^{(0)} p v^2 \cos(T_1) \quad (3.103)$$

$$\frac{\partial^2 \theta_{a2}}{\partial T_1^2} + v^2 \theta_{a2} = g_\epsilon^{(0)} p v^2 \theta_{a1} \sin(T_1) - 2 \frac{\partial^2 \theta_{a1}}{\partial T_1 \partial T_2} - 4\alpha_2 p v^2 \theta_{a1} \frac{\partial \theta_{a1}}{\partial T_1} \quad (3.104)$$

$$\begin{aligned} \frac{\partial^2 \theta_{a3}}{\partial T_1^2} + v^2 \theta_{a3} = & \frac{\theta_{a1}^3 v^2}{6} - \frac{\partial^2 \theta_{a1}}{\partial T_2^2} - 2 \frac{\partial^2 \theta_{a2}}{\partial T_1 \partial T_2} - 2 \frac{\partial^2 \theta_{a1}}{\partial T_1 \partial T_3} - \alpha_2 \theta_{a1}^3 v^2 + \dots \\ & - 2\alpha_2 \frac{\partial^2 \theta_{a1}}{\partial T_1^2} p \theta_{a1}^2 v^2 - 4\alpha_2 \frac{\partial \theta_{a1}^2}{\partial T_1} p \theta_{a1} v^2 + g_\epsilon^{(0)} p \theta_{a2} v^2 \sin(T_1) + \dots \\ & + \frac{g_\epsilon^{(0)} p \theta_{a1}^2 v^2 \cos(T_1)}{2} - 4\alpha_2 \frac{\partial \theta_{a1}}{\partial T_2} p \theta_{a1} v^2 - 4\alpha_2 \frac{\partial \theta_{a2}}{\partial T_1} p \theta_{a1} v^2 + \dots \\ & - 4\alpha_2 \frac{\partial \theta_{a1}}{\partial T_1} p \theta_{a2} v^2 - \alpha_2 g_\epsilon^{(0)} p \theta_{a1}^2 v^2 \cos(T_1) \end{aligned} \quad (3.105)$$

\vdots \vdots

The solution has been calculated up to the third order and is given on the form:

$$\theta_a(t; \epsilon) = \epsilon \theta_{a1} + \epsilon^2 \theta_{a2} + \epsilon^3 \theta_{a3} + O(\epsilon^4) \quad (3.106)$$

The first order approximation θ_{a1} is given by:

$$\theta_{a1} = a \cos(\varphi) - \frac{g_\epsilon^{(0)} p v^2}{v^2 - 1} \cos(T_1) \quad (3.107)$$

The instantaneous phase $\varphi(\tau)$ is going to be defined later on the text in order to keep a solid line of analysis. The system being studied in this section does not have an excitation acting on it, but the parameters related to gravity oscillate in time. This variation causes

²⁹Remembering that the homogeneous response has to be calculated only for the first equation. From the second equation on, only the inhomogeneous response must be calculated.

the system to be unstable for some conditions, which is found at the very first term of the approximated solution.

The amplitude of response of this term is divided by a function of v , which has zeros at $v = \pm 1$. Once this parameter is always positive, if $v = 1$ then the first order approximation shows a parametric resonance. If $v = 1$, it is known that the solution presented above is mathematically not valid, but this term would certainly lead to a resonance, hence the conclusion.

Proceeding to the second order approximation, the term θ_{a2} is given by:

$$\theta_{a2} = \Theta_{T_1+\varphi}^{(s)} \sin(T_1 + \varphi) + \Theta_{T_1-\varphi}^{(s)} \sin(T_1 - \varphi) + \Theta_{2T_1}^{(s)} \sin(2T_1) + \Theta_{2\varphi}^{(s)} \sin(2\varphi) \quad (3.108)$$

, where the terms Θ are all constants.

The amplitude of the first two terms of Eq. (3.108) are given by:

$$\Theta_{T_1+\varphi}^{(s)} = -\frac{ag_\epsilon^{(0)} pv^2(4\alpha_2 pv^2 - v + 1)}{2(v-1)(v+\frac{1}{2})} \quad (3.109)$$

$$\Theta_{T_1-\varphi}^{(s)} = -\frac{ag_\epsilon^{(0)} pv^2(4\alpha_2 pv^2 + v + 1)}{2(v+1)(v-\frac{1}{2})} \quad (3.110)$$

These first terms of the second order approximation show that there is a harmonic parametric resonance (Eq. (3.109)) and a subharmonic parametric resonance (Eq. (3.110)) for $v = \frac{1}{2}$. The amplitudes of the latter two terms are given by:

$$\Theta_{2T_1}^{(s)} = \frac{\left(g_\epsilon^{(0)}\right)^2 p^2 v^4 (4\alpha_2 pv^2 - v^2 + 1)}{2(v+1)^2(v-1)^2(v+2)(v-2)} \quad (3.111)$$

$$\Theta_{2\varphi}^{(s)} = -\frac{2a^2\alpha_2 pv}{3} \quad (3.112)$$

The amplitude of the third term, shown in Eq. (3.111) shows harmonic parametric resonance and also superharmonic parametric resonance for $v = 2$. The amplitude of the fourth term is the same amplitude found on the previous case, where gravity had not been taken into consideration. Analyzing the amplitude of all the terms, it is possible to infer that the first two ones are a result of the interaction between the homogeneous response

(considering zero gravity) and the response due to parametric excitation. The third term does not depend on the amplitude of free oscillation of the system (a), and the fourth term is not affected by the presence of gravity.

On the numerator of the terms affected by gravitational field, there are polynomial factors that depend on the system parameters only. One possible way to avoid parametric resonance would be to find values of p as a function of v so that these polynomials vanish. This investigation is chosen not to be carried out on this work.

Secular terms found on this approximation led to no correction of the oscillation amplitude. Hence, it is possible to proceed to the next order.

The third order approximation term is given by:

$$\begin{aligned} \theta_{a3} = & \Theta_{\varphi+2T_1}^{(c)} \cos(\varphi + 2T_1) + \Theta_{\varphi-2T_1}^{(c)} \cos(\varphi - 2T_1) + \Theta_{T_1+2\varphi}^{(c)} \cos(T_1 + 2\varphi) + \dots \\ & + \Theta_{T_1-2\varphi}^{(c)} \cos(T_1 - 2\varphi) + \Theta_{T_1}^{(c)} \cos(T_1) + \Theta_{3T_1}^{(c)} \cos(3T_1) + \Theta_{3\varphi}^{(c)} \cos(3\varphi) \quad (3.113) \end{aligned}$$

The amplitude of each of the seven terms that compose θ_{a3} is listed below:

$$\begin{aligned} \Theta_{\varphi+2T_1}^{(c)} = & -\frac{a \left(g_\epsilon^{(0)}\right)^2 p^2 v^4 (6v^4 - 13v^2 + 4)}{32(v+1)(v^2-1)^2(4v^2-1)} + \dots \\ & + \alpha_2 \frac{a \left(g_\epsilon^{(0)}\right)^2 p^2 v^4 (88pv^2 - 292pv^4 + 122pv^6 - 8pv^8 + 30v^2 + 9v^4 - 4v^6 - 8)}{16(v-1)^2(v+1)^3(4v^2-1)} + \dots \\ & - 5\alpha_2^2 \frac{a \left(g_\epsilon^{(0)}\right)^2 p^4 v^8 (v^4 - 6v^2 + 2)}{16(v-1)^2(v+1)^3(4v^2-1)(v^2-4)} \quad (3.114) \end{aligned}$$

$$\begin{aligned} \Theta_{\varphi-2T_1}^{(c)} = & \frac{a \left(g_\epsilon^{(0)}\right)^2 p^2 v^4 (6v^4 - 13v^2 + 4)}{24(v^2-1)^2(v-1)(3v-1)(4v^2-1)} + \dots \\ & - \alpha_2 \frac{a \left(g_\epsilon^{(0)}\right)^2 p^2 v^4 (88pv^2 - 292pv^4 + 122pv^6 - 8pv^8 + 30v^2 + 9v^4 - 4v^6 - 8)}{16(v-1)^2(v+1)^3(4v^2-1)} + \dots \\ & + \alpha_2^2 \frac{a \left(g_\epsilon^{(0)}\right)^2 p^4 v^8 (v^4 - 6v^2 + 2)}{16(v-1)^2(v+1)^3(4v^2-1)(v^2-4)} \quad (3.115) \end{aligned}$$

$$\Theta_{T_1+2\varphi}^{(c)} = -\frac{a g_\epsilon^{(0)} p v^2 \left(4 g_\epsilon^{(0)} p v^5 - 4 g_\epsilon^{(0)} p v^3 - 4 a v^2 + a\right)}{96(v+1)^2(v-1)(v^2-\frac{1}{4})(v+\frac{1}{3})} + \dots$$

$$\begin{aligned}
& +\alpha_2 (ag_\epsilon^{(0)}pv^2 (g_\epsilon^{(0)}p^2v^5(-96v^4 + 228v^2 + 84)+ \dots \\
& +ap(48v^{10} + 80v^9 - 180v^8 - 404v^7 - 126v^6 + 336v^5 + 330v^4 + 4v^3 - 72v^2 - 16v) + \dots \\
& +a(-24v^8 + 114v^6 - 63v^4 - 39v^2 + 12))) \times \\
& \left(144(v-1)^2(v+1)^3(v^2-4)(v^2-\frac{1}{4})(v+\frac{1}{3}) \right)^{-1} + \dots \\
& +\alpha_2^2 (4ag_\epsilon^{(0)}p^3v^5 (3g_\epsilon^{(0)}pv^4(-2v^4 + 11v^2 + 3)+ \dots \\
& +a(12v^8 + 20v^7 - 59v^6 - 105v^5 + 42v^4 + 105v^3 + 9v^2 - 20v - 4))) \times \\
& \left(48(v-1)^2(v+1)^3(v^2-4)(v^2-\frac{1}{4})(v+\frac{1}{3}) \right)^{-1} \tag{3.116}
\end{aligned}$$

$$\begin{aligned}
\Theta_{T_1-2\varphi}^{(c)} = & -\frac{ag_\epsilon^{(0)}pv^2 (4g_\epsilon^{(0)}pv^5 - 4g_\epsilon^{(0)}pv^3 - 4av^2 + a)}{96(v-1)^2(v+1)(v^2-\frac{1}{4})(v-\frac{1}{3})} + \dots \\
& -\alpha_2 (ag_\epsilon^{(0)}pv^2 (g_\epsilon^{(0)}p^2v^5(-96v^4 + 228v^2 + 84)+ \dots \\
& +ap(-48v^{10} + 80v^9 + 180v^8 - 404v^7 + 126v^6 + 336v^5 - 330v^4 + 4v^3 + 72v^2 - 16v) + \dots \\
& +a(24v^8 - 114v^6 + 63v^4 + 39v^2 - 12))) \times \\
& \left(144(v+1)^2(v-1)^3(v^2-4)(v^2-\frac{1}{4})(v-\frac{1}{3}) \right)^{-1} + \dots \\
& -\alpha_2^2 (4ag_\epsilon^{(0)}p^3v^5 (3g_\epsilon^{(0)}pv^4(-2v^4 + 11v^2 + 3)+ \dots \\
& +a(12v^8 - 20v^7 - 59v^6 + 105v^5 + 42v^4 - 105v^3 + 9v^2 + 20v - 4))) \times \\
& \left(48(v+1)^2(v-1)^3(v^2-4)(v^2-\frac{1}{4})(v-\frac{1}{3}) \right)^{-1} \tag{3.117}
\end{aligned}$$

$$\begin{aligned}
\Theta_{T_1}^{(c)} = & -g_\epsilon^{(0)}pv^2 (a^2(8v^8 - 50v^6 + 84v^4 - 50v^2 + 8) + \dots \\
& + (g_\epsilon^{(0)})^2 p^2v^4(28v^4 - 47v^2 + 10)) \times \\
& \left(32(v^2-1)^4(v^2-4)(v^2-\frac{1}{4}) \right)^{-1} + \dots \\
& -\alpha_2 (g_\epsilon^{(0)}pv^2 (a^2p(48v^{10} - 321v^8 + 576v^6 - 408v^4 + 96v^2) + \dots \\
& +a^2(-32v^{10} + 184v^8 - 236v^6 + 32v^4 + 68v^2 - 16) + \dots \\
& + (g_\epsilon^{(0)})^2 p^2v^4(16pv^6 - 68pv^4 + 16pv^2 - 24v^4 + 102v^2 - 24))) \times \\
& \left(32(v^2-1)^4(v^2-4)(v^2-\frac{1}{4}) \right)^{-1} + \dots \\
& -\alpha_2^2 (g_\epsilon^{(0)}pv^6 (a^2p^2(128v^8 - 832v^6 + 1536v^4 - 1088v^2 + 256)+ \dots \\
& + (g_\epsilon^{(0)})^2 p^4v^2(-128v^2 + 32))) \times \\
& \left(32(v^2-1)^4(v^2-4)(v^2-\frac{1}{4}) \right)^{-1} \tag{3.118}
\end{aligned}$$

$$\begin{aligned}
\Theta_{3T_1}^{(c)} &= \frac{\left(g_\epsilon^{(0)}\right)^3 p^3 v^6 (8v^4 - 23v^2 + 18)}{24(v^2 - 1)^3(v^2 - 4)(v^2 - 9)} + \dots \\
&+ \alpha_2 \frac{\left(g_\epsilon^{(0)}\right)^3 p^3 v^6 (40pv^2 - 22pv^4 + v^2 - 4)}{4(v^2 - 1)^3(v^2 - 4)(v^2 - 9)} + \dots \\
&+ \alpha_2^2 \frac{\left(g_\epsilon^{(0)}\right)^3 p^5 v^{10}}{(v^2 - 1)^3(v^2 - 4)(v^2 - 9)}
\end{aligned} \tag{3.119}$$

$$\Theta_{3\varphi}^{(c)} = -\frac{a^3}{192}(1 - 6\alpha_2 + 36\alpha_2 pv^2 + 96\alpha_2^2 p^2 v^2) \tag{3.120}$$

It is known that, in case small divisors are found (i.e. resonant terms appear), if one desires to know the amplitude of the system near these critical frequencies, then special treatment must be given to these equations. Once gravity induced instability is not the core subject of this work, this analysis is not being performed in this section.

Analyzing the denominator of the amplitude terms of the third order approximation term, it is possible to find harmonic parametric resonances, subharmonic parametric resonances for $v = \frac{1}{2}$ and $v = \frac{1}{3}$ and also superharmonic parametric resonances at $v = 2$ and $v = 3$. Further order terms have not been calculated, but it is possible to notice a trend on the occurrence of subharmonic and superharmonic parametric resonances for values of $\frac{1}{i}$ and i for $i \in \mathbb{Z}_+^*$.

For the terms at which there is an interaction between the acceleration of gravity and the amplitude of free oscillation of the system, sub and superharmonic parametric resonances are found. However, once there is an interaction with the amplitude of free oscillation of the system, a small amount of damping should help to make these terms decrease along time.

On the other hand, there are terms generated purely by the presence of gravity, with no influence of the transient response of the system. These terms present superharmonic parametric resonances only, and ways to make these terms less significant should be investigated.

On the process of eliminating secular terms from the third order approximation term, considering the system is not near any resonant condition, a correction for the frequency of oscillation is found. The instantaneous phase is, for this case:

$$\varphi(\tau) = v(1 - \epsilon^2 a^2 v_c - \epsilon^2 g_c)\tau \tag{3.121}$$

, where v_c is exactly the same as given by Eq. (3.99) and g_c is given by:

$$g_c = - \frac{\left(g_\epsilon^{(0)}\right)^2 p^2 v^2 (32\alpha_2^2 p^2 v^6 + \alpha_2 (16pv^6 - 12pv^4 + 8pv^2 - 8v^4 - 14v^2 + 4) - 2v^4 + 5v^2)}{8(v^2 - 1)^2(4v^2 - 1)} \quad (3.122)$$

This brings an important conclusion about the detuning. Although on the response of the system there is an interaction between the amplitude of free oscillation a and the amplitude of the terms brought by the gravitational field, these two amplitudes act separately on the detuning of the system. An important feature about the dimensionless gravitational constant g_ϵ is that it is inversely proportional to the square of the rotating speed of the system. Hence, the higher the rotating speed the less influent this term is, and consequently less detuning and parametric resonances are expected.

From this investigation including gravity, the main conclusion to be drawn is that, one must avoid integer values of the parameter v , especially the unity. Additionally, the system parameters must be chosen so that the value of g_ϵ is as low as possible (e.g. high rotating speeds and highest possible distance from the pendulum's pin to the center of the rotor, so that the radius of the pendulum bob can be increased.). On further analyses, gravity is not being considered.

3.3.3.6 Nonlinear analysis with zero gravity and small oscillations on the carrier disk's angular speed

In this section, a system with two rotors is considered. One of the rotors spins at constant angular speed and is attached to the second one through a torsional spring. The latter rotor has a centrifugal pendulum vibration absorber installed on it. Basically, the system is the same one shown in Fig. 3.7. Additionally, the latter rotor is subjected to the actuation of an oscillating torque.

The Multiple Scales Method is also suitable for the analysis of systems with more than one degree of freedom. However, the amount of algebra resulting from the application of this method is so extensive that it would be humanly impossible to perform it without the help of a symbolic mathematics toolbox. Therefore, calculations have been carried up to the second

order.

The first step for the application of the method is to write the equations of motion on their dimensionless forms. In this case, the equations are:

$$\begin{aligned} \left(\frac{1}{\mu} - v^2\right) \tilde{\theta}_t'' + v^2 \frac{d^2 f_a(\theta_a)}{d\theta_a^2} \theta_a'^2 \sin \theta_a + v^2 \frac{df_a(\theta_a)}{d\theta_a} \left(\theta_a'' \sin \theta_a + 2\theta_a'(\theta_a' + \tilde{\theta}_t' + 1) \cos \theta_a\right) + \dots \\ + v^2 f_a(\theta_a) \left((\theta_a'' + \tilde{\theta}_t'') \cos \theta_a - (\theta_a' + \tilde{\theta}_t' + 1)^2 \sin \theta_a\right) + \frac{v^2}{\beta^2 a \mu} \tilde{\theta}_t = G \cos(n\tau) \end{aligned} \quad (3.123)$$

, for the disk and:

$$\begin{aligned} (1 + v^2 p(f_a^2(\theta_a) - 1)) (\theta_a'' + \tilde{\theta}_t'') + 2v^2 p \frac{df_a(\theta_a)}{d\theta_a} f_a(\theta_a) \theta_a' (\theta_a' + \tilde{\theta}_t' + 1) + \dots \\ + v^2 f_a(\theta_a) \left(\tilde{\theta}_t'' \cos \theta_a + (\tilde{\theta}_t' + 1) \sin \theta_a\right) = 0 \end{aligned} \quad (3.124)$$

, for the pendulum.

Regarding the excitation term of Eq. (3.123), n is the order of the oscillating torque and its amplitude G is given by:

$$G = \frac{T}{(I_a + m_a \epsilon_a^2) \Omega^2} \quad (3.125)$$

, where T is the physical amplitude of the oscillating torque.

The amplitude of the excitation is a small parameter. In order to represent its smallness explicitly, the parameter G_0 is introduced, so that:

$$G = \epsilon G_0 \quad (3.126)$$

, and Eq. (3.123) reads:

$$\begin{aligned} \left(\frac{1}{\mu} - v^2\right) \tilde{\theta}_t'' + v^2 \frac{d^2 f_a(\theta_a)}{d\theta_a^2} \theta_a'^2 \sin \theta_a + v^2 \frac{df_a(\theta_a)}{d\theta_a} \left(\theta_a'' \sin \theta_a + 2\theta_a'(\theta_a' + \tilde{\theta}_t' + 1) \cos \theta_a\right) + \dots \\ + v^2 f_a(\theta_a) \left((\theta_a'' + \tilde{\theta}_t'') \cos \theta_a - (\theta_a' + \tilde{\theta}_t' + 1)^2 \sin \theta_a\right) + \frac{v^2}{\beta^2 a \mu} \tilde{\theta}_t = \epsilon G_0 \cos(n\tau) \end{aligned} \quad (3.127)$$

Once the equations are in the appropriate form, it is necessary to propose an expansion

for both of the variables. The expansions are proposed in the following forms:

$$\theta_a(T_1, T_2; \epsilon) = \epsilon \theta_{a1} + \epsilon^2 \theta_{a2} + O(\epsilon^3) \quad ; \quad T_1 = \tau, T_2 = \epsilon \tau \quad (3.128)$$

$$\tilde{\theta}_t(T_1, T_2; \epsilon) = \epsilon \tilde{\theta}_{t1} + \epsilon^2 \tilde{\theta}_{t2} + O(\epsilon^3) \quad ; \quad T_1 = \tau, T_2 = \epsilon \tau \quad (3.129)$$

The next step is to replace Eqs. (3.128) and (3.129) into Eqs. (3.127) and (3.124) and to equate the like powers of ϵ . This, as seen before, leads to a series linear partial differential equations to be solved.

Interestingly, the left-hand side of the i -th equation on this series is given by:

$$\underbrace{\begin{bmatrix} \mu^{-1} & v^2 \\ (1+v^2) & 1 \end{bmatrix}}_{\mathbf{M}_\phi} \underbrace{\left\{ \begin{array}{c} \partial^2 \tilde{\theta}_{ti} / \partial T_1^2 \\ \partial^2 \theta_{ai} / \partial T_1^2 \end{array} \right\}}_{\partial_1^2 \boldsymbol{\theta}_i} + \underbrace{\begin{bmatrix} v^2 & -v^2 \\ \beta^2 a \mu & v^2 \\ 0 & v^2 \end{bmatrix}}_{\mathbf{K}_\phi} \underbrace{\left\{ \begin{array}{c} \tilde{\theta}_{ti} \\ \theta_{ai} \end{array} \right\}}_{\boldsymbol{\theta}_i} \quad (3.130)$$

, where the dimensionless mass and stiffness matrices \mathbf{M}_ϕ and \mathbf{K}_ϕ are the same ones found on the linear analysis performed at section 3.3.2.1. In order to obtain a shorthand notation, the array of variables $\{\tilde{\theta}_{ti} \theta_{ai}\}^T$ is denoted $\boldsymbol{\theta}_i$, and the second derivative of such array with respect to the timescale T_1 is denoted $\partial_1^2 \boldsymbol{\theta}_i$.

The series of equations to be solved, up to the second order, is then:

$$\mathbf{M}_\phi \partial_1^2 \boldsymbol{\theta}_1 + \mathbf{K}_\phi \boldsymbol{\theta}_1 = \begin{Bmatrix} G_0 \\ 0 \end{Bmatrix} \cos(n\tau) \quad (3.131)$$

$$\begin{aligned} \mathbf{M}_\phi \partial_1^2 \boldsymbol{\theta}_2 + \mathbf{K}_\phi \boldsymbol{\theta}_2 &= \begin{Bmatrix} 2v^2 - 4\alpha_2 v^2 \\ -4\alpha_2 v^2 \end{Bmatrix} \theta_{a1} \frac{\partial \theta_{a1}}{\partial T_1} + \begin{Bmatrix} 2v^2 \\ -2v^2 \end{Bmatrix} \theta_{a1} \frac{\partial \tilde{\theta}_{t1}}{\partial T_1} + \dots \\ &+ \begin{Bmatrix} -2v^2 \\ -2 \end{Bmatrix} \frac{\partial^2 \theta_{a1}}{\partial T_1 \partial T_2} + \begin{Bmatrix} -2\mu^{-1} \\ -2(v^2 + 1) \end{Bmatrix} \frac{\partial^2 \tilde{\theta}_{t1}}{\partial T_1 \partial T_2} \end{aligned} \quad (3.132)$$

\vdots
 \vdots

Before solving the equations, it is important to keep in mind that the solutions to be calculated are responses of a two-degree-of-freedom system. Hence, if they are represented in terms of the dimensionless parameters, these terms are usually long, and equations may become too long and with poor readability. In order to avoid this, once the linear system

with mass and stiffness matrices \mathbf{M}_ϕ and \mathbf{K}_ϕ has already been studied, the responses are written in terms of its modal parameters.

Recalling the parameters, the system is undamped and consequently has two pairs of complex conjugate eigenvalues $\pm j\chi_1$ and $\pm j\chi_2$, being χ_1 the lowest eigen-order and χ_2 the greatest. Each pair of complex conjugate eigenvalues $\pm j\chi_i$ is related to an eigenvector ψ_i , which is of the form:

$$\psi_i = \begin{Bmatrix} \Gamma_i \\ 1 \end{Bmatrix} \quad (3.133)$$

, where Γ_i is the ratio between the amplitude of the carrier disk and the amplitude of the pendulum bob for the i -th mode.

These parameters are all represented by long expressions when written in terms of the dimensionless parameters, and hence they help to shorten equations. A latter parameter to be introduced is the following determinant:

$$\Delta = \det (\mathbf{K}_\phi - \mathbf{M}_\phi n^2) \quad (3.134)$$

When calculating the inhomogeneous response of the system to an oscillating torque of order n , the matrix $\mathbf{K}_\phi - \mathbf{M}_\phi n^2$ has to be inverted, and hence this determinant has to be calculated. The definition of this parameter also helps to shorten the equations. Additionally, the inverse of this matrix is:

$$\mathbf{\Lambda} = (\mathbf{K}_\phi - \mathbf{M}_\phi n^2)^{-1} = \Delta^{-1} \begin{bmatrix} (v^2 - n^2) & v^2(n^2 + 1) \\ n^2(v^2 + 1) & \mu^{-1}(\frac{v^2}{\beta^2 a} - n^2) \end{bmatrix} \quad (3.135)$$

With these parameters it is possible to write the solution for the first order approximation $\boldsymbol{\theta}_1$:

$$\boldsymbol{\theta}_1 = A_1 \begin{Bmatrix} \Gamma_1 \\ 1 \end{Bmatrix} \cos(\chi_1 T_1 + \beta_1) + A_2 \begin{Bmatrix} \Gamma_2 \\ 1 \end{Bmatrix} \cos(\chi_2 T_1 + \beta_2) + \mathbf{\Lambda} \begin{Bmatrix} G_0 \\ 0 \end{Bmatrix} \cos(nT_1) \quad (3.136)$$

, where A_1 , A_2 , β_1 and β_2 are constants to be calculated from the initial value problem.

According to the method, the solution of the first equation must be full, i.e. it must contain both the homogeneous and the inhomogeneous responses. From the second equation

on, only the inhomogeneous response has to be calculated.

This solution brings the knowledge on the orders for which the system has primary resonances, which are, as expected, $n = \chi_1$ and $n = \chi_2$. The tuning of the dimensionless parameters must be performed so that n lies in a special zone which none of the eigen-orders can reach. Therefore, primary resonances can be easily avoided and must not be investigated.

Once Eq. (3.136) is composed by three terms, when substituted into Eq. (3.132), the right-hand side of the resulting equation will be composed by 18 terms, and calculating the responses for each of them takes a lot of work. Once detuning and gravity induced instability have been investigated through simpler models, it is chosen to use the current two-degree-of-freedom model to study the presence of primary and secondary resonances only³⁰.

The advantage of studying the resonant conditions only is that it is not necessary to calculate the response of the system to all the terms, but only to the ones that may lead to small divisor terms when resonant orders are reached. Through experience with the method, thirteen independent circular terms³¹ are expected on the right-hand side of Eq. (3.132). The frequency³² of these terms is: $\chi_1, \chi_2, 2\chi_1, 2\chi_2, 2n, \chi_1 + n, \chi_1 - n, \chi_2 + n, \chi_2 - n, \chi_1 + \chi_2$ and $\chi_2 - \chi_1$.

Among these terms, the ones with frequency of χ_1 and χ_2 are the terms that generate secular terms and must be eliminated. For frequencies far from resonant frequencies, these terms are the only ones that generate secular terms. However, the same cannot be said if the frequency of another a given term tends to χ_1 or χ_2 . The method of multiple scales handles this case, and a short example is presented below.

Imagine that, for a given expansion, one of the equations to be solved is:

$$\mathbf{M}_\phi \partial_1^2 \boldsymbol{\theta}_1 + \mathbf{K}_\phi \boldsymbol{\theta}_1 = A_1 \{\Gamma_1 \ 1\}^T \cos(\chi_1 T_1) + \{F \ 0\}^T \cos(\omega T_1) \quad ; \quad \omega \rightarrow \chi_1 \quad (3.137)$$

The first term on the right-hand side of this equation would generate a secular term and hence it must be eliminated. The second term, however, will have a small divisor for the condition $\omega \rightarrow \chi_1$. If ω is away from χ_1 or χ_2 , the method follows as before. On the other

³⁰Being the secondary resonances calculated from the second order term only

³¹A circular term is a sinusoidal function, i.e. a sine or a cosine.

³²Remembering that, in this case the frequency is in the τ -domain, and not in the physical time domain.

hand, if it is close to χ_1 , then the following term is introduced:

$$\omega = \chi_1 + \epsilon\sigma \quad (3.138)$$

, where σ represents the proximity of ω to χ_1 and ϵ is used to represent the smallness of σ explicitly.

With this constraint for ω , the second term on the right-hand side of Eq. (3.137) reads:

$$\begin{aligned} \{F \ 0\}^T \cos(\omega T_1) &= \{F \ 0\}^T \cos((\chi_1 + \epsilon\sigma)T_1) \\ &= \{F \ 0\}^T \cos(\chi_1 T_1 + \sigma\epsilon T_1) \\ &= \{F \ 0\}^T \cos(\chi_1 T_1 + \sigma T_2) \\ &= \{F \ 0\}^T (\cos(\chi_1 T_1) \cos(\sigma T_2) - \sin(\chi_1 T_1) \sin(\sigma T_2)) \end{aligned} \quad (3.139)$$

Once the time scales T_1 and T_2 are independent, the terms with instantaneous phase of σT_2 are constant on the time scale T_1 . Therefore, the term on Eq. (3.139) also generates secular terms and must be eliminated. Notice that a small divisor term has been replaced by another that generates secular terms.

From the condition for the vanishing of secular terms it is possible to find dependency relationships between A_1 and F . Considering the case of a steady state response, these relationships are usually referred to as frequency response equations. From these equations it is possible to infer stability of response and important phenomena, such as *jumping*.

Going back to Eq. (3.132), it is possible to define which terms may lead to small divisor ones. Remembering that n is defined to be positive, and $\chi_1 < \chi_2$, then the four conditions where secondary resonances may appear are: $2n \rightarrow \chi_1$, $2n \rightarrow \chi_2$, $\chi_1 + n \rightarrow \chi_2$ and $\chi_2 - n \rightarrow \chi_1$. These cases are referred to as case 1 to 4, respectively, and are analyzed separately.

An information that is going to be used on all four cases is the terms that would generate secular terms on the original equation. They are:

$$\begin{aligned} \theta_{sec}^{(2)} &= \Theta_{\chi_1}^{(c)} \cos(\chi_1 T_1 + \beta_1) + \Theta_{\chi_1}^{(s)} \sin(\chi_1 T_1 + \beta_1) + \dots \\ &\quad + \Theta_{\chi_2}^{(c)} \cos(\chi_2 T_1 + \beta_2) + \Theta_{\chi_2}^{(s)} \sin(\chi_2 T_1 + \beta_2) \end{aligned} \quad (3.140)$$

From the analysis of the terms in $\Theta_{\chi_1}^{(c)}$, $\Theta_{\chi_1}^{(s)}$, $\Theta_{\chi_2}^{(c)}$ and $\Theta_{\chi_2}^{(s)}$, if n is far from any resonant condition, then:

$$\frac{\partial A_1}{\partial T_2} = \frac{\partial A_2}{\partial T_2} = \frac{\partial \beta_1}{\partial T_2} = \frac{\partial \beta_2}{\partial T_2} = 0 \quad (3.141)$$

With these information it is now possible to analyze the four secondary resonances.

Case 1: $2n \rightarrow \chi_1$

In this case, the term that generates a small divisor term on the response of Eq. (3.132) is:

$$\Theta_{2n}^{(s)} \sin(2nT_1) = \Theta_{2n}^{(s)} (\sin(\chi_1 T_1) \cos(\sigma T_2) + \sin(\sigma T_2) \cos(\chi_1 T_1)) \quad (3.142)$$

The term in this equation must be added to the term from Eq. (3.140) and this result must vanish. Therefore:

$$\theta_{sec}^{(2)} + \Theta_{2n}^{(s)} (\sin(\chi_1 T_1) \cos(\sigma T_2) + \sin(\sigma T_2) \cos(\chi_1 T_1)) = 0 \quad (3.143)$$

From the conditions for $\sin(\chi_2 T_1)$ and $\cos(\chi_2 T_1)$ to vanish, the following equations are obtained:

$$2A_2 \chi_2 \mu^{-1} \frac{\partial \beta_2}{\partial T_2} (\Gamma_2 \mu v^2 + 1) = 0 \quad (3.144)$$

$$2A_2 \chi_2 \frac{\partial \beta_2}{\partial T_2} (v^2 + \Gamma_2 + 1) = 0 \quad (3.145)$$

$$2\chi_2 \mu^{-1} \frac{\partial A_2}{\partial T_2} (\Gamma_2 \mu v^2 + 1) = 0 \quad (3.146)$$

$$2\chi_2 \frac{\partial A_2}{\partial T_2} (v^2 + \Gamma_2 + 1) = 0 \quad (3.147)$$

From these equations, ignoring the case of trivial response for A_2 , the resulting condition is:

$$\frac{\partial A_2}{\partial T_2} = \frac{\partial \beta_2}{\partial T_2} = 0 \quad (3.148)$$

This result was expected, because the small divisor term did not introduce any new secular terms with frequency χ_2 . The conditions for vanishing $\sin(\chi_1 T_1)$ and $\cos(\chi_1 T_1)$ lead

to more complicated equations:

$$\begin{aligned} \frac{G_0^2}{\Delta^2} \left((2\alpha_2 - 1 - n^2)nv^6 + (2\alpha_2 + v^2)n^5v^2 + (1 - 4\alpha_2)n^3v^4 \right) \sin(\sigma T_2 - \beta_1) + \dots \\ + 2A_1\chi_1 \frac{\partial \beta_1}{\partial T_2} (\mu^{-1} + v^2\Gamma_1) = 0 \end{aligned} \quad (3.149)$$

$$\begin{aligned} \frac{G_0^2}{\Delta^2} \left((2\alpha_2 p + n^2)nv^6 + (2\alpha_2 p - v^2 - 1)n^5v^2 + (1 - 4\alpha_2 p)n^3v^4 \right) \sin(\sigma T_2 - \beta_1) + \dots \\ + 2A_1\chi_1 \frac{\partial \beta_1}{\partial T_2} (1 + v^2 + \Gamma_1) = 0 \end{aligned} \quad (3.150)$$

$$\begin{aligned} \frac{G_0^2}{\Delta^2} \left((2\alpha_2 - 1 - n^2)nv^6 + (2\alpha_2 + v^2)n^5v^2 + (1 - 4\alpha_2)n^3v^4 \right) \cos(\sigma T_2 - \beta_1) + \dots \\ + 2\chi_1 \frac{\partial A_1}{\partial T_2} (\mu^{-1} + v^2\Gamma_1) = 0 \end{aligned} \quad (3.151)$$

$$\begin{aligned} \frac{G_0^2}{\Delta^2} \left((2\alpha_2 p + n^2)nv^6 + (2\alpha_2 p - v^2 - 1)n^5v^2 + (1 - 4\alpha_2 p)n^3v^4 \right) \cos(\sigma T_2 - \beta_1) + \dots \\ + 2\chi_1 \frac{\partial A_1}{\partial T_2} (1 + v^2 + \Gamma_1) = 0 \end{aligned} \quad (3.152)$$

Although Eqs. from (3.149) to (3.152) represent conditions for the vanishing of secular terms, they are written in terms of $\sin(\sigma T_2 - \beta_1)$ and $\cos(\sigma T_2 - \beta_1)$, sinusoids in terms of other time scales. This is undesirable, because this system of four equations becomes nonautonomous.

In order to avoid it, the following change of variables is proposed:

$$\gamma_1 = \sigma T_2 - \beta_1 \quad (3.153)$$

$$\frac{\partial \beta_1}{\partial T_2} = \sigma - \frac{\partial \gamma_1}{\partial T_2} \quad (3.154)$$

Furthermore, in order to find the steady state response of the system, the amplitudes and phases may not vary in any time scale. Hence, it is necessary that:

$$\frac{\partial A_1}{\partial T_2} = \frac{\partial \gamma_1}{\partial T_2} = 0 \quad (3.155)$$

Substituting Eqs. from (3.153) to (3.155) into Eqs. from (3.149) to (3.152) leads directly to $\cos \gamma_1 = 0$, therefore $\sin \gamma_1 = \pm 1$. From these results it is possible to find four conditions for A_1 :

$$A_1^{(1)} = \pm \frac{G_0^2}{\Delta^2} \left(\frac{(2\alpha_2 - 1 - n^2)nv^6 + (2\alpha_2 + v^2)n^5v^2 + (1 - 4\alpha_2)n^3v^4}{2\chi_1\sigma(\mu^{-1} + v^2\Gamma_1)} \right) \quad (3.156)$$

$$A_1^{(2)} = \pm \frac{G_0^2}{\Delta^2} \left(\frac{(2\alpha_2p + n^2)nv^6 + (2\alpha_2p - v^2 - 1)n^5v^2 + (1 - 4\alpha_2p)n^3v^4}{2\chi_1\sigma(1 + v^2 + \Gamma_1)} \right) \quad (3.157)$$

From the first order approximation term, it is known that the parameter A_1 dictates the amplitude of vibration of the first mode shape while A_2 dictates the amplitude of the second one. Once the resonant condition being achieved is the eigen-order χ_1 , then the system imposes conditions for A_1 only, i.e. A_2 is defined exclusively through the initial value problem.

The first important feature to be noticed is that in both cases, A_1 is a product between the fraction G_0^2/Δ^2 and a function of the order of excitation and system parameters. Once Γ_1 is always positive, A_1 will have zeros at $n = \chi_1$ and $n = \chi_2$. As in this case $n \rightarrow \chi_1/2$, the function A_1 does not have poles in both cases, i.e. it is limited.

Additionally, the parameter σ , which represents the nearness of $2n$ to χ_1 , multiplies the denominator of A_1 in both cases. Hence, it is possible to normalize A_1 using σ , G_0 and Δ for further analysis.

There are two key dimensionless parameters to be varied. The first one is β . One must remember that β is proportional to the rotating speed of the system. Hence, analyzing the variation of A_1 along β provides knowledge on how the system may behave in different rotating speeds. The second one is q , a parameter which is linked directly to the stability of the system. Lower values of q (near zero) imply on higher inertias of the pendulum, while greater values of this parameter (near the unity) imply on lower inertia of the pendulum bob. One must remember that, from the linear analysis, a key condition for stability is $0 < q \leq 1$.

Therefore, on the following analysis, a normalized version of the parameter A_1 is varied along β . These graphics are generated for different values of q and results are discussed. In Figs. 3.22 and 3.23, these results are shown for $q = 0.003125$. Besides, the curves are generated for three cases: the epicycloidal, the cycloidal and the circular paths.

In both conditions it is possible to see that the system may present higher amplitudes

Case 1: $A_1^{(1)} - q = 0.003125$

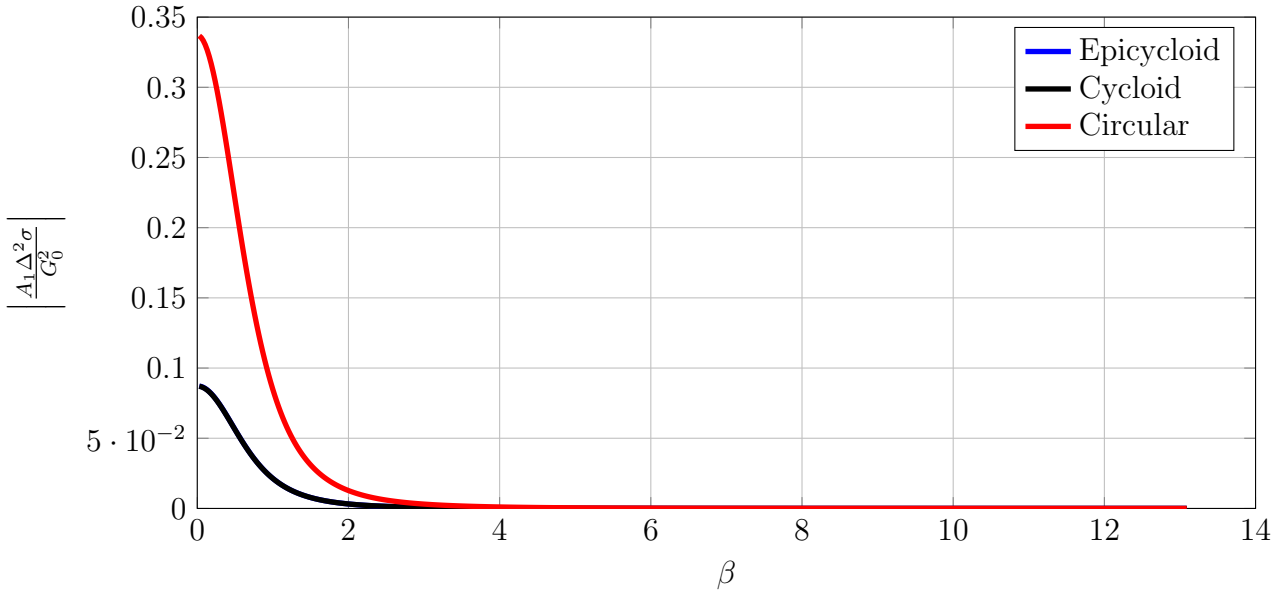


Figure 3.22: Normalized variation of A_1 from Eq. (3.156) along β with $q = 0.003125$

Case 1: $A_1^{(2)} - q = 0.003125$

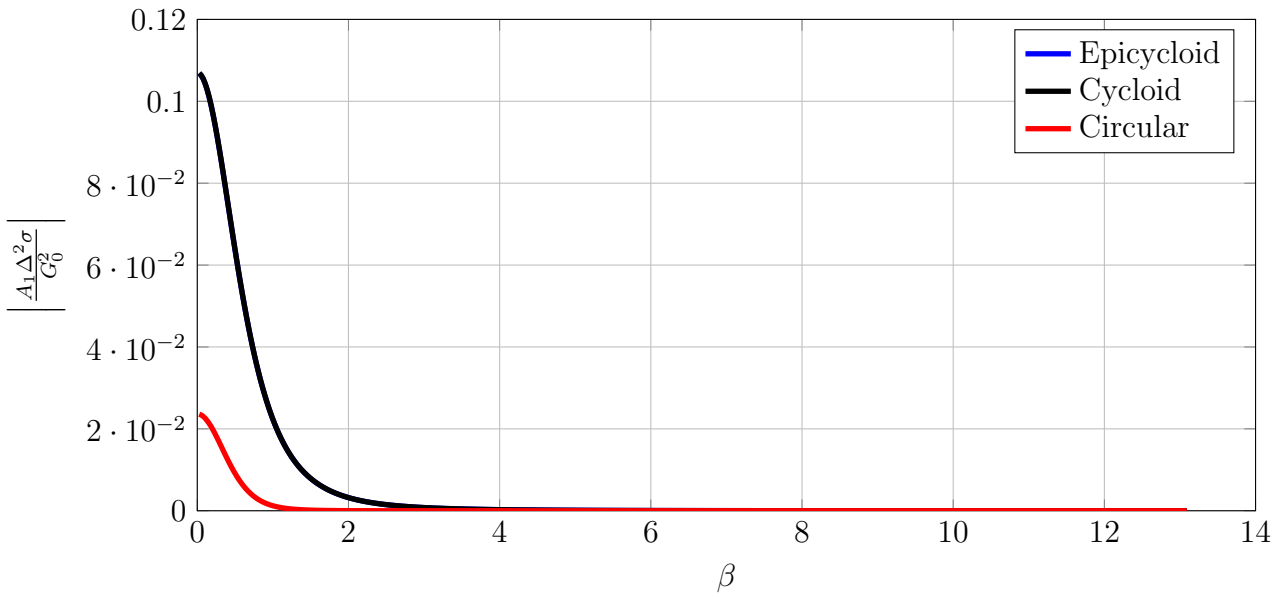


Figure 3.23: Normalized variation of A_1 from Eq. (3.157) along β with $q = 0.003125$

for low values of β , below $\beta = 3$, which mean low rotating speeds. For higher values of β , all the curves tend to zero. For the condition $A_1^{(1)}$, the epicycloid and the cycloid (which are superposed on the figure) have shown to provide lower amplitudes than the circular path. For the condition $A_1^{(2)}$ epicycloid and the cycloid have shown to provide low, but the lowest amplitudes have been generated on the circular path. Also, in this case both values for A_1 are lower than one, because the pendulum bob has high inertia.

The results for $q = 0.32031$ are shown in Figs. 3.24 and 3.25. In this case, higher amplitudes are found on $A_1^{(1)}$ for $\beta < 7$ and on $A_1^{(2)}$ for $\beta < 3$. For higher values of β , all the curves tend to zero. For the condition $A_1^{(2)}$, the performance of both paths is similar. For the condition $A_1^{(1)}$, however, for low values of beta the non-circular paths have shown to be way better than the circular path.

Case 1: $A_1^{(1)}$ - $q = 0.32031$

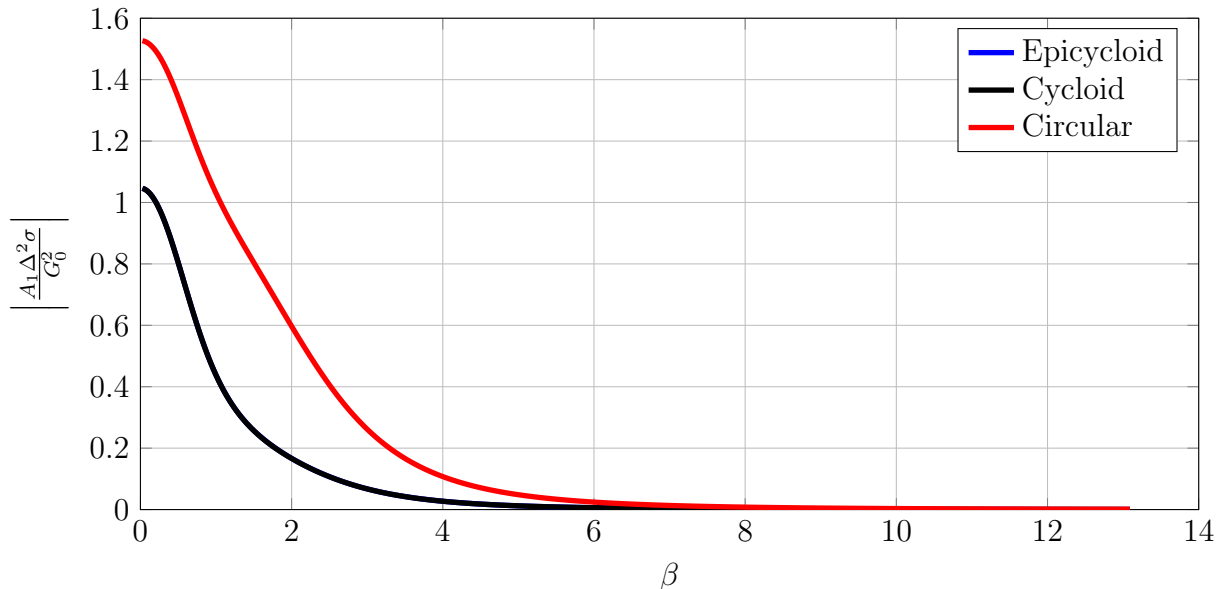


Figure 3.24: Normalized variation of A_1 from Eq. (3.156) along β with $q = 0.32031$

The results for different values of q have shown to evolve progressively, and hence it is possible to proceed to $q = 0.95469$ without omitting any important feature. The results for this condition are shown in Figs. 3.26 and 3.27. For the condition $A_1^{(1)}$ the epicycloid and the cycloid have shown to generate comparatively lower amplitudes than the other paths. However, although the inertia of the pendulum for this case is low, the amplitude of both responses is also low. Furthermore, they tend to zero as β increases.

Case 1: $A_1^{(2)} - q = 0.32031$

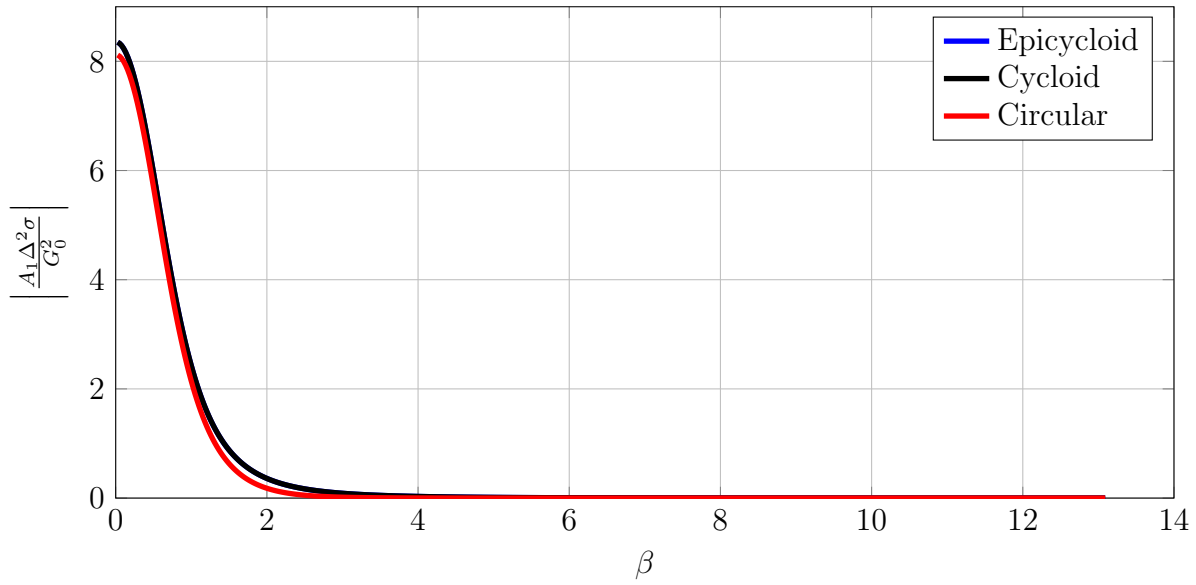


Figure 3.25: Normalized variation of A_1 from Eq. (3.157) along β with $q = 0.32031$

Case 1: $A_1^{(1)} - q = 0.95469$

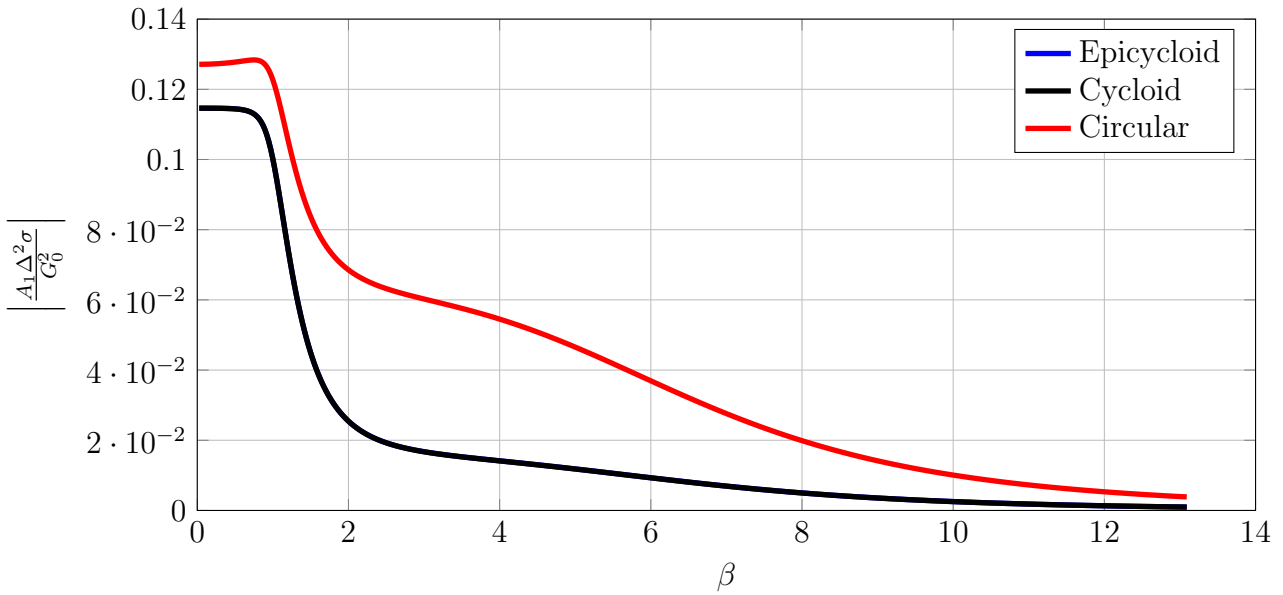


Figure 3.26: Normalized variation of A_1 from Eq. (3.156) along β with $q = 0.95469$

For the condition $A_1^{(2)}$, shown in Fig. 3.27, high amplitudes are noticed for $\beta < 3$ and both paths produced comparatively equivalent results. For higher values of beta, the curves tend to zero.

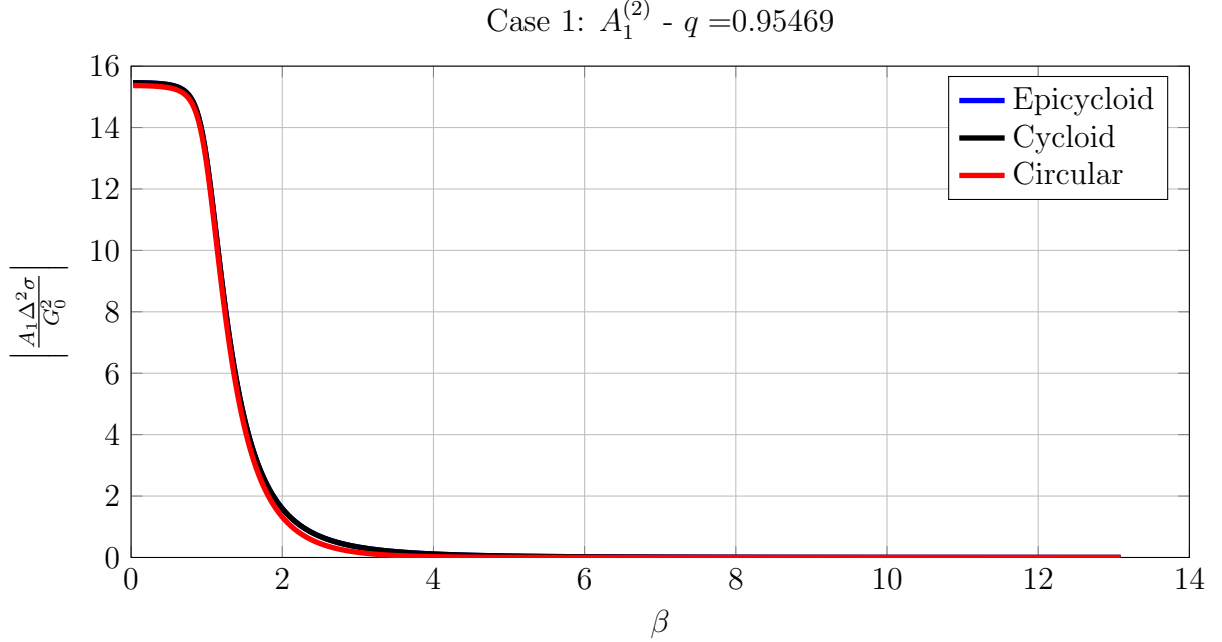


Figure 3.27: Normalized variation of A_1 from Eq. (3.157) along β with $q = 0.95469$

For the case when $2n \rightarrow \chi_1$, the conditions $A_1^{(1)}$ and $A_1^{(2)}$ exist for any combination of the parameters except for $\sigma = 0$. Hence, both responses are possible for any rotating speed, and the mechanism that allows for the system to “choose” which response is being followed is still to be studied, yet it is known that it depends strongly on the initial conditions of the system.

Also, in this case the condition $A_1^{(1)}$ has shown greater amplitudes than $A_1^{(2)}$ for lower values of q , i.e., for pendulums with high inertia. For greater values of q , the condition $A_1^{(2)}$ has shown greater amplitudes. In all the cases, higher rotating speeds are desirable to reduce the amplitude of the terms generated by this secondary resonance.

Case 2: $2n \rightarrow \chi_2$

On the previous case, the whole mathematical procedure necessary to get to the frequency response equations Eqs. (3.156) and (3.157) was shown. In this case and on the following two ones the mathematical procedure is exactly the same, and hence in these cases

it is chosen to proceed directly to the frequency response equations.

Analogously to the previous case, the resonant condition being achieved is χ_2 , and hence the system imposes conditions for the amplitude A_2 only. The term A_1 , in this case, is exclusively defined by the initial conditions. The conditions imposed for A_2 are:

$$A_2^{(1)} = \pm \frac{G_0^2}{\Delta^2} \left(\frac{n\mu v^2(n^2 - v^2)(n^2 v^2 + 2\alpha_2 n^2 - 2\alpha_2 v^2 + v^2)}{2\sigma\chi_2(\Gamma_2 v^2 \mu + 1)} \right) \quad (3.158)$$

$$A_2^{(2)} = \pm \frac{G_0^2}{\Delta^2} \left(\frac{nv^2(n^2 - v^2)(n^2 v^2 + n^2 + 2\alpha_2 p v^2 - 2\alpha_2 p n^2)}{2\sigma\chi_2(v^2 + \Gamma_2 + 1)} \right) \quad (3.159)$$

Once $2n \rightarrow \chi_2$, the term Δ is not null. Furthermore, although the term Γ_2 is negative, as shown in Fig. 3.10, it is not capable of creating a pole on either $A_2^{(1)}$ or $A_2^{(2)}$. However, the eigen-order χ_2 tends to the infinity for low rotating speeds, as seen in Fig. 3.8. Once the numerator of both conditions for A_2 is $O(\chi_2^5)$ while the denominator is $O(\chi_2)$, large amplitudes are expected for low rotating speeds.

The results for $q = 0.003125$ are shown in Figs. 3.28 and 3.29. In both cases, all the paths produced comparatively similar results, with high amplitudes on the whole range of values of β and even higher amplitudes for low values of β . Because of the asymptotic behavior of χ_2 along Ω , the amplitudes do not tend to zero as β increases. Instead, they tend to a constant value, which is lower than the one found at lower rotating speeds but also very critical.

Decreasing the inertia of the pendulum bob makes possible to reach $q = 0.32031$. The results for this value of q are shown in Figs. 3.30 and 3.31. Once more, in both cases the three paths produced comparatively similar results, with higher amplitudes for lower values of β and the amplitudes tending asymptotically to lower but nonzero values as β is increased. However, in this case the amplitudes are much less critical than the ones found for the pendulum bob with high inertia.

Reducing even more the inertia of the pendulum bob leads to the value of $q = 0.95469$ and the results are shown in Figs. 3.32 and 3.33. In the condition $A_2^{(1)}$, the values for the amplitude found for $\beta > 2$ are not critical, even though they are not null. Also, in this case the epicycloidal and the cycloidal paths produced slightly smaller amplitudes than the circular path. In the condition $A_2^{(2)}$, the results from both paths are comparatively equivalent,

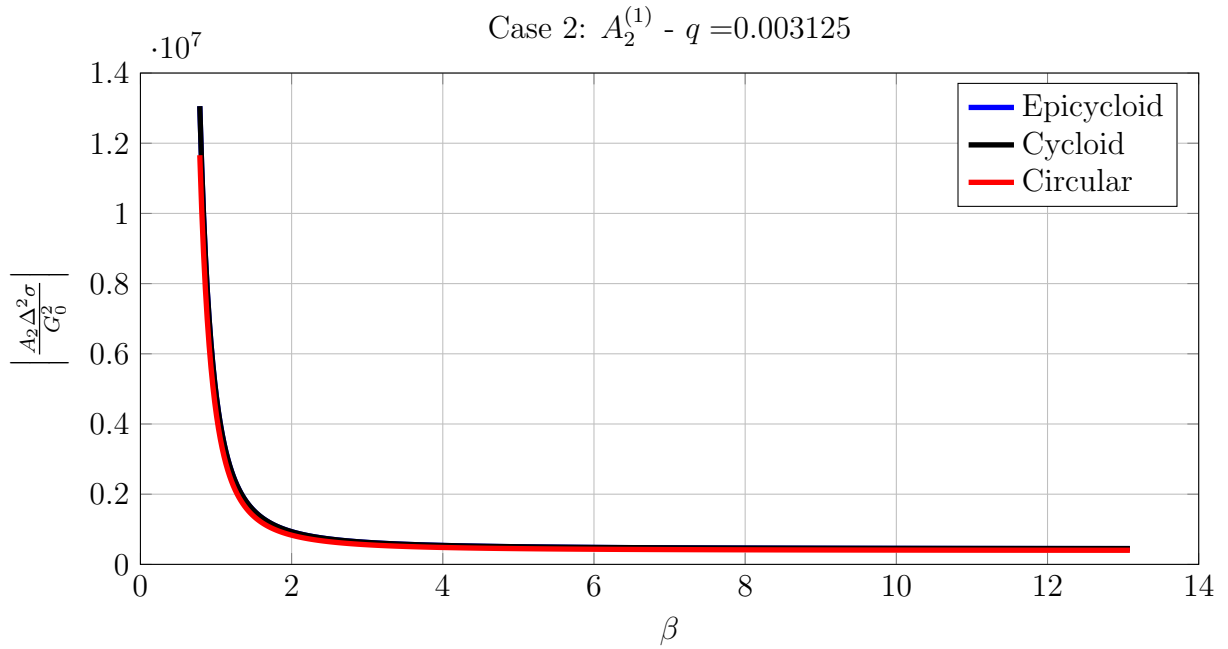


Figure 3.28: Normalized variation of A_2 from Eq. (3.158) along β with $q = 0.003125$

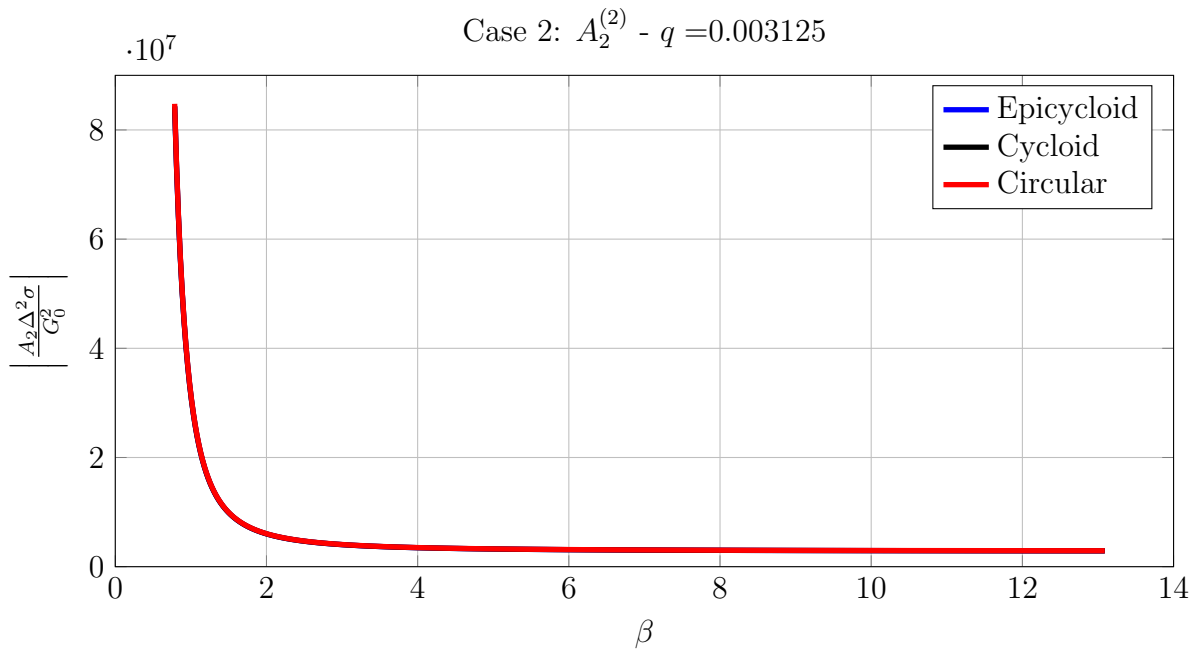


Figure 3.29: Normalized variation of A_2 from Eq. (3.159) along β with $q = 0.003125$

Case 2: $A_2^{(1)} - q = 0.32031$

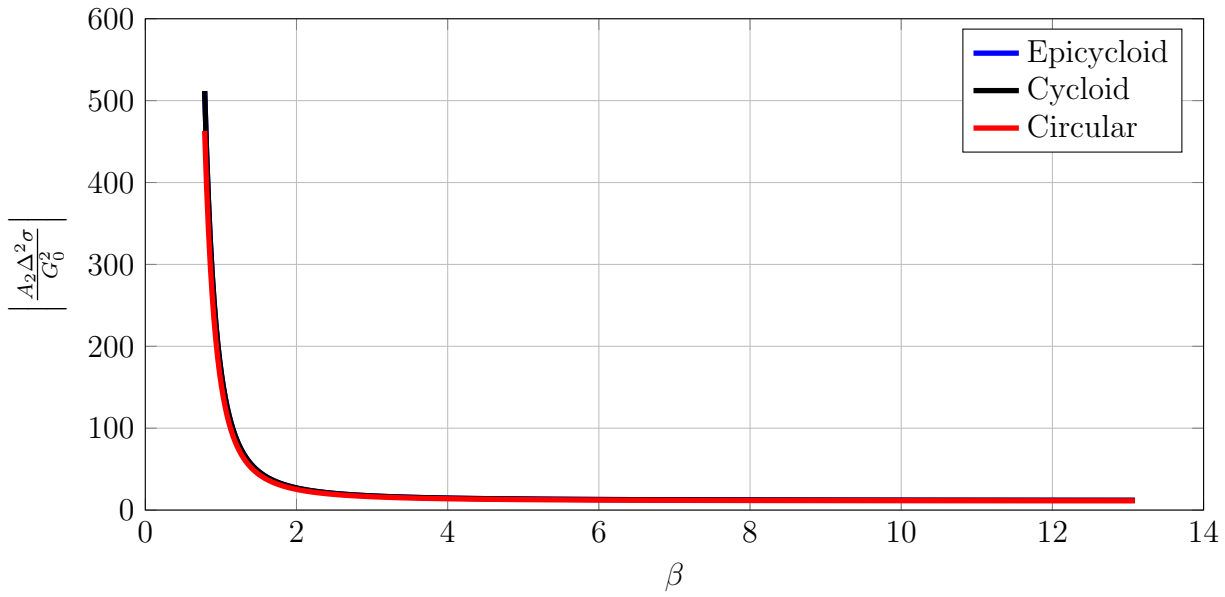


Figure 3.30: Normalized variation of A_2 from Eq. (3.158) along β with $q = 0.32031$

Case 2: $A_2^{(2)} - q = 0.32031$

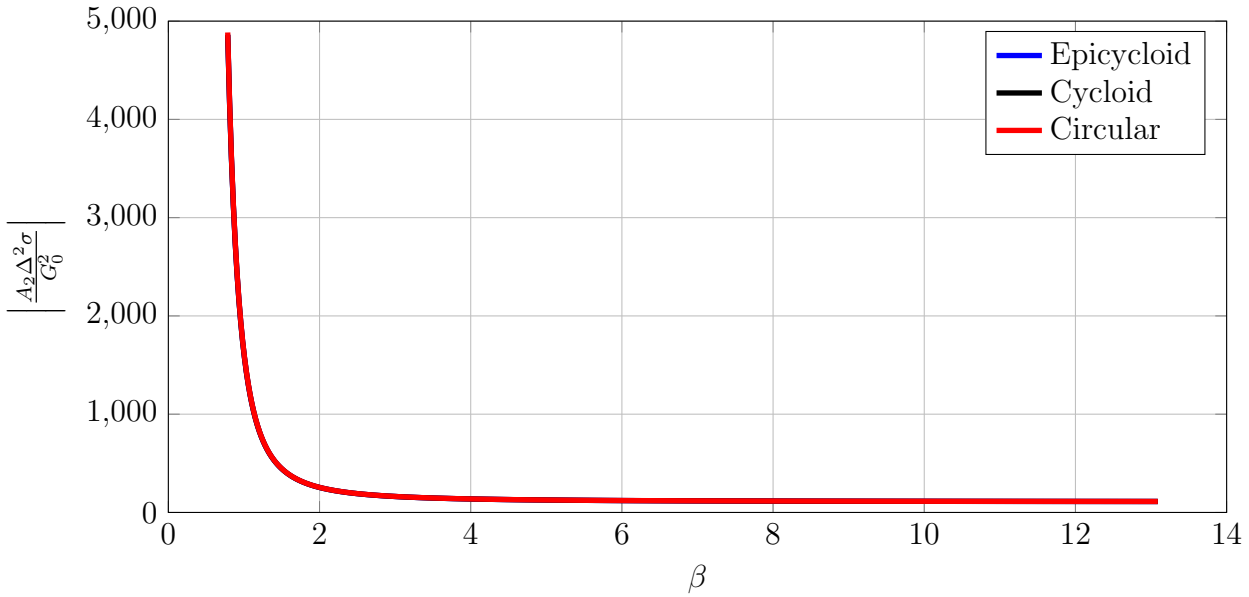


Figure 3.31: Normalized variation of A_2 from Eq. (3.159) along β with $q = 0.32031$

and their amplitude is significantly smaller than for smaller values of q .

Case 2: $A_2^{(1)} - q = 0.95469$

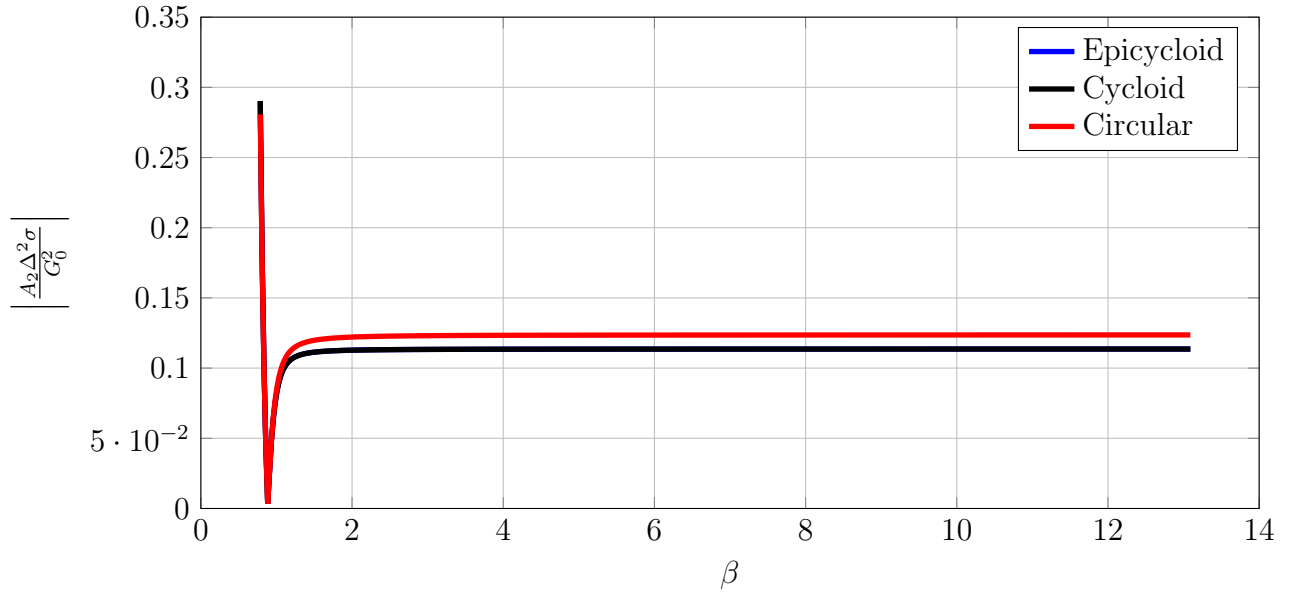


Figure 3.32: Normalized variation of A_2 from Eq. (3.158) along β with $q = 0.95469$

Case 2: $A_2^{(2)} - q = 0.95469$

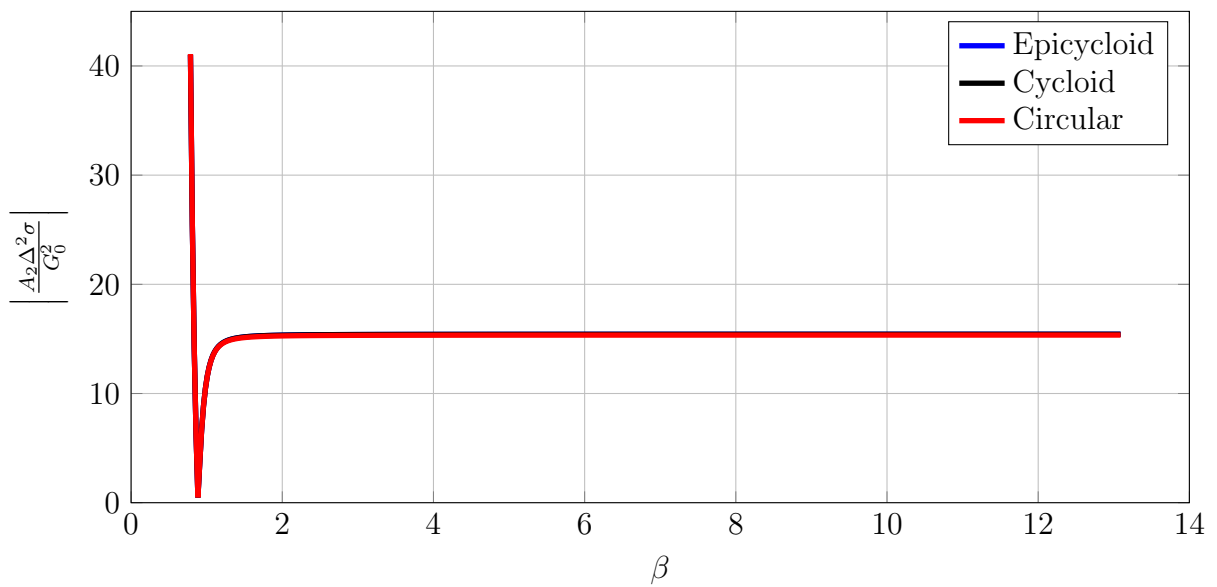


Figure 3.33: Normalized variation of A_2 from Eq. (3.159) along β with $q = 0.95469$

For the case where $2n \rightarrow \chi_2$ a much more critical condition was found. In this case

it was shown that pendulum bobs with lower inertia tend to make this secondary resonance less prominent. Also, lower rotating speeds, directly associated to lower values of β tend to make this secondary resonance much more critical.

Case 3: $\chi_1 + n \rightarrow \chi_2$

This case differs from the previous ones because the secondary resonance is caused by a term resulting from the interaction between the response to excitation and the free oscillation response of the system. Hence, the system must impose conditions for both of the terms A_1 and A_2 . The mathematical procedure is the same from case one, what allows one to proceed directly to the frequency response equations:

$$\left(\frac{A_2}{A_1}\right)_1 = \pm \frac{G_0}{\Delta} \left(\frac{\mu v^2 ((v^2 - n^2)(1 + \Gamma_1(1 - 2\alpha_2(1 + n)))\chi_1 + nv^2\Gamma_1(n^2 + 1))}{2\sigma\chi_2(\Gamma_2\mu v^2 + 1)} \right) \quad (3.160)$$

$$\left(\frac{A_2}{A_1}\right)_2 = \pm \frac{G_0}{\Delta} \left(\frac{v^2 ((v^2 - n^2)(\chi_1 + 2\Gamma_1\alpha_2 p(n + \chi_1)) + n^3\Gamma_1(v^2 + 1))}{2\sigma\chi_2(v^2 + \Gamma_2 + 1)} \right) \quad (3.161)$$

In this case the procedure led to a relationship between A_1 and A_2 in the form of a ratio. Hence it is not possible to determine stability based on these conditions, because they depend strongly on the initial value problem. However, the terms on the right-hand side of Eqs. (3.160) and (3.161) are capable of providing information on how strong this secondary resonance be if the initial conditions allow the existence of nonzero A_1 .

As done in the previous cases, this ratio can be normalized through the parameters G_0 , Δ and σ . Also, this normalized ratio has been analyzed for many different values of q and the result is qualitatively the same. Hence, for this analysis an intermediate value of q is adopted. For $q = 0.54688$, the results for the two conditions for the ratio A_2/A_1 are shown in Figs. 3.34 and 3.35.

In both cases, the ratio has a singularity at $\beta = 0$, but right after this singularity the value of the ratio is low, but increases very rapidly with β . In all the cases the different paths were not able to produce comparatively different results. Therefore, in case the initial conditions allow for the presence of the term A_1 with significant amplitude, then A_2 may reach high amplitudes. Additionally, a small amount of damping may avoid the term A_1 to have significant amplitude for a long period, hence avoiding this secondary resonance to

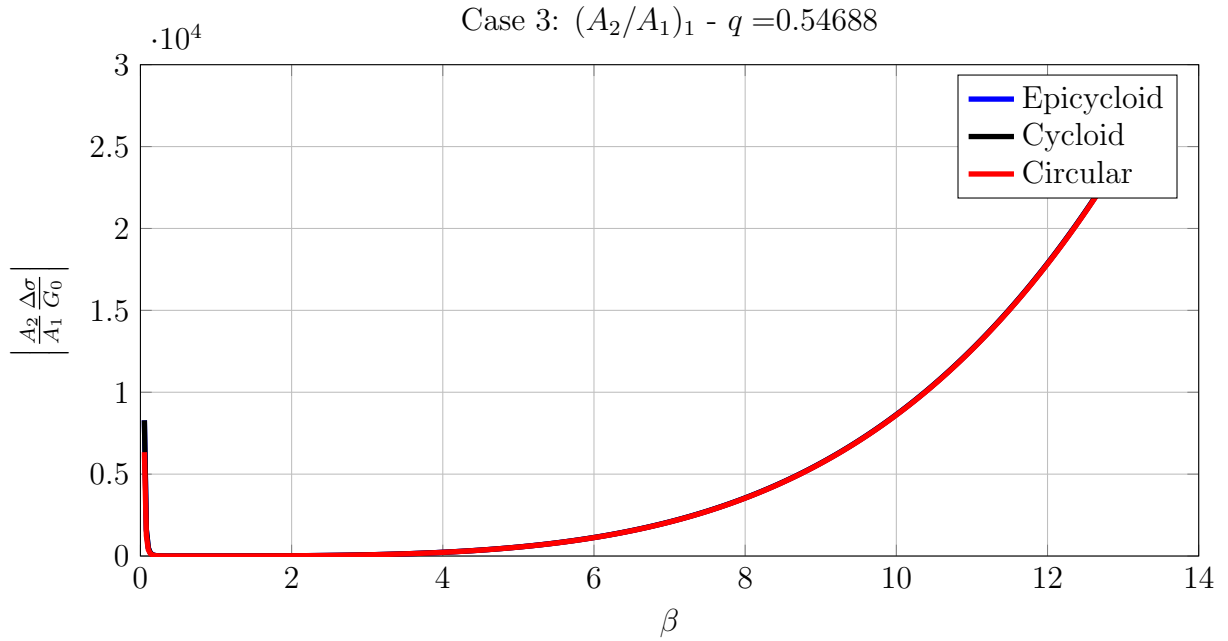


Figure 3.34: Normalized variation of the ratio A_2/A_1 from Eq. (3.160) along β with $q = 0.54688$

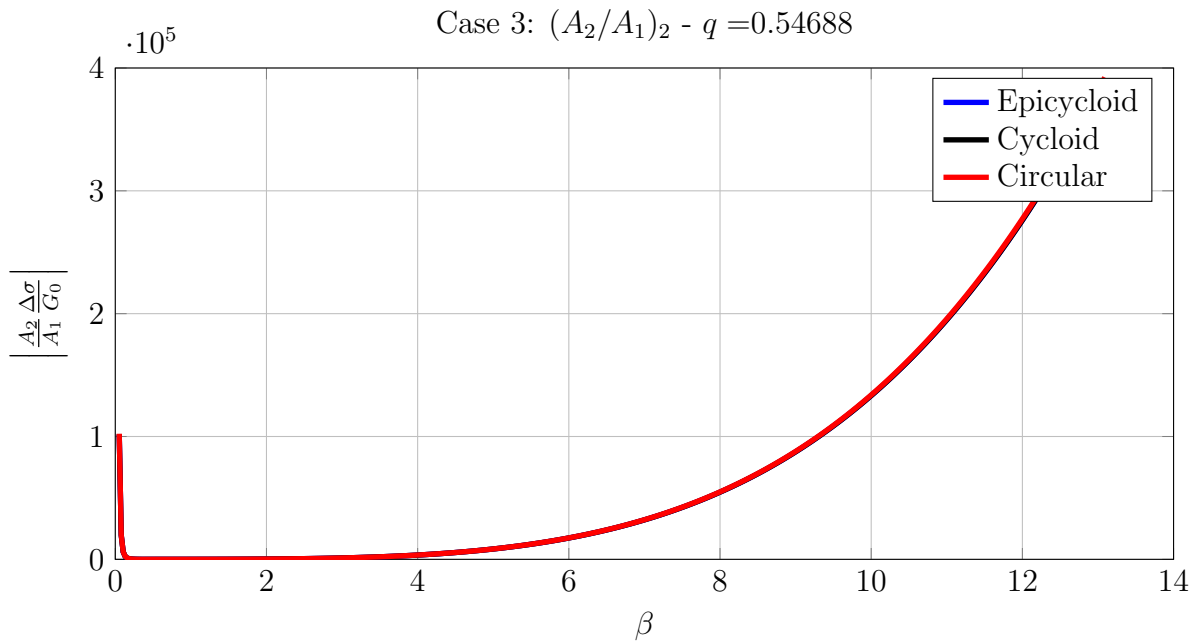


Figure 3.35: Normalized variation of the ratio A_2/A_1 from Eq. (3.161) along β with $q = 0.54688$

occur.

Case 4: $\chi_2 - n \rightarrow \chi_1$

Analogously to the previous case, in this case the secondary resonance is also generated by the interaction between a free oscillation response and a forced response. Hence, the conditions from the frequency response equation must also involve both A_1 and A_2 . These conditions for the case 4 are:

$$\left(\frac{A_1}{A_2}\right)_1 = \pm \frac{G_0}{\Delta} \left(\frac{\mu v^2 ((v^2 - n^2)(\Gamma_2(2\alpha_2(1 - n) - \chi_2) - \chi_2) + \Gamma_2 n v^2 (n^2 + 1))}{2\sigma \chi_1 (1 + \Gamma_1 v^2 \mu)} \right) \quad (3.162)$$

$$\left(\frac{A_1}{A_2}\right)_2 = \pm \frac{G_0}{\Delta} \left(\frac{v^2 ((v^2 - n^2)(2\alpha_2 p \Gamma_2 n v^2 (1 - \chi_2) - \chi_2) + \Gamma_2 n^3 (v^2 + 1))}{2\sigma \chi_1 (v^2 + \Gamma_1 + 1)} \right) \quad (3.163)$$

Like in the previous case, the relationship provided by the frequency response equations is a ratio between A_1 and A_2 , and hence stability cannot be inferred from these equations. However, in case the initial conditions lead to significant amplitude of A_2 , the right-hand side term of Eqs. (3.162) and (3.163) allows for the investigation of the behavior of A_1 .

Additionally, the parameters G_0 , Δ and σ can once more be used to normalize the ratio being studied. For a given pendulum bob with high inertia, it is possible to achieve the value of $q = 0.003125$, and the results for this value are shown in Figs. 3.36 and 3.37

The results show a similar behavior for both conditions stated for the ratios between A_1 and A_2 . For low values of beta the ratio has high values, but as β increases, it rapidly decreases, tending to zero asymptotically. It means that even if there is a certain amplitude A_2 due to initial conditions, if the rotating speed is high enough, then this secondary resonance becomes less relevant.

For lower values of the inertia of the pendulum bob, this behavior did not change significantly. Hence, it was chosen to proceed for a very small inertia for the pendulum bob, leading to a high value of q near the unity. This value is of $q = 0.95469$, and results are shown in Figs. 3.38 and 3.39

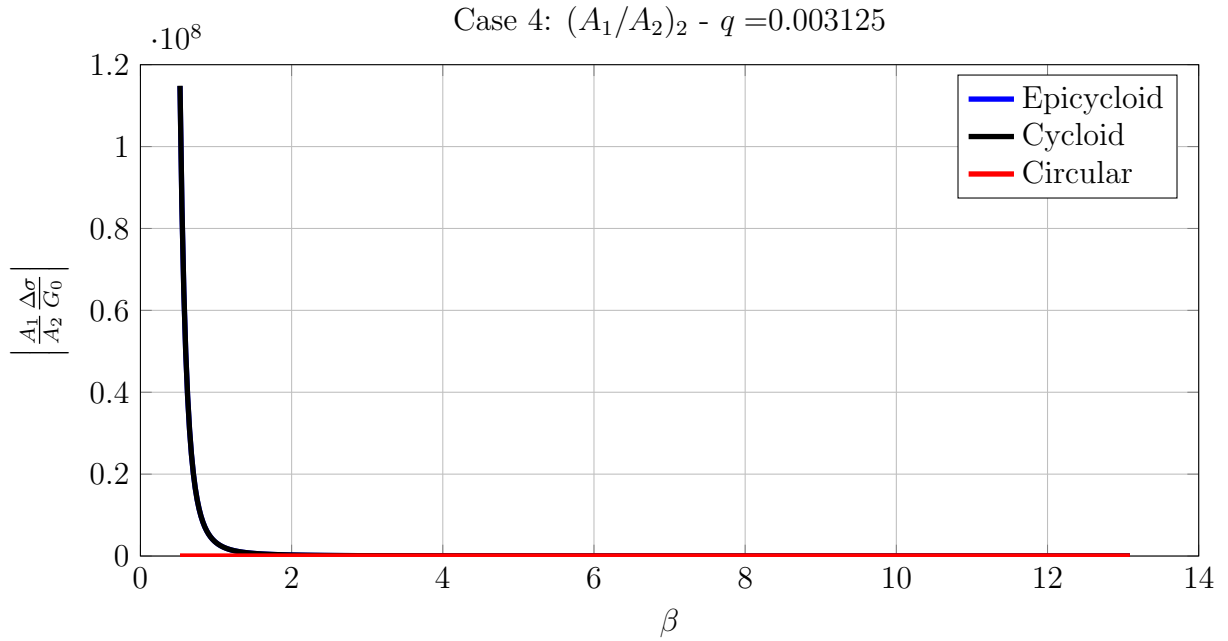


Figure 3.36: Normalized variation of the ratio A_1/A_2 from Eq. (3.162) along β with $q = 0.003125$

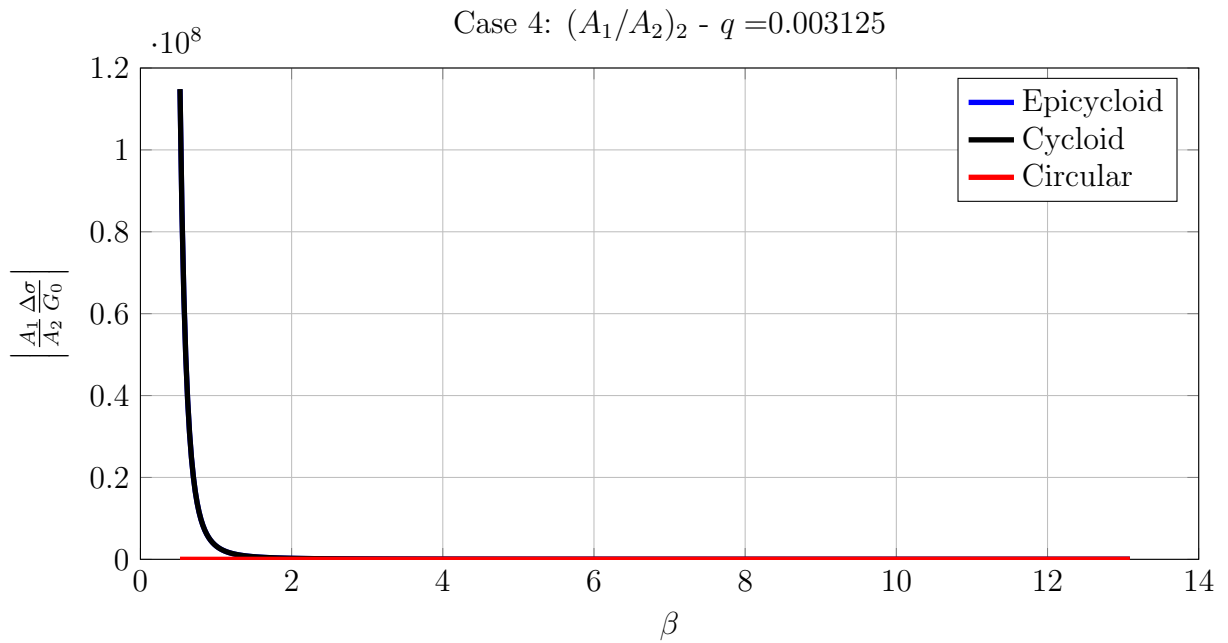


Figure 3.37: Normalized variation of the ratio A_1/A_2 from Eq. (3.163) along β with $q = 0.003125$

Case 4: $(A_1/A_2)_1 - q = 0.95469$

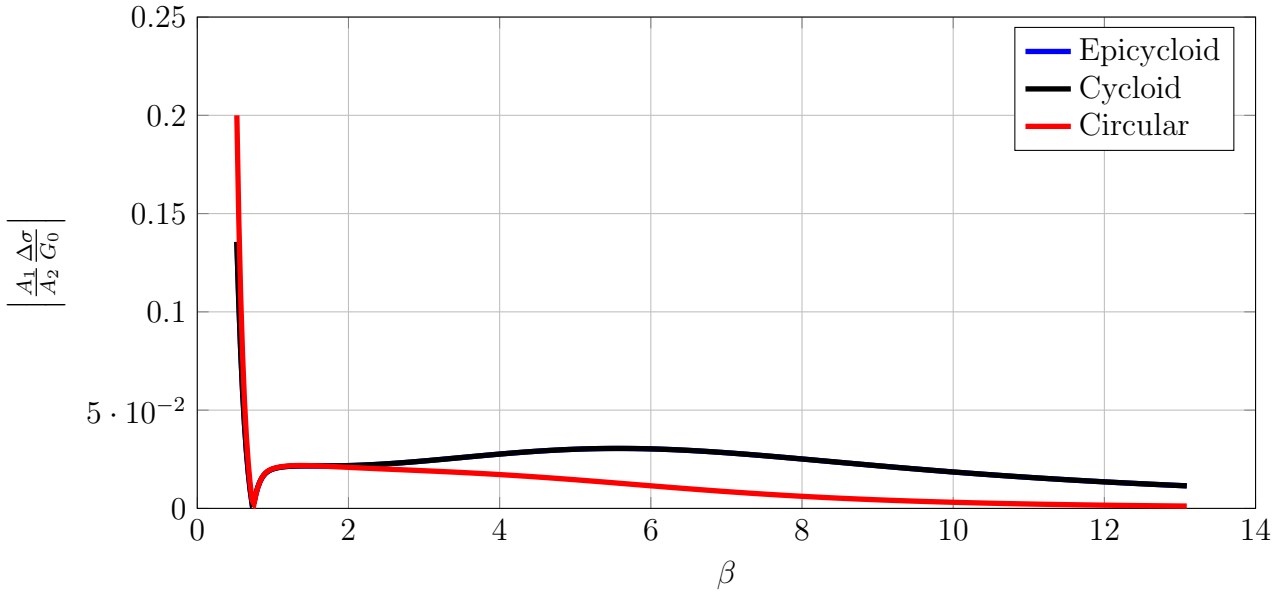


Figure 3.38: Normalized variation of the ratio A_1/A_2 from Eq. (3.162) along β with $q = 0.95469$

Case 4: $(A_1/A_2)_2 - q = 0.95469$

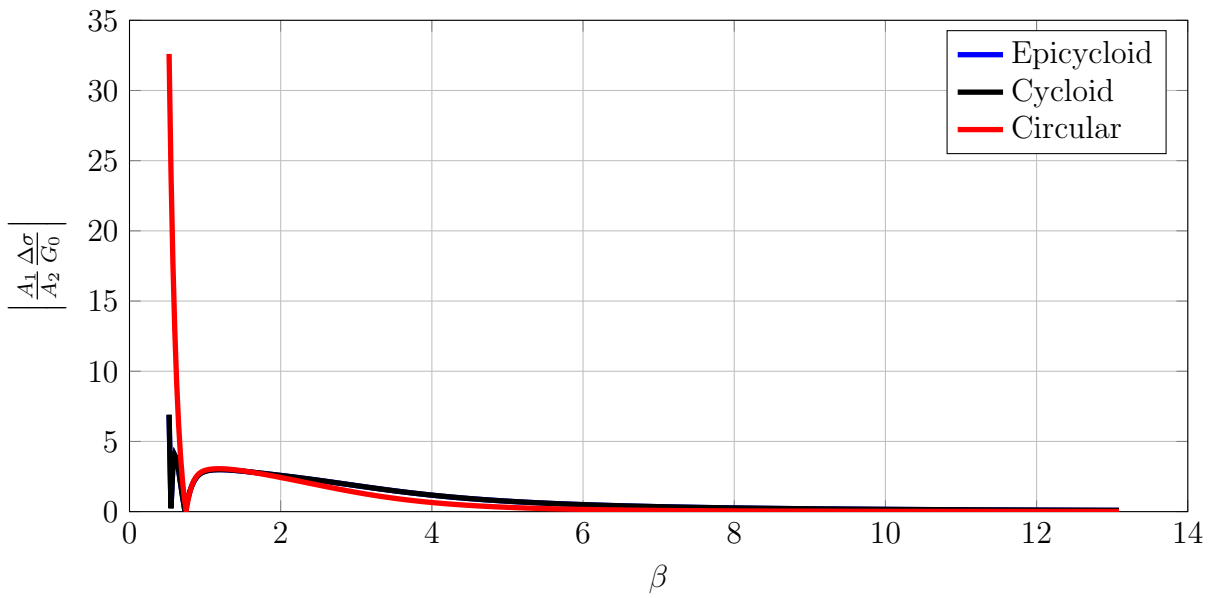


Figure 3.39: Normalized variation of the ratio A_1/A_2 from Eq. (3.163) along β with $q = 0.95469$

For this condition, the behavior found for both ratios is the same. However, the value of the ratios is much smaller, indicating that if secondary resonances occur, reducing the inertia of the pendulum bob may help make them less relevant.

Collecting the results from all four cases there are then two important conclusions to be drawn: one of them about the rotating speed of the system and another one regarding the inertia of the pendulum bob.

Yet this conclusion already shows up from the linear analysis, on the analysis of the secondary resonances for the two-degree-of-freedom system, it becomes very clear that, regardless of the path being used, instability problems may occur if the system operates below a certain rotating speed. Most of the secondary resonances of the second order term approximation have shown lower amplitudes in case the rotating speed is sufficiently high. Therefore, centrifugal pendulums may not be suitable to applications where the rotating speed is low.

Still about the rotating speed, in practical terms, if centrifugal pendulums are to be installed on a gearbox, it is recommended that it is installed on the end which has the greatest rotating speed, which is often the input shaft.

The second conclusion has a rather antagonistic meaning. From the literature it is known that, in order to obtain better behavior and performance from CPVAs, the amplitude of the swing angle must be kept as low as possible. It can be done through increasing the distance from the pinning point of the pendulum to the center of the rotor or through increasing the inertia of the pendulum.

The first alternative does not bring any undesirable effect to the system, but it is limited by the system's geometry. The second alternative brings good results on the linear case. However, as shown in all the four cases, high values for the inertia of the pendulum bob may turn the secondary resonances more significant, and hence the stability of the system may be harmed.

Therefore, increasing the inertia of the pendulum bob is possible, but it brings the risk of creating relevant secondary resonances. On the other hand, reducing the inertia of the pendulum bob may reduce its performance, but make it less prone to secondary resonances.

Yet bifurcations have not been investigated, these results are in agreement with some

of the conclusions of the work of Alsuwayian and Shaw (2002). The authors mention that paths other than the circular one do not present significant improvements compared to the easily manufactured circular path, yet in some circumstances the cycloidal path produces better behavior. The results shown in this section show precisely the same trend.

4 Application of the CPVA on the Clutch Disk of the Powertrain

The goal to be achieved on this chapter is to gather the knowledge from the analysis on chapters 2 and 3 to design a proper CPVA to be installed on the clutch disk of the powertrain under investigation.

On chapter 2 the powertrain is analyzed under static and dynamic conditions. From these tests it was possible to obtain the required data to make a linear representative model of the torsional dynamics of the driveline. On chapter 3, a deep analysis of the CPVA is performed, including different paths, linear and nonlinear analyses of many subjects including performance, detuning and stability.

Therefore, there is plenty of knowledge on the powertrain itself and on centrifugal pendulums, making it possible to design CPVAs and to test their effectiveness through simulations using the dynamic model developed in chapter 2.

In order to achieve this goal, this chapter is organized in the following order: on the first part two design techniques for the CPVA are presented. Then, on the second part, simulations are performed using the linear models of the powertrain and the nonlinear models of the pendulum absorbers. The results are analyzed and the effectiveness and suitability of the centrifugal pendulum vibration absorber for this application is discussed.

4.1 Design Techniques for CPVAs

On this section, two design techniques for CPVAs are presented. Both of them have been developed based on the linear analysis of a rotor with a CPVA installed on it.

The linear analysis represents well the dynamics of this system for small displacements, what is said on the literature (Wilson (1941), Alsuwayian and Shaw (2002), Chao *et al.* (1997)) to be an essential condition for the good behavior of the pendulum. Furthermore, stability of the system can be better inferred on nonlinear analyses, where large displacements

are considered. From these analyses in which are found on the literature and have been performed on section 3.3.3 of this work, there are two ways of controlling instabilities: the choice of noncircular paths or the reduction of inertia of the pendulum bob. For some cases, the use of an epicycloidal path may help to attenuate certain secondary resonances. However, the use of pendulum bobs with less inertia made secondary resonances less critical.

Therefore, if secondary resonances are found, two actions can be taken: either the path of the pendulum must be changed, which requires any further computation of parameters, or the pendulum must be redesigned so that the inertia of the bob is reduced. In both cases the design techniques to be presented are still suitable. Besides, design techniques for CPVAs have not been found on the literature and the ones presented in this work can be a starting point for the development of more advanced techniques in the future.

Before heading to the techniques, the No-Resonance Zone or Resonance Suppression Zone is a central feature of the application of centrifugal pendulum vibration absorbers, and careful analysis of this feature lead to robust design of the CPVA. Hence, the importance and the usage of this feature is discussed separately, on the next section.

4.1.1 Resonance Tuning vs. Inertia Tuning

Both of the terms on the title of this section are proposed by Wilson (1941), and refer to different types of tuning of the CPVA that are presented and discussed below.

From the various applications of tuned mass dampers on vibrating structures, it is well known that, if such structure vibrates with high amplitudes on a specifically narrow range of frequencies, or in a single frequency, a tuned mass damper should be installed on this structure and its resonant frequency, when isolated from other structures, should be exactly the same frequency for which the original structure presents problems.

Once the CPVA is the analogous of a tuned mass damper but for orders of vibration instead of frequencies themselves, the obvious idea is to tune the pendulum absorber to the target order that presents excessive amplitude of vibration. This type of tuning is referred to as *Resonance Tuning*, and yet theoretically perfect, it presents several difficulties for practical implementation.

One of them is related to detuning of the pendulum. Once the centrifugal pendulum is essentially a nonlinear device, the frequency of oscillation of the pendulum is expected to be slightly different for different amplitudes of oscillation of the pendulum. Therefore, its tuning may be harmed because of the amplitude of vibration, and undesired amplitudes may appear. Other factors that may cause such detuning are the manufacturing tolerances and wear. Some cases may require tolerances to be too tight, while in other cases detuning caused by wear (due to change on the radius of the pendulum) may cause the system to vibrate after short usage.

An alternative to this inconvenience is brought by Wilson (1941). In his work, the author replaces the pendulum by an equivalent inertia for the pendulum bob, which varies according to the frequency of oscillation. This approach may be considered simplistic when compared to recent research, but it was very elegant considering the resources available at the time this work was published.

After calculating the natural frequencies of the system in terms of this equivalent inertia, the author found out that, for some values of such inertia, the system would have no natural frequency. This result is one of the first expressions found on the literature for the No-Resonance Zone.

Then, the author suggests that the pendulum must be designed so that the value of this equivalent inertia lies on the range of values for which the system does not have any natural frequency, and refers to this procedure as *Inertia Tuning*. Once the values for the physical parameters of the pendulum must assure its tuning frequency lies on a zone instead of a single value, it enables one to make a design that compensates for detuning caused by high amplitudes, manufacturing tolerances and wear. In some cases, the performance of the pendulum may improve with wear, up to the design limits.

This idea is adapted to this work through the use of the parameters derived in chapter 3. A scheme to improve visualization of the parameters to be proposed is shown in Fig. 4.1.

The first known parameter is the target order, referred to as n_t . This order must lie inside the No-Resonance Zone of the system. The width of such zone depends on the parameters of the pendulum and of the rotor at which it is installed only. It is possible to see at Fig. 4.1 that it starts at $n = v$ and ends at $n = \sqrt{(1 - q + v^2)/q}$. Hence, the parameter

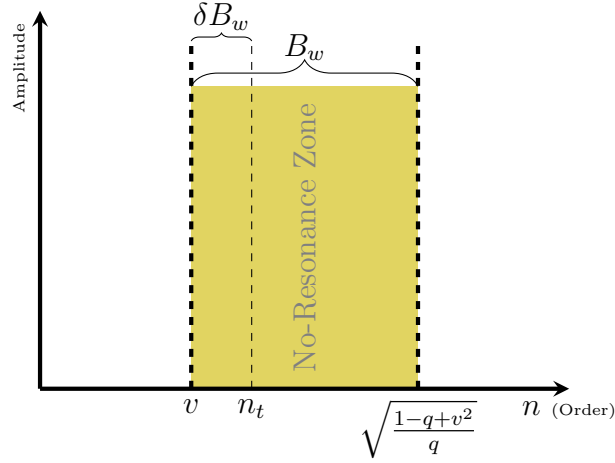


Figure 4.1: Parameters for tuning of CPVAs considering the No-Resonance Zone.

B_w , the bandwidth of the No-Resonance Zone can be written as:

$$B_w = \sqrt{\frac{1 - q + v^2}{q}} - v \quad (4.1)$$

The parameter B_w is a design parameter that can be chosen by the designer, and the choice of wider or narrower band has direct impact on some parameters of the pendulum. This impact is discussed later on the text.

The position of the order n_t on the order axis is given by $n_t = v + \delta B_w$, therefore v can be written as:

$$v = n_t - \delta B_w \quad (4.2)$$

where the parameter δ must lie between zero and the unity, and places n_t on a desired position inside the No-Resonance Zone. This parameter must also be chosen by the designer and also has direct consequences on the parameters of the pendulum. One must notice that $\delta = 0$ leads to *Resonance Tuning*.

Through simple manipulation of Eq. (4.1), it is possible to isolate q as:

$$q = \frac{1 + v^2}{1 + (B_w + v)^2} \quad (4.3)$$

As B_w and v are real, q will always be positive and lower than the unity, as it should be. The influence of δ , B_w and n_t on v is pretty simple and clear, as shown in Fig. 4.1. However, their influence on μ gives important information on the choice of the parameters for the tuning of the pendulum, and hence it must be studied carefully. The parameter μ can be written in terms of B_w and v through the use of Eqs. (4.3) and (3.34):

$$\mu = \frac{(B_w + v)^2 - v^2}{(1 + (B_w + v)^2)v^2(v^2 + 1)} \quad (4.4)$$

If $B_w \rightarrow 0$, then according to Eq. (4.2), $v \rightarrow n_t$, therefore:

$$\mu_{\min} = \lim_{B_w \rightarrow 0} \mu = 0 \quad (4.5)$$

The expression on Eq. (4.5) provides prior knowledge on which is the minimum value for μ in order to design a pendulum which is capable of deal with the desired order. Furthermore, the use of the parameters δ and B_w will not lead to unacceptable values of μ . Also, when $B_w \rightarrow 0$, the parameter q becomes:

$$q_{\max} = 1 \quad (4.6)$$

Hence it is also possible to know beforehand that the maximum achievable value for q for a given application will not be greater than one for positive values of B_w . If B_w tends to high values, then these parameters have to be analyzed more carefully.

The lower bound for the No-Resonance Zone is v , a parameter that must be at least positive. Therefore, the maximum allowable value for B_w would force v to tend to zero. This would force μ to tend to the infinity, according to Eq. (4.4), and q to tend to 0, according to Eq. (4.3). However, these conditions are all subjected to $n_t = \delta B_w$. Once n_t is constant, this implies that these conditions are valid for $\delta \rightarrow 0$, i.e. the *Resonance Tuning* case.

These conditions are contradicting, because *Resonance Tuning* requires that $n_t = v$, and in this case $v = 0 \neq n_t$. Therefore, the project of the pendulum must always consider a finite width for B_w . Consequently, in order to understand the influence of B_w on μ , it is necessary to analyze the derivative of μ with respect to B_w , which is given by:

$$\frac{\partial \mu}{\partial B_w} = (2B_w^3 \delta (4v + B_w)(2v^2 + 1) + 2B_w^2 \delta (11v^4 + 8v^2 + 1) + 2B_w v \delta (5v^4 + 6v^2 + 1) + \dots$$

$$+2v(v + B_w)(v^2 + 1)^2 \times (v^3(v^2 + 1)^2((B_w + v)^2 + 1)^2)^{-1} \quad (4.7)$$

Through simple inspection of Eq. (4.7), once B_w , δ and v are always positive, then the derivative of μ with respect to B_w is always positive, indicating that wider bandwidths require necessarily larger μ . On the other hand, the derivative of the parameter q with respect to B_w is given by:

$$\frac{\partial q}{\partial B_w} = -\frac{2v^3 + 2B_w(\delta + 1)v^2 + 2(\delta B_w^2 + 1)v + 2B_w(1 - \delta)}{(1 + (B_w + v)^2)^2} \quad (4.8)$$

As B_w and v are positive and $0 < \delta \leq 1$, the derivative of q with respect to B_w is always negative, and hence wider bandwidths tend to reduce the value of q . The value of the parameter q also has a minimum, which has already been proven in this work to be zero. This sets a maximum value for the parameter μ in terms of v . However, v is maximum if δ or B_w equals zero, what sets $v = n_t$, and it is minimum when $\delta = 1$, what sets $v = n_t - B_w$. This leads to the following relationship:

$$\frac{1}{n_t^2(n_t^2 + 1)} \leq \mu_{\max} \leq \frac{1}{(n_t - B_w)^2((n_t - B_w)^2 + 1)} \quad (4.9)$$

If the value of δ has already been set, then the maximum value for μ is:

$$\mu_{\max} = \frac{1}{(n_t - \delta B_w)^2((n_t - \delta B_w)^2 + 1)} \quad (4.10)$$

It is also important to verify the behavior of μ along δ , which can be done by analyzing the derivative of μ with respect to this parameter. It is given by:

$$\frac{\partial \mu}{\partial \delta} = \frac{2B_w^2(B_w^2(B_w + 4v)(2v^2 + 1) + B_w(11v^4 + 8v^2 + 1) + 5v^5 + 6v^3 + 1)}{v^3(v^2 + 1)^2(B_w^2 + 2B_w v + v^2 + 1)^2} \quad (4.11)$$

Through inspection of Eq. (4.11), it is direct to see that if B_w and v are positive, which is always true, then the derivative of μ with respect to δ is always positive, and hence greater values of δ lead to greater values of μ .

Consequently, on the design of a CPVA, the designer must have the a priori information on the target order to be dealt with, i.e. the parameter n_t . The next step is to choose values for δ and B_w , taking into account that the increase on any of these values leads to an increase on the value of μ , and a decrease on any of these values generates a decrease on μ .

An important point to be discussed on this section is the dependence of μ on the value of the target order to be dealt with. The smallest maximum (Eq. (4.9)) value for μ depends only on such order and is suitable for a first analysis on any application. These values are presented on Table 4.1.

Table 4.1: Values of $\min(\mu_{\max})$ for usual values of n_t .

n_t	$\min(\mu_{\max})$
0.5	3.20000000
1.0	0.50000000
1.5	0.13675214
2.0	0.05000000
2.5	0.02206897
3.0	0.01111111
3.5	0.00616095
4.0	0.00367647
4.5	0.00232389
5.0	0.00153846
5.5	0.00105785
6.0	0.00075075

Firstly, the value $\min(\mu_{\max})$ refers to the term on the left of Eq. (4.9). Hence, if the parameters B_w and δ are chosen, then the maximum value for μ can be increased. For low values of the target order, the value of μ may be too large. This may turn the application of the centrifugal pendulum unsuitable for some applications, once system modifications are often required to be small.

The target orders from 1.5 to 3.0 are the firing frequencies for four stroke engines with 3, 4, 5 and 6 cylinders, the most usual engines running on worldwide vehicle applications. For these orders the maximum value of μ may vary between 1.11% and 13.67%, depending on the target order. For these orders, these values are small enough to be considered small modifications, and at the same time large enough to allow the absorber to have good performance and low amplitudes. For higher orders, the maximum permissible values for μ tend to be smaller and the range of permissible values becomes narrower. For these orders and

above, suitability must be analyzed.

It is also possible to analyze the influence of the bandwidth on manufacturing tolerances. From Eq. (3.18), it is possible to isolate the parameter ϵ_a as follows:

$$\epsilon_a = \frac{1}{2} \left(\frac{R_p}{v^2} + \sqrt{\frac{R_p^2}{v^4} - 4r_{ga}^2} \right) \quad (4.12)$$

The value of ϵ_a is replaced on this expression by the sum of its nominal value $\bar{\epsilon}_a$ and the manufacturing error ϱ . Also, the parameter v is replaced by $n_t - \delta B_w$. Therefore:

$$\bar{\epsilon}_a + \varrho = \frac{1}{2} \left(\frac{R_p}{(n_t - \delta B_w)^2} + \sqrt{\frac{R_p^2}{(n_t - \delta B_w)^4} - 4r_{ga}^2} \right) \quad (4.13)$$

In this case it is assumed that R_p and r_{ga} do not contain error. If $B_w = 0$, then the right-hand side of Eq. (4.13) tend to $\bar{\epsilon}_a$, because in this case $v = n_t$. Hence, the tolerance ϱ goes to zero. On the other hand, if $B_w \neq 0$ and $\delta = 1$, the target order n_t would be at the right-hand limit of the No-Resonance Zone, causing the error ϱ to be the maximum acceptable error. Hence, the maximum tolerance margin must be the half of it, i.e.:

$$\varrho_{\max} = \pm \frac{1}{2} \left(\frac{R_p}{2(n_t - B_w)^2} - \bar{\epsilon}_a + \sqrt{\frac{R_p^2}{4(n_t - B_w)^4} - r_{ga}^2} \right) \quad (4.14)$$

From Eq. (4.14) it is direct to see that the wider the No-Resonance Zone, the less the manufacturing or wear tolerances must be tight, showing the huge advantage of *Inertia Tuning* against *Resonance Tuning*.

With the introduction of the parameters B_w , δ and n_t , it is now possible to propose two different design techniques, which are shown on the next two sections.

4.1.2 Design Technique 1: Design for Tuning

The design technique presented in this section is sought to reduce the detuning caused by high amplitudes of vibration of the pendulum bob. The inertia of the carrier disk (I_t) and the radius at which the pendulum is pinned (R_p) are considered to be known. Also, the parameters B_w and δ are considered to be chosen by the designer, and the target order n_t is also known a priori. An important condition is that the path to be used in this case is the epicycloid.

The first two parameters to be calculated are μ and v , which follow directly from the value of the target order n_t and the choice of the parameters δ and B_w . Their formulae are:

$$v = n_t - \delta B_w \quad (4.15)$$

$$\mu = \frac{(B_w + v)^2 - v^2}{v^2(v^2 + 1)(1 + (B_w + v)^2)} \quad (4.16)$$

For the next steps, the value of the parameter p , the ratio between the effective length of the pendulum (ϵ_a) and the radius at which the pendulum is pinned (R_p) is required. At this point the detuning reduction is considered on this procedure. For the case at which the carrier disk spins at constant angular speed, nonlinear analyses performed on chapter 3 have shown that a detuning term shows up on the calculation of the third order term of the approximated response of the system. This detuning term is shown to vanish if the value of p is the root of the following polynomial¹:

$$-(18v^2 + 1)p^4 + (18v^2 - 1)p^3 + (24v^2 + 21)p^2 - (24v^2 + 40)p + 20 = 0 \quad (4.17)$$

where v is given by Eq. (4.15). More specifically, the polynomial from Eq. (4.17) has four roots, but only one of them lies between 0 and 1, and this root is the value to be used for p .

With this value it is possible to calculate the effective length of the pendulum bob ϵ_a and also the parameter b , using the following expressions:

$$\epsilon_a = R_p p \quad (4.18)$$

$$b = \frac{1}{1 - v^2 p} \quad (4.19)$$

¹Refer to Eq. (3.99)

The parameter b is the ratio between the inertia of the pendulum bob about its pinning point ($I_a + m_a \epsilon_a^2$) and its inertia about its center of mass (I_a). Depending on the values of p and v , it may be difficult to find a geometry that generates a suitable value for b . One must notice that:

$$b = \frac{I_a + m_a \epsilon_a^2}{I_a} = 1 + \frac{\epsilon_a^2}{r_{ga}^2} \quad (4.20)$$

where r_{ga} is the radius of gyration of the pendulum bob. Therefore, the parameter b is purely defined by geometry.

With these parameters, it is possible to calculate the mass and inertia of the pendulum bob about its center of gravity through the following expressions:

$$m_a = \frac{\mu I_t (b - 1)}{\epsilon_a^2 + R_p^2 (p^2 - \mu(1 + p))(b - 1)} \quad (4.21)$$

$$I_a = \frac{m_a \epsilon_a^2}{b - 1} \quad (4.22)$$

4.1.3 Design Technique 2: Design for Geometry

Although the previous design technique is proposed to minimize detuning due to large amplitude vibration, it has two main drawbacks: it demands the path of the pendulum to be epicycloidal and it forces the designer to create a certain geometry to suit the value of b . Once this parameter is always greater than one, if the calculations demands that b is very close to 1 it may be difficult to create such geometry, because in this case the radius of gyration of the pendulum must be large, leading to a large pendulum bob. In such cases, if detuning due to large amplitudes is not a relevant problem, one can impose a value for b and calculate p instead, as it is shown along the text.

The application of this technique demands that I_t , R_p and n_t are known. Also, the designer must choose suitable values for B_w , δ and b , and they are free to choose among the circular, cycloidal or epicycloidal paths.

Similarly to the previous case, once the values of n_t , δ and B_w are available, it is possible

to directly calculate v and μ using the formulae:

$$v = n_t - \delta B_w \quad (4.23)$$

$$\mu = \frac{(B_w + v)^2}{v^2(v^2 + 1)(1 + (B_w + v)^2)} \quad (4.24)$$

Once p is not available, but v and b are, it is possible to calculate p through the expression:

$$p = \frac{b - 1}{bv^2} \quad (4.25)$$

Then, all the parameters of the pendulum can be calculated as follows:

$$\epsilon_a = R_p p \quad (4.26)$$

$$m_a = \frac{\mu I_t (b - 1)}{\epsilon_a^2 + R_p^2 (p^2 - \mu(1 + p))(b - 1)} \quad (4.27)$$

$$I_a = \frac{m_a \epsilon_a^2}{b - 1} \quad (4.28)$$

At this point, both techniques for the design of CPVAs have been presented. It is now possible to use them to make different designs of pendulum absorbers and to test them through simulations.

4.2 Simulations

In this chapter simulations are performed using the linear model of the powertrain at 8th and 9th gears and the nonlinear equations of motion for the CPVA. Before performing the simulations, it is necessary to design the pendulum. Furthermore, some project limitations must be taken into account for this design.

These limitations are basically generated by the prototype layout designed by ZF engineers. Therefore this layout and the project limitations are presented on the following section.

4.2.1 Layout of The Clutch Disk with a CPVA and Project Limitations

One of the main goals of this work is to assess the suitability of the use of a CPVA on a clutch disk for the reduction of torsional vibration in a gearbox, leading to possible reduction of the rattle noise. For this reason, the author of this work, together with the ZF engineers, were required to design a prototype of a clutch disk where it would be possible to install CPVAs for field tests.

The starting point for the prototype was a clutch disk that currently equips the vehicle under investigation. The design chosen for the pendulum absorber was the bifilar suspension design, because it does not require parts to roll and the tuning of the pendulum depends on the mass of the pendulum bob only, and not on its inertia. The digital drawing of the prototype is shown in Fig. 4.2.

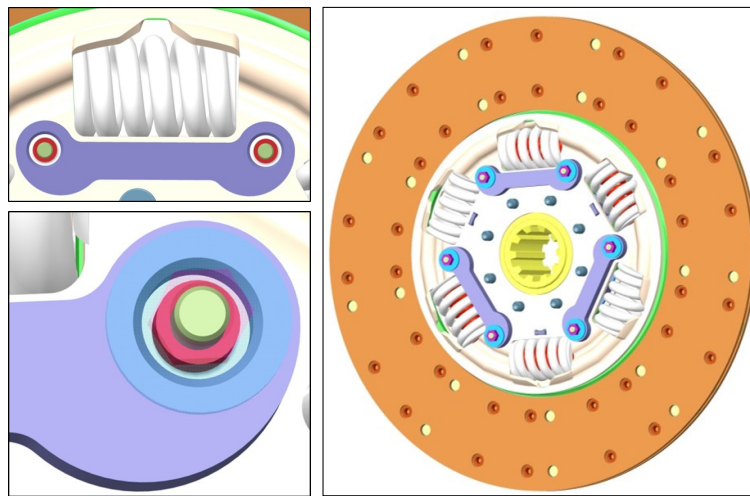


Figure 4.2: ZF prototype layout of clutch disk with bifilar CPVAs.

Because of the position of the springs, this is the layout that allows the pendulum bobs to be as far as possible from the center of the clutch hub. However, this distance is not as large as desired, providing the pendulums with an R_p of approximately 71,88mm. As it has been shown in this work, small R_p lead to large amplitudes of the pendulum and increased mass of the pendulum bob.

On the drawing shown in Fig. 4.2, the clutch disk is equipped with three pendulums, and this was though so that the effective inertia of the pendulum bob could be increased by

adding more pendulums, based on the linear analysis performed on section 3.2. Non unison responses may occur, as shown in Chao *et al.* (1997), but the use of a single CPVA is not possible for imbalance reasons.

The mass of each pendulum bob is controlled by its thickness, which is limited because excessively thick pendulums would touch the flywheel, leading to poor performance of the system. With the thickness limit, the greatest mass that can be achieved by combining the three pendulums is of 315g.

With these values in mind, it is possible to analyze the model of the powertrain and to perform a linear estimation of the amplitude of vibration of the pendulum bob. It is known that these estimations are not realistic if amplitudes grow large, but once the amplitude of vibration of the pendulum bob should be kept small, as literature says, it provides good estimations for the amplitude of vibration of the pendulum, that can be directly linked to the mass of the pendulum bob.

This analysis is done as follows: on the first step it is necessary to obtain a linearized model of the powertrain with the pendulum bob installed on it. The next step is to suppose a maximum acceptable amplitude of vibration at a given rotating speed of the engine. It is advisable to notice that this amplitude is the one after the installation of the pendulum, and not the peak amplitude found on the measurements. The rotating speed, on the other hand, must be directly related to critical rattling speeds found on the original vehicle. In this case, the amplitude is chosen to be of 700rad/s² of torsional acceleration at 800 rpm.

Although there is a linear model to be analyzed and a given condition of amplitude and frequency, the parameters of the pendulum are still unknown. However, in order to design the pendulum, two parameters must be set: δ and B_w . The first parameter must lie between zero and one, and the second one has to be positive. Once it is known that a bandwidth of one order is a very high value, both of the parameters can be varied from zero to one leading to a complete analysis.

Hence, the amplitude of the swing angle of the pendulum can be estimated for each pair (B_w, δ) , leading to a surface. Also, for each pair (B_w, δ) the mass of the pendulum bob with bifilar suspension design can be defined, leading to a second surface. These surfaces are shown in Figs. 4.3 and 4.4, respectively.

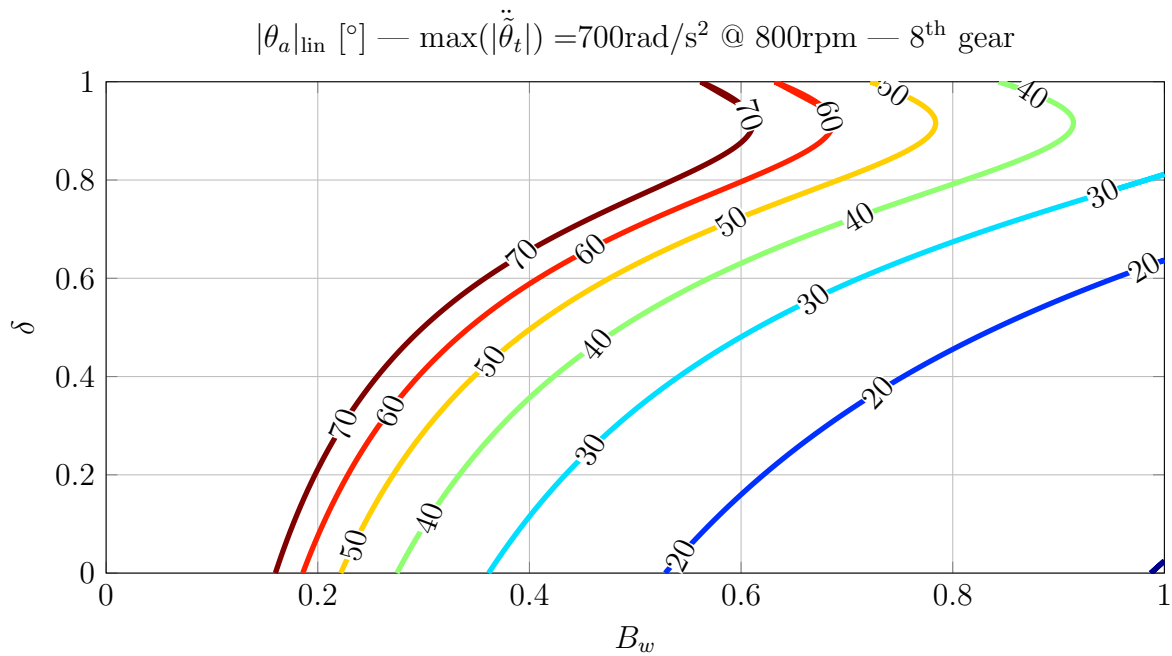


Figure 4.3: Contour levels of the surface of swing angles through (B_w, δ) for 8th gear.

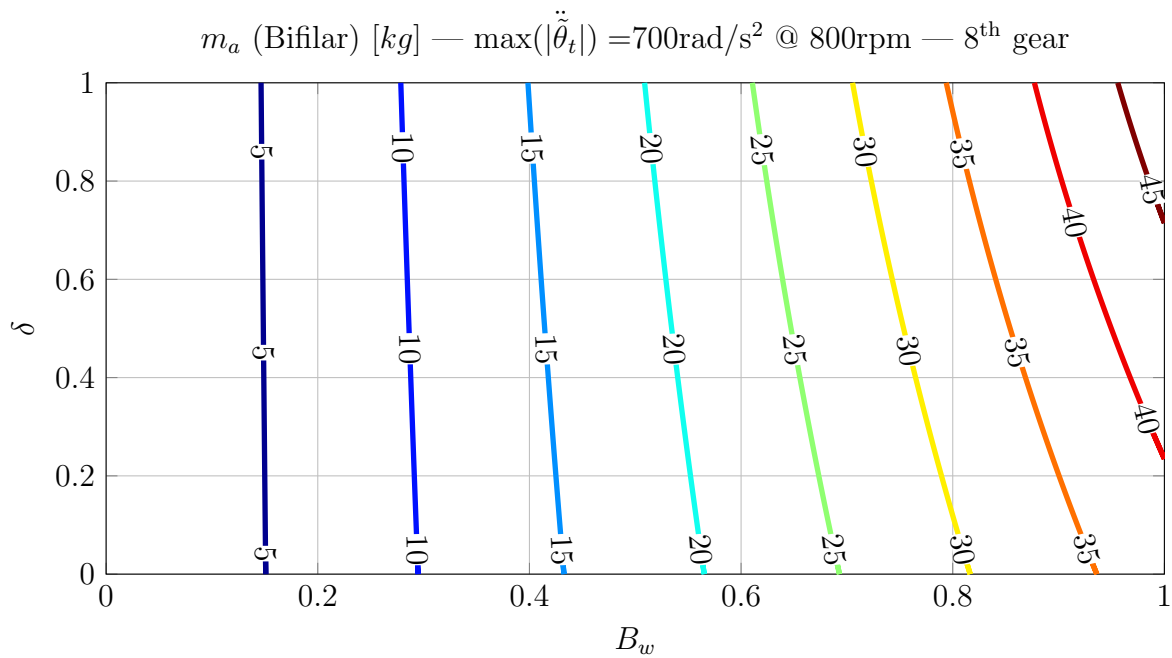


Figure 4.4: Contour levels of the surface of mass of bifilar pendulum bob through (B_w, δ) for 8th gear.

Analyzing both graphics, it is possible to verify that the thicker the bandwidth B_w , the greater is the swing angle of the pendulum, and the lighter the pendulum bob has to be. Large values of δ tend to increase the swing angle of the pendulum bob and also to increase its mass. Therefore, greater values for B_w and lower values for δ are preferable.

It is also very clear that, given the project constraints, through this analysis the pendulum would not be suitable for this application. In order to obtain a swing angle of $\pm 40^\circ$, for instance, which is already considered high, a pendulum bob of at least $10kg$ is required. However, one must consider that this analysis is being carried out considering a worst case scenario, i.e. high amplitude at a considerably low rotating speed.

Another important fact to bear in mind when designing pendulums for powertrains is that for different gears the equivalent inertia of the gearbox is different, and the design of the pendulum should assure stability and good performance for all gears. For this reason, the same graphics found in Figs. 4.3 and 4.4 are plotted for the 9th gear in Figs. 4.5 and 4.6.

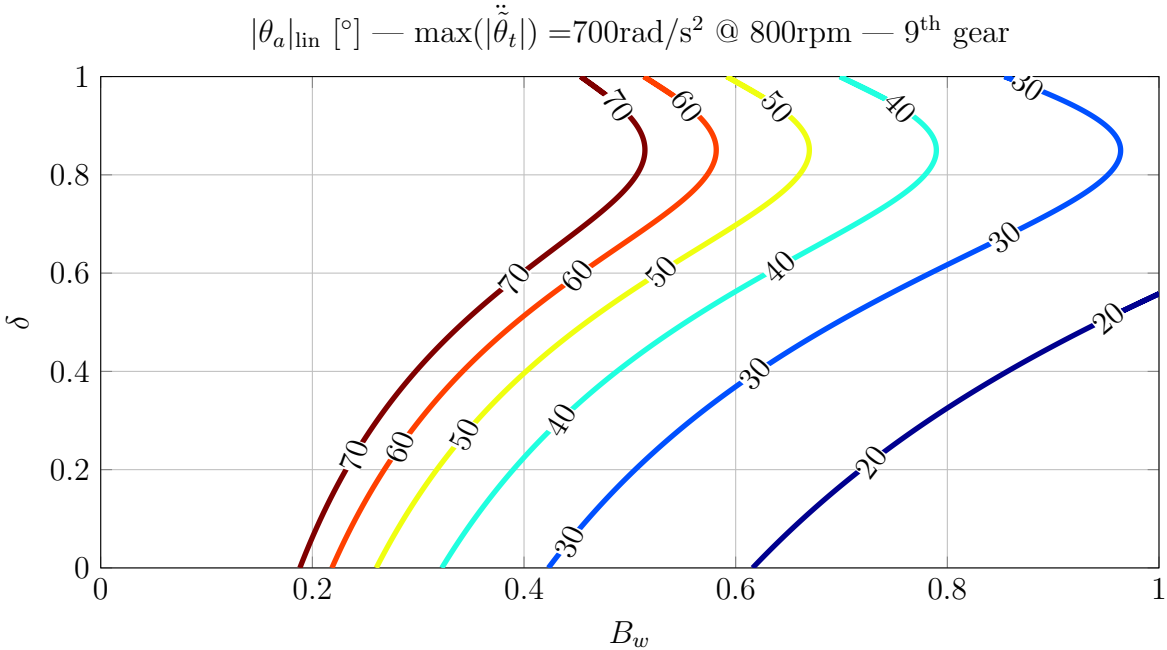


Figure 4.5: Contour levels of the surface of swing angles through (B_w, δ) for 9th gear.

Once the equivalent inertia of the gearbox is increased when higher gears are shifted, as the parameter μ is constant given a pair (B_w, δ) , the inertia of the pendulum is required to be greater in order to keep the same performance. Hence, if a given inertia is suitable for a low gear pair, it may have decreased performance for high gear pairs. On the other hand,

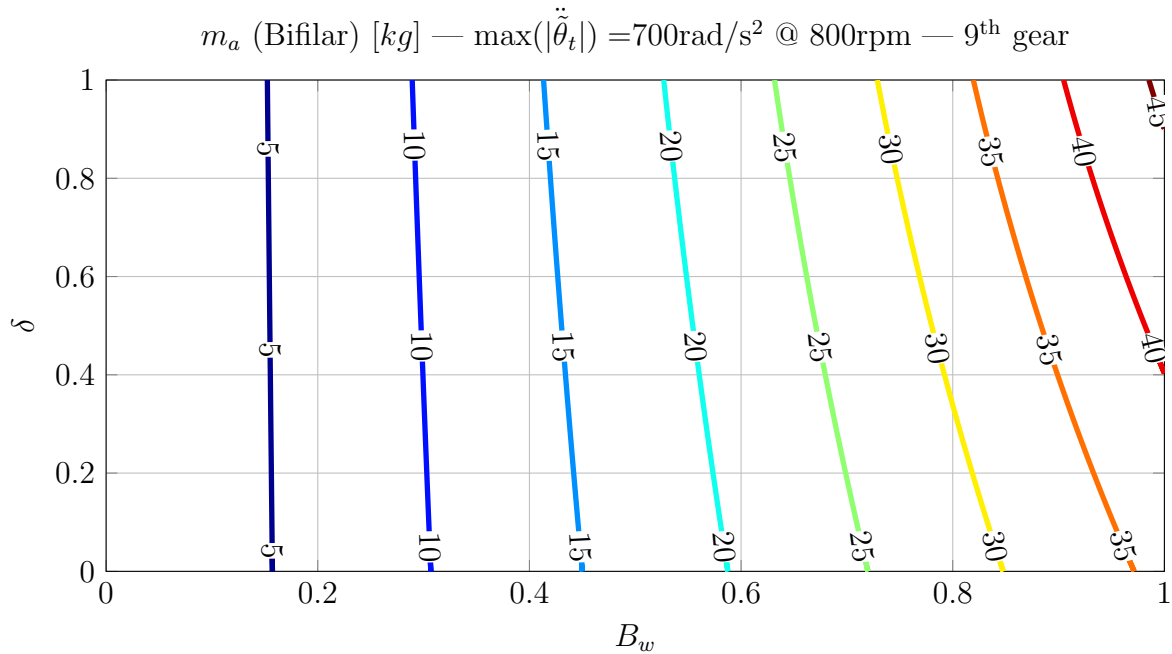


Figure 4.6: Contour levels of the surface of mass of bifilar pendulum bob through (B_w, δ) for 9th gear.

a value of inertia that is suitable for a high gear pair may generate a value for μ which is higher than the maximum acceptable for a low gear pair, becoming unstable for low gears.

A pendulum suitable for all gear pairs is not being designed in this work because it would need 16 linear models to be equalized, one for each available speed of the gearbox. Furthermore, due to project constraints the mass of the pendulum bob would never be as high as possible for this layout, making this design pointless.

From the project constraints, the pendulum bob with the maximum allowed mass is still expected to be unstable. However, the conditions for which it will become unstable are still unknown. If the pendulum becomes unstable and increases vibration on noncritical speeds, or raise some amplitudes to noncritical levels, but it reduces amplitudes on critical speeds, it would still be a solution for the torsional vibration problem, once the goal is to reduce the amplitude of vibration on the gearbox to a level which generates no subjectively unpleasant noise.

These facts guide the simulation planning to be executed, and a detailed discussion about which simulations are to be performed and what results are to be analyzed from them

is presented on the next section.

4.2.2 Simulation Planning

As it was shown in the last section, the project limitations are very tight, and allow for an inertia of the pendulum bob that would not be able to cause any benefit to the system. However, this analysis was done based on the assumption that the system behaves linearly, which is not true for high amplitudes. Therefore, the simulations performed on this chapter are divided in three sets.

On the first set, two simulations are performed considering the powertrain models for 8th and 9th gears without any pendulum. These simulations are the control simulations, and are used as a reference for comparison with the upcoming simulations in which pendulums are going to be considered.

On the second set, the project limitations are obeyed. The parameters of two pendulum bobs are calculated, one for the eighth gear and another for the ninth, both with the maximum allowable mass. Then simulations with the circular path are performed, because great amplitudes are expected and this path is defined for any angle of the pendulum². On the results, pendulum stability and amplitude attenuation are observed.

On the third set, project limitations are neglected and the circular, cycloidal and epicycloidal paths are tested. For the circular and the cycloidal paths the design for geometry is used, while for the epicycloidal path, the design for tuning is used. On the results, the amplitude of the swing angle of the pendulum bob and the amplitude of vibration of the gearbox are observed. Table 4.2 has the summarized information about all the simulations.

The input for all the simulations is the measurement response of the flywheel obtained in Run 4, at the desired gear. The measurements from this run were chosen because in this case the torsional friction was capable of eliminating the first resonance of the system. Hence, the dynamics of the flywheel is much less influenced by the powertrain in this Run than on the first ones at which clutch disks with much less friction had been used.

²The cycloid and the epicycloid are defined for $\pm 90^\circ$ only.

Table 4.2: Summarized information about the simulations.

Set	Simulation	Gear	Path	B_w	δ	b
1	1	8	—	—	—	—
1	2	9	—	—	—	—
2	1	8	Circular	0.00975	0.5	40000
2	2	9	Circular	0.01014	0.5	40000
3	1	8	Circular	0.5	0.5	40000
3	2	8	Cycloid	0.5	0.5	40000
3	3	8	Epicycloid	0.5	0.5	—
3	4	9	Circular	0.5	0.5	40000
3	5	9	Cycloid	0.5	0.5	40000
3	6	9	Epicycloid	0.5	0.5	—

Another important detail about the simulations is that, in all cases a single pendulum is considered. The use of more than one pendulum is usual, mainly for balancing purposes, but it may generate non-unison responses, which are chosen not to be studied in this work.

Regarding the numerical method for integration, all the simulations are performed using the `ode45` routine from Matlab R2010a [®]. The parameters of this integrator are set to maximize accuracy.

4.2.3 Simulation Results

The simulations from Set 1 are used for reference only. Therefore, the first results to be presented are the ones obtained from the simulations from Set 2, at which all the design constraints have been obeyed. The results for the first simulation of the second set are shown in Figs. 4.7 and 4.8.

The first feature to be noticed is the fact that the high amplitude peak related to gear rattle phenomenon occurred on a slightly lower engine speed than was found on the measurements. As this is an approximated model, small divergences were expected. Although this frequency imprecision occurred, the model still represents well the behavior of the powertrain, and this feature does not invalidate further analyses and conclusions.

From Fig. 4.7 it is possible to verify that the pendulum designed to this case was not

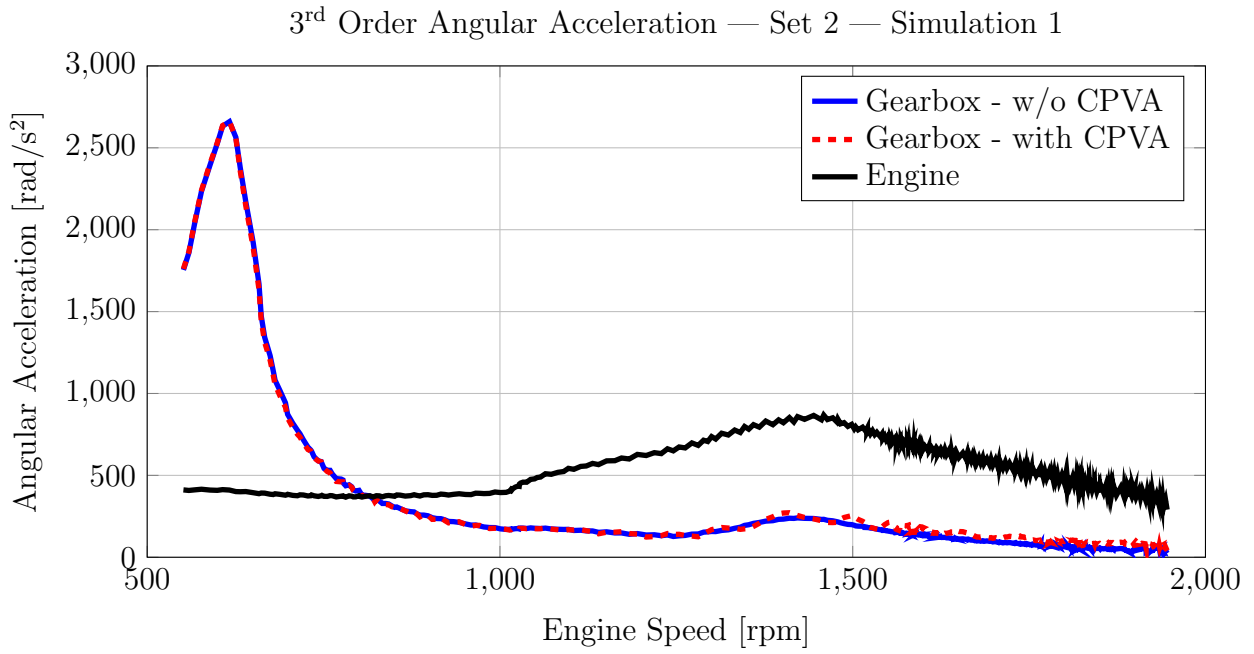


Figure 4.7: Angular acceleration from Simulation 1 from Set 2.

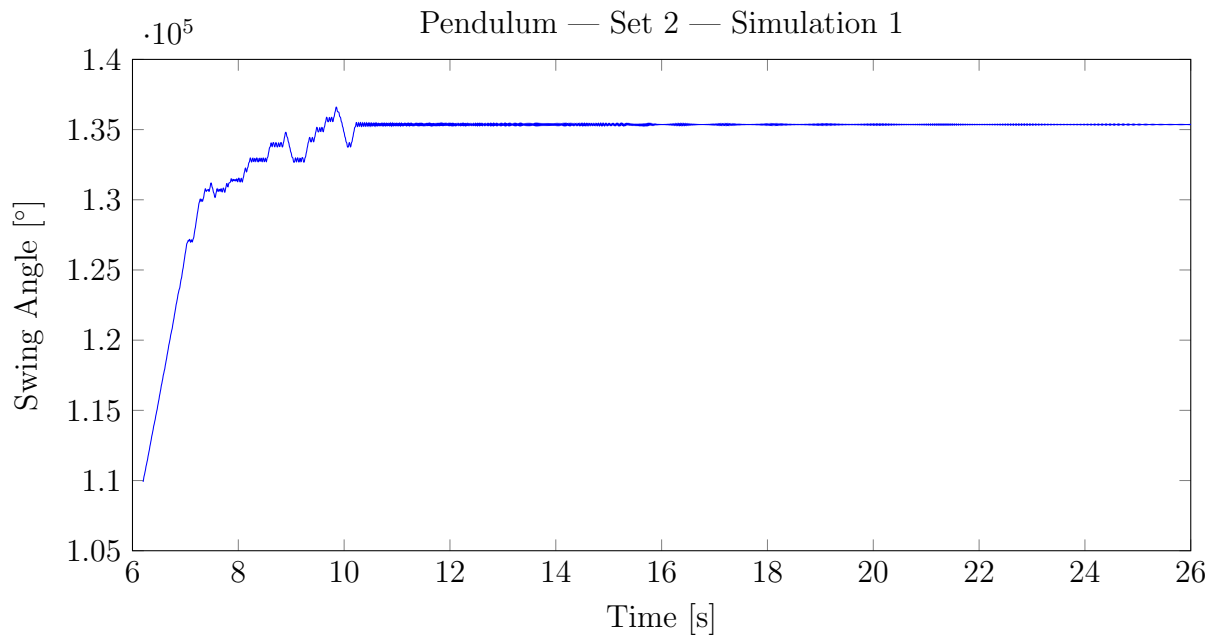


Figure 4.8: Swing angle of the pendulum bob from Simulation 1 from Set 2.

capable of providing any improvement to the dynamics of the system. Great and unacceptable amplification still occurs between 600 and 1000 rpm, and the 3rd order amplitude of angular acceleration of the gearbox is the same for all engine speeds. From Fig. 4.8 it is also possible to verify that for low engine speeds, at the beginning of the simulation, the pendulum became unstable. After that, for higher engine speeds it started to oscillate about a given position, but no improvement on the system response was found. The results for the 6th order are similar.

The results of simulation 2 from the second set are shown in Figs. 4.9 and 4.10. Regarding the reduction of amplitude of angular acceleration on the gearbox, the results are similar to what is found for the eighth gear, i.e., no amplitude reduction was found for all engine speeds. In Fig. 4.10 it is possible to see that, in this case, the pendulum did not become unstable, but the amplitudes of its swing angle are up to $\pm 80^\circ$, which is prohibitive. As for the previous case, the results for the sixth order are similar.

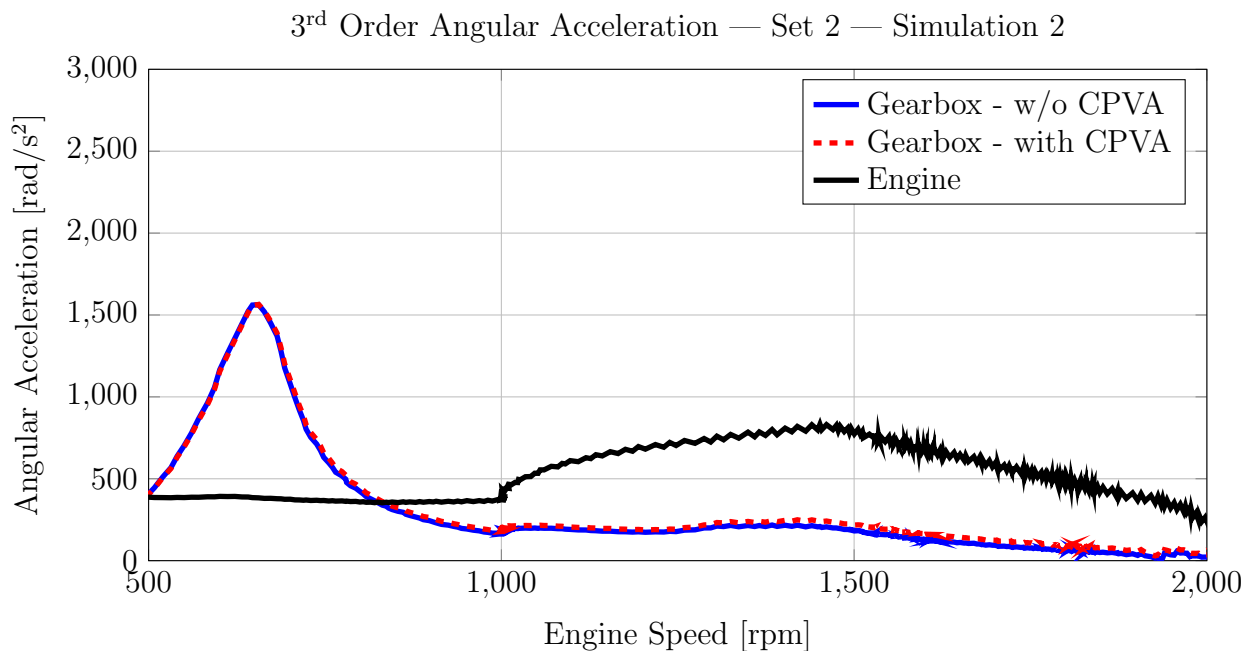


Figure 4.9: Angular acceleration from Simulation 2 from Set 2.

All the designs tested on Set 2 have been designed considering that the mass of the pendulum bob has its maximum value of 315g. In order to reach this mass, the bandwidth B_w had to be chosen to be very low, nearly of 1% of an order of vibration. As a result, this tuning is very close to resonance tuning, which should force the amplitude of vibration of the

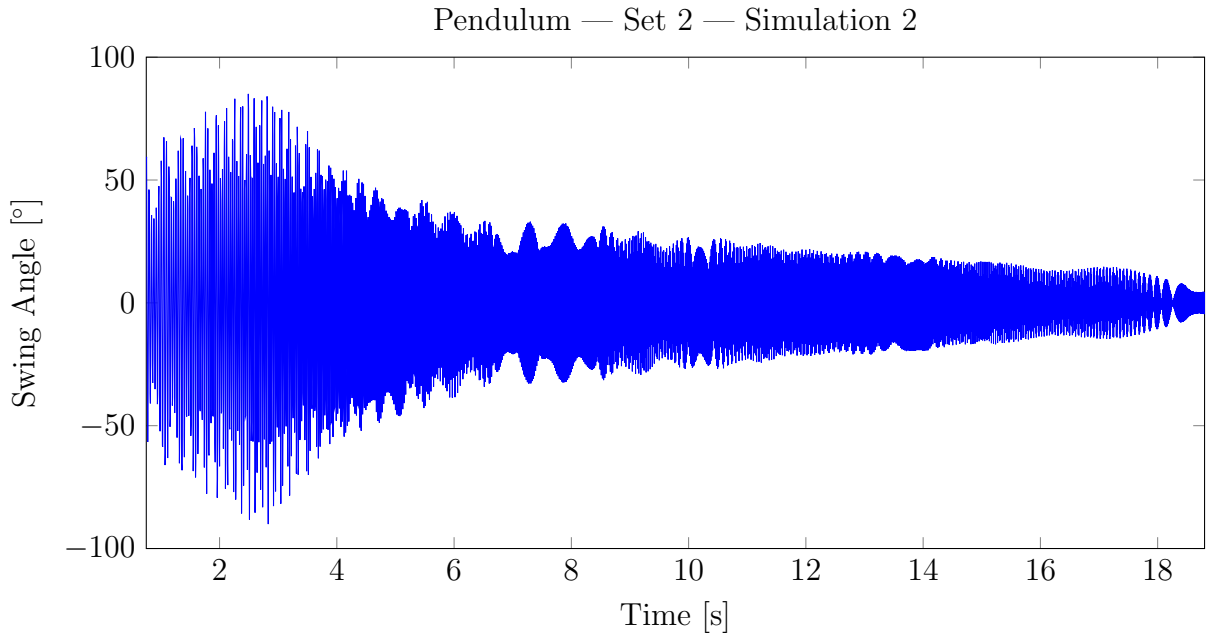


Figure 4.10: Swing angle of the pendulum bob from Simulation 2 from Set 2.

gearbox to become very low.

However, as the maximum allowable mass of the pendulum bob, and also the maximum radius of pinning R_p are very low, the amplitude of vibration of the pendulum bob became very large, leading to the instability found in Fig. 4.8. In this case, stability was not able to contribute for amplification of the original amplitude of vibration.

On the other hand, the pendulums were not able to reduce the amplitude of vibration of the gearbox, even in the case where no instability was found. This is due to the detuning caused by large amplitudes of swing of the pendulum bob, which made this solution ineffective.

These first conclusions are in accordance with the literature, which mentions that, for good performance, the amplitude of the swing angle of the pendulum bob must be kept as low as possible, avoiding detuning and instability.

At this point the results from the Set 2 of simulations have already been presented. The discussion is now turned to the results from the Set 3. Simulations 1 to 3 from set 3 are performed in 8th gear while simulations 4 to 6 are performed in 9th gear. In Fig. 4.11, the

amplitude of vibration of the gearbox for simulations 1 to 3 is presented.

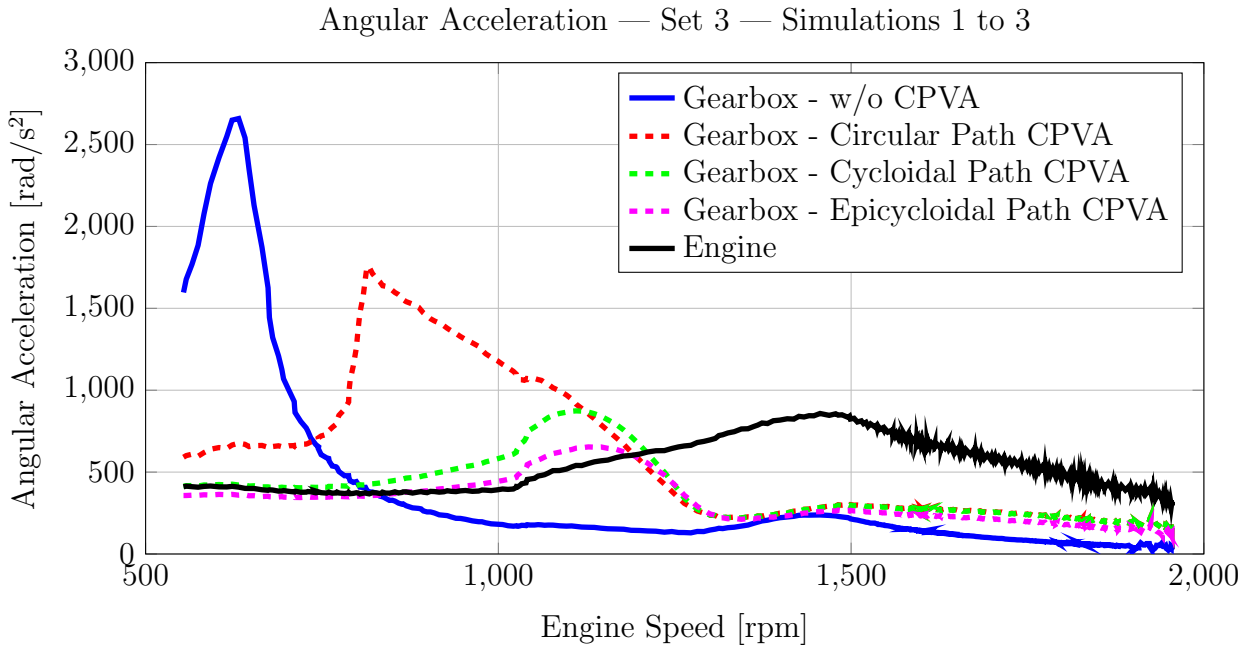


Figure 4.11: Angular acceleration from Simulations 1 to 3 from Set 3.

In both cases, where the CPVA was applied, the gear rattle peak, shown at the original blue curve disappears. However, in the case where the circular path CPVA was applied, another peak shows up in a higher rotating speed, with amplitude of nearly 1700rad/s^2 , which according to experience, is very likely to induce rattle noise.

The cycloidal path CPVA has exactly the same parameters of the circular path CPVA, and its performance is shown to be a lot better. There is not any peak of vibration on the gearbox for this case and the maximum amplitude found is below 1000rad/s^2 , which is known not to induce subjectively unacceptable rattle noise, although it can still induce wear.

It is possible to say that even better results were obtained using the epicycloidal path CPVA. However, its design is different from the previous two cases, and as it is going to be shown further on the text, its inertia is almost twice the inertia of the pendulums of the previous cases, what explains the even lower amplitudes.

The third and sixth order amplitudes of the swing angles of the pendulums are shown in Figs. 4.12 and 4.13. The most relevant part of the amplitude of the pendulums is found in

the 3rd order response. Yet their parameters are different, the cycloidal and the epicycloidal pendulums have nearly the same performance. Swing angles are most of the time below $\pm 30^\circ$, which is acceptable, and no peak is found, indicating few detuning.

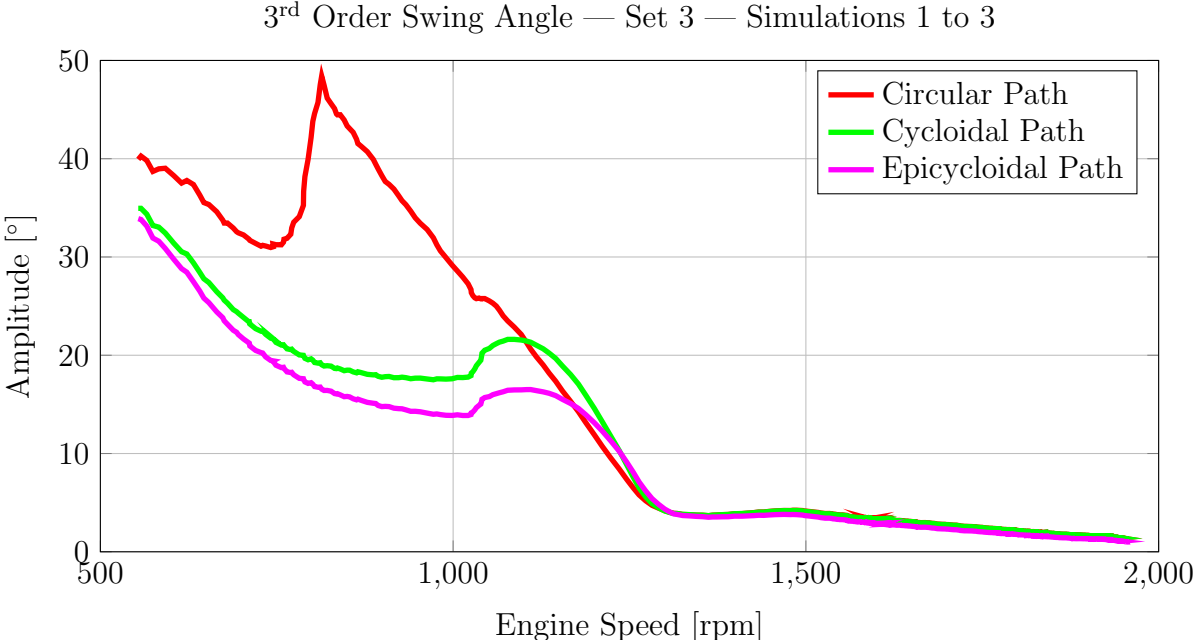


Figure 4.12: 3rd order swing angle response of the pendulums from Simulations 1 to 3 from Set 3.

The circular path pendulum has the worst behavior. It presents amplitudes above $\pm 30^\circ$ for engine speeds below 1000rpm, the most critical region. Furthermore, it presents a peak of vibration which has the same shape of the one seen in Fig. 4.11 on the response of the gearbox. The shape of this peak suggests a jump phenomenon due to a softening-like nonlinear stiffness and requires further investigation.

The results for the amplitude of vibration at the gearbox for simulations 4 to 6 from set 3 are shown in Fig. 4.14. In all cases where the CPVA has been applied, once more the peak related to gear rattle, shown in the original blue curve, vanishes. Both the cycloidal and epicycloidal path pendulums have better performance than the circular path one, but in this case no instability was found on the circular path one.

The third and sixth order amplitudes of the swing angle of both pendulums are shown in Figs. 4.15 and 4.16. In this case, once again the most relevant part of the amplitude of the swing angles is at the third order.

6th Order Swing Angle — Set 3 — Simulations 1 to 3

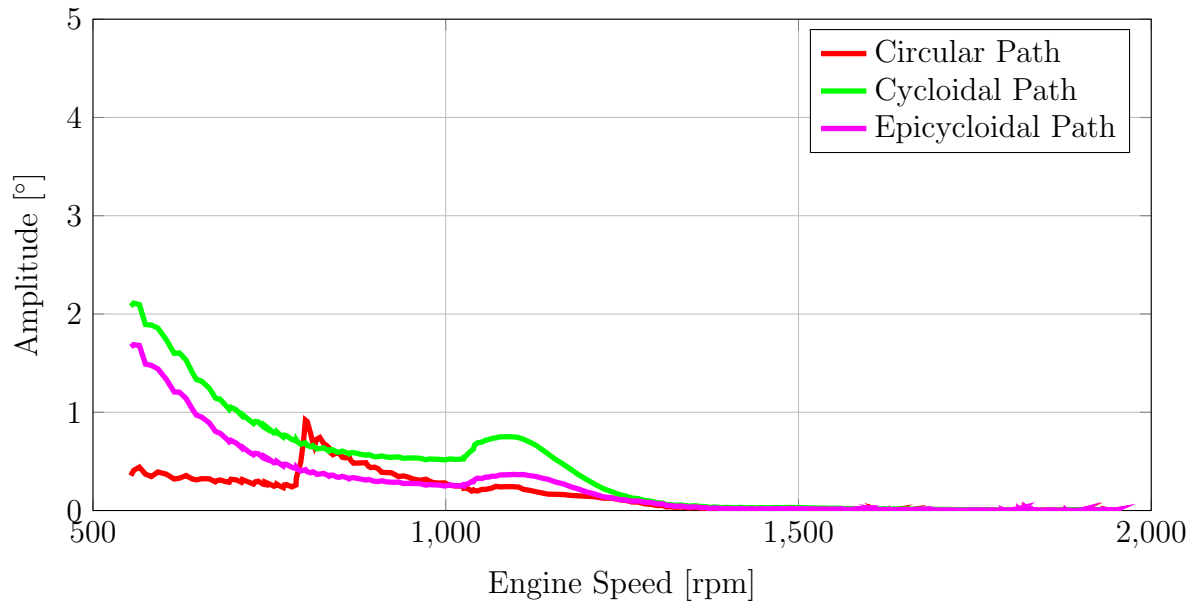


Figure 4.13: 6th order swing angle response of the pendulums from Simulations 1 to 3 from Set 3.

Angular Acceleration — Set 3 — Simulations 4 to 6

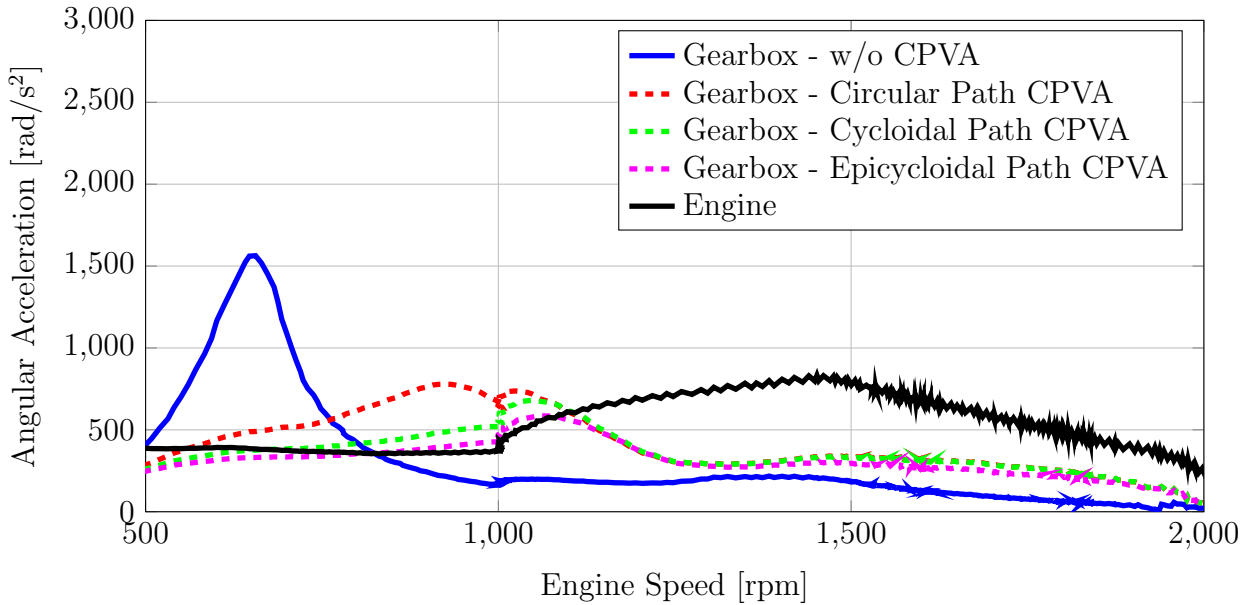


Figure 4.14: Angular acceleration from Simulations 4 to 6 from Set 3.

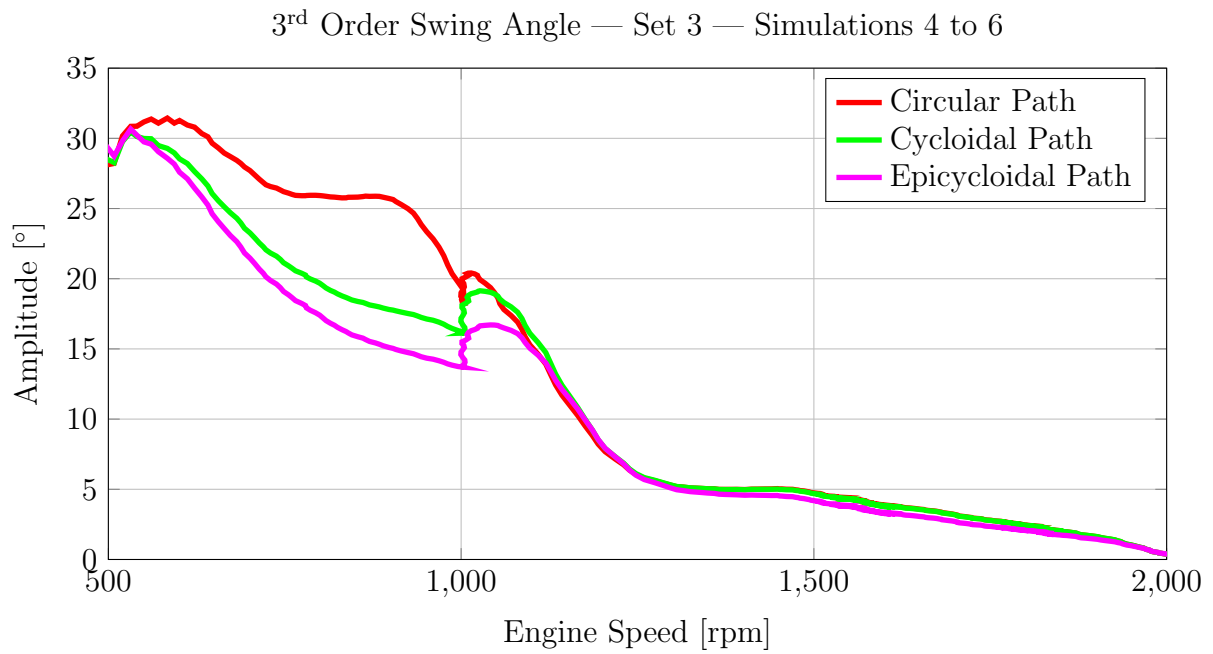


Figure 4.15: 3rd order swing angle response of the pendulums from Simulations 4 to 6 from Set 3.

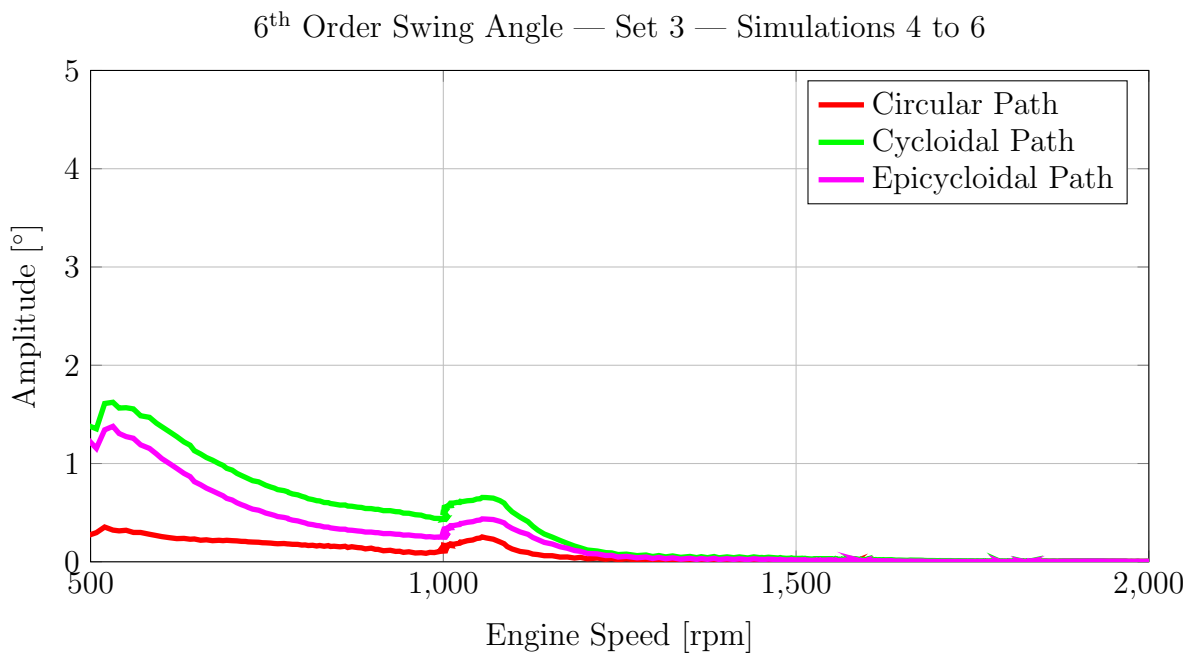


Figure 4.16: 6th order swing angle response of the pendulums from Simulations 4 to 6 from Set 3.

Unlike the previous case, in this case the circular path pendulum did not become unstable, and therefore its performance is worse but close to the one of the cycloidal and the epicycloidal pendulums. The swing angle of both pendulums remained below $\pm 30^\circ$ most of the time.

In all six simulations from Set 3, the design parameters of the circular and cycloidal path pendulums are the same. Different parameters are chosen for the epicycloidal path pendulum because its design technique is different from the one used on the other cases. All the design and physical parameters can be found in Tables 4.3 and 4.4.

Table 4.3: Design and physical parameters for simulations 1 to 3 from Set 3.

Simulation	1	2	3
δ	0.5	0.5	0.5
B_w	0.5	0.5	0.5
$R_p[mm]$	71.88	71.88	71.88
b	40000.0	40000.0	4.1
a	1.3504	1.3504	1.5001
$\mu[\%]$	0.40	0.40	0.40
$I_a[kg.m^2]$	$4.186.10^{-8}$	$4.186.10^{-8}$	$4.536.10^{-4}$
$m_a[kg]$	18.532	18.532	27.228
$\epsilon_a[mm]$	9.74	9.74	6.90
$\varrho_{\max}[mm]$	1.76	1.76	2.90
$m_{\text{bif}}[kg]$	18.533	18.533	36.011

Table 4.4: Design and physical parameters for simulations 4 to 6 from Set 3.

Simulation	4	5	6
δ	0.5	0.5	0.5
B_w	0.5	0.5	0.5
$R_p[mm]$	71.88	71.88	71.88
b	40000.0	40000.0	4.1
a	1.3504	1.3504	1.5001
$\mu[\%]$	0.40	0.40	0.40
$I_a[kg.m^2]$	$4.013.10^{-8}$	$4.013.10^{-8}$	$4.349.10^{-4}$
$m_a[kg]$	17.768	17.768	26.105
$\epsilon_a[mm]$	9.74	9.74	6.90
$\varrho_{\max}[mm]$	1.76	1.76	2.90
$m_{\text{bif}}[kg]$	17.769	17.769	34.526

In all cases, the parameters δ and B_w are fixed and R_p is a design limitation, also constant for all cases. The parameter b is chosen for simulations 1, 2, 4 and 5, because in

these cases the design for geometry is used. The higher this parameter, the closer the ideal pendulum is to a particle mass attached to a massless rod. On simulations 3 and 6, the value of b is defined by the no detuning constraint.

All the other parameters are a result from the values of the first four ones. Because μ depends on the choice of the target order n_t (which is obviously 3 in this case), B_w and δ , this parameter is constant for all cases.

The parameter a indicates how much the inertia of the gearbox is increased by the use of CPVAs. For circular and cycloidal paths it is increased on nearly 35%, while for simulations 3 and 6 it is increased on almost 50%.

The parameters I_a and m_a refer to the parameters of an ideal pendulum. However, ϵ_a is the radius of the ideal and of the real pendulum. In both cases, it reached acceptable values. Also, the parameter ϱ_{\max} indicates the manufacturing and wear tolerance for those radii. In all cases the tolerances are very loose, which eases manufacturing and allows for good performance in the presence of wear.

Finally, the parameter m_{bif} is the mass of the bifilar pendulum bob resulting from this project. In both cases, these masses have elevated values, and the design for tuning, used on simulations 3 and 6 provided a mass which is nearly twice the mass for the other cases. The increased value for the pendulum mass is due to the fact that the radius R_p is too small for this application.

On Tables 4.5 and 4.6, the same parameters are recalculated for $R_p = 200\text{mm}$. As R_p is increased, ϵ_a and ϱ_{\max} also increase, but still remain in acceptable values. The mass of the pendulum bob m_{bif} decreases considerably, indicating that, with proper values for R_p , this solution may be suitable. The parameter a , however remains unaltered for all simulations, showing that, yet the mass of the pendulum bob has decreased, its increase on the inertia of the gearbox does not depend on R_p . The parameter a is an important parameter for the design of the synchronizers.

These are the results obtained from the simulations performed in this work. On the next chapter the conclusions of the present thesis, contributions and perspectives for future research are presented.

Table 4.5: Recalculated design and physical parameters for simulations 1 to 3 from Set 3.

Simulation	1	2	3
δ	0.5	0.5	0.5
B_w	0.5	0.5	0.5
$R_p[mm]$	200.00	200.00	200.00
b	40000.0	40000.0	4.1
a	1.3504	1.3504	1.5001
$\mu[\%]$	0.40	0.40	0.40
$I_a[kg.m^2]$	$4.186.10^{-8}$	$4.186.10^{-8}$	$4.536.10^{-4}$
$m_a[kg]$	2.394	2.394	3.517
$\epsilon_a[mm]$	27.11	27.11	19.19
$\varrho_{\max}[mm]$	4.89	4.89	8.08
$m_{\text{bif}}[kg]$	2.394	2.394	4.651

Table 4.6: Recalculated design and physical parameters for simulations 4 to 6 from Set 3.

Simulation	4	5	6
δ	0.5	0.5	0.5
B_w	0.5	0.5	0.5
$R_p[mm]$	200.00	200.00	200.00
b	40000.0	40000.0	4.1
a	1.3504	1.3504	1.5001
$\mu[\%]$	0.40	0.40	0.40
$I_a[kg.m^2]$	$4.013.10^{-8}$	$4.013.10^{-8}$	$4.349.10^{-4}$
$m_a[kg]$	2.295	2.295	3.372
$\epsilon_a[mm]$	27.11	27.11	19.19
$\varrho_{\max}[mm]$	4.89	4.89	8.08
$m_{\text{bif}}[kg]$	2.295	2.295	4.460

5 Conclusion

At this point, all the relevant methods, analyses and results have already been presented. Therefore, the goal of this chapter is to present the conclusions of this work, as well as the contributions and innovations and perspectives for future research.

5.1 Discussion and Conclusions

At the first chapter, an introduction of the main NVH phenomena related to powertrain dynamics and also an introduction to the history and the basic features of CPVAs is presented. One of the most important facts presented in this chapter is that CPVAs are one of the most effective solutions for mitigation of torsional vibration. Besides, its usage on vehicle powertrains has only been discontinued due to its cost.

It is true that its usage in the late 1940s had the objective of eliminating crankshaft vibration, and was not related to rattle noise. However, the latter has become a very important issue, and this solution was rarely applied for the reduction of rattle noise for historical reasons. Other solutions such as the dual mass flywheel have been developed, but have shown to be very expensive, and its usage is limited to critical or high budget applications.

Centrifugal pendulums have shown to be very effective, and the simplicity of its conception suggests a potentially cheaper solution, when compared to the complexity of dual-mass flywheels. However, the cost analysis must not be focused on a single solution, mainly due to the results shown in chapter 3.

On the third chapter of this work, a very deep analysis of the dynamic characteristics of the CPVA is presented. One of the most important features of this solution is that it creates a zone at which few or no natural frequencies are present. This eliminates undesirable amplifications that occur at some critical speeds, which lead to rattle noise. On the results shown in chapter 4, it is very clear that the result of the application of well tuned CPVAs with the correct paths is the complete mitigation of vibration peaks at the gearbox that led

to gear rattle.

Once amplification regions are no longer present, it is no longer necessary to produce clutch disks with torsional friction. Furthermore, there are many parameters on the design of the gearbox such as placement of bearings, gear lashes and shape, tolerances, and others, which are designed for the reduction of noise intensity when teeth impacts occur. Once resonances that affect the gearbox are no longer present, these parameters can be relaxed, leading to possible reduction of the cost of the gearbox.

The point of the powertrain at which the CPVA is installed is also of great importance. Regarding the gearbox, the pendulums could be installed on the input shaft or on any secondary shaft. Installing the pendulum at the input shaft lead to an important advantage and an important drawback.

The advantage is that after the coupling of the clutch set, the input shaft has the same rotating speed as the engine. This means that the order of excitation, related to the firing frequency, is constant regardless of the shifted gear, and hence the pendulum must be designed for a single order. On the other hand, the working principle of the gearbox requires the inertia of the input shaft to be as low as possible, in order to improve service life of the synchronizers and shiftability, i.e., to reduce the effort the driver needs to make to shift a given gear. The use of CPVAs on the input shaft would increase this inertia.

In contrast, the CPVAs could be installed on the output shaft of the gearbox. This would lead to no increase of the inertia of the input shaft. However, because of the different gear ratios available at the gearbox, the order of excitation on the output shaft varies and the design of the CPVAs may become very difficult.

Another possibility would be to install the CPVAs on the engine flywheel. It allows for a greater distance between the pendulum and the geometric center of the rotor, which is good. However, as the inertia of the flywheel is large, the inertia of the pendulums would have to be high, which is undesirable. A possibility that must be studied is the reduction of the inertia of the flywheel parallel to the use of CPVAs on it. It would be the same of exchanging a simple inertia by an dynamically active one.

There is still a fourth possibility mentioned in the work of Wilson (1941), which is to replace the crankshaft counterweights by CPVAs. It would potentially eliminate the need for

viscous dampers on engines, allow for reduction of the inertia of the flywheel, eliminate the need for torsional friction at the clutch disk and possibly allow for a cheaper gearbox design.

An important fact on this discussion is that car manufacturers usually buy different parts, like engines, gearboxes and clutch sets, from different companies, and lots of politics and negotiation are involved on the decision of the point at which the CPVAs must be installed. However, this discussion is kept into the academic scope.

On chapter 3, linear and nonlinear analyses are performed on systems with one and two rotors and centrifugal pendulums. On the linear analyses, once small displacements are an assumption, it is possible to verify the existence of the No-Resonance Zone or the Resonance Suppression Zone. Its parameters are verified to be independent from all the system parameters, except for the inertia of the disk at which it is installed.

Nonlinear analyses performed on the same chapter were able to show that, if the rotating speed of the system is not excessively low and the amplitude of the pendulum is kept low, then the project of the pendulum can be based on the existence of such zone. However, the path of the pendulum plays an important role on the tuning of its parameters, and the cycloidal and epicycloidal paths have shown to reduce the effect of detuning and hence to be more effective than the circular one.

On chapter 4, two design techniques for centrifugal pendulums are presented. One of them allows for the choice of the pendulum geometry, while the second allows for the elimination of a given detuning term. Also, a prototype of a clutch disk with CPVAs is presented.

From simulation results it was possible to verify that, if the design constrains are obeyed, then the maximum permissible inertia of the pendulum, which is very low for this application, makes this solution unsuitable for this case, once no improvements on the amplitude of vibration of the gearbox are found. Low inertia of the pendulum bobs led to high amplitude of vibration and consequently detuning, which annihilated the performance of the CPVA.

If the inertia of the pendulums is increased, then the amplitude of the swing angles are lowered and all paths can be tested. The design for the circular and cycloidal paths is exactly the same, while the design for the epicycloidal path took detuning into consideration.

In all the results, it is clear that pendulums with cycloidal paths are less prone to detuning, and their performance for high amplitudes is definitely much superior to the pendulums with circular paths. The lowest amplitude of vibration of the gearbox was obtained using the pendulum with epicycloidal path. However, its design led to a pendulum which has twice as much inertia as the cycloidal path one, and the reduction of amplitude of vibration of the gearbox is not as significant. Therefore, either the cycloidal or epicycloidal paths are better choices than the circular paths.

It is very clear that a pendulum bob of nearly $18kg$ is impracticable for this application. The high value of its mass is simply due to the fact that the maximum radius at which the pendulum can be pinned on the disk is still too small. If it is raised to $0,2m$, then the inertia of the pendulum bob required to obtain exactly the same result drops to $2,4kg$, which is much more realistic. Additionally, the advantage of the designs proposed in this work is that, as predicted by Wilson (1941), the manufacturing tolerances are very loose even when such radius is low, and apart from cheaper manufacturing, it results in good performance even in the presence of wear.

Consequently, taking into account the prototype layout available, the use of CPVAs for the reduction of gear rattle is unsuitable for this application. However, it may be suitable if a new layout of clutch disk is proposed, allowing the radius of installation of the pendulum to be greater. Also, the use of non-circular paths is reinforced.

Regarding the objectives of this work, the five stated goals have been achieved successfully, and the execution of this work led directly to experience and knowledge gain for all the parts involved.

5.2 Contributions

Due to the nature of this work and its organization, the contributions are grouped in chapters 3 and 4. The most relevant contributions and their motivation are described in the following.

The literature on centrifugal pendulums is composed of works that date from the beginning of the twentieth century up to works from the current days. Therefore, it is possible

to find many different theoretical and experimental studies on these devices. However, as in any research field, it was possible to find some problems that this thesis tries to address.

The first one is related to the choice of the degrees of freedom used to describe the motion of the pendulum. On the most current works, almost all published on the present century, the coordinate used to describe the motion of the pendulum bob is the arc-length traveled by the center of mass of the pendulum bob. Based on this choice, the equations of motion of the system can be written in a more convenient form. The convenience of this form is due to the fact that, through varying a single parameter, the equation is able to represent a pendulum with circular, cycloidal or epicycloidal path. Furthermore, the final form of the equations of motion makes them suitable for the application of the Krylov-Bogoliubov Method of Averaging (KB-Averaging), a method for the calculation of approximate responses of a nonlinear system.

However, there are some drawbacks involved on this choice. The first and simplest one is that the arc-length provides an indirect measure of the swing angle of the pendulum bob. In fact, the calculation of the swing angle based on the arc-length traveled by the pendulum bob is simple, but is an unnecessary step to be performed.

The second one is that this approach allows for the choice of a circular, cycloidal or epicycloidal path through the variation of a single parameter. However, it does not allow for any other trajectory to be tested with the same convenience, and there is not a work on the literature that proves that optimal paths belong to this family of paths. If other types of path are to be tested, this formulation leads to mathematical inconvenience.

The third disadvantage related to the choice of this coordinate is actually about the application of the KB-Averaging. This choice is made in a way that the equations of motion are in a suitable form for the application of this method. However, this method is shown in the work of Nayfeh (1981) to lead to incomplete expansions, where frequency correction terms are absent. Furthermore, the same author affirms that this method leads to an unnecessary amount of algebra.

In order to address these issues, in this work, the coordinate chosen to describe the motion of the pendulum bob is its own swing angle. Therefore, the results from any analysis bring direct data on the angle domain, without intermediate steps.

In order to address the problem of the paths, a dimensionless shape function for each path is proposed. This shape function is described as a power series, allowing for the test of any path with no increased mathematical complexity. Furthermore, these shape functions are application-independent, i.e., once calculated, they are valid for any application.

With this proposal, another mathematical difficulty had to be addressed. The cycloidal and epicycloidal paths are described in terms of an angle which is not the swing angle of the pendulum. There is a function that describes the swing angle in terms of the secondary angle, but it is not invertible, which increases the difficulty to calculate the desired power series.

This obstacle has been overcome by the use of implicit differentiation, which allowed for the calculation of the power series directly in terms of the swing angle, without the need for inverting a non invertible function. The coefficients of the shape functions for the circular, cycloidal and epicycloidal paths are shown to be rational, therefore, with infinite precision.

The third issue has been overcome by the choice of the Method of Multiple Scales, instead of the KB-Averaging. It is a more precise method, generates less algebra and has the advantage of not requiring the equations of motion to be in any specific form. Furthermore, the use of this method, not used in the literature on centrifugal pendulums, led to a set of linear differential equations to be solved, which were of the same form of the equations analyzed on the linear analysis of this work, what made the calculations much more direct.

Another subject which has not been explored in the literature is the presence of gravity on horizontal rotors with CPVAs. This subject is studied in this work, and depends on the linearity assumption it may lead to a linear time-varying system or a nonlinear autonomous one.

The linear time varying cases can be studied using the Floquet Theory, which addresses linear time varying systems with periodic coefficients. The case at which the rotor spins at constant speed, after convenient adimensionalization leads to the Mathieu equation, which has been exhaustively studied. The two degrees of freedom case can also be studied using the Floquet Theory. In both cases, it was shown that stability is achieved if the angular speed of the rotor is above a certain limit.

The nonlinear autonomous case could be studied using the Method of Multiple Scales.

The results show that the presence of gravity may lead to sub or super harmonic secondary resonances, which tend to be less influent as the rotating speed of the system increases.

Finally, the last contribution of this work are the two design techniques proposed for the project of CPVAs. One of them is suitable for circular, cycloidal or epicycloidal paths, and allows for the choice of different geometries for the pendulum bob. The second one is designed exclusively for the epicycloidal path, and aims to vanish the detuning term found on the third order approximation of the nonlinear response of the system.

5.3 Future Research

Although there are significant contributions in this work, there are still many subjects related to powertrains and CPVAs that deserve special attention. The most relevant ones are listed below:

- **Improve the modeling of the powertrain.** Although a representative model was obtained in this work, some imperfections led to imprecision, mainly on the placement of the peak related to gear rattle. Therefore the modeling of the powertrain must be improved. Special attention must be given to the model of damping, which is fundamental on the representativeness of the model.
- **Calculate higher approximations for nonlinear response.** The Method of Multiple Scales was applied in this work and good results were obtained. However, most analyses were truncated at the second or third order. Higher order terms should be calculated to increase accuracy of the approximations.
- **Try other paths.** One of the main advantages of the formulation shown in this work is that paths which are not circular, cycloidal or epicycloidal can be tested with no increased difficulty. Therefore, further paths should be tested. Furthermore, optimization algorithms can be applied to calculate the coefficients of the shape function of a supposedly unknown optimal path.
- **Apply CPVA on other points of the powertrain.** It is known that it is possible to apply the CPVA on the engine flywheel, for example, exchanging simple inertia by

dynamically active inertia. Further studies should be performed to assess the suitability of this solution.

- **Propose and build suitable prototypes.** The prototype proposed in this work is shown not to be suitable for this application due to project limitations. However, once the CPVAs are an effective and potentially low cost solution, different prototypes should be proposed, allowing for the application of this technology on vehicles.

References

- ALSUWAYIAN, A.S. and SHAW, S.W. Performance and dynamic stability of general-path centrifugal pendulum vibration absorbers. **Journal of Sound and Vibration**, 2002.
- ALSUWAYIAN, A.S. and SHAW, S.W. Steady state responses in systems of nearly-identical torsional vibration absorbers. **ASME Journal of Vibration and Acoustics**, 2003.
- BRAMWELL, A.; DONE, G.; DONE, G. and BALMFORD, D. **Bramwell's Helicopter Dynamics**. Referex Engineering. American Institute of Aeronautics and Astronautics, 2001. ISBN 9780750650755.
- CHAO, C.P.; LEE, C.T. and SHAW, S.W. Non-unison dynamics of multiple centrifugal pendulum vibration absorbers. **Journal of Sound and Vibration**, 1997.
- CHAO, C.P. and SHAW, S.W. The dynamic response of multiple pairs of subharmonic torsional vibration absorbers. **Journal of Sound and Vibration**, 2000.
- DENMAN, H.H. Tautochronic bifilar pendulum torsion absorbers for reciprocating engines. **Journal of Sound and Vibration**, 1992.
- DORMAND, J.R. and PRINCE, P.J. A family of embedded runge-kutta formulae. **Journal of Computational and Applied Mathematics**, v. 6, 1980.
- DREXL, H.J. **Motor Vehicle Clutches**. Verlag Moderne Industrie, 1999.
- DUQUE, E.L.; LEMES, D.V.; GALVANI, S.A. and NIGRO, F.E.B. Analyzing the torsional vibration of engines in dynamometer previewing the impacts in clutch disc calibration. **SAE Technical Paper 2004-01-3247**, 2004.
- GOZEN, S.; OLSON, B.J.; SHAW, S.W. and PIERRE, C. Resonance suppression in multi-degree-of-freedom rotating flexible structures using order-tuned absorbers. **Journal of Vibration and Acoustics**, v. 134, December 2012.
- HADDOW, A.G. and SHAW, S.W. Centrifugal pendulum vibration absorbers: An experimental and theoretical investigation. **Nonlinear Dynamics**, 2003.

- HAUPT, O. Über lineare homogene differentialgleichungen 2. ordnung mit periodischen koeffizienten. **Math Ann. Bd.**, v. 79, February 1918.
- HILL, G.W. On the part of the motion of lunar perigee which is a function of the mean motions of the sun and moon. **Acta mathematica**, v. 8, February 1886.
- LEE, C.T. and SHAW, S.W. The non-linear dynamic response of paired centrifugal pendulum vibration absorbers. **Journal of Sound and Vibration**, 1997.
- LEMES, D V. **Commercial Vehicle Powertrain - Control of the torsional vibration amplitudes via damping of the clutch disc torsional dampers (Unpublished)**. 2015 *planned*. Master's Thesis. University of Campinas.
- LIGIER, J.; BARON, É. and FRANÇAIS DU PÉTROLE, I. **Acyclisme et vibrations: Dépouillement**. Acyclisme et vibrations: applications aux moteurs thermiques et aux transmissions. Technip, 2002. ISBN 9782710808176.
- MIYASATO, H H. **Simulação do fenômeno de gear rattle em modelos de trem de potência automotivos**. 2011. Master's Thesis. University of Campinas.
- MIYASATO, H H. **Modeling of the Clutch Squeal Phenomenon and Practical Possibilities for its Mitigation**. 2015. Doctorate Thesis. University of Campinas.
- MIYASATO, H.H.; SIMIONATTO, V.G.S. and DIAS JR., M. Numerical investigation on the nonlinear behaviour of powertrain systems: Focus on clutch modifications. In **10^a Conferência Brasileira de Dinâmica, Controle e Aplicações**. 2011a.
- MIYASATO, H.H.; SIMIONATTO, V.G.S. and DIAS JR., M. Study of the gear rattle phenomena in automotive powertrain systems. In **Proceedings of the 21st International congress of Mechanical Engineering**. 2011b.
- MIYASATO, H.H.; SIMIONATTO, V.G.S. and DIAS JR., M. Linear powertrain models for nvh phenomena evaluation. In **Proceedings of the XV International Symposium on Dynamic Problems of Mechanics**. 2013.
- NAYFEH, A. **Introduction to perturbation techniques**. Wiley classics library. Wiley, 1981. ISBN 9780471080336.
- NESTER, T.M.; HADDOW, A.G.; SHAW, S.W.; BREVICK, J.E. and BOROWSKI, V.J. Vibration reduction in a variable displacement engine using pendulum absorbers. **SAE Technical Paper 2003-01-1484**, 2003.

- NESTER, T.M.; SCHMITZ, P.M.; HADDOW, A.G. and SHAW, S.W. Experimental observations of centrifugal pendulum vibration absorbers. In **The 10th International Symposium on Transport Phenomena and Dynamics of Rotating Machinery**. 2004.
- OLSON, B.J. and SHAW, S.W. Vibration absorbers for cyclic rotating flexible structures: linear and nonlinear tuning. In **ASME Conference on Smart Materials, Adaptive Structures and Intelligent Systems**. 2008.
- OLSON, B.J. and SHAW, S.W. Vibration absorbers for a rotating flexible structure with cyclic symmetry: nonlinear path design. **Nonlinear Dynamics**, v. 60, September 2009.
- OLSON, B.J.; SHAW, S.W. and PIERRE, C. Order-tuned vibration absorbers for cyclic rotating flexible structures. In **ASME 2005 International Design Engineering Technical Conferences and Computers and Information in Engineering Conference**. 2005.
- PERESTRELO, L T R. **Modelagem do trem de potência automotivo para estudo de trepidação (Judder)**. 2013. Master's Thesis. University of Campinas.
- RUSCH, A.; LEHMANN, S. and HEPPELLE, W. Centrifugal pendulum and clutch disc having the latter. July 3 2014. US Patent App. 14/200,627.
- SEAMAN, R.L.; JOHNSON, C.E. and HAMILTON, R.F. Component inertial effects on transmission design. **SAE Technical Paper 841686**, 1984.
- SHAW, S.W.; ACAR, M.A.; FEENY, B.F. and GEIST, B.K. **Modal Properties of Rotating Shafts with Order-Tuned Absorbers**. 2014.
- SIMIONATTO, V. G. S. **Estudo dos fenômenos de Shuffle e Clunk em trens de potência automotivos**. 2011. Master's Thesis. University of Campinas.
- SIMIONATTO, V.G.S.; MIYASATO, H.H. and DIAS JR., M. Insights on centrifugal pendulum vibration absorber part one: Dynamic modeling and behaviour of eigenvalues and eigenvectors along rotating speed. In **Proceedings of the ASME 2013 International Mechanical Engineering Congress and Exposition**. 2013.
- SLANE, J. and TRAGESSER, S. Analysis of periodic nonautonomous inhomogeneous systems. **Nonlinear Dynamics and Systems Theory**, v. 2, March 2011.
- STEINEL, K. Clutch tuning to optimize noise and vibration behavior in trucks and buses. In **IX Congresso e Exposição Internacionais da Tecnologia da Mobilidade**. 2000.

STOKER, J.J. **Nonlinear Vibrations in Mechanical and Electrical Systems.** New York: Interdiscience Publisher, 1950.

WEDIN, A. **Reduction of Vibrations in Engines using Centrifugal Pendulum Vibration Absorbers.** 2011. Master's Thesis. Chalmers University of Technology.

WILSON, W. **Practical Solution of Torsional Vibration Problems: Vibration measurement and analysis.** N. v. IV in Practical solution of torsial vibration problems. Chapman & Hall, 1969.

WILSON, W.K. **Practical Solutions of Torsional Vibration Problems.** John Wiley and Sons Inc., 1941.

Appendix A -Auxiliary information from the powertrain

Extra information about the powertrain of the vehicle under investigation is shown in this appendix.

A.1 Powerflow Diagram of the ZF 16AS 2631 TO Gearbox

The powerflow diagram of the gearbox used on the vehicle was obtained from its maintenance manual, and is shown in Fig. A.1.

A.2 Energy Equivalence Approach for powertrain modeling

The goal of this appendix is to introduce the Energy Equivalence Approach, shown in the work of Ligier *et al.* (2002).

The main objective of this method is to represent a system with gearings such as the one shown in Fig. A.2, namely “system A”, using the equations of motion of a simpler system, such as the one shown in Fig. A.3, namely “system B”. The main advantage is that the equations of motion of system “B” are considered easier to derive.

As indicated in Fig. A.2, system “A” has six rotors with inertias I_1 to I_6 respectively. Bodies 1 and 2, 3 and 4, and 5 and 6 are linked to each other through the springs K_{12} , K_{34} and K_{56} respectively. Inertias 2 and 3, and 4 and 5 are constrained to each other with the condition that there is no slipping between the surfaces of the disks (they act like gearings), therefore, four degrees of freedom are enough to describe the dynamics of such system. The gear ratios are called n_{23} and n_{45} , defined as following:

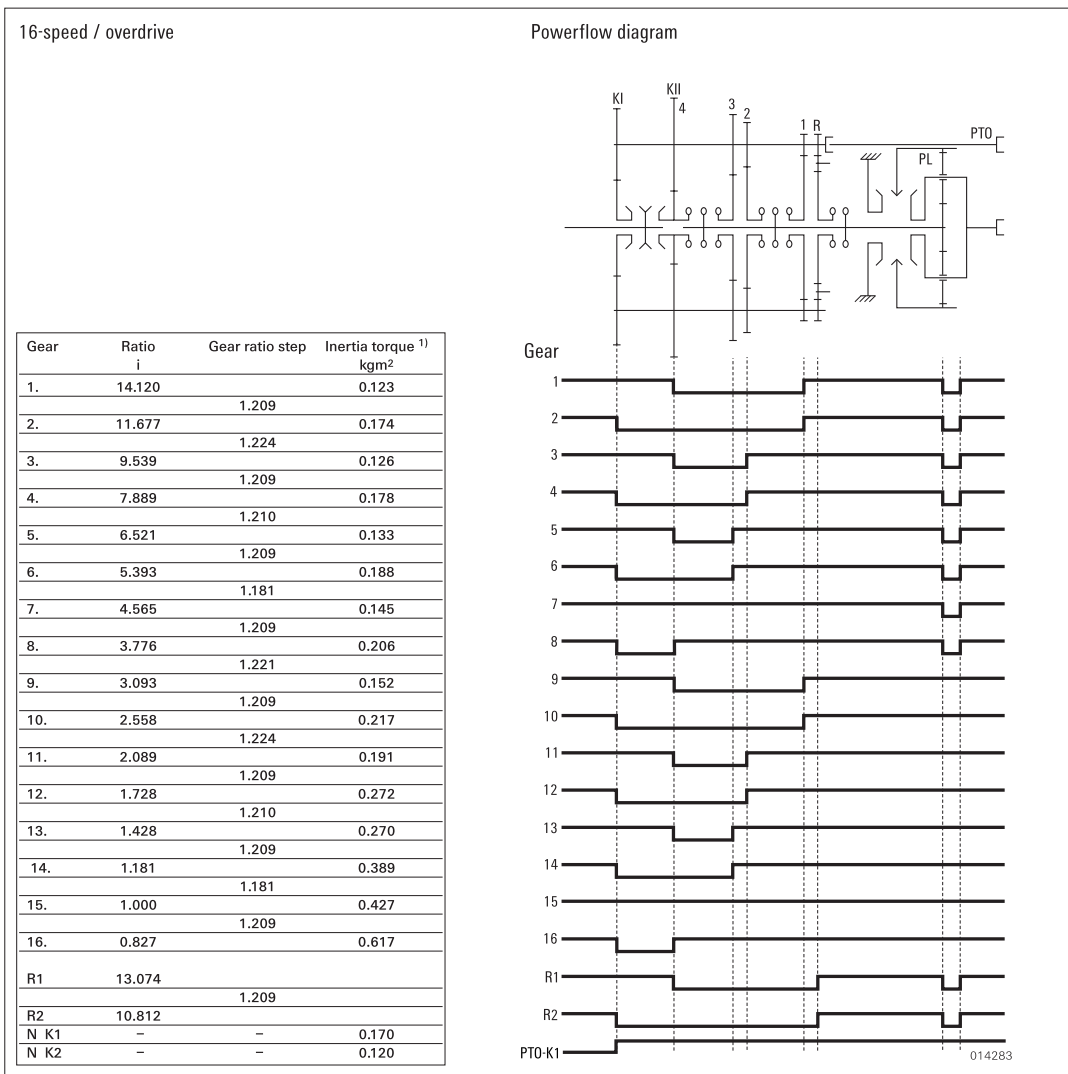
$$n_{23} = -\dot{\theta}_2/\dot{\theta}_3 \tag{A.1}$$

**2.2.11 Trucks Product Family 3:
Technical Data 16-Speed / Overdrive**

Number of forward gears:	16
Number of reverse gears:	2
Length in mm:	953
Ratio range:	Forwards 14.12 - 0.83
	Reverse 13.07 - 10.81

max. input torque (traction/coasting)*:	2 600 Nm
Input speed:	max. 2 500 rpm (traction) max. 2 800 rpm (coasting)
Output speed:	max. 3 200 rpm (coasting)
Oil volume (in liters):	approx. 13
Weight:	252 kg**
<i>Center of gravity: Refer to install. drawing (Sec. 4.1.1)</i>	

* Approximate value: Depends on type of vehicle and vehicle data as well as the prevailing operating conditions.
 ** Without peripherals, oil fill, PTOs, Intarder, clutch, release fork, release shaft, release bearing, push rod, and clutch actuator.
 Weight: Release fork, release shaft, release bearing, push rod, and clutch actuator approx. 10 kg.



1) Values relate to input end.

Figure A.1: Powerflow diagram of ZF 16AS 2631 TO Gearbox

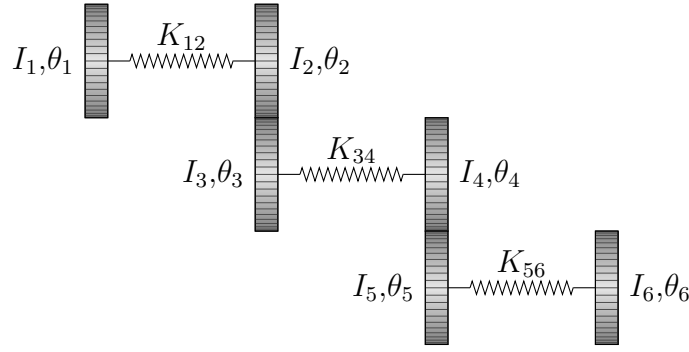


Figure A.2: Example of system to be simplified (System A).

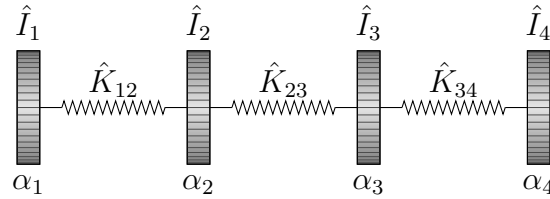


Figure A.3: Simplification of torsional system (System B).

$$n_{45} = -\dot{\theta}_4/\dot{\theta}_5 \quad (\text{A.2})$$

Hence, in Fig. A.3 there is a simplified version of system “A”, also with four degrees of freedom, but with equivalent inertias, \hat{I}_1 to \hat{I}_4 , and equivalent springs \hat{K}_{12} , \hat{K}_{23} and \hat{K}_{34} .

In system “A”, the displacements of the inertias 1 to 6 are named θ_1 to θ_6 , while in system “B”, the displacements of the bodies 1 to 4 are called α_1 to α_4 . As both systems behave statically differently, there is a relationship between the degrees of freedom α_i and θ_j . In this case, the primary shaft of the gearbox is taken as reference (bodies 1 and 2 of system “A”). Hence, if a displacement α_i represents a degree of freedom θ_j that is not on the primary shaft, it must be converted, using the appropriate gear ratios, to the equivalent displacement of the primary shaft.

Considering this, and the fact that the displacements α_1 , α_2 , α_3 and α_4 represent the degrees of freedom θ_1 , θ_2 , θ_4 and θ_6 , the relationships between them are:

$$\alpha_1 = \theta_1 \quad (\text{A.3})$$

$$\alpha_2 = \theta_2 \quad (\text{A.4})$$

$$\alpha_3 = \theta_4 n_{23} \quad (\text{A.5})$$

$$\alpha_4 = \theta_6 n_{23} n_{45} \quad (\text{A.6})$$

Given the relationships, the first step is to calculate the equivalent inertias, and this is done by identically equating the kinetic energies $E_A^{(k)}$ and $E_B^{(k)}$ of the systems ‘‘A’’ and ‘‘B’’ respectively. The expression for $E_A^{(k)}$ is:

$$E_A^{(k)} = \frac{1}{2} \sum_{i=1}^6 I_i \dot{\theta}_i^2 \quad (\text{A.7})$$

Applying the gearing constraints, this equation becomes:

$$E_A^{(k)} = \frac{1}{2} \left[I_1 \dot{\theta}_1^2 + \left(I_2 + \frac{I_3}{n_{23}^2} \right) \dot{\theta}_2^2 + \left(I_4 + \frac{I_5}{n_{45}^2} \right) \dot{\theta}_4^2 + I_6 \dot{\theta}_6^2 \right] \quad (\text{A.8})$$

On the other hand, the expression for the total kinetic energy of system ‘‘B’’ is:

$$E_B^{(k)} = \frac{1}{2} \sum_{i=1}^4 \hat{I}_i \dot{\alpha}_i^2 \quad (\text{A.9})$$

Replacing Eqs. from (A.3) to (A.6) on Eq. (A.9), it becomes:

$$E_B^{(k)} = \frac{1}{2} \left[\hat{I}_1 \dot{\theta}_1^2 + \hat{I}_2 \dot{\theta}_2^2 + \hat{I}_3 n_{23}^2 \dot{\theta}_4^2 + \hat{I}_4 n_{23}^2 n_{45}^2 \dot{\theta}_6^2 \right] \quad (\text{A.10})$$

Now, given that all $\dot{\theta}_i(t)$ are functions of time, if one states that the functions $E_A^{(k)}$ and $E_B^{(k)}$ are simply equal, it would be possible to find solutions that are valid for some values of t and not for all t , which is desired. Hence, to find a valid solution for the entire time domain, it must be stated that both functions are identically equal, i.e.:

$$E_A^{(k)} \equiv E_B^{(k)} \quad (\text{A.11})$$

From this statement, it is possible to obtain:

$$\hat{I}_1 = I_1 \quad (\text{A.12})$$

$$\hat{I}_2 = I_2 + \frac{I_3}{n_{23}^2} \quad (\text{A.13})$$

$$\hat{I}_3 = \left(I_4 + \frac{I_5}{n_{45}^2} \right) \frac{1}{n_{23}^2} \quad (\text{A.14})$$

$$\hat{I}_4 = \frac{I_6}{n_{23}^2 n_{45}^2} \quad (\text{A.15})$$

The second step is to calculate the equivalent stiffnesses, which is done by identically equalling the total elastic potential energies for systems “A” and “B”, given by $E_A^{(p)}$ and $E_B^{(p)}$ respectively. The expression for $E_A^{(p)}$ is:

$$E_A^{(p)} = \frac{1}{2} \sum_{i=1}^3 K_{\langle 2i-1 \rangle \langle 2i \rangle} (\theta_{2i} - \theta_{2i-1})^2 \quad (\text{A.16})$$

After replacing Eqs. (A.1) and (A.2) on Eq. (A.16) and rearranging the terms, it follows that:

$$\begin{aligned} E_A^{(p)} = & \frac{1}{2} \left[\theta_1^2 (K_{12}) + \theta_2^2 \left(K_{12} + \frac{K_{34}}{n_{23}^2} \right) + \dots \right. \\ & \dots + \theta_4^2 \left(K_{34} + \frac{K_{56}}{n_{45}^2} \right) + \theta_6^2 (K_{56}) + \dots \\ & \dots + \theta_1 \theta_2 (-2K_{12}) + \theta_2 \theta_4 \left(-\frac{2K_{34}}{n_{23}^2} \right) + \dots \\ & \left. \dots + \theta_4 \theta_6 \left(-\frac{2K_{56}}{n_{45}^2} \right) \right] \quad (\text{A.17}) \end{aligned}$$

On the other hand, the expression for $E_B^{(p)}$ is:

$$E_B^{(p)} = \frac{1}{2} \sum_{i=1}^3 \hat{K}_{\langle i \rangle \langle i+1 \rangle} (\alpha_{i+1} - \alpha_i)^2 \quad (\text{A.18})$$

Replacing Eqs. from (A.3) to (A.6) on Eq. (A.18) and reordering terms results in:

$$\begin{aligned}
E_B^{(p)} = \frac{1}{2} & \left[\theta_1^2(\hat{K}_{12}) + \theta_2^2(\hat{K}_{12} + \hat{K}_{23}) + \dots \right. \\
& \dots + \theta_4^2(\hat{K}_{23} + \hat{K}_{34})n_{23}^2 + \theta_6^2(\hat{K}_{34}n_{23}^2n_{45}^2) + \dots \\
& \dots + \theta_1\theta_2(-2\hat{K}_{12}) + \theta_2\theta_4(-2\hat{K}_{23}n_{23}) + \dots \\
& \left. \dots + \theta_4\theta_6(-2\hat{K}_{34}n_{23}^2n_{45}^2) \right] \tag{A.19}
\end{aligned}$$

At this point, and for the same reasons as for the calculus of the inertias, it must be stated that:

$$E_A^{(p)} \equiv E_B^{(p)} \tag{A.20}$$

Finally, the equivalent values for stiffness are obtained:

$$\hat{K}_{12} = K_{12} \tag{A.21}$$

$$\hat{K}_{23} = \frac{K_{34}}{n_{23}^2} \tag{A.22}$$

$$\hat{K}_{34} = \frac{K_{56}}{n_{23}^2n_{45}^2} \tag{A.23}$$

It must be reinforced here that the equivalent values of inertia and stiffness calculated so far are valid when the system is described in the coordinates α_i . In order to obtain the matrices that describe the equivalent system in the physical coordinates θ_i , a coordinate transformation must be performed. Once it is done, it is possible to verify that, for the example given in this section, the matrices for systems A and B are identical.

On the other hand, one may choose to simply calculate the eigenvalues and eigenvectors from the system represented in the coordinates α_i , knowing that the eigenvalues are exactly the same from the original system, and the eigenvectors must undergo a coordinate transformation (given by Eqs. from (A.3) to (A.6)) in order to be equal to the ones from the original system, if necessary.

A.3 Generalized method to impose motion of known degrees of freedom on linear time invariant systems

The goal of this appendix is to show a general way to impose the motion of some known degrees of freedom on a linear time-invariant model. Let the LTI system be of the form:

$$\mathbf{M}\ddot{\mathbf{x}} + \mathbf{C}\dot{\mathbf{x}} + \mathbf{K}\mathbf{x} = \mathbf{f}(t)$$

As the time response of some of the degrees of freedom of the system are known, these time responses are grouped on an array $\mathbf{g}(t)$, while the unknown variables are grouped in \mathbf{x}_u . The matrices \mathbf{A}_k and \mathbf{A}_u are defined so that:

$$\mathbf{x} = \mathbf{A}_k\mathbf{g}(t) + \mathbf{A}_u\mathbf{x}_u$$

One must notice that, once the known degrees of freedom are going to be imposed, their part on the array $\mathbf{f}(t)$ is of no use. In order to eliminate it, it suffices to left multiply the whole equation by \mathbf{A}_u^T . After making it and replacing the terms in \mathbf{x} and its derivatives by the terms shown in the previous equation, the system becomes:

$$\bar{\mathbf{M}}\ddot{\mathbf{x}}_u + \bar{\mathbf{C}}\dot{\mathbf{x}}_u + \bar{\mathbf{K}}\mathbf{x}_u = \bar{\mathbf{f}}(t)$$

, where:

$$\begin{aligned}\bar{\mathbf{M}} &= \mathbf{A}_u^T\mathbf{M}\mathbf{A}_u \\ \bar{\mathbf{C}} &= \mathbf{A}_u^T\mathbf{C}\mathbf{A}_u \\ \bar{\mathbf{K}} &= \mathbf{A}_u^T\mathbf{K}\mathbf{A}_u\end{aligned}$$

$$\bar{\mathbf{f}}(t) = \mathbf{A}_u^T\mathbf{f}(t) - \mathbf{A}_u^T\mathbf{M}\mathbf{A}_k\ddot{\mathbf{g}}(t) - \mathbf{A}_u^T\mathbf{C}\mathbf{A}_k\dot{\mathbf{g}}(t) - \mathbf{A}_u^T\mathbf{K}\mathbf{A}_k\mathbf{g}(t)$$

The order of the system is reduced, because the known degrees of freedom are eliminated from the left-hand side, and the known array $\mathbf{g}(t)$ becomes part of the excitation array.

Appendix B -Auxiliary results for the Review on Tuned Mass Dampers

All the relevant mathematical deductions for the review on tuned mass dampers are shown in this appendix.

B.1 Proof: Radicand real and nonnegative

In this section it is necessary to show that the term inside the square root in the equation below is greater or equal to zero:

$$r_{1,2}^2 = \frac{1}{2} \left(1 + \beta^2(1 + \mu) \mp \sqrt{(1 + \beta^2(1 + \mu))^2 - 4\beta^2} \right)$$

Hence, the following inequality is to be proven:

$$(1 + \beta^2(1 + \mu))^2 \geq 4\beta^2$$

Once both sides of the inequality are squared, it leads to the analysis of two inequalities. The first inequality is:

$$1 + \beta^2(1 + \mu) \geq 2\beta$$

Reordering the terms, it is easy to verify that:

$$(\beta - 1)^2 \geq -\beta^2\mu$$

, which is always true for real values of β and real nonnegative values of μ .

The second inequality is:

$$-(1 + \beta^2(1 + \mu)) \leq -2\beta$$

, which is obviously the same as the first one, and hence the result is the same.

□

B.2 Proof: Square of dimensionless eigenfrequency is always real and positive

In this section it is necessary to show that the smallest dimensionless eigenfrequency r_1 from the expression:

$$r_{1,2}^2 = \frac{1}{2} \left(1 + \beta^2(1 + \mu) \mp \sqrt{(1 + \beta^2(1 + \mu))^2 - 4\beta^2} \right)$$

is a real nonnegative number. It will happen if and only if:

$$1 + \beta^2(1 + \mu) \geq \sqrt{(1 + \beta^2(1 + \mu))^2 - 4\beta^2}$$

, because it has already been proven that the radicand in this inequality is nonnegative.

Assuming that μ is nonnegative, it is possible to square both sides of the inequality and obtain:

$$0 \geq -4\beta^2.$$

, which is always true for real values of β , and the equality only holds if $\beta = 0$.

□

B.3 Proof: Smallest dimensionless eigenfrequency is less than or equal to β

In this section it is necessary to show that the dimensionless eigenfrequency r_1 is always less than or equal to β . In this case, it will be easier to start from the square of r_1 , which must be less than or equal to β^2 :

$$r_1^2 = \frac{1}{2} \left(1 + \beta^2(1 + \mu) - \sqrt{(1 + \beta^2(1 + \mu))^2 - 4\beta^2} \right) \leq \beta^2$$

After some rearrangements it is easy to obtain:

$$1 + \beta^2(1 + \mu) - 2\beta^2 \leq \sqrt{(1 + \beta^2(1 + \mu))^2 - 4\beta^2}$$

Squaring both sides leads to:

$$-4\beta^2(1 + \beta^2(1 + \mu)) + 4\beta^4 \leq -4\beta^2$$

And after some simplifications, the inequality reduces to:

$$\beta^2\mu \geq 0$$

, which is true for real values of β and real nonnegative values of μ , and the equality only holds if $\beta = 0$.

□

B.4 Proof: Greatest dimensionless eigenfrequency is greater than or equal to β

In this section it is necessary to show that the dimensionless eigenfrequency r_2 is always greater than or equal to β . In this case, it will be easier to start from the square of r_2 , which must be greater than or equal to β^2 :

$$r_2^2 = \frac{1}{2} \left(1 + \beta^2(1 + \mu) + \sqrt{(1 + \beta^2(1 + \mu))^2 - 4\beta^2} \right) \geq \beta^2$$

After some rearrangements it is easy to obtain:

$$1 + \beta^2(1 + \mu) - 2\beta^2 \geq -\sqrt{(1 + \beta^2(1 + \mu))^2 - 4\beta^2}$$

It has already been proven that the term on the right hand side of this inequality is real and nonpositive (the radicand is nonnegative, and the result from the square root is

multiplied by minus one). If the term on the right hand side is proven to be nonnegative, then the inequality will be confirmed.

For such term to be nonnegative, considering that β and μ are real and the latter is nonnegative, the necessary and sufficient condition is:

$$1 + \beta^2(1 + \mu) \geq 2\beta^2$$

Reordering the terms leads to:

$$(\beta - 1)^2 \geq -\beta^2\mu$$

, which is always true for the conditions stated for β and μ .

□

B.5 Proof: Asymptotic behavior of gap between dimensionless eigenfrequencies as a function of β

In this section the asymptotic behavior of the gap between the dimensionless eigenfrequencies as a function of the parameter β is demonstrated.

Firstly, the formula for such gap is given by:

$$r_2 - r_1 = \sqrt{\frac{1}{2} \left(1 + \beta^2(1 + \mu) + \sqrt{(1 + \beta^2(1 + \mu))^2 - 4\beta^2} \right)} + \dots \\ - \sqrt{\frac{1}{2} \left(1 + \beta^2(1 + \mu) - \sqrt{(1 + \beta^2(1 + \mu))^2 - 4\beta^2} \right)}$$

Differentiating this formula with respect to β would be prohibitive. Hence, before that, meaningful simplification is achieved by simply squaring both sides of this equation and then taking the square root of the result. Once it has already been shown that $r_2 > r_1$ the result

of this procedure will be a positive number as is the expression $r_2 - r_1$:

$$\begin{aligned}\sqrt{(r_2 - r_1)^2} &= |r_2 - r_1| = \\ r_2 - r_1 &= \sqrt{(\beta - 1)^2 + \beta^2\mu}\end{aligned}$$

The first derivative of this expression with respect to β is given by:

$$\frac{\partial(r_2 - r_1)}{\partial\beta} = \frac{\beta(\mu + 1) - 1}{\sqrt{(\beta - 1)^2 + \beta^2\mu}}$$

In order to verify asymptotic behavior, the limit of such derivative must tend to a constant value, which is verified below for β tending to zero and to the infinity:

$$\begin{aligned}\lim_{\beta \rightarrow 0} \frac{\partial(r_2 - r_1)}{\partial\beta} &= -1 \\ \lim_{\beta \rightarrow \infty} \frac{\partial(r_2 - r_1)}{\partial\beta} &= \sqrt{\mu + 1}\end{aligned}$$

Once both asymptotes exist and their slopes have already been calculated, the limit of the difference between the actual value of the gap and the slope of the asymptote multiplied by β must be constant and equal to the independent term on the function that describes the asymptote. Hence:

$$\begin{aligned}\lim_{\beta \rightarrow 0} (r_2 - r_1) - (-\beta) &= 1 \\ \lim_{\beta \rightarrow \infty} (r_2 - r_1) - \beta\sqrt{\mu + 1} &= \frac{1}{\sqrt{\mu + 1}}\end{aligned}$$

With these results, the following asymptotes are defined:

$$\begin{aligned}\lim_{\beta \rightarrow 0} (r_2 - r_1) &\rightarrow 1 - \beta \\ \lim_{\beta \rightarrow \infty} (r_2 - r_1) &\rightarrow \beta\sqrt{\mu + 1} + \frac{1}{\sqrt{\mu + 1}}\end{aligned}$$

Also, the minimum of this curve is reached when its derivative equals zero, i.e.:

$$\frac{\partial(r_2 - r_1)}{\partial\beta} = 0 \Leftrightarrow \beta = \frac{1}{1 + \mu} \Rightarrow r_2 - r_1 = \frac{\mu}{1 + \mu}$$

□

B.6 Proof: Asymptotic behavior of gap between dimensionless eigenfrequencies as a function of μ

In this section the asymptotic behavior of the gap between the dimensionless eigenfrequencies as a function of the parameter μ is demonstrated.

Firstly, the formula for such gap is given by:

$$r_2 - r_1 = \sqrt{\frac{1}{2} \left(1 + \beta^2(1 + \mu) + \sqrt{(1 + \beta^2(1 + \mu))^2 - 4\beta^2} \right)} + \dots \\ - \sqrt{\frac{1}{2} \left(1 + \beta^2(1 + \mu) - \sqrt{(1 + \beta^2(1 + \mu))^2 - 4\beta^2} \right)}$$

Differentiating this formula with respect to μ would be prohibitive. Hence, before that, meaningful simplification is achieved by simply squaring both sides of this equation and then taking the square root of the result. Once it has already been shown that $r_2 > r_1$ the result of this procedure will be a positive number as is the expression $r_2 - r_1$:

$$\sqrt{(r_2 - r_1)^2} = |r_2 - r_1| = \\ r_2 - r_1 = \sqrt{(\beta - 1)^2 + \beta^2\mu}$$

The first derivative of this expression with respect to μ is given by:

$$\frac{\partial(r_2 - r_1)}{\partial\mu} = \frac{\beta^2}{2\sqrt{(\beta - 1)^2 + \beta^2\mu}}$$

For small values of μ , it is possible to verify that:

$$\lim_{\mu \rightarrow 0} \frac{\partial(r_2 - r_1)}{\partial\mu} = \frac{\beta^2}{2|\beta - 1|}$$

$$\lim_{\mu \rightarrow 0} (r_2 - r_1) - \frac{\beta^2}{2|\beta - 1|} \mu = |\beta - 1|$$

And hence, the following asymptote is defined:

$$\lim_{\mu \rightarrow 0} (r_2 - r_1) \rightarrow \frac{\beta^2}{2|\beta - 1|} \mu + |\beta - 1|$$

For higher values of μ , however, the limit of the derivative of the gap with μ tending to the infinity is undefined:

$$\lim_{\mu \rightarrow \infty} \frac{\partial(r_2 - r_1)}{\partial\mu} \rightarrow \infty$$

, and hence no asymptotic behavior is verified.

□

B.7 Proof: Normalized FRF for a 1-DOF system with multiple similar TMDs

In this section, it is necessary to show the derivation of the normalized frequency response function for a system with one degree of freedom which has n similar tuned mass dampers attached to it.

The mass of the carrier structure is m_t , its stiffness is k_t , and its vertical displacement is described by the degree of freedom x_t . The mass of the p -th TMD is $m_a^{(p)} = m_a$, its stiffness is $k_a^{(p)} = k_a$ and its vertical displacement is described by the degree of freedom $x_a^{(p)}$. Furthermore, a sinusoidal force, given by $F(\omega, t)$, acting on the carrier structure is considered. Hence, the $n + 1$ equations of motion are given by:

$$\begin{cases} m_t \ddot{x}_t + k_t x_t + \sum_{p=1}^n k_a (x_t - x_a^{(p)}) = F(\omega, t) \\ m_a \ddot{x}_a^{(p)} + k_a (x_a^{(p)} - x_t) = 0 \quad , p \in \{1, \dots, n\} \end{cases}$$

The steady state response must be calculated, and therefore, in order to ease the calculations, the proposed solutions and the excitation are expressed in terms of a complex exponential function. Consequently, the following relationships are assumed:

$$x_t(t) = \Re \left[\check{x}_t e^{j\omega t} \right]; \quad x_a^{(p)}(t) = \Re \left[\check{x}_a^{(p)} e^{j\omega t} \right]; \quad F(\omega, t) = \Re \left[\check{F} e^{j\omega t} \right]$$

, where \check{x}_t , $\check{x}_a^{(p)}$ and \check{F} are complex constants.

Replacing these relations on the equation of motion for the p -th tuned mass damper leads to:

$$-m_a \omega^2 \check{x}_a^{(p)} + k_a \check{x}_a^{(p)} - k_a \check{x}_t = 0$$

, from which it is possible to isolate $\check{x}_a^{(p)}$:

$$\check{x}_a^{(p)} = \frac{k_a \check{x}_t}{k_a - m_a \omega^2}, \quad p \in \{1, \dots, n\}$$

Now, replacing the complex exponential relations on the equation of motion for the carrier structure leads to:

$$-m_t \check{x}_t \omega^2 + k_t \check{x}_t + \sum_{p=1}^n k_a (\check{x}_t - \check{x}_a^{(p)}) = \check{F}$$

But, from the other n equations it was possible to isolate the term $\check{x}_a^{(p)}$. Hence, it can be replaced in this equation, leading to:

$$-m_t \check{x}_t \omega^2 + k_t \check{x}_t + \sum_{p=1}^n k_a \left(\check{x}_t - \frac{k_a \check{x}_t}{k_a - m_a \omega^2} \right) = \check{F}$$

The argument in the summation term does not depend on the variable p , and hence the result of this operation is n times this argument. With this and some simplifications, it is possible to calculate the following ratio:

$$\frac{\check{x}_t}{\check{F}} = \frac{k_a - m_a \omega^2}{(k_t - m_t \omega^2)(k_a - m_a \omega^2) - n k_a m_a \omega^2}$$

It is now possible to calculate this ratio in terms of the dimensionless parameters:

$$\beta = \frac{\omega_a}{\omega_t}; \quad \omega_a = \sqrt{\frac{k_a}{m_a}}; \quad \omega_t = \sqrt{\frac{k_t}{m_t}}; \quad \mu = \frac{m_a}{m_t}; \quad r = \frac{\omega}{\omega_t}$$

It must be taken into account that when these dimensionless parameters are considered, specially r , a change in the time base from t to $\tau = \omega_t t$ is implicit. Hence, after some simplifications, taking the absolute value on both sides of the equation leads directly to the normalized frequency response function for the carrier structure, given by:

$$\frac{|x_t(\tau)|}{|F(r, \tau)|/k_t} = \frac{\beta^2 - r^2}{r^4 - r^2(1 + \beta^2(1 + n\mu)) + \beta^2}$$

□

B.8 Derivation: Equations of motion for a single torsional disk with a CPVA

In this section, the equations of motion for a purely torsional disk with a CPVA attached to it are shown. The free body diagram for the disk and for the pendulum are shown in Fig. B.1.

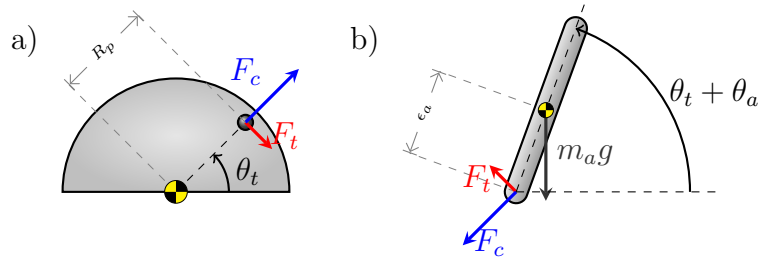


Figure B.1: Free body diagrams for disk and pendulum.

The summation of moments on the disk about its center of mass ($\sum M_t$) must be equal to its polar moment of inertia (I_t) multiplied by its absolute angular acceleration ($\ddot{\theta}_t$). Hence:

$$\sum M_t = I_t \ddot{\theta}_t = -F_t R_p$$

In order to eliminate the term F_t , which is an inner effort, from this equation, the summation of the forces on the tangential direction of the pin trajectory ($\sum F_{td}$), acting on the pendulum is calculated, and it must be equal to the product between the acceleration of its center of mass on the same direction (a_{td}) and its mass (m_a). Therefore:

$$\sum F_{tg} = m_a a_{td} = F_t - m_a g \cos \theta_t = m_a (R_p \ddot{\theta}_t + \epsilon_a (\ddot{\theta}_t + \ddot{\theta}_a) \cos \theta_a - \epsilon_a (\dot{\theta}_t^2 + \dot{\theta}_a^2) \sin \theta_a)$$

Isolating F_t in this equation and replacing it on the first one leads to the first equation of motion, which describes the dynamics of the disk:

$$(I_t + m_a R_p^2 + m_a R_p \epsilon_a \cos \theta_a) \ddot{\theta}_t + m_a R_p \epsilon_a \ddot{\theta}_a \cos \theta_a - m_a R_p \epsilon_a (\dot{\theta}_t + \dot{\theta}_a)^2 \sin \theta_a + m_a R_p g \cos \theta_t = 0$$

In order to obtain the second equation of motion, one merely has to obtain the summation of the moments acting on the pendulum about the point where it is pinned to the disk ($\sum M_p$). This summation term equals to the product between the polar moment of inertia of the pendulum bob about its center of mass (I_a) and its absolute angular acceleration ($\ddot{\theta}_a + \ddot{\theta}_t$) plus a correction term due to the fact that the summation is not obtained about its center of mass. This term is the product between the mass of the pendulum bob (m_a), the acceleration of its center of mass on its tangential direction (a_{tp}) and the distance between its center of mass and the pin (ϵ_a). Consequently:

$$\sum M_p = I_a (\ddot{\theta}_a + \ddot{\theta}_t) + m_a a_{tp} \epsilon_a = -m_a \epsilon_a g \cos(\theta_t + \theta_a)$$

, where:

$$a_{tp} = (\ddot{\theta}_t + \ddot{\theta}_a) \epsilon_a + \ddot{\theta}_t R_p \cos \theta_a + \dot{\theta}_t^2 R_p \sin \theta_a$$

Replacing this term on the previous equation leads to the second equation of motion, which describes the dynamics of the pendulum bob:

$$(I_a + m_a \epsilon_a^2) \ddot{\theta}_a + (I_a + m_a \epsilon_a^2 + m_a \epsilon_a R_p \cos \theta_a) \ddot{\theta}_t + m_a \epsilon_a R_p \dot{\theta}_t^2 \sin \theta_a + m_a \epsilon_a g \cos(\theta_t + \theta_a) = 0$$

□

B.9 A brief introduction to the Floquet theory applied to one-degree-of-freedom systems

In this section a brief introduction to the Floquet theory for one-degree-of-freedom systems is shown. It is based on the work by Stoker (1950).

The goal is to study the solutions for linear time varying equations of the following form:

$$\frac{d^2w}{dz^2} + p(z)\frac{dw}{dz} + q(z)w = 0 \quad , \quad \begin{cases} p(z) = p(z + \zeta) \\ q(z) = q(z + \zeta) \end{cases}$$

, i.e. $p(z)$ and $q(z)$ are periodic in z with period ζ .

Once it is a homogeneous differential equation of second order, it must have two linearly independent solutions w_1 and w_2 , and the final solution must be a linear combination of them, whose coefficients are to be determined by the initial values for z . The couple (w_1, w_2) is called the fundamental solution set.

If the set of solutions (w_1, w_2) is a fundamental set, then the wronskian:

$$\Delta(z) = \begin{vmatrix} w_1 & w_2 \\ \frac{dw_1}{dz} & \frac{dw_2}{dz} \end{vmatrix} := \begin{vmatrix} w_1 & w_2 \\ w_1' & w_2' \end{vmatrix} \neq 0$$

, must not identically vanish. If it did, then the pair (w_1, w_2) would not be linearly independent, and hence not a fundamental set of solutions.

As a consequence of the periodicity of $p(z)$ and $q(z)$, if $(w_1(z), w_2(z))$ is a fundamental set, then $(w_1(z + \zeta), w_2(z + \zeta))$ also is. This does not imply, however, that w_1 and/or w_2 are periodic.

As any solution can be written as a linear combination of $w_1(z)$ and $w_2(z)$, so can the solutions $w_1(z + \zeta)$ and $w_2(z + \zeta)$, and consequently:

$$\begin{bmatrix} a_{11} & a_{12} \\ a_{21} & a_{22} \end{bmatrix} \begin{Bmatrix} w_1(z) \\ w_2(z) \end{Bmatrix} = \begin{Bmatrix} w_1(z + \zeta) \\ w_2(z + \zeta) \end{Bmatrix}$$

, where:

$$\det([a_{ij}]) = \begin{vmatrix} a_{11} & a_{12} \\ a_{21} & a_{22} \end{vmatrix} \neq 0$$

It is not always true that the solutions $w_i(z)$ are periodic, although $p(z)$ and $q(z)$ are. However, there are some solutions that are simply multiplied by a constant factor σ when there is a shift of $\zeta \in \mathbb{R}$, i.e. there are solutions where:

$$w_i(z + \zeta) = \sigma w_i(z)$$

As a consequence of this, from the relationship between the fundamental sets $(w_1(z), w_2(z))$ and $(w_1(z+\zeta), w_2(z+\zeta))$, it is possible to obtain the following homogeneous algebraic system:

$$\begin{bmatrix} a_{11} - \sigma & a_{12} \\ a_{21} & a_{22} - \sigma \end{bmatrix} \begin{Bmatrix} w_1(z) \\ w_2(z) \end{Bmatrix} = \begin{Bmatrix} 0 \\ 0 \end{Bmatrix}$$

Clearly, the only nontrivial solutions for this problem are the roots of the polynomial in the equation below, namely the characteristic equation:

$$\sigma^2 - (a_{11} + a_{22})\sigma + \det([a_{ij}]) = 0$$

Once $[a_{ij}]$ is nonsingular, its determinant will never be zero, and hence the values of σ can be determined. Furthermore, if the roots are simple (i.e. not multiple), then there are two linearly independent solutions of the form:

$$w_i(z) = e^{\alpha_i z} \varphi(z)$$

, being $\alpha_i \in \mathbb{C}^*$ and $\varphi(z + \zeta)$ periodic with period ζ in z .

Applying a one period shift, it is possible to obtain:

$$\sigma_i w_i(z) = w_i(z + \zeta) = e^{\alpha_i(z+\zeta)} \varphi(z + \zeta) = e^{\alpha_i \zeta} e^{\alpha_i z} \varphi(z) = e^{\alpha_i \zeta} w_i(z)$$

Consequently, the assumption of $\varphi(z)$ as a periodic function with period ζ in z leads

to:

$$\sigma_i = e^{\alpha_i \zeta}$$

, with σ_i and α_i not necessarily real.

These constants are closely related to the boundedness of the normal solutions w_1 and w_2 . For this reason, σ_i is called a Floquet multiplier and α_i is a Floquet exponent. Boundedness is given by $|\sigma_i| \leq 1$ or $\Re[\alpha_i] \leq 0$, where the equalities represent the limit of the boundedness. Otherwise, the solutions are unbounded.

Another important consequence of the form assumed for the normal solutions is that once α_i may be complex, the exponential $e^{\alpha_i z}$ may be a periodic function. Particularly, if $\sigma_i = -1$, then the period of the normal solution $w_i(z)$ is 2ζ , and not ζ as firstly expected.

The conclusions obtained so far are valid if the roots of the characteristic equation σ_1 and σ_2 are different. If there is only one root σ with multiplicity 2, then the normal solutions are given by:

$$\begin{cases} w_1(z) = e^{\alpha z} \varphi_1(z) \\ w_2(z) = e^{\alpha z} \left(\frac{az}{\sigma \zeta} \varphi_1(z) + \psi_1(z) \right) \end{cases} \quad | \quad \psi_1(z + \zeta) = \psi_1(z)$$

B.10 Introduction to the general Floquet theory

The goal of this section is to introduce the main features from the general Floquet theory. It is based on the work by Slane and Tragesser (2011).

The object of study are homogeneous and autonomous systems defined by:

$$\dot{\mathbf{x}} = \mathbf{A}(t)\mathbf{x}$$

, where the matrix $\mathbf{A}(t)$ is $n \times n$ time varying and periodic with period ζ in t .

The first step is to define the fundamental matrix $\mathbf{X}(\mathbf{t})$, which is a matrix function whose columns are linearly independent solutions of $\dot{\mathbf{x}} = \mathbf{A}(t)\mathbf{x}$. It is non singular and

not unique. If $\mathbf{X}(t_0) = \mathbf{I}$, where \mathbf{I} is the identity matrix, then $\mathbf{X}(t)$ is called the principal fundamental matrix.

From this definition it follows directly that:

- If $\mathbf{X}(t)$ is a fundamental matrix, then $\mathbf{Y}(t) = \mathbf{X}(t)\mathbf{B}$ for any nonsingular constant matrix \mathbf{B} .
- If $\mathbf{A}(t)$ is ζ -periodic and $\mathbf{X}(t)$ is a fundamental matrix, then so is $\mathbf{X}(t + \zeta)$, and there exists a nonsingular constant matrix \mathbf{B} such that $\mathbf{X}(t + \zeta) = \mathbf{X}(t)\mathbf{B}$.

Since the matrix \mathbf{B} is constant, it can be easily calculated by setting $t = 0$, and then:

$$\mathbf{B} = \mathbf{X}^{-1}(0)\mathbf{X}(\zeta)$$

Especially, if $\mathbf{X}(t)$ is the principal fundamental matrix, then:

$$\mathbf{B} = \mathbf{X}(\zeta)$$

From the Floquet-Lyapunov theorem, any fundamental matrix of the aforementioned system must be of the form:

$$\mathbf{X}(t) = \mathbf{\Phi}(t)e^{\mathbf{K}t}$$

, where $\mathbf{\Phi}(t)$ is a nonsingular continuous ζ -periodic $n \times n$ matrix function, and \mathbf{K} is some constant matrix.

From the previous definitions, it is possible to say that:

$$\mathbf{X}(t + \zeta) = \mathbf{\Phi}(t + \zeta)e^{\mathbf{K}(t+\zeta)} = \mathbf{\Phi}(t)e^{\mathbf{K}t}e^{\mathbf{K}\zeta} = \mathbf{X}(t)e^{\mathbf{K}\zeta} = \mathbf{X}(t)\mathbf{B}$$

, from which it is directly concluded that:

$$\mathbf{B} = e^{\mathbf{K}\zeta}$$

Furthermore, if $\mathbf{X}(t)$ is the principal fundamental matrix, then:

$$\mathbf{B} = e^{\mathbf{K}\zeta} = \mathbf{X}(\zeta)$$

The eigenvalues of \mathbf{K} are called the characteristic Floquet exponents (α_i), while the eigenvalues of \mathbf{B} are the Floquet multipliers (σ_i). The matrix \mathbf{B} is called the monodromy matrix. The relationship between the exponents and the multipliers is:

$$\alpha_i = \frac{\ln \sigma_i}{\zeta}$$

Once α_i and σ_i need not be real, carrying analyses considering the multipliers is more convenient than through the exponents, for avoiding the calculation of a complex logarithm.

The main advantage brought by this theory is that, just by determining the monodromy matrix, it is possible to infer the system's stability beforehand.

B.11 Introduction to the extended Floquet theory

The goal of this section is to introduce the results brought by the work of Slane and Tragesser (2011) on the analysis of inhomogeneous systems with periodic coefficients.

The system to be studied is of the form:

$$\dot{\mathbf{x}} = \mathbf{A}(t)\mathbf{x} + \mathbf{g}(t)$$

, where the matrix $\mathbf{A}(t)$ and the array $\mathbf{g}(t)$ are ζ -periodic.

The solution to this equation is readily expressible in terms of the *principal fundamental matrix* $\mathbf{X}(t)$ as follows:

$$\mathbf{x}(t) = \mathbf{X}(t) \left[\mathbf{x}(0) + \int_0^t \mathbf{X}^{-1}(\tau)\mathbf{g}(\tau)d\tau \right]$$

The same solution after precisely n periods ($n \in \mathbb{Z}_+^*$), is given by:

$$\mathbf{x}(n\zeta) = \underbrace{\mathbf{X}^n(\zeta)\mathbf{x}(0)}_{\text{Homogeneous}} + \underbrace{\left(\sum_{i=1}^n \mathbf{X}^i(\zeta) \right) \int_0^\zeta \mathbf{X}^{-1}(\tau)\mathbf{g}(\tau)d\tau}_{\text{Inhomogeneous}}$$

The boundedness of the homogeneous solution is given by the existence of the limit $\lim_{n \rightarrow \infty} \mathbf{X}^n(\zeta)$, which is defined by the following theorem:

Theorem 1 (Limits of Powers Theorem). *Given a complex square matrix \mathbf{X} , the limit $\lim_{n \rightarrow \infty} \mathbf{X}^n$ exists if and only if $\rho[\mathbf{X}(\zeta)] < 1$ or $\rho[\mathbf{X}(\zeta)] = 1$, where 1 is the only eigenvalue on the unit circle and is semisimple.*

When it exists, this limit is the projector onto the null space of $(\mathbf{I} - \mathbf{A})$ along its range space.

This theorem is complemented by the following one:

Theorem 2 (Cesàro summability). *Given a complex square matrix \mathbf{X} , such matrix is Cesàro summable if and only if $\rho[\mathbf{X}(\zeta)] < 1$ or $\rho[\mathbf{X}(\zeta)] = 1$ where each eigenvalue on the unit circle is semisimple.*

If the Cesàro limit exists, it is given by:

$$\lim_{n \rightarrow \infty} \frac{1}{n} \left(\mathbf{I} + \sum_{i=1}^{n-1} \mathbf{X}^i \right) = \mathbf{G}$$

, where \mathbf{G} is the projector onto the null space of $(\mathbf{I} - \mathbf{A})$ along its range space, the very same from the Limits of Powers Theorem, in case it exists. The matrix \mathbf{G} will not be null if and only if 1 is an eigenvalue of \mathbf{X} .

It is important to notice that if $\lim_{n \rightarrow \infty} \mathbf{X}^n$ exists, it implies that \mathbf{G} exists, but the converse is not true, once the Cesàro sum is the limit of the arithmetic mean of the n partial sums of a series with n tending to the infinity. In other words, if a series does not converge but oscillates around a mean value, the limit does not exist but the Cesàro sum does.

With these results it is now clear that the homogeneous response of this system will only be unbounded in case there are eigenvalues on the unit circle that are not semisimple or in case there are eigenvalues outside it.

Now, turning the discussion to the boundedness of the inhomogeneous solution, it turns out that the integral term is calculated over a single well defined period, and hence it is constant. Consequently, the boundedness of this term depends exclusively on the boundedness of the summation term, given by the following theorem:

Theorem 3 (Neumann series). *Given a complex square matrix \mathbf{X} , if the Neumann series $\mathbf{I} + \sum_{i=1}^{\infty} \mathbf{X}^i$ converges, both statements hold:*

- $\rho[\mathbf{X}] < 1$
- $\lim_{n \rightarrow \infty} \mathbf{X}^n = \mathbf{0}$

and if they do, the Neumann series converges.

It is important to mention that if $\lim_{n \rightarrow \infty} \mathbf{X}^n = \mathbf{0}$, then $(\mathbf{I} - \mathbf{X})^{-1}$ exists and

$$\lim_{n \rightarrow \infty} \mathbf{I} + \sum_{i=1}^n \mathbf{X}^i = (\mathbf{I} - \mathbf{X})^{-1}$$

If the eigenvalues of $\mathbf{X}(\zeta)$ all lie inside the unit circle, or if there are some semisimple ones on the unit circle that are other than 1, then the summation term converges. If 1 is the only multiplier on the unit circle, even if it is semisimple the summation term will diverge. Obviously, divergence also occurs when there are non semisimple eigenvalues on the unit circle or when they lie outside it.

The results from this extension are then summarized on Table 3.1.

B.12 Proof: s_i^2 from Eq. (3.33) is negative

The goal of this section is to prove that the parameter $s_{1,2}^2$ shown in Eq. (3.33) is always negative.

In order to ease further analyses, the following parameters are defined:

$$q = 1 - \mu v^2(v^2 + 1); \quad r = \mu(v^2 + 1) + 1 + \frac{1}{\beta^2 a}$$

, so that:

$$s_{1,2}^2 = \frac{v^2}{2q} \left(-r \pm \sqrt{r^2 - \frac{4q}{\beta^2 a}} \right)$$

The first thing to prove is that the radicand is in \mathbb{R}_+ . Hence, it is necessary to prove that:

$$\left(\mu v^2(v^2 + 1) + 1 + \frac{1}{\beta^2 a} \right)^2 - \frac{4(1 - \mu v^2(v^2 + 1))}{\beta^2 a} \geq 0$$

This expression can be rearranged to:

$$\left(1 - \frac{1}{\beta^2 a} \right)^2 + \left(2 + \mu v^2(v^2 + 1) + \frac{6}{\beta^2 a} \right) \mu v^2(v^2 + 1) \geq 0$$

Once a and μ are real and positive, and β and v are real, then this inequality will always hold and the radicand will always be greater than or equal to zero.

It is easy to see that r is positive, but nothing can be said about q . Once the radicand is proven to be positive, this directly constraints q to:

$$q \geq 0$$

On the other hand, if the result of the square root is greater than r , one of the squared eigenvalues will be real and positive, leading directly to instability. Hence, the parameter q must be positive.

The positiveness of q is assured by the relationship:

$$\mu > \frac{1}{v^2(v^2 + 1)}$$

□

B.13 Proof: Asymptotic behavior of eigen-order χ_1

The goal of this section is to prove the asymptotic behavior of χ_1 when Ω tends to zero and to the infinity.

Firstly, the following parameters are introduced:

$$q = 1 - \mu v^2(v^2 + 1); \quad \beta_\Omega = \frac{\beta}{\Omega}$$

Then, the eigen-order χ_1 can be written as:

$$\chi_1 = \frac{v}{\sqrt{2q}} \left(\left(\frac{1-q}{v^2} + 1 + \frac{1}{\beta_\Omega^2 \Omega^2 a} \right) - \sqrt{\left(\frac{1-q}{v^2} + 1 + \frac{1}{\beta_\Omega^2 \Omega^2 a} \right)^2 - \frac{4q}{\beta_\Omega^2 \Omega^2 a}} \right)^{1/2}$$

After squaring both sides and rearranging some terms, it is possible to obtain:

$$\frac{2q\chi_1^2}{v^2} = \left(\frac{1-q}{v^2} + 1 + \frac{1}{\beta_\Omega^2 \Omega^2 a} \right) - \sqrt{\left(\frac{1-q}{v^2} + 1 + \frac{1}{\beta_\Omega^2 \Omega^2 a} \right)^2 - \frac{4q}{\beta_\Omega^2 \Omega^2 a}}$$

Performing more rearrangements and squaring both sides again leads to:

$$-2 \left(\frac{2q\chi_1^2}{v^2} \right) \left(\frac{1-q}{v^2} + 1 + \frac{1}{\beta_\Omega^2 \Omega^2 a} \right) + \left(\frac{2q\chi_1^2}{v^2} \right)^2 = -\frac{4q}{\beta_\Omega^2 \Omega^2 a}$$

From this point on it is possible to apply both limits, with Ω tending to zero and to

the infinity. For the first limit, it is convenient to multiply both sides of the equation by Ω^2 , which leads to:

$$-2 \left(\Omega^2 \left(\frac{1-q}{v^2} + 1 \right) + \frac{1}{\beta_\Omega^2 a} \right) \left(\frac{2q\chi_1^2}{v^2} \right) + \Omega^2 \left(\frac{2q\chi_1^2}{v^2} \right)^2 = -\frac{4q}{\beta_\Omega^2 a}$$

Applying the limit with $\Omega \rightarrow 0$ on both sides provides the following expression:

$$\left(\lim_{\Omega \rightarrow 0} \Omega^2 \right) \left(\frac{-4(1-q)q}{\beta_\Omega^2 v^4 a} \lim_{\Omega \rightarrow 0} \chi_1^2 + \frac{4q^2}{v^4} \lim_{\Omega \rightarrow 0} \chi_1^4 \right) - \frac{4q}{\beta_\Omega^2 v^2 a} \lim_{\Omega \rightarrow 0} \chi_1^2 = -\frac{4q}{\beta_\Omega^2 a}$$

If $\lim_{\Omega \rightarrow 0} \chi_1$ exists, then this expression reduces to:

$$\frac{1}{v^2} \lim_{\Omega \rightarrow 0} \chi_1^2 = 1$$

, and hence:

$$\lim_{\Omega \rightarrow 0} \chi_1 = v$$

This proof is completed by Appendix B.15, where it is shown that $\chi_1 \leq v$ if $q \leq 1$.

Returning now to the following expression:

$$\chi_1 = \frac{v}{\sqrt{2q}} \left(\left(\frac{1-q}{v^2} + 1 + \frac{1}{\beta_\Omega^2 \Omega^2 a} \right) - \sqrt{\left(\frac{1-q}{v^2} + 1 + \frac{1}{\beta_\Omega^2 \Omega^2 a} \right)^2 - \frac{4q}{\beta_\Omega^2 \Omega^2 a}} \right)^{1/2}$$

It is rather direct to see that if Ω tends to the infinity, then χ_1 tends to zero. Hence, the asymptotic behavior of χ_1 is proven. □

B.14 Proof: Asymptotic behavior of eigen-order χ_2

The goal of this section is to prove the asymptotic behavior of χ_2 when Ω tends to zero and to the infinity.

Firstly, the following parameters are introduced:

$$q = 1 - \mu v^2(v^2 + 1); \quad \beta_\Omega = \frac{\beta}{\Omega}$$

Then, the eigen-order χ_2 can be written as:

$$\chi_2 = \frac{v}{\sqrt{2q}} \left(\left(\frac{1-q}{v^2} + 1 + \frac{1}{\beta_\Omega^2 \Omega^2 a} \right) + \sqrt{\left(\frac{1-q}{v^2} + 1 + \frac{1}{\beta_\Omega^2 \Omega^2 a} \right)^2 - \frac{4q}{\beta_\Omega^2 \Omega^2 a}} \right)^{1/2}$$

Applying the limit with $\Omega \rightarrow \infty$ on both sides, the result is straightforward:

$$\lim_{\Omega \rightarrow \infty} \chi_2 = \sqrt{\frac{1-q+v^2}{q}}$$

Now, for the case where $\Omega \rightarrow 0$, some rearrangements must be performed. In the expression for χ_2 , it is possible to rewrite it putting the factor $1/\Omega$ in evidence:

$$\chi_2 = \underbrace{\left(\frac{v}{\Omega \sqrt{2q}} \right)}_{\text{Part: I}} \underbrace{\left(\left(\Omega^2 \left(\frac{1-q}{v^2} + 1 \right) + \frac{1}{\beta_\Omega^2 a} \right) + \sqrt{\left(\Omega^2 \left(\frac{1-q}{v^2} + 1 \right) + \frac{1}{\beta_\Omega^2 a} \right)^2 - \frac{4q\Omega^4}{\beta_\Omega^2 a}} \right)}_{\text{Part: II}}^{1/2}$$

When Ω tends to zero, it is very clear that part II of this expression tends to a constant, while part I tends to the infinity. Hence, it is straightforward to conclude that:

$$\lim_{\Omega \rightarrow 0} \chi_2 \rightarrow \infty$$

Therefore, the asymptotic behavior of χ_2 is proven. □

B.15 Proof: Maximum value of eigen-order χ_1

The goal of this section is to prove that the eigen-order χ_1 is always lower than or equal to v . Once χ_1 is given by:

$$\chi_1 = \frac{v}{\sqrt{2q}} \left(\left(\frac{1-q}{v^2} + 1 + \frac{1}{\beta_\Omega^2 \Omega^2 a} \right) - \sqrt{\left(\frac{1-q}{v^2} + 1 + \frac{1}{\beta_\Omega^2 \Omega^2 a} \right)^2 - \frac{4q}{\beta_\Omega^2 \Omega^2 a}} \right)^{1/2}$$

, the inequality to be solved is:

$$\frac{v}{\sqrt{2q}} \left(\left(\frac{1-q}{v^2} + 1 + \frac{1}{\beta_\Omega^2 \Omega^2 a} \right) - \sqrt{\left(\frac{1-q}{v^2} + 1 + \frac{1}{\beta_\Omega^2 \Omega^2 a} \right)^2 - \frac{4q}{\beta_\Omega^2 \Omega^2 a}} \right)^{1/2} \leq v$$

It is possible to square both sides and perform some rearrangements to obtain:

$$\left(\frac{1-q}{v^2} + 1 + \frac{1}{\beta^2 a} \right) - \sqrt{\left(\frac{1-q}{v^2} + 1 + \frac{1}{\beta^2 a} \right)^2 - \frac{4q}{\beta^2 a}} \leq 2q$$

In order to eliminate the square root, it is isolated and both sides are squared once more. After some rearrangements it is possible to achieve the interesting expression:

$$-q(1-q) \leq 0$$

, which is true if and only if:

$$0 < q \leq 1$$

Hence,

$$\chi_1 \leq v \Leftrightarrow 0 < q \leq 1 \Rightarrow v \in \mathbb{R}; \mu \in \mathbb{R}_+$$

□

B.16 Proof: Minimum value of eigen-order χ_2

The goal of this section is to prove that the eigen-order χ_2 is always greater than or equal to $\sqrt{\frac{1-q+v^2}{q}}$. Once χ_2 is given by:

$$\chi_2 = \frac{v}{\sqrt{2q}} \left(\left(\frac{1-q}{v^2} + 1 + \frac{1}{\beta^2 a} \right) + \sqrt{\left(\frac{1-q}{v^2} + 1 + \frac{1}{\beta^2 a} \right)^2 - \frac{4q}{\beta^2 a}} \right)^{1/2}$$

, the inequality to be solved is:

$$\frac{v}{\sqrt{2q}} \left(\left(\frac{1-q}{v^2} + 1 + \frac{1}{\beta^2 a} \right) + \sqrt{\left(\frac{1-q}{v^2} + 1 + \frac{1}{\beta^2 a} \right)^2 - \frac{4q}{\beta^2 a}} \right)^{1/2} \geq \sqrt{\frac{1-q+v^2}{q}}$$

It is possible to square both sides and perform some rearrangements to obtain:

$$\left(\frac{1-q}{v^2} + 1 + \frac{1}{\beta^2 a} \right) + \sqrt{\left(\frac{1-q}{v^2} + 1 + \frac{1}{\beta^2 a} \right)^2 - \frac{4q}{\beta^2 a}} \geq \frac{2(1-q+v^2)}{v^2}$$

In order to eliminate the square root, it is isolated and both sides are squared once more:

$$\frac{-4q}{\beta^2 a} \geq 4 \left(\frac{1-q}{v^2} + 1 \right)^2 - 4 \left(\frac{1-q}{v^2} + 1 \right) \left(\frac{1-q}{v^2} + 1 + \frac{1}{\beta^2 a} \right)$$

, which reduces to

$$q \leq 1$$

Hence,

$$\chi_2 \geq \sqrt{\frac{1-q+v^2}{q}} \Leftrightarrow q \leq 1$$

□

B.17 Derivation: Equations of motion for a single torsional disk with a General Path CPVA

The goal of this section is to exhibit the derivation of the equations of motion of a single torsional disk with a General Path CPVA. A pendulum with general path is represented in Fig. B.2.

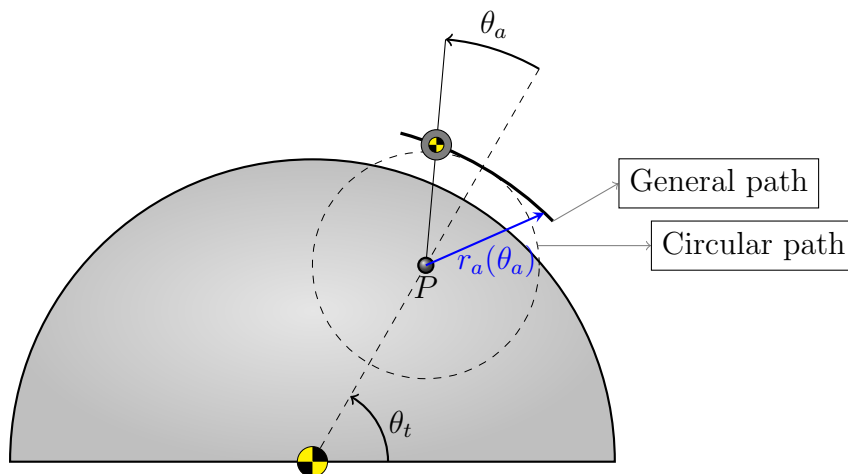


Figure B.2: Representation of a general path pendulum.

The mass of the pendulum is represented by a point that is free to slide on the rod, that is pinned to the point P . Although this mass is free to slide, it is constrained to remain on the General path indicated in the figure. One must notice that this path is not circular. The circular one is indicated by the dashed circumference around the point P . In order to locate the center of mass of the pendulum with respect to the point P , the relative angle θ_a is used. The distance of the center of mass of the pendulum bob to the point P is then given by $r_a(\theta_a)$.

The position of the center of mass of the pendulum bob, considering that the point P is at a distance R_p from the center of the disk is:

$$\begin{aligned} P_x &= R_p \cos \theta_t + r_a(\theta_a) \cos(\theta_a + \theta_t) \\ P_y &= R_p \sin \theta_t + r_a(\theta_a) \sin(\theta_a + \theta_t) \end{aligned}$$

The speed of this point is given by the first derivative P_x and P_y with respect to time

in the respective directions, and is given by:

$$\dot{P}_x = -R_p \dot{\theta}_t \sin \theta_t - r_a(\theta_a)(\dot{\theta}_a + \dot{\theta}_t) \sin(\theta_a + \theta_t) + \frac{dr_a(\theta_a)}{d\theta_a} \dot{\theta}_a \cos(\theta_a + \theta_t)$$

$$\dot{P}_y = R_p \dot{\theta}_t \cos \theta_t + r_a(\theta_a)(\dot{\theta}_a + \dot{\theta}_t) \cos(\theta_a + \theta_t) + \frac{dr_a(\theta_a)}{d\theta_a} \dot{\theta}_a \sin(\theta_a + \theta_t)$$

Its acceleration in x and y directions is then given by:

$$\begin{aligned} \ddot{P}_x &= -R_p \left(\ddot{\theta}_t \sin \theta_t + \dot{\theta}_t^2 \cos \theta_t \right) + \dots \\ &\quad - r_a(\theta_a) \left((\ddot{\theta}_a + \ddot{\theta}_t) \sin(\theta_a + \theta_t) + (\dot{\theta}_a + \dot{\theta}_t)^2 \cos(\theta_a + \theta_t) \right) + \dots \\ &\quad + \frac{dr_a(\theta_a)}{d\theta_a} \left(\ddot{\theta}_a \cos(\theta_a + \theta_t) - 2\dot{\theta}_a(\dot{\theta}_a + \dot{\theta}_t) \sin(\theta_a + \theta_t) \right) + \dots \\ &\quad + \frac{d^2 r_a(\theta_a)}{d\theta_a^2} \dot{\theta}_a^2 \cos(\theta_a + \theta_t) \\ \ddot{P}_y &= R_p \left(\ddot{\theta}_t \cos \theta_t - \dot{\theta}_t^2 \sin \theta_t \right) + \dots \\ &\quad + r_a(\theta_a) \left((\ddot{\theta}_a + \ddot{\theta}_t) \cos(\theta_a + \theta_t) - (\dot{\theta}_a + \dot{\theta}_t)^2 \sin(\theta_a + \theta_t) \right) + \dots \\ &\quad + \frac{dr_a(\theta_a)}{d\theta_a} \left(\ddot{\theta}_a \sin(\theta_a + \theta_t) + 2\dot{\theta}_a(\dot{\theta}_a + \dot{\theta}_t) \cos(\theta_a + \theta_t) \right) + \dots \\ &\quad + \frac{d^2 r_a(\theta_a)}{d\theta_a^2} \dot{\theta}_a^2 \sin(\theta_a + \theta_t) \end{aligned}$$

The free body diagrams for this system are shown in Fig. B.3.

The summations of efforts in x and y directions for the pendulum body are then:

$$\begin{aligned} m_a \ddot{P}_x &= F_x \\ m_a \ddot{P}_y &= F_y - m_a g \end{aligned}$$

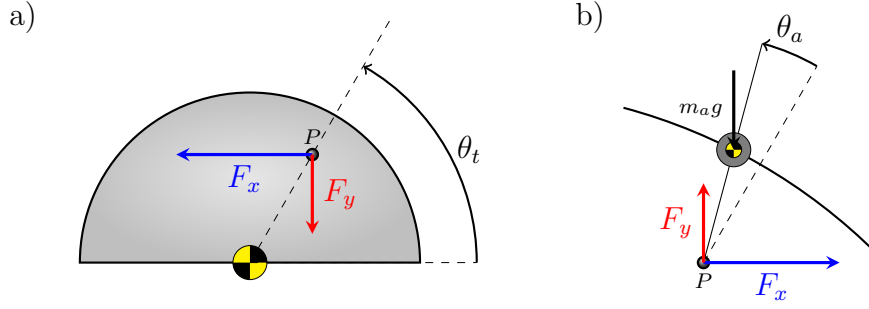


Figure B.3: Free body diagrams for disk with general path CPVA.

The summation of moments at the disk about its center of mass is:

$$I_t \ddot{\theta}_t = R_p (F_x \sin \theta_t - F_y \cos \theta_t)$$

Replacing the two previous equations on this one makes possible to find the equation of motion for the disk, given by:

$$\begin{aligned} & (I_t + m_a R_p^2) \ddot{\theta}_t + m_a R_p \frac{d^2 r_a(\theta_a)}{d\theta_a^2} (\dot{\theta}_a^2 \sin \theta_a) + \dots \\ & + m_a R_p \frac{dr_a(\theta_a)}{d\theta_a} \left(\ddot{\theta}_a \sin \theta_a + 2\dot{\theta}_a (\dot{\theta}_a + \dot{\theta}_t) \cos \theta_a \right) + \dots \\ & + m_a R_p r_a(\theta_a) \left((\ddot{\theta}_a + \ddot{\theta}_t) \cos \theta_a - (\dot{\theta}_a + \dot{\theta}_t)^2 \sin \theta_a \right) + m_a R_p g \cos \theta_t = 0 \end{aligned}$$

The equation of motion of the pendulum can be obtained directly by making the summation of the moments about the point P :

$$\sum M_P = I_a (\ddot{\theta}_a + \ddot{\theta}_t) + m_a \left(\ddot{P}_y \cos(\theta_a + \theta_t) - \ddot{P}_x \sin(\theta_a + \theta_t) \right) r_a(\theta_a)$$

Replacing all the terms on this equation leads to the equation of motion for the pendulum:

$$\begin{aligned} & (I_a + m_a r_a^2(\theta_a)) (\ddot{\theta}_a + \ddot{\theta}_t) + 2m_a \frac{dr_a(\theta_a)}{d\theta_a} r_a(\theta_a) \dot{\theta}_a (\dot{\theta}_a + \dot{\theta}_t) + \dots \\ & + m_a r_a(\theta_a) \left(R_p (\ddot{\theta}_t \cos \theta_a + \dot{\theta}_t^2 \sin \theta_a) + g \cos(\theta_t + \theta_a) \right) = 0 \end{aligned}$$

B.18 List of derivatives of the radius of the general path in terms of the function $g(\theta_r)$

In this appendix the derivatives of $r_a(\theta_a)$ with respect to θ_a as functions of $g(\theta_r)$ are shown up to the eighth order. The first one has already been shown in section 3.3.3, and is given by:

$$\frac{d}{d\theta_a} (r_a(\theta_a)) = \left(\frac{\frac{dx_p}{d\theta_r} x_p + \frac{dy_p}{d\theta_r} y_p}{\frac{dx_p}{d\theta_r} y_p - \frac{dy_p}{d\theta_r} x_p} \right) r_a(\theta_a(\theta_r)) = g(\theta_r) r_a(\theta_a)$$

The higher ones, up to the eighth order are listed below. In this appendix only, the notation g' means differentiation with respect to θ_a :

$$\frac{d^2}{d\theta_a^2} (r_a(\theta_a)) = (g^2 + g') r_a(\theta_a)$$

$$\frac{d^3}{d\theta_a^3} (r_a(\theta_a)) = (g^3 + 3g'g + g'') r_a(\theta_a)$$

$$\frac{d^4}{d\theta_a^4} (r_a(\theta_a)) = (3g'^2 + 6g'g^2 + g^4 + 4g''g + g''') r_a(\theta_a)$$

$$\frac{d^5}{d\theta_a^5} (r_a(\theta_a)) = (15g'^2g + 10g'g^3 + 10g''g' + g^5 + 10g''g^2 + 5g'''g + g^{IV}) r_a(\theta_a)$$

$$\begin{aligned} \frac{d^6}{d\theta_a^6} (r_a(\theta_a)) = & (10g''^2 + 60g''g'g + 20g''g^3 + 15g'^3 + 45g'^2g^2 + 15g'g^4 + 15g'''g' + \dots \\ & + g^6 + 15g'''g^2 + 6g^{IV}g + g^V) r_a(\theta_a) \end{aligned}$$

$$\begin{aligned} \frac{d^7}{d\theta_a^7} (r_a(\theta_a)) = & (70g''^2g + 105g''g'^2 + 210g''g'g^2 + 35g''g^4 + 35g'''g'' + 105g'^3g + \dots \\ & + 105g'^2g^3 + 21g'g^5 + 105g'''g'g + 21g^{IV}g' + g^7 + 35g'''g^3 + \dots \\ & + 21g^{IV}g^2 + 7g^Vg + g^{VI}) r_a(\theta_a) \end{aligned}$$

$$\begin{aligned} \frac{d^8}{d\theta_a^8} (r_a(\theta_a)) = & (280g''^2g' + 280g''^2g^2 + 280g''g'''g + 840g''g'^2g + 560g''g'g^3 + \dots \\ & + 56g''g^5 + 56g^{IV}g'' + 35g'''^2 + 210g'''g'^2 + 420g'''g'g^2 + 70g'''g^4 + \dots \\ & + 105g'^4 + 420g'^3g^2 + 210g'^2g^4 + 28g'g^6 + 168g^{IV}g'g + 28g^Vg' + \dots \\ & + g^8 + 56g^{IV}g^3 + 28g^Vg^2 + 8g^{VI}g + g^{VII}) r_a(\theta_a) \end{aligned}$$

B.19 List of functions from $E_0(p)$ to $E_8(p)$ for the epicycloid

In this appendix the functions from $E_0(p)$ to $E_8(p)$ are defined for the polynomial approximation of the epicycloid. Only the functions with even subscripts are not identically null.

$$E_0(p) = 1$$

$$E_2(p) = -\frac{3(p-1)}{(p-2)^2}$$

$$E_4(p) = \frac{(p-1)}{(p-2)^5} (15p^3 + 13p^2 - 103p + 70)$$

$$E_6(p) = \frac{(p-1)}{(p-2)^8} (63p^6 + 1607p^5 - 6577p^4 + 6301p^3 + 3341p^2 - 7378p + 2650)$$

$$E_8(p) = \frac{(p-1)}{(p-2)^{11}} \left(\begin{array}{l} 255p^9 + 38325p^8 + 34809p^7 - 1195927p^6 + 3926985p^5 + \dots \\ -5681495p^4 + 4083785p^3 - 1314990p^2 + 90652p + 17592 \end{array} \right)$$

B.20 Table of values of $p_1(v)$ for given values of v

In this section a table of values for the root $p_1(v)$ are provided for vanishing the 3rd detuning term. Results are shown in Table B.1.

Table B.1: Some values of $p_1(v)$

v	$p_1(v)$	v	$p_1(v)$
0.0	0.8541019662	4.1	0.0473131498
0.1	0.8525478078	4.2	0.0451807130
0.2	0.8476795230	4.3	0.0431875773
0.3	0.8388182755	4.4	0.0413219965
0.4	0.8246073691	4.5	0.0395734251
0.5	0.8026277710	4.6	0.0379323753
0.6	0.7690045650	4.7	0.0363902932
0.7	0.7193477645	4.8	0.0349394517
0.8	0.6538332015	4.9	0.0335728566
0.9	0.5814012026	5.0	0.0322841662
1.0	0.5123060889	5.1	0.0310676196
1.1	0.4512515101	5.2	0.0299179745
1.2	0.3988581452	5.3	0.0288304527
1.3	0.3542515219	5.4	0.0278006920
1.4	0.3162477087	5.5	0.0268247038
1.5	0.2837377878	5.6	0.0258988355
1.6	0.2557807170	5.7	0.0250197372
1.7	0.2316043011	5.8	0.0241843328
1.8	0.2105815757	5.9	0.0233897931
1.9	0.1922040714	6.0	0.0226335128
2.0	0.1760581689	6.1	0.0219130899
2.1	0.1618057625	6.2	0.0212263067
2.2	0.1491689128	6.3	0.0205711134
2.3	0.1379177989	6.4	0.0199456133
2.4	0.1278612778	6.5	0.0193480488
2.5	0.1188394746	6.6	0.0187767900
2.6	0.1107179403	6.7	0.0182303235
2.7	0.1033830215	6.8	0.0177072427
2.8	0.0967381705	6.9	0.0172062387
2.9	0.0907009872	7.0	0.0167260927
3.0	0.0852008334	7.1	0.0162656682
3.1	0.0801768991	7.2	0.0158239049
3.2	0.0755766251	7.3	0.0153998124
3.3	0.0713544112	7.4	0.0149924649
3.4	0.0674705510	7.5	0.0146009962
3.5	0.0638903514	7.6	0.0142245952
3.6	0.0605833998	7.7	0.0138625015
3.7	0.0575229520	7.8	0.0135140021
3.8	0.0546854197	7.9	0.0131784277
3.9	0.0520499380	8.0	0.0128551494
4.0	0.0495980006	8.1	0.0125435761